Autonomous control for adaptive ships with hybrid propulsion and power generation

Geertsma, Rinze

DOI
10.4233/uuid:ad81b0ee-76be-4054-a7e8-bd2eeecdb156

Publication date
2019

Document Version
Final published version

Citation (APA)
Geertsma, R. (2019). *Autonomous control for adaptive ships: with hybrid propulsion and power generation*. [Dissertation (TU Delft), Delft University of Technology]. https://doi.org/10.4233/uuid:ad81b0ee-76be-4054-a7e8-bd2eeecdb156

Autonomous Control for Adaptive Ships

with Hybrid Propulsion and Power Generation

AUTONOMOUS CONTROL FOR ADAPTIVE SHIPS

WITH HYBRID PROPULSION AND POWER GENERATION

Proefschrift

ter verkrijging van de graad van doctor
aan de Technische Universiteit Delft,
op gezag van de Rector Magnificus prof. dr. ir. T. H. J. J. van der Hagen,
voorzitter van het College voor Promoties,
in het openbaar te verdedigen op dinsdag 8 januari 2019 om 15:00 uur

door

Rinze Dirk GEERTSMA

Master of Science in Marine Engineering, University College London, United Kingdom,
geboren te Kollum, Nederland.

Dit proefschrift is goedgekeurd door de promotoren:

Promotor: Prof. ir. J. J. Hopman
Promotor: Prof. dr. R. R. Negenborn

Samenstelling promotiecommissie:

Rector Magnificus	voorzitter
Prof. ir. J. J. Hopman	Technische Universiteit Delft
Prof. dr. R. R. Negenborn	Technische Universiteit Delft

Onafhankelijke leden:

Prof. dr. ir. P. H. A. J. M. van Gelder	Technische Universiteit Delft
Prof. dr. ir. M. Cao	Rijksuniversiteit Groningen
Prof. dr. S. Delprat	University of Valenciennes and Hainaut-Cambresis (France)
Prof. M. Figari	Univerity of Genoa (Italy)

Overige leden:

Ir. K. Visser	Technische Universiteit Delft

The research in this dissertation is part of the research programme 'ShipDrive: A Novel Methodology for Integrated Modelling, Control, and Optimisation of Hybrid Ship Systems' with project number 13276, which is partly financed by the Netherlands Organisation for Scientific Research (NWO), domain Applied and Engineering Sciences (TTW) and by the Royal Netherlands Navy.

Keywords: Ship propulsion, Non-linear control systems, Marine systems, Modelling and simulation, Validation, Power systems

Printed by: KLTZ (TD) Rinze Dirk Geertsma, MSc, CEng

Front & Back: Ministerie van Defensie en De Betekenaar

ISBN 978-90-829766-0-1

An electronic version of this dissertation is available at
http://repository.tudelft.nl/.

If I have seen further, it is by standing on the shoulders of giants

Isaac Newton

Thanks to the support of Coby, Jelmer and Lienke

CONTENTS

SUMMARY

SHIPPING plays a crucial role in modern society, as it enables world trade, provides resources such as fossil fuels and allows harvesting renewable resources, such as wind, wave and tidal energy from the oceans, now and in the future. However, shipping needs to significantly reduce its impact on the environment, as it emits the most polluting emissions of all types of transport and increasingly disturbs ecologically sensitive underwater environments with its noise. At the same time, the diversity of modern shipping puts pressure on the manoeuvrability, availability and maintainability of ships and their power and propulsion systems, in order to perform its function more reliably and with less crew, or, in future, autonomously. The commercial availability of power electronic converters and lithium-ion batteries has led to an exponential increase in the variety and complexity of propulsion and power generation architectures. This variety and complexity provides an opportunity to design hybrid propulsion and power generation architectures that use a combination of direct mechanical propulsion, electrical propulsion, combustion power supply and energy storage, to reduce emissions and noise as well as improve manoeuvrability, availability and maintainability.

As the complexity of the system architecture increases, the degrees of freedom in control increase. Advanced control strategies that use these degrees of freedom in control are required to achieve the full potential of the selected architectures. As such, many intelligent control strategies have been investigated and applied in other applications such as the automotive industry and land based micro-grids. However, advanced control strategies have only most recently been investigated and applied in maritime applications, and only reductions in fuel consumption and emissions, of 15% to 35%, have been quantified for some cases. Improvements in other criteria, such as propulsion availability, radiated noise and maintenance cost are crucial for effective hybrid power and propulsion systems as well, but have not yet been established.

In this PhD thesis, we therefore investigate how advanced control strategies for hybrid propulsion and power generation architectures can autonomously achieve the best multi-objective trade-off between the measures of effectiveness (MOEs) fuel consumption, emissions, radiated noise, propulsion availability, manoeuvrability and maintainability due to engine mechanical and thermal loading. We first perform a literature review to establish the benefits and challenges of the various architectures and their control strategies in relation to ship functions and ship types. Then, we establish a dynamic simulation model, benchmark manoeuvres and measures of performance (MOP) in order to quantify holistic system performance over the MOEs listed above. We use these MOPs to quantify the improvements with three novel control strategies and finally propose a layered control strategy that can autonomously adapt to changing ship functions, using the proposed control strategies.

The review has identified three promising control strategies that utilise the degrees of freedom provided by the controllable pitch propeller (CPP) for mechanical propulsion,

by the power split between the main engine and electric drive for hybrid propulsion, and by the power split between the diesel generator and the energy storage in hybrid power supply:

- Adaptive pitch control (APC) for diesel mechanical and hybrid propulsion with controllable pitch propellers combines the angle of attack approach for propeller pitch control (Vrijdag *et al.* 2010) with slow integrating speed control for diesel engine fuel injection;
- Parallel adaptive pitch control (PAPC) for hybrid propulsion with CPP uses a combination of slow integrating speed control for the main engines and torque control for the electric drive, both for electric motor assist and power take-off;
- A novel approach for the charge depleting Equivalent Consumption Minimisation Strategy (ECMS) for hybrid propulsion with hybrid power generation can achieve near optimum fuel consumption and can be used to generate the torque setpoint for the PAPC strategy.

In order to quantify holistic performance, we have first proposed a novel hybrid propulsion and hybrid power generation model. This model is based on a previous Mean Value First Principle (MVFP) diesel engine model that has been improved to reflect modern turbocharger and Miller-timing behaviour based on advanced diesel engine theory. The engine model has been validated with Factory Acceptance Test (FAT) measurements and predicts most parameters within 5% accuracy, including the exhaust gas receiver temperature T_{d}, which will be used to quantify engine thermal loading in combination with the air excess ratio λ and the exhaust valve temperature T_{ev}. The complete mechanical propulsion system model with CPP has been validated with the Sea Acceptance Test (SAT) measurements of the case study *Holland* class Patrol Vessel, using the existing baseline control strategy. Quantitative validation has demonstrated that the propulsion system model credibly predicts propulsion system behaviour within 5% accuracy.

Subsequently, we have proposed to use simulation experiments of three straight line manoeuvres: sailing at constant speed, slam start acceleration from 0 kts to full speed and intermediate sprints, for example from 0 to 5, 5 to 10 and 10 to 15 kts, to obtain the following specific Measures of Performance (MOP):

- Fuel consumption per mile as a function of ship speed;
- Average air excess ratio as a function of ship speed;
- Air excess ratio fluctuations due to waves as a function of ship speed;
- Acceleration time for slam start and intermediate sprint accelerations;
- Minimum air excess ratio during slam start and intermediate sprint accelerations;
- Cavitation plot for slam start and intermediate sprint accelerations.

With the proposed simulation model and MOPs, we have proposed and investigated the performance over multiple MOEs for three novel control strategies and come to the following conclusions:

- Adaptive pitch control (APC) for mechanical propulsion with CPP enables to select the optimum trade-off between cavitation risk, engine thermal loading and speed of acceleration by varying the fuel increase rate limitation R_X and the minimum air excess ratio λ_{min}, while achieving the best possible fuel consumption. For the case study patrol vessel, the adaptive pitch control strategy reduces fuel consumption by 5% to 15% compared to the baseline transit mode at ship speeds from 6 to 15 kts, and reduces acceleration time from 0 to 15 kts during slam start by 32% compared to the baseline manoeuvre mode and by 84% for an intermediate sprint from 10 to 15 kts, without thermally overloading the engine;
- Parallel adaptive pitch control (PAPC) for hybrid propulsion enables to select the trade-off between cavitation risk, engine thermal loading and speed of acceleration by varying the fuel increase rate limitation R_X and minimum air excess ratio λ_{min}, while achieving the best possible fuel consumption above 15 kts, similar to APC. Moreover, PAPC reduces acceleration time of intermediate sprints at high speed and the slam start acceleration by 50% for the case study frigate. Below 15 kts, fuel consumption can be reduced by running on the electric drive in speed control, fed from the diesel generators, thus maintaining maximum pitch and running at shaft speeds below minimum diesel engine speed. PAPC in combination with an engine with a wide operating envelope, for example due to sequential turbocharging, can enable a further fuel consumption and emission reduction of 7% and a significant reduction in running hours, at a transit speed of 18 kts for the case study frigate with sequentially turbocharged diesel engines.
- The proposed novel Equivalent Consumption Minimisation Strategy (ECMS) for hybrid propulsion with hybrid power supply can contribute significantly to cleaner shipping, particularly if the batteries are recharged from the shore grid in between missions. Simulation results demonstrate that fuel consumption and associated CO_2 emissions can be reduced by 5% to 10% for a typical operating profile, within 1-2% of the global optimum solution. The simulation results of a case study tug show that, with unknown load demand, 6% fuel savings can be achieved with ECMS, while the simple ECMS with a constant equivalence factor s is not robust against changes in the operating profile, but performs better than the existing rule based controller over all investigated operating profiles.

Finally, we have proposed a layered control strategy that can autonomously adapt to changing ship functions, using APC and PAPC in its primary control layer and ECMS in its secondary control layer, as illustrated in Figure 7.1. We have discussed how additional control objectives can be included in this control strategy and how alternative power sources, such as gas and dual fuel engines, fuel cells and ultra capacitor or flywheel energy storage can be integrated in hybrid propulsion and power supply architectures and controlled with the proposed control strategies, by changing its control objectives, weights, setting and constraints. The proposed hybrid propulsion and power generation architecture and associated control strategies can therefore contribute significantly to the urgently required reduction of the impact of shipping on the environment, while more autonomously achieving its increasingly diverse missions at sea.

SAMENVATTING

SCHEEPVAART speelt nu en in de toekomst een cruciale rol in de hedendaagse maatschappij, omdat het de wereld economie draaiende houdt, voorziet in grondstoffen, zoals fossiele brandstoffen, en de mogelijkheid biedt om duurzame energie op te wekken, zoals windenergie, energie van golven en getijde energie. Maar scheepvaart moet haar effect op de natuurlijke omgeving verminderen, aangezien schepen de meest vervuilende uitlaatgassen uitstoten van alle vormen van transport en in toenemende mate ecologisch gevoelige omgevingen verstoren met hun onderwater geluid. Tegelijkertijd vereist de diversiteit van moderne scheepvaart meer en meer manoeuvreerbaarheid, beschikbaarheid en onderhoudbaarheid van schepen en haar energie systemen, om haar functie betrouwbaarder en met minder bemanning of, in de toekomst, autonoom uit te voeren. De commerciële beschikbaarheid van vermogenselektronica en lithium-ion batterijen heeft geleid tot een exponentiële toename van de verscheidenheid en complexiteit van voortstuwing en energie-opwekking systemen. Deze verscheidenheid en complexiteit biedt een kans om hybride voortstuwing en energie-opwekking architecturen te ontwerpen die een combinatie van directe mechanische voortstuwing, elektrische voortstuwing, energie-opwekking met verbrandingsmotoren en energie-opslag gebruiken om schadelijke uitlaatgassen en onderwatergeluid te verminderen, en tegelijkertijd de manoeuvreerbaarheid, beschikbaarheid en onderhoudbaarheid te verbeteren.

Met de toename van de complexiteit van de architectuur neemt ook het aantal vrijheidsgraden voor de regeling toe. Geavanceerde regelstrategieën die meerdere vrijheidsgraden gebruiken, zijn nodig om alle mogelijkheden van dergelijke hybride architecturen te benutten. Daarom zijn veel slimme regelstrategieën onderzocht en toegepast in andere toepassingen zoals de automobiel industrie en lokale elektrische netwerken op land. Voor maritieme toepassingen worden geavanceerde regelstrategieën echter pas recent onderzocht en toegepast en alleen besparingen in brandstofverbruik en schadelijke uitstoot zijn voor enkele gevallen bepaald. Verbeteringen op andere gebieden, zoals de beschikbaarheid van de voortstuwing, uitgestraald geluid en onderhoudskosten zijn echter ook essentieel voor effectieve hybride energie systemen, maar zijn nog niet vastgesteld.

In dit proefschrift onderzoeken we daarom hoe geavanceerde regelstrategieën voor hybride voortstuwing en energie architecturen autonoom de beste mogelijke prestaties kunnen bereiken voor de effectiviteit-indicatoren brandstofverbruik, uitstoot, uitgestraald geluid, beschikbaarheid van voortstuwing, manoeuvreerbaarheid en onderhoudbaarheid als gevolg van thermische belasting. We hebben eerst een literatuuronderzoek uitgevoerd om de voordelen en uitdagingen van de verschillende architecturen en regelstrategieën in kaart te brengen in relatie tot de scheepsfunctie en het type schip. Vervolgens hebben we een dynamisch simulatiemodel bepaald, met referentie manoeuvres en prestatie indicatoren om de algehele effectiviteit van het systeem over de gekozen

indicatoren te bepalen. We hebben deze prestatie indicatoren gebruikt om de verbeteringen met drie nieuwe regelstrategieën te kwantificeren en hebben uiteindelijk een gelaagde regelstrategie voorgesteld die zich autonoom aanpast aan een veranderende scheepsfunctie, met behulp van de drie voorgestelde regelstrategieën:

- De adaptieve schroefspoed regeling voor diesel mechanische en hybride voortstuwing met verstelbare schroef combineert de aanstroom-hoek aanpak voor de schroefspoed regeling (Vrijdag e.a., 2010) met langzaam integrerende toerenregeling voor de brandstofinspuiting van de dieselmotor;
- De parallelle adaptieve schroefspoed regeling voor hybride voortstuwing met verstelbare schroef benut een combinatie van langzaam integrerende toerenregeling voor de hoofdmotoren met koppelregeling voor de elektromotor, zowel tijdens elektrische ondersteuning als elektrische levering van energie aan het scheepsnet;
- Een nieuwe aanpak voor ontladende gelijkwaardig verbruik minimalisatie strategie voor hybride voortstuwing met hybride energie opwekking kan een bijna optimaal brandstofverbruik bereiken en kan gebruikt worden om het gewenste koppel voor de parallelle adaptieve schroefspoed regeling te bepalen.

Om de effectiviteit van hybride energie systemen te kwantificeren, hebben we eerst een nieuw hybride voortstuwings- en energie-opwekkingsmodel voorgesteld. Dit model is gebaseerd op een eerder gemiddelde-waarde fysisch dieselmotor model die verbeterd is om moderne turbine gedreven compressoren en Miller-timing te beschrijven, gebaseerd op geavanceerde dieselmotor theorie. Het dieselmotor model is gevalideerd met fabriek acceptatie testen en voorspelt de meeste parameters met een nauwkeurigheid van +/-5%, inclusief de temperatuur in het uitlaatgassen kanaal voor de turbo T_{d}, die we gebruiken om de thermische belasting van de motor te kwantificeren in combinatie met de luchtovermaat λ en de uitlaatklep temperatuur T_{ev}. Het complete model van mechanische voortstuwing met verstelbare schroef is gevalideerd met varende beproevingen van de praktijkstudie met een *Holland* klasse patrouilleschip, die gebruikt maakt van een conventionele regelstrategie. De validatie heeft aangetoond dat het model het gedrag van de voortstuwing met een nauwkeurigheid van +/-5% voorspelt.

Vervolgens hebben we simulatie experimenten van drie manoeuvres in rechte lijn voorgesteld: varen met constante snelheid, maximale acceleratie van 0 knopen naar maximale snelheid en tussensprints, bijvoorbeeld van 0 to 5, 5 tot 10, en 10 tot 15 knopen, om de volgende prestatie indicatoren vast te stellen:

- Brandstofverbruik per mijl als een functie van de scheepssnelheid;
- Gemiddelde luchtovermaat als een functie van de scheepssnelheid;
- Luchtovermaat schommelingen door golven als een functie van de scheepssnelheid;
- Acceleratietijd voor maximale acceleratie en tussensprints;
- Laagste luchtovermaat tijdens maximale acceleratie en tussensprints;
- Cavitatie plot voor maximale acceleratie en tussensprints.

Met het voorgestelde simulatie model en de prestatie indicatoren, hebben we de effectiviteit voor meerdere criteria onderzocht voor de drie nieuwe regelstrategieën en komen we tot de volgende conclusies:

- De adaptieve schroefspoed regeling voor mechanische voortstuwing met verstelbare schroef maakt het mogelijk om de optimale keuze te maken tussen het risico op cavitatie, thermische belasting van de dieselmotor en acceleratiesnelheid door de maximale toename van brandstofinspuiting R_X en de minimale luchtovermaat λ_{min} te variëren, terwijl de regeling het laagst mogelijke brandstofverbruik realiseert. Voor de praktijkstudie met het patrouilleschip kan de adaptieve schroefspoed regeling het brandstofverbruik en de gerelateerde uitstoot met 5% tot 15% verminderen in vergelijking met de conventionele transit regelstrategie, op scheepssnelheden tussen 6 en 15 knopen, en verkort de acceleratietijd van 0 tot 15 knopen tijdens maximale acceleratie met 32% vergeleken met de conventionele manoeuvreer regelstrategie en met 84% voor tussensprints van 10 tot 15 knopen, zonder de motor thermisch over te belasten;
- De parallelle adaptieve schroefspoed regeling voor hybride voortstuwing maakt het mogelijk om de optimale keuze te maken tussen het risico op cavitatie, thermische overbelasting en acceleratiesnelheid door de maximale toename van de brandstofinspuiting R_X en de minimale luchtovermaat λ_{min} te variëren, terwijl de regeling het laagst mogelijke brandstofverbruik realiseert, vergelijkbaar met de adaptieve schroefspoedregeling. Veder verkort de parallelle adaptieve schroefspoedregeling de acceleratietijd van tussensprints bij hoge snelheid en de maximale acceleratie met 50% voor de praktijkstudie met een fregat. Tot 15 knopen kan de regeling brandstof besparen door met een toerenregeling op de elektromotor te varen, gevoed vanuit de diesel generatoren, en zo de maximale schroefspoed te handhaven met een astoerental lager dan het minimum toerental van de dieselmotor. De parallelle adaptieve schroefspoed regeling kan in combinatie met een motor met een groot operatiebereik, bijvoorbeeld door sequentiële drukvulling, brandstofverbruik en emissies verder beperken met 7% en draaiuren van de dieselgeneratoren beperken door de elektrische energie te voorzien vanuit de elektromotor, bij een economische snelheid van 18 knopen voor de praktijkstudie met een fregat met sequentiële drukvulling op de dieselmotoren.
- De voorgestelde gelijkwaardig verbruik minimalisatie strategie voor hybride voortstuwing met hybride energie opwekking kan aanzienlijk bijdragen aan schonere scheepvaart, met name als de batterijen herladen worden van een walvoorziening tussen missies. Resultaten van simulaties laten zien dat brandstofverbruik en de gerelateerde CO_2 uitstoot met 5% tot 10% verminderd kan worden voor een typisch operatieprofiel van een sleepboot, binnen 1-2% van de globaal optimale oplossing. De simulatieresultaten van een praktijkstudie met een sleepboot laten verder zien dat, met een onbekende belasting, 6% brandstof kan worden bespaard met deze regeling, alhoewel een eenvoudige gelijkwaardig verbruik minimalisatie strategie met een constante evenwaardigheidsfactor s niet robuust is voor veranderingen in het operatieprofiel, maar wel beter presteert dan de bestaande regeling op basis van heuristiek voor alle onderzochte operatieprofielen.

Tenslotte hebben we een gelaagde regelstrategie voorgesteld die zich autonoom aanpast aan een veranderende scheepsfunctie, met behulp van de parallelle adaptieve schroefspoed regeling op het eerste niveau van de regeling en de gelijkwaardig verbruik minimalisatie strategie op het tweede regelniveau, zoals getoond in Figuur 7.1. We hebben besproken hoe aanvullende regeldoelen kunnen worden meegenomen in deze gelaagde regelstrategie, en hoe alternatieve vermogensbronnen, zoals gas- en gecombineerde brandstof motoren, brandstofcellen, ultra condensatoren en vliegwiel energie opslag geïntegreerd kunnen worden in hybride voortstuwing en energie architecturen en met de voorgestelde strategieën kunnen worden geregeld, door de regeldoelen, gewichten, instellingen en randvoorwaarden aan te passen. De voorgestelde hybride energie architecturen kunnen daarmee aanzienlijk bijdragen aan de zeer noodzakelijke vermindering van de invloed van scheepvaart op de omgeving, terwijl die scheepvaart zelfstandiger haar in toenemende mate diverse missies op zee kan uitvoeren.

PREFACE

FOUR years ago, I embarked at Delft University of Technology to start one of the most inspiring, rewarding and eye-opening journeys of my life. The Royal Netherlands Navy gave me the trust and opportunity to immerse myself into a world of fresh ideas, endless inspiration and novel and refreshing views; views on engineering and technology, but also views on life and politics. While I expected to become more certain about the engineering choices the Navy and society in general have to make, the journey has made me realise that there is so much more to learn, for me, for my academic friends and for mankind. However, I also believe that ever growing science can provide us with so many more opportunities. Opportunities to take better care of the world, provide access to wealth and happiness for more people and create a sustainable and more peaceful world for our children and future generations. Many people have made it possible for me to embark on this journey, sail though it while staying afloat, and arrive in the final port successfully, with this dissertation as a result. I would like to thank everyone and spend some words on some of them here.

First and foremost, I would like to thank my family, Coby, Jelmer and Lienke, for sailing this journey with me. In particular, the first two years were choppy, with me trying to catch up with my academic skills that had been underused for 15 years. In those years, I spent quite some weekends trying to catch up with my linear algebra, mathematics and control theory, sometimes with guidance to useful online courses from my first paranymph Ivo Marx. Also my mind was regularly distracted with thoughts about the direction of my research, at moments I should really have focused on family life. Later years became easier with following seas, sometimes with higher sea-states when deadlines arrived. I am very thankful that Coby was always there to draw me back into family life and keep track of my priorities. In particular, the holidays and the weekend walks on the beach, in the dunes and in the woods around Alkmaar with her, Jelmer, Lienke and our dog Shailo were good to re-energise and give air to the mind.

Equally important has been the support of my wider family during these four years and life before my PhD. First of all, I would like to thank my mum, Nynke Geertsma, for her support throughout my life and for looking after the kids, for example during various conference trips. But also my brothers, Henk en Frans with their families, my parents-in-law, Leen en Nel van Tilburg, and all brothers- and sisters-in-law with their families have always been a great support. I am very thankful for the nice and inclusive bond we have with our families and look forward to celebrate the defence ceremony with all of you. I would also like to make a special mention to my dad, Durk Geertsma, who unfortunately has not made it to be part of this journey. I know he would have been very proud of me reaching this point and I would like to acknowledge that the basis for my academic career was laid down in the three primary school years that he was my teacher. I also believe the circle is complete now, as the teacher in me has now finally appeared during the courses I have given, with the BKO qualification as a result. Finally, I believe

he would have thoroughly enjoyed the Defence Ceremony and he will be with me in my thoughts.

During my 20-year-career in the Royal Netherlands Navy, I have experienced endless opportunities to develop myself into an experienced engineer and leader. These opportunities range from studying for an MSc. in Marine Engineering at University College London in 1998, through bearing technical responsibility and leading experienced engineers at a very young age, to working with inspiring leaders within the United Kingdom and Netherlands Ministries of Defence. While I have always strived to contribute to the development of naval engineering and contributed with various IMarEST and IEEE conference papers, I am extremely grateful for the opportunity to read for a PhD at Delft University of Technology in full-time employment of the Navy. In particular, I would like to thank Rear-Admiral (ME, ret) ir. Klaas Visser and Vice-Admiral dr. ir. Arie-Jan de Waard for creating this opportunity for me and for the Navy, while Rear-Admiral (ME, ret) ir. Klaas Visser has also been an inspiring supervisor and room-mate during the four years at Delft University of Technology. I truly believe these four years at Delft University of Technology have enabled me to contribute more fundamentally to the development of marine and naval engineering and I am looking forward to make a difference in the Defence Materiel Organisation, as the associate editor of the Journal of Marine Engineering and Technology, and as a chairman of the international Ship Control Systems Symposium, thanks to the opportunities the Royal Netherlands Navy has given me.

The most important lesson that I have learned during these four years is that the progress of science can only be achieved by many researchers contributing tiny steps. Maybe the greatest contribution of Isaac Newton was the realisation that even the greatest scientists can only see further 'by standing on the shoulders of giants'. I feel I also have been standing on the shoulders of many giants. For the complete list of my giants, I can refer to the References section. However, I would like to refer to some of my giants specifically. First of all, I would like to thank my supervision team. Prof. ir. Hans Hopman has been strong from the start in concisely defining the problem. Prof. dr. Rudy Negenborn has been the perfect scientific role model. He always provided excellent feedback on my written work impressively fast, was supportively critical when I took on extra work that distracted from research and always kept me focussed to deliver on journal publications and my final dissertation. On the other side, ir. Klaas Visser has been an enormous motivation throughout the four years. First of all, he was always the first to emphasise on the achievements, such as good presentations, contributions to projects and publications, but also on contributions outside my research, such as organising the international Ship Control System Symposium. Secondly, he always recognised opportunities for application of research results in new research proposals or development projects with industry. And, finally, his busy diary kept reminding me, what a privilege it was to have four years to focus on one research subject.

Apart from my direct supervision team, the ideas from, discussions with and previous work by the Marine Engineering Group has contributed enormously to my work. First of all, many of my modelling and control ideas build on earlier work from the Marine Engineering group performed by prof. ir. Douwe Stapersma, late dr. ir. Hugo Grimmelius dr. ir. Paul Schulten, dr. ir. Peter de Vos, dr. ir. Milinko Godjevac and dr. ir. Arthur Vrijdag. In particular, the angle of attack control strategy proposed in the disser-

tation of dr. ir. Arthur Vrijdag has turned out a very important building block for my work. Secondly, the colleagues of the ShipDrive and GasDrive research programmes, Ioana Georgescu, Ali Haseltalab, Lindert van Biert and Harsh Sapra, have stimulated me to publish at a high level and to work together in raising the profile of our group. Equally important, I have really enjoyed the drinks and dinners that were often organised spontaneously with the PhD candidates of Maritime and Transport Technology and the many discussions we had about research, the culture in the scientific world, life and politics.

While the atmosphere at Delft University of Technology has always been very inspiring, my research has built equally on work from other universities and researchers. I have developed an enormous respect for academics across the world, as academia turns out to be a very competitive and demanding environment. Academics need to teach and inspire the next generation, they need to perform research at the highest level and they need to engage with industry and other researchers to gain funding for their research. I am therefore also very grateful for the international network that I established over the past four years, with excellent researchers from all over the world. In particular, I would like to thank the international Ship Control Systems Symposium technical subcommittee, and in particular Michele Martelli, for the excellent cooperation in preparing the international Ship Control Systems Symposium 2018, and the colleagues in the MOSES steering committee, in particular Francesco Baldi and Gerasimos Theotokatos for involving me. Moreover, I really enjoyed working together on a joint paper with Andrea Corraddu, Luca Oneto, Gert-Jan Meijn and Miltiades Kalikatzarakis. I truly hope these international coöperations will continue and many more will follow.

While my research obviously has had a strong input from academia, which can clearly be identified in the References, another important compass to sail on was the ShipDrive user committee. The practical discussions during the user committee meeting, the extensive information of the state-of-the-art of current products and the extensive information the user committee provided for the case studies has been of crucial importance to demonstrate the applicability of my research and therefor to get it published in high impact journals. I would like to thank the Royal Netherlands Navy, the Defence Material Organisation, Damen Schelde Naval Shipbuilding, Damen Shipyards Gorinchem, Royal IHC, CroonWolter&Dros, HYPS and RH Marine, and in particular all their experts that joined the user group meetings or hosted me for various technical meetings, for their excellent contribution and for providing practical case studies.

An important part of working at Delft University of Technology and at the Netherlands Defence Academy is teaching, of course. I truly enjoyed this part of the work. A large part of my teaching activity consisted of supervising Bachelor and Masters students graduation projects, both at Delft University of Technology and the Netherlands Defence Academy. The work of the students and the discussions I had with them have contributed to the development of my research. Therefore, I would like to thank Ruben de Jong, Irene Rollema, Roeland Schillings, Casper Volger, Hugo Engelbrecht, Niels Jacobsen, Katelijne van Houten, Jesse van Zwol, Perry Eeuwijk, ir. Jasper Vollbrandt, ir. Miltiadis Kalikatzarakis and ir. Joris Rusman for the effort they put into their graduation projects and for contributing to my research with their research findings. Moreover, I am particularly proud that the work of all three MSc. students, Jasper, Miltiades and Joris,

has led to a publication, while the work of my second paranymph, Miltiadis, has led to a journal publication, which forms the main part of Chapter 6 of my dissertation.

In summary, I have thoroughly enjoyed my four years in the academic world and have met so many new inspiring colleagues and friends. I have grown an enormous respect for my academic friends and I hope to stay in touch with many of you and to keep contributing to research in marine and naval engineering alongside my responsibilities in the Navy. I truly believe that good cooperation between academia, industry and the Navy will lead to ships with less impact on our environment and better performance to deliver safety from sea, as such contributing to a sustainable and more peaceful world for our children and future generations.

Rinze Dirk Geertsma
Alkmaar, November 2018

1

INTRODUCTION

The world of system integration faces many challenges: the expanding range of propulsion alternatives due to electric drives, the expanding range of power sources due to fuel cell and battery technology, the choice between alternating or direct current (AC or DC) electrical distribution, the integration of multiple functions and objectives in one design, and the development of control strategies over multiple control layers, such as the functional, system and component layers. The ShipDrive project aims to develop the necessary methodologies to solve these challenges and has the following main objectives:

- *to define a fundamental design and optimisation methodology for integrating hybrid ship design installations; and*
- *to define control strategies, based on functional criteria, for hybrid systems on several control layers.*

This PhD thesis is part of the ShipDrive project and, first, aims to develop a methodology to quantify improvements over multiple objectives due to applying hybrid propulsion and power generation architectures, and, second, aims to propose novel control strategies that can autonomously adapt to various ship functions. While the candidate architectures in this thesis were established through a literature review, the ShipDrive work of Ioana Georgescu aims to develop a quantitative methodology to compare, select and size various propulsion and power supply architectures during the early stage ship design. Moreover, the ShipDrive work of Ali Haseltalab aims to develop advanced control strategies for DC electrical distribution, as opposed to AC distribution in this thesis. Combined, these three research directions will address the complete ShipDrive scope as summarised above.

This chapter introduces the research in this PhD thesis, and is organised as follows: First, the motivation is covered in Section 1.1, before introducing its objectives in Section 1.2. Then, Section 1.3 and 1.4 define the propulsion and power generation architectures and control strategies that will be addressed. Subsequently, Section 1.5 describes the problem statement and research questions, followed by the proposed approach in Section 1.6, the outline and structure of the thesis in Section 1.7 and its scientific contributions in Section 1.8.

1

1.1. MOTIVATION

THE United Nations emissions gap report UN, (2017) identifies an urgent need to reduce CO_2 emissions across the globe to meet the goals of the Paris Agreement. Therefore, the 72nd Marine Environmental Protection Committee meeting of the International Maritime Organisation (IMO) agreed to 'reduce total annual global shipping emissions by 50% over 2008 by 2050', in its *initial strategy on greenhouse gas emissions reduction for ships* (IMO MEPC 72, 2018). While improved planning of vessel operations (Li *et al.* 2017a,b), either with manned or autonomous vessels (H. Zheng *et al.* 2017a,b), and improved route planning (L. Chen *et al.* 2017; Liu *et al.* 2017a,b), taking into account weather conditions (Perera *et al.* 2017; Vettor *et al.* 2016; Zaccone *et al.* 2017, 2018) can all help reduce emissions, single ships also need to reduce emissions for a given operating profile. Economic studies suggest that, in shipping, the transition to alternative fuels, such as LNG, bio-methanol or synthetic fuels, will be gradual, and that diesel, dual fuel and gas engines will continue to provide most propulsion and electric power over the next decades (Taljegard *et al.* 2014). Therefore, increasing efficiency of propulsion and electrical power supply with diesel engines, using these fuels, is even more important.

According to estimates in the UN emission gap report, shipping can contribute 0.7 $GtCO_2$ emission reduction by increasing its efficiency (UN, 2017). While the savings potential of most individual design aspects, such as waste heat recovery (Benvenuto *et al.* 2014; Cignitti *et al.* 2017; De La Fuente *et al.* 2015; Mondejar *et al.* 2017; Shu *et al.* 2013), hull coatings and lubrications, and hull design have been quantified in Brynolf *et al.* (2016) and Schulten *et al.* (2017), efficiency improvements of the complete propulsion chain, from tank to propeller, and the interactions between the engine, propeller and hull can also be significant, but have not yet been studied systematically. Therefore, a detailed study of various propulsion architectures, including their control strategy is required to quantify how much efficiency can be gained in the complete propulsion chain.

While the pressure to reduce fuel consumption and emissions has increased, the operating profile of multifunction ships has become increasingly diverse: offshore and windfarm construction vessels perform numerous tasks, such as transit and critical dynamic positioning (DP) operations (Barcellos, 2013; MER, 2008); heavy crane vessels, such as the *Pioneering Spirit*, exhibit an increased capacity and complexity for diverse offshore operations (Ovrum *et al.* 2015); naval ships perform traditional patrol operations in open sea, but are also deployed in littoral operations; and tugs require full bollard pull when towing and require limited power during transit or standby (Boonen, 2016; de Groote *et al.* 2014; Volker, 2013). Moreover, the shipping industry is pushing towards reduced crews, more autonomous systems, remote control and autonomous shipping (Burmeister *et al.* 2014; Kretschmann *et al.* 2017; Wrobel *et al.* 2017). Therefore, when studying efficiency improvements for propulsion and electrical power supply, the impact on holistic ship performance and aspects such as manoeuvrability, propulsion availability and maintainability also need to be considered.

1.2. MEASURES OF EFFECTIVENESS

IN this PhD thesis, we aim to compare propulsion and power supply architectures and control strategies over various measures of succes to achieve its operational objec-

Figure 1.1: HNLMS Rotterdam with electric propulsion.

tives, including reducing its environmental impact. We use the term measures of effectiveness (MOE) from system engineering to refer to these high levels measures of succes (Roedler *et al.* 2005). While literature is available on the potential reduction of fuel consumption and emissions of specific propulsion and power supply architectures, most literature does not consider the impact on other MOEs. However, to support the trends towards more demanding operating profiles, reduced maintenance and remote or autonomous shipping, while reducing the environmental impact, the trade-off between various MOEs needs to be considered. Therefore, in this thesis, we consider all MOEs that are primarily affected by the propulsion and power generation architecture and its control:

1. fuel consumption;
2. emissions;
3. radiated noise;
4. propulsion availability;
5. manoeuvrability; and
6. maintainability due to engine mechanical and thermal loading.

Chapter 3 will define Measures of Performance (MOP) to quantify these MOEs. These MOPs quantify physical attributes during system operation in specified operational conditions, as defined for system engineering (Roedler *et al.* 2005).

1.3. PROPULSION AND POWER GENERATION ARCHITECTURES

THE commercial availability of power electronic converters has led to an exponential increase in the variety and complexity of propulsion and power generation architectures, starting with the introduction of electric propulsion in the 1990s for various

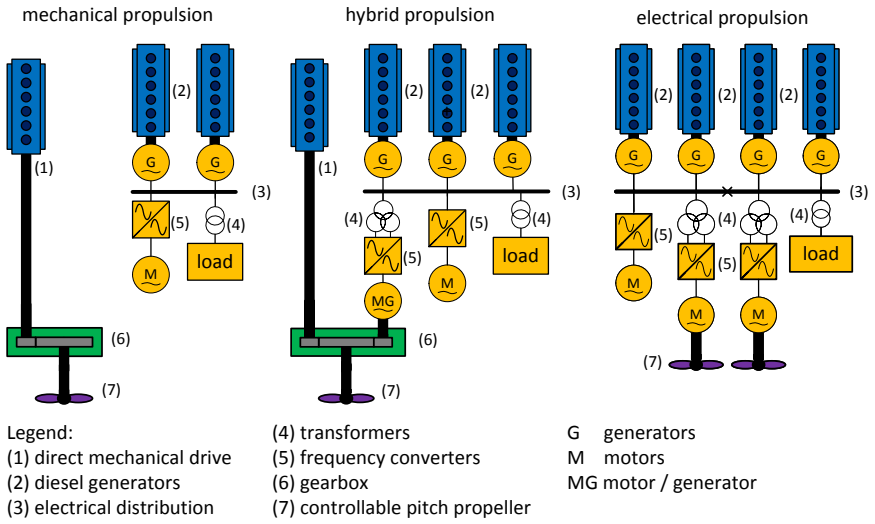

Figure 1.2: Schematic representation of propulsion architecture qualification, from Geertsma *et al.* (2017a).

ship types, such as cruise ships and capital naval ships, like *HNLMS Rotterdam* shown in Figure 1.1. While electrical propulsion is more efficient at low speed, it introduces additional conversion losses of 5% to 15% of the propulsive power in electrical components such as generators, power converters, transformers and electric motors. Therefore, full electric propulsion seems only viable for ships that have an auxiliary electrical load of a similar magnitude as the propulsion load. When the auxiliary load is only a fraction of the required propulsive power for full speed and the ship also sails at low speeds a significant amount of time, then a combination of mechanical propulsion for high speed and electrical propulsion for low speeds, classified as hybrid propulsion in this thesis, provides advantages of both architectures. Thus, hybrid propulsion has been applied to many ship types recently. Summarising, the propulsion architectures for ships can be classified into the following categories, as illustrated in Figure 1.2.:

- mechanical propulsion: propulsion provided by one or more combustion engines connected to a propulsor either directly or through a gearbox;
- electrical propulsion: propulsion provided by one or more electric motors connected to a propulsor either directly or through a gearbox;
- hybrid propulsion: propulsion provided by a combination of one or more combustion engines and electric machines connected to a propulsor.

For mechanical, electrical and hybrid propulsion, until recently, diesel engines have provided most power, while some applications that require high power density have used gas turbines as an alternative combustion power supply. The development of power dense lithium-ion battery technologies for the automotive industry can provide power and energy dense energy storage with good life cycle performance (Capasso *et al.* 2014), thus enabling electrical vehicles (EV) and hybrid electrical vehicles (HEV) for automotive

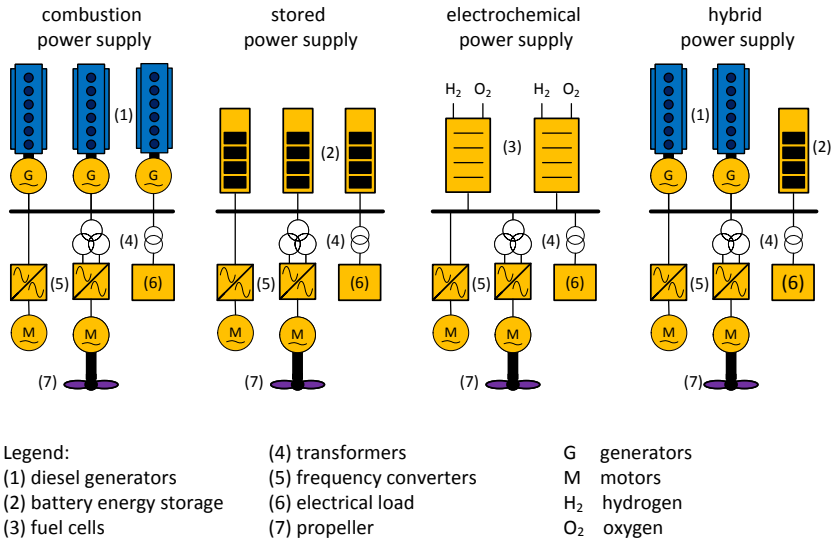

Figure 1.3: Schematic representation of power generation architecture qualification, from Geertsma *et al.* (2017a).

applications. These battery technologies have also enabled the use of energy storage on board ships, initially in combination with combustion power supply from diesel engines, later as the only power source on board short range vessels, such as ferries. Similarly, fuel cells have been applied in some niche maritime applications, such as submarines (Psoma *et al.* 2002; Sattler, 2000; van Biert *et al.* 2016). Thus, the power generation architectures can be classified in:

- combustion power supply: power supply from combustion engines only;
- electrochemical power supply: power supply from electrochemical sources, such as fuel cells, only;
- stored power supply: power supply from energy storage, such as batteries, flywheel or ultra capacitors only; and
- hybrid power supply: power supply from a combination of two or more types of power supply as listed above.

These architectures are illustrated in Figure 1.3 and can utilise either Alternating Current (AC), as primarily considered in this thesis, or Direct Current (DC) distribution systems, as considered in the various works of Haseltalab et al. (Haseltalab *et al.* 2017a,b, 2016), or a hybrid combination. The variety and complexity of all possible combinations with the propulsion and power generation architectures above provides an opportunity to design hybrid propulsion and power supply architectures that reduce emissions and noise as well as improve manoeuvrability, availability and maintainability.

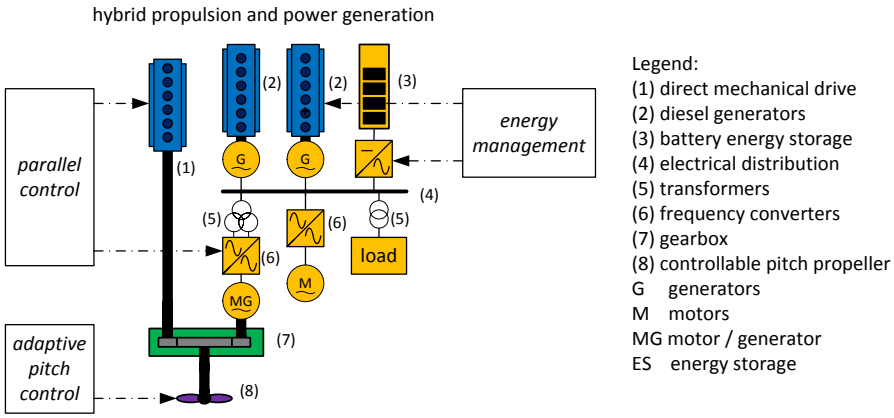

Figure 1.4: Schematic representation of the degrees of freedom in control and the associated control strategies.

1.4. CONTROL STRATEGIES

MODERN control strategies for hybrid propulsion and power generation architectures provide additional degrees of freedom in control to improve system effectiveness for various MOEs and influence the trade-off between these MOEs. First, mechanical propulsion with Controllable Pitch Propellers (CPPs) can utilise pitch control to adapt the working point of the propeller and diesel engine, thus influencing fuel consumption, emissions, cavitation noise and engine thermal loading. Secondly, hybrid propulsion can vary the power split between the electric drive and the propulsion diesel engine with parallel control, when both are driving the propeller. Thus, the operating point of the propulsion diesel engine and the electric drive can be adapted, influencing fuel consumption, emissions, engine thermal loading and loading of the electric drive and the power generation system. Finally, hybrid power generation can vary the power split between the diesel generators and the energy storage system with energy management, thus influencing the fuel consumption and emissions of the diesel generators, the loading of the battery and the energy storage and its state of charge. These degrees of freedom in control, which can ultimately be combined for hybrid propulsion with CPP and hybrid power generation, are illustrated in Figure 1.4.

Advanced control strategies that use these degrees of freedom in control are required to achieve the full potential of the selected architectures. As such, many intelligent control strategies have been investigated and applied in other applications such as the automotive industry and land based micro-grids. However, advanced control strategies have only most recently been investigated and applied in maritime applications, and only reductions in fuel consumption and emissions, of 15% to 35%, have been quantified for some cases. While improvements in other criteria, such as propulsion availability, radiated noise and maintenance cost are crucial for effective hybrid power and propulsion systems as well, the holistic performance of these advanced control strategies over all MOEs identified in Section 1.2 needs to be investigated.

1.5. PROBLEM STATEMENT AND RESEARCH QUESTIONS

Holistic system performance can be influenced significantly due to the increasing complexity of propulsion and power generation architectures and the additional degrees of freedom in control from CPPs, electric drives and energy storage. While some of the MOEs listed in Section 1.2, such as manoeuvrability, radiated noise and thermal loading, depend on the dynamic behaviour of the various subsystems and their interaction, system analysis with dynamic simulation models is required. These simulation models need to include the control strategy as it strongly influences the operating point of the various subsystems. Subsequently, the simulation models can be used to develop and compare advanced control strategies, that use the additional degrees of freedom in control to realise the best possible trade-off between the MOE listed in Section 1.2 for the ships mission. Thus, the following problem statement is answered in this dissertation:

> *How can advanced control strategies for hybrid propulsion and power generation architectures autonomously achieve the best multi-objective trade-off for diverse ship operations?*

This problem statement leads to the following research questions, first on the quantification of propulsion and power generation architectures and controls strategies:

1. Which candidate propulsion and power generation architectures are suitable for which ship type and which combination of ship functions?
2. What candidate control strategies can be identified to improve on the MOEs fuel consumption, emissions, radiated noise, propulsion availability, manoeuvrability and maintainability due to engine mechanical and thermal loading?
3. What simulation model can be used to quantify MOEs fuel consumption, emissions, radiated noise, propulsion availability, manoeuvrability and maintainability due to engine mechanical and thermal loading?
4. What benchmark manoeuvres and Measures of Performance (MOP) can quantify the MOEs listed above?

then on control strategies:

5. What control strategy can be used for controllable pitch propellers to provide the best possible performance against an adaptive trade-off between the various conflicting MOEs listed in Section 1.2?
6. What control strategy can be used for the power split between the propulsion engine and electric drive in hybrid propulsion to provide the best possible performance against an adaptive trade-off between the various conflicting MOEs?
7. What control strategy can be used for the power split between various power sources in hybrid power supply to provide the best possible performance against an adaptive trade-off between the various conflicting MOEs?

and, finally, on adaptation of the control strategy to changing ship functions:

8. How can the performance trade-off between the various MOEs be autonomously adapted for changing ship functions?

1

1.6. PROPOSED APPROACH

THIS PhD thesis first aims to propose a methodology to quantify performance improvements in fuel consumption, emissions, radiated noise, propulsion availability, manoeuvrability and maintainability due to applying hybrid propulsion and power generation architectures with autonomous control strategies for adaptive ships, and, second, aims to propose novel control strategies that can autonomously adapt to various ship functions. In order to establish candidate architectures for various ship types and answer Research Question 1, in this thesis, we use a literature review and a qualitative analysis to identify the benefits and challenges of the various propulsion and power generation architectures and establish which architectures are expected to be promising for which ship type, now and in the future, and we obtain general trends about which operating profile and power split between propulsion and electrical loads leads to which candidate architectures for certain ship types, functions and operations. This review can be further supported by a more quantitative approach, in which performance of various propulsion and power generation architectures is captured in mathematical models, as proposed in the ShipDrive studies from Georgescu et al. (Georgescu *et al.* 2015, 2018, 2017, 2016). In order to establish the candidate control architectures and answer Research Question 2, we also use a literature review. We particularly focus on how we can use the additional degrees of freedom in control that the controllable pitch propeller, hybrid propulsion and hybrid power supply provide and review developments in maritime as well as automotive and microgrid research fields. Subsequently, dynamic simulation models are required to quantify the MOPs of the chosen candidate architectures and control strategies.

While existing simulation models either require too much detailed calibration information or require too much simulation time for whole ship system performance analysis, we propose a novel hybrid propulsion and power generation system model and validate the model with measurements performed during the Factory Acceptance Test of the diesel engine and during the Sea Acceptance Test of the case study Patrol Vessel, thus answering Research Question 3. For the validation of the model, we use its two transit and manoeuvre control strategies as a baseline. Subsequently, the proposed model can be used to quantify MOEs fuel consumption, emissions, radiated noise, propulsion availability, manoeuvrability and maintainability. In order to quantify these MOEs and answer Research Question 4, we propose benchmark manoeuvres to establish consistent MOPs to compare various propulsion and power generation architectures and their control strategies.

Depending on the candidate propulsion and power generation architectures, the control strategy can use the additional degrees of freedom: propeller pitch, power split between the main engine and electric drive and the power split between the diesel generator and the energy storage. The three proposed tertiary control strategies utilising these degrees of freedom in control are adaptive pitch control to answer Research Question 5, parallel control for hybrid propulsion to answer Research Question 6 and an energy management strategy based on Equivalent Consumption Minimisation Strategy (ECMS) for hybrid power generation to answer Research Question 7. These primary and secondary control strategies can subsequently be adapted to various ship functions with a functional control layer as illustrated in Figure 1.5 to answer Research Question 8. The

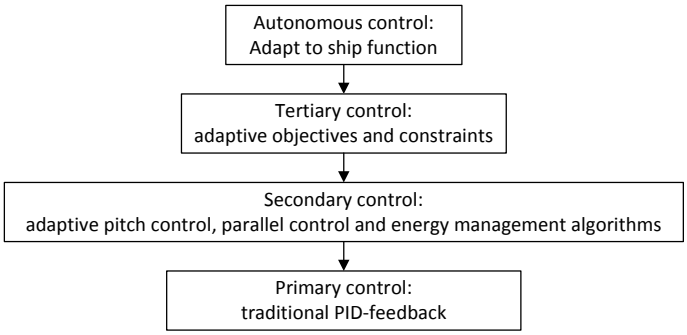

Figure 1.5: Schematic representation of the structure of autonomous control for adaptive ships.

schematic representation of the proposed methodology and the reading guide for this thesis are illustrated in Figure 1.6.

1.7. THESIS OUTLINE

THE PhD thesis is organised as follows, as illustrated in Figure 1.6:

- In **Chapter 2** propulsion and power generation topologies are reviewed. A novel classification in mechanical, electrical and hybrid propulsion and combustion, electrochemical, stored and hybrid power supply is proposed. Subsequently, the benefits and challenges of the various combinations of propulsion and power supply topologies for various ship functions and their expected future application are discussed and the applicable control strategies and their potential performance improvement are reviewed. Finally, the chapter proposes the following control strategies for further consideration in this thesis: adaptive pitch control; parallel control of the propulsion diesel engine and the electric drive for hybrid propulsion; and advanced energy management strategies for hybrid power generation.
- In **Chapter 3** a novel dynamic mean value propulsion system model is proposed. After the introduction and validation of the model, benchmark manoeuvres and Measures of Performance (MOP) are proposed to quantify fuel consumption, rate of acceleration, engine thermal loading and propeller cavitation, in order to evaluate performance improvements of conventional and advanced control strategies, and compare propulsion architectures against predefined MOPs.
- In **Chapter 4** a novel adaptive pitch control strategy for diesel mechanical and hybrid propulsion with controllable pitch propellers is proposed, which combines the angle of attack approach for propeller pitch control (Vrijdag *et al.* 2010) with slow integrating speed control for diesel engine fuel injection. The benchmark manoeuvres are performed to establish the improvements of the proposed MOPs with the novel control strategy compared with the baseline combinator curve control strategy for a case study patrol vessel.
- In **Chapter 5** a novel parallel control strategy is proposed for hybrid propulsion with fixed or controllable pitch propellers, which combines the adaptive pitch

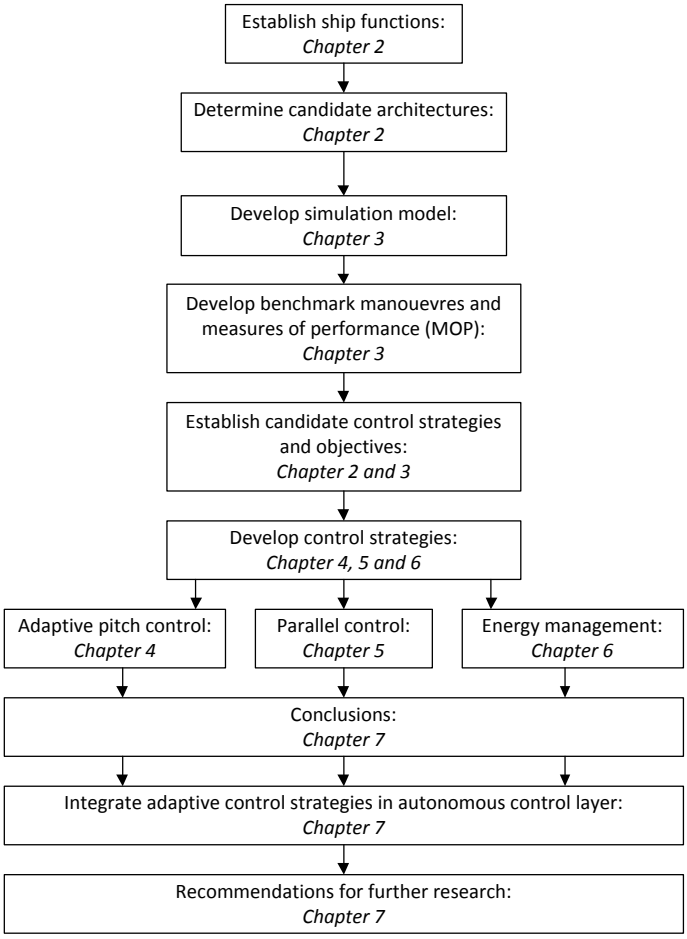

Figure 1.6: Schematic representation of the methodology proposed in this thesis and reading guide.

control strategy with torque control for the electric drive. The benchmark manoeuvres are performed to establish the improvements of the proposed MOPs with the novel control strategy compared with a number of alternative baseline control strategies for a case study frigate.

- In **Chapter 6** a novel energy management strategy is proposed for hybrid propulsion and hybrid power supply. This strategy aims to determine the optimal power-split between three or more different power sources, in real-time, and to optimally deplete the battery packs over the mission profile. To this end, a Mixed-Integer Non-Linear optimisation Problem is formulated and solved by combining Branch & Bound and Convex optimisation. In a simulation study of a case study tug, the fuel consumption of two novel energy management strategies are compared with the global optimum fuel consumption established with Dynamic Programming

(DP), assuming apriori knowledge of the operating profile and with the fuel consumption for a simple rule-based (RB) controller.

- **Chapter 7** summarises the conclusions and proposes the concept and design structure for autonomous control that can adapt the control system performance to changing ship functions and discusses the relation of the proposed autonomous control structure to the proposed control strategies: adaptive pitch control, parallel control for hybrid propulsion and energy management for hybrid power supply. Finally, recommendations for further research are dicussed.

1.8. CONTRIBUTIONS

THE main contributions of this dissertation with respect to understanding the performance trade-off for hybrid power and propulsion system topologies and their control strategies are as follows:

- a survey of the development and application of hybrid power and propulsion architectures and their control strategies for ships in **Chapter 2** and published in Geertsma *et al.* (2017a);
- classification of the propulsion topology into mechanical propulsion, electrical propulsion and hybrid propulsion in **Chapter 2** and published in Geertsma *et al.* (2017a);
- classification of the power system topology in combustion power supply, electrochemical power supply, stored power supply and hybrid power supply in **Chapter 2** and published in Geertsma *et al.* (2017a);
- a review of the benefits and challenges of the various combinations of the propulsion and power supply topologies and its expected future application in **Chapter 2** and published in Geertsma *et al.* (2017a);
- a review of the benefits and challenges of the various control strategies for the propulsion and power supply topologies and its expected future development in **Chapter 2** and published in Geertsma *et al.* (2017a).

The main contributions with regard to assessing performance of propulsion and power generation systems are as follows:

- a Mean Value First Principle (MVFP) diesel engine model that can accurately predict engine performance for comparative system and control studies and can be calibrated with FAT measurements and without compressor and turbine maps in **Chapter 3** and published in Geertsma *et al.* (2017c);
- a novel validated ship propulsion model that can provide new insights in the influence of a control strategy on performance of ship propulsion with controllable pitch propellers, hybrid propulsion and hybrid power generation across various MOEs, such as fuel consumption, rate of acceleration, engine thermal loading and propeller cavitation in **Chapter 3** and published in Geertsma *et al.* (2017c);
- benchmark manoeuvres and Measures of Performance (MOP) to quantify fuel consumption, rate of acceleration, engine thermal loading and propeller cavitation, in

order to evaluate performance improvements of conventional and advanced control strategies, and compare propulsion architectures against predefined MOPs in **Chapter 3** and published in Geertsma *et al.* (2017c).

Finally, the main contributions to advanced control strategies for mechanical and hybrid propulsion and for hybrid power supply systems are as follows:

- a novel adaptive pitch control strategy for diesel mechanical and hybrid propulsion with controllable pitch propellers, which combines the angle of attack approach for propeller pitch control Vrijdag *et al.* (2010) with slow integrating speed control for diesel engine fuel injection in **Chapter 4** and published in Geertsma *et al.* (2018);
- quantification of performance improvement with the proposed adaptive pitch control strategy for a case study patrol vessel compared to the current baseline control strategy in **Chapter 4** and published in Geertsma *et al.* (2018);
- a novel parallel adaptive pitch control strategy in **Chapter 5** that is based on the results of previous research reported in Geertsma *et al.* (2017b,d);
- quantification performance improvement with the proposed parallel adaptive pitch control strategy (PAPC) for a case study frigate with hybrid propulsion, compared with a number of alternative control strategies in **Chapter 5**;
- a novel approach for the on-line solution of the charge depleting ECMS control problem for hybrid propulsion with hybrid power generation. This approach uses discrete variables for the various engines and operating modes, thus splitting the problem formulation in convex sub-problems, and combines branch and bound with convex optimisation. This approach is applied to an ECMS approach without and with operator load estimation in **Chapter 6** and published in Kalikatzarakis *et al.* (2018);
- a comparison of the optimality and robustness of the ECMS strategies with and without operator load estimation strategies with a rule-based strategy as applied on a case study tug and with the global optimum from Dynamic Programming (DP), assuming apriori knowledge on the operating profile in **Chapter 6** and published in Kalikatzarakis *et al.* (2018);
- a novel concept and design structure for autonomous control that can adapt the holistic control system performance to changing ship functions and the relation of the proposed adaptive layered control structure to the proposed control strategies: adaptive pitch control, parallel control for hybrid propulsion and energy management for hybrid power supply in **Chapter 7**.

2

REVIEW OF DEVELOPMENTS IN ARCHITECTURES AND CONTROL

The recent trend to design more efficient and versatile ships has increased the variety in hybrid propulsion and power supply architectures. In order to improve performance with these architectures, intelligent control strategies are required, while mostly conventional control strategies are applied at present. This chapter aims to answer Research Question 1 and 2: 'Which candidate propulsion and power generation architectures are suitable for which ship type and which combination of ship functions?' and 'What control strategy can be used for the power split between the propulsion engine and electric drive in hybrid propulsion to provide the best possible performance against an adaptive trade-off between the various conflicting MOEs? '

First, this chapter classifies ship propulsion topologies into mechanical, electrical and hybrid propulsion, and power supply topologies into combustion, electrochemical, stored and hybrid power supply in Section 2.1. Subsequently, the chapter reviews mechanical propulsion in Section 2.2, electrical propulsion in Section 2.3 and hybrid propulsion in Section 2.4 and the power system topologies in Section 2.5. Moreover, the chapter reviews combined architectures, such as hybrid propulsion with hybrid power supply in Section 2.6 and hybrid propulsion with DC hybrid power supply in Section 2.7. For all these power and propulsion architectures, the chapter reviews the benefits and challenges, the application on ships and the control strategies. Because research on these advanced architectures and control strategies for ships is limited, each section also reviews relevant literature from associated fields, such as terrestrial microgrid and hybrid electrical vehicle technology. Finally, Section 2.8 summarises the developments, benefits, drawbacks and application trends of the power and propulsion system architectures, and reviews the available control strategies and their benefits, Section 2.9 reviews the research opportunities and Section 2.10 summarises the conclusions and recommendations.

Parts of this chapter have been published in Applied Energy **194** (2017), Geertsma *et al.* (2017a).

2.1. INTRODUCTION

THE trade-off between efficiency and adaptability to diverse operating profiles has led to a growing variety of power and propulsion architectures, which can be categorised as follows:

- Mechanical propulsion, electrical propulsion or a hybrid combination of both;
- Power generation with combustion engines, fuel cells, energy storage or a hybrid combination; and
- AC or DC electrical distribution.

As complexity of the system architecture increases, the degrees of freedom in control increase. However, most advanced propulsion architectures still use the same traditional control strategies: fixed combinator curves, fixed frequency generators, rule-based use of batteries and operator-controlled configuration settings. Conversely, research in the maritime and automotive domain has shown that advanced architectures with traditional control do not significantly reduce fuel consumption or emissions while cost and complexity of the system do increase (Sciarretta *et al.* 2014; Volker, 2013).

Nevertheless, advanced control strategies for maritime applications have hardly been developed yet. The limited research in optimisation of battery deployment and intelligent use of DC architectures has, however, shown that smart control strategies can deliver reductions of 10 to 35% in fuel consumption and emissions (Bosich *et al.* 2013; Breijs *et al.* 2016; Butcher *et al.* 2009; Rampen *et al.* 2014; Zadeh *et al.* 2013; Zahedi *et al.* 2013, 2014). Analysis of the impact on other criteria has hardly been covered. Therefore, holistic research into and development of smart control strategies to improve performance on various criteria is urgently required to achieve the benefits of advanced architectures for future smart ships. In order to direct this research, applicable control strategies have to be reviewed for each architecture, as well as their performance on the criteria listed above.

While extensive reviews are available on automotive hybrid electric vehicles architectures and their control strategies (Emadi *et al.* 2005; Koot *et al.* 2005; Sciarretta *et al.* 2014; Wirasingha *et al.* 2011), such a review is lacking on power and propulsion architectures for ships and their control strategies. Moreover, the classification in parallel, series and series-parallel (Emadi *et al.* 2005; Silvas *et al.* 2015) hybrid electric vehicles does not apply to ship's power and propulsion architectures, as ships can have multiple propulsion engines, electric propulsion motors, diesel generators, fuel cells and energy storage systems. Therefore, this chapter provides a survey of the development and application of hybrid power and propulsion architectures and their control strategies for ships.

2.2. MECHANICAL PROPULSION

PRIOR to the 19th century, ships were propelled by oars and sails. Then, the development of the steam engine led to the introduction of mechanical propulsion. Over the 19th and 20th centuries, the driving engines developed from reciprocal steam engines and steam turbines into diesel engines and, for some applications, gas turbines. A detailed historical review of these developments can be found in Curley, (2012).

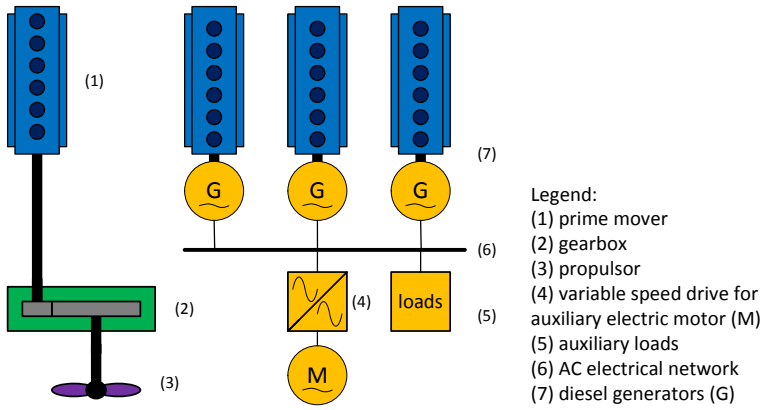

Figure 2.1: Typical mechanical propulsion system.

A typical architecture for a modern ship with mechanical propulsion is presented in Figure 2.1. A prime mover (1), typically a diesel engine or gas turbine, drives the propulsor (3), typically a propeller, either directly or through a gearbox (2). Alternative prime movers are steam turbines in combination with a (nuclear) steam raising plant and gas turbines. However, this review focuses on diesel engines, as most ships use them due to their high fuel efficiency.

A separate electrical AC network (6) is required for generating and distributing electric power of auxiliary loads (5), such as variable speed drives (4), heating ventilation and air-conditioning (HVAC) and other mission-critical and auxiliary systems. Diesel, steam-turbine or gas-turbine generators (7) feed this electrical network.

For large cargo ships, driven by low speed diesel engines, no gearbox is required and reversing can be achieved by reversing engine rotation. On the other hand, smaller ships do require a gearbox to reduce the engine speed, as they are driven by medium- or high-speed diesel engines. This gearbox can also be used for reversing shaft rotation.

The most applied propulsor is a Fixed Pitch Propeller (FPP). It requires a reversible engine or gearbox for stopping and reversing. Alternatively, a controllable pitch propeller (CPP) can provide negative thrust for stopping and reversing. Other propulsors are water jets, surface piercing propellers, cycloïdal propellers, paddle wheels, whale-tails, and magneto hydrodynamic propulsion (Carlton, 2012). Furthermore, propulsion and steering can be combined in steerable thrusters. This review, however, will be limited to propellers, although the same principles and control strategies apply to other propulsors as well. Therefore, the characteristics of the FPP and CPP will be introduced next in more detail.

2.2.1. FIXED PITCH PROPELLER

When the propulsor in a mechanical propulsion plant is an FPP, the ship's resistance, propeller and gearbox determine the load characteristic of the diesel engine. This load characteristic is referred to as the *propeller curve* (Klein Woud *et al.* 2012). In Figure 4.3,

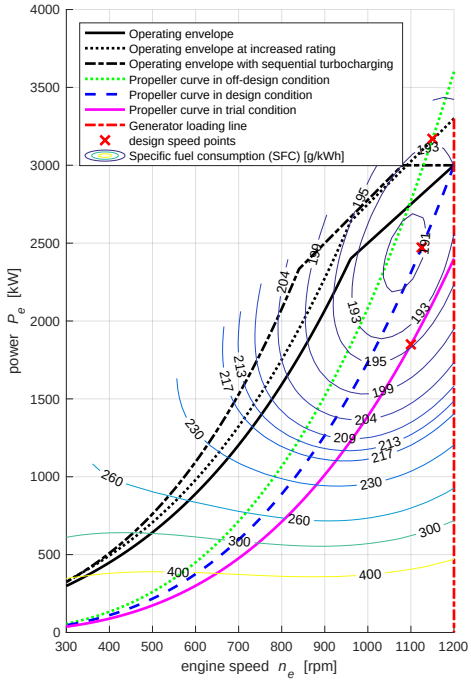

Figure 2.2: Three propeller curves and the generator loading line in three diesel engine operating envelopes with typical SFC contour plot.

three propeller curves have been plotted, representing the load experienced by the diesel engine in trial condition, design condition, and off-design condition (Stapersma, 2005).

The propeller curves have been plotted in the *engine operating envelope*. This operating envelope shows the maximum power the engine can deliver as a function of engine speed. Moreover, Figure 4.3 shows the specific fuel consumption (SFC) of the engine as a function of engine speed and delivered power. This specific plot is derived from a quadratic fit model of a typical medium speed diesel engine.

The propeller curves, operating envelope, and SFC contour plot represent stationary conditions, without acceleration and deceleration. When operating in stationary conditions, the diesel engine delivers a constant power output at a constant engine speed. For example, the design speed could be achieved in the operating point at 1125 rpm and 2450 kW, indicated by the design speed point on the design condition propeller curve in Figure 4.3. At this design condition, the specific fuel consumption is 191 g/kWh. On the other hand, in the off-design condition due to heavy weather and hull fouling, the design speed will be achieved in the operating point at 1150 rpm and 3150 kW, leading to an average specific fuel consumption of 193 g/kWh.

However, in dynamic conditions, such as steaming in heavy weather and turning, the actual load fluctuates around the average operating point of the propeller curve (van Spronsen *et al.* 2001; Vrijdag, 2009). The off-design condition shown in Figure 4.3 repre-

sents the average increase in load. In order to prevent overloading from the fluctuation around the average load, sufficient margin between the propeller curve and the engine operating-envelope is required. This can be achieved by selecting an engine with an increased rating (see Figure 4.3).

However, an overrated engine increases the cost of the propulsion plant and increases fuel consumption as the average operating point may now have a greater distance from the optimal fuel consumption, which is close to the maximum loading line. Alternatively, selecting an engine with a broader operating envelope in part load has recently become possible. A broader operating envelope can be achieved with sequential turbocharging, a waste gate, or variable turbine geometry (Klein Woud *et al.* 2012). For instance, sequential turbocharging (STC) widens the operating envelope by switching off a turbocharger when exhaust gas flow is too low for effective performance.

In conclusion, the challenge with an FPP is to match the diesel engine, gearbox, propeller and ship's resistance, so that the engine can run safely within its operating envelope across the speed range of the engine. The minimum speed of the ship is limited by the minimum engine speed limit. For reversing, either the engine or the gearbox needs to be reversible.

2.2.2. CONTROLLABLE PITCH PROPELLER

To overcome the challenges mentioned above, a CPP can be used (Klein Woud *et al.* 2012), because propeller pitch introduces an additional degree of control. Reducing the pitch reduces propeller thrust, and the power absorbed by the engine at a certain shaft speed. This allows the thrust to be reduced below the value of minimum engine speed and full pitch. Moreover, reversing pitch enables the thrust to be reversed without reversing the engine or gearbox. CPP thus directly improves manoeuvrability and the control strategy can be used to improve performance.

2.2.3. BENEFITS AND CHALLENGES OF MECHANICAL PROPULSION

Mechanical propulsion is particularly efficient at design speed, between 80 and 100% of top speed. In this range the diesel engine operates in its most efficient working point (see Figure 4.3). Moreover, mechanical propulsion consists of only three power conversion stages, the main engine, the gearbox and the propeller, which leads to low conversion losses. Because the limitations on NO_x emissions for Tier II and Tier III engines are expressed in g/kWh, efficient operation, leading to lower power output, will also lead to lower NO_x emission, bearing in mind that the limitations for high speed engines are lower than those for low speed engines. Finally, the purchase cost of mechanical propulsion is low, due to its low complexity. This justifies the application of mechanical propulsion for transport ships, as illustrated with the energy analysis performed on a deadweight tanker, which converts 88 % of its energy in the main diesel engines (Baldi *et al.* 2014). This study thus concludes that, for these ship types, fuel consumption and emissions can best be reduced by recovering waste heat in exhaust gas and cooling water to generate auxiliary electrical power and heating.

However, matching the engine for the design speed also fixes plant behaviour for the rest of the operating envelope. A CPP can add an additional freedom of control at

the cost of increased system complexity. Nevertheless, mechanical propulsion faces the following challenges:

- The manoeuvrability is limited by the engine's operating envelope. Manoeuvrability can be improved with CPP but remains limited to prevent engine overloading.
- High static and dynamic engine loading can increase the required maintenance effort for the engine. Application of CPP with an appropriate control strategy can reduce static and dynamic loading (Guillemette *et al.* 1997; Stapersma, 2005; van Spronsen *et al.* 2001).
- Mechanical propulsion has an increased fuel efficiency and high emissions when sailing at speeds below 70% of top speed, because engine fuel consumption significantly increases below 50% of rated power (see Figure 4.3).
- Mechanical propulsion exhibits limited reliability, because failure of any of the components in the drive train directly leads to loss of propulsion.
- The NO_x emissions of the main propulsion engine are determined by its operating points in the operating envelope. In automotive, diesel engine research has shown that the NO_x emissions during the world-harmonized light-duty vehicle test cycle (WLTC), with increased acceleration profile, are much higher than the current Euro 6 standard of 80 mg/km, which is assessed in the new European driving cycle (NEDC) with more constant loading (Ko *et al.* 2017). This trend is confirmed by NO_x measurements performed on a 300kW MAN4L20/27 research engine without NO_x abatement technology at the Netherlands Defence Academy shown in Figure 2.3, from Linden, (2017). Similarly, diesel mechanical propulsion during acceleration is likely to lead to high NO_x emissions due to the high cylinder temperature caused by the turbolag. NO_x emissions for ships in this situation are likely to occur at a higher rate in g/kWh than the specified Tier 2 or Tier 3 standard.
- The radiated noise performance is limited due to the mechanical transmission path from the engine to the propeller, although isolation measures can improve this.
- Radiated noise performance due to cavitation is limited, particularly in dynamic conditions, but can be improved with CPP and a proper control strategy (Vrijdag, 2009).

The control strategies for mechanical propulsion should be aimed at addressing these challenges.

2.2.4. APPLICATION OF MECHANICAL PROPULSION

After the introduction of the steam engine, most ships used mechanical propulsion. In order to meet the challenges listed above, various electrical architectures have replaced purely mechanical propulsion for many applications. However, mechanical propulsion remains the preferred architecture for ships that sail at a single cruise speed most of the time, because its fuel efficiency at full load is high. Examples of such ship types are cargo ships and fast crew suppliers.

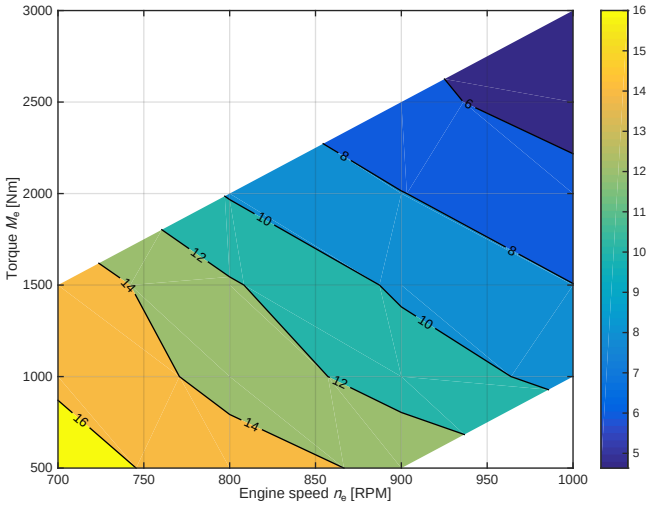

Figure 2.3: NO_X measurement results in g/kWh of MAN4L20/27 research engine on Netherlands Defence Academy in contour plot, from Linden, (2017).

With mechanical propulsion, other ship types would operate at low power in the operating envelope of the engine in certain operating modes. For example tugs only require 20% of their maximum power required for towing during transit, and offshore vessels operate at very low power during DP. For these ship types, mechanical propulsion would lead to poor specific fuel consumption and high emissions. Thus, electric or hybrid propulsion could be considered to improve part-load fuel efficiency. Nevertheless, over 50% of tugs operating around the globe consist of mechanical propulsion.

Alternatively, ships with a limited number of distinct operating modes can benefit from mechanical propulsion with multiple shafts and / or multiple engines on one shaft, through a gearbox with clutches. These engines can be of the same type or of different types. Such configurations with multiple engines and shafts can also improve propulsion availability. For example, many naval frigates utilise combined diesel or gas-turbine (CODOG) or combined diesel and gas-turbine (CODAG) propulsion plants. While many European navies and the US Navy in their new designs opt for hybrid or full electric propulsion, many smaller navies still apply mechanical propulsion, even in recent vessels.

Dredging ships currently still mostly apply mechanical propulsion with also a direct mechanical drive on the dredging pumps. Their dynamic operating profile and the arduous dynamic loading of both propulsion and dredging pumps due to inconsistencies in the dredge spoil, are motivations to consider electrical drives for both the dredging pumps and propulsion.

Finally, many yachts consist of mechanical propulsion. An important aspect of yacht design is to achieve the maximum top speed with the smallest possible installed power. The high efficiency of mechanical propulsion at the design point, enables high speed.

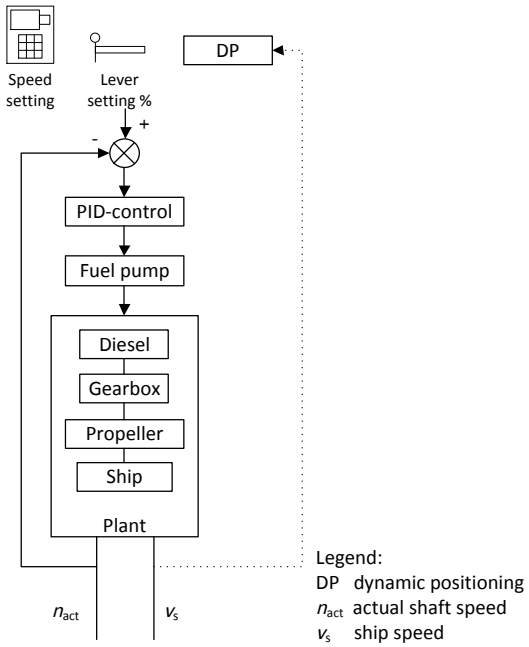

Figure 2.4: Control loop with standard engine governor for mechanical propulsion with fixed pitch propeller.

However, requirements to improve the comfort when sailing at low speeds and improve the flexibility in operation have led to the development of hybrid yacht concepts (Loon *et al.* 2016).

2.2.5. CONTROL STRATEGIES FOR MECHANICAL PROPULSION

This section covers the control strategies for mechanical propulsion that have been implemented in ships or published in research.

GOVERNOR SPEED CONTROL

The standard control strategy for mechanical propulsion with a fixed pitch propeller is to control engine speed as a function of the lever setting. The diesel engine's speed governor typically fulfils this task with a PID controller. Most ships are equipped with a lever that sets the reference shaft speed as a percentage of full speed. Alternatively, the actual reference shaft speed can be entered. Ships can also be controlled with the DP system. Then the DP system generates the actual shaft or engine speed setting. The standard control loop is illustrated in Figure 2.4.

Many publications have concluded speed control leads to unnecessary engine load disturbances (Faber, 1993; Guillemette *et al.* 1997; Stapersma *et al.* 2004, 2009; van Spronsen *et al.* 2001; Vrijdag, 2009). Faber, (1993) argues that running the engine with constant fuel injection leads to more constant thermal loading of the engine and better fuel-efficiency. Nevertheless, industry primarily uses speed control, because it provides

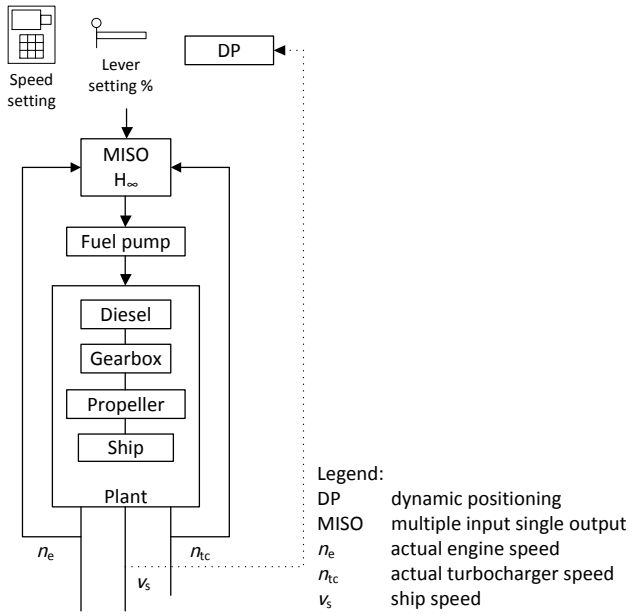

Figure 2.5: Control loop for state feedback control.

over-speed protection and a nearly linear relationship between the speed setting and the resulting ship speed.

N. Xiros, (2002) proposes a method for robust PID speed governor design that increases load disturbance attenuation compared to traditional PID control. This method utilises the H_∞ norm of the closed-loop transfer function from propeller disturbance to shaft rpm. D-action is required, in order to achieve robust control with higher order dynamical terms. However, it is not possible to directly implement the D-term on the speed feedback signal, due to torque fluctuation from engine and propeller. To overcome this, Xiros proposes predicting the speed derivative from the measured shaft torque and the system dynamics model, thus achieving robust PID H_∞ control that significantly attenuates disturbances due to wind, waves and turns.

STATE FEEDBACK CONTROL WITH ENGINE AND TURBOCHARGER SPEED MEASUREMENT

N. Xiros, (2002) also proposes a method for H_∞ state feedback controller synthesis using engine and turbocharger speed as state variables. This allows a single disturbance origin, for example the propeller load. Furthermore, the method allows separate scalar H_∞ norm requirements for the state variables. The schematic representation of state feedback control is illustrated in Figure 2.5. The improvements that can be achieved with this method have not been quantified and this needs further research.

ADAPTIVE SPEED CONTROL

When the mechanical propulsion plant consists of a fixed pitch propeller, the freedom of control is limited. Moreover, the speed control loop aims to maintain engine speed,

causing considerable fluctuation of engine loading during disturbances from waves and manoeuvring (van Spronsen *et al.* 2001; Vrijdag, 2009). Both Royal Netherlands Navy (RNLN) and Canadian frigates with mechanical propulsion have suffered from significant increased maintenance costs due to dynamic engine overloading (Guillemette *et al.* 1997; van Spronsen *et al.* 2001).

Guillemette *et al.* (1997) propose an 'optimal' speed controller that adapts the diesel engine speed feedback signal to the governor via an amplifier. It determines the optimum value for this amplifier real-time, with a cost function that trades off future predicted engine speed fluctuation and fuel rack actuation due to predicted engine load disturbance. Current engine load disturbance is estimated using a Kalman filter. Future engine load disturbance is predicted using autocorrelation of statistical data, based on the current estimated load disturbance. Even though the case study has a CPP, pitch is held constant. The work demonstrates that, with maximum cost attributed to fuel rack actuation–counterintuïtively–the engine speed fluctuation reduces from the situation with governor speed control. When maximum cost is attributed to engine speed fluctuation, it reduces even further –as expected. However, Guillemette *et al.* (1997) do not confirm whether the combination of an estimated load disturbance and a predicted future load disturbance using autocorrelation of statistical data can lead to robust control in a practical environment with additional measurement disturbances. The proposed test bed and shipboard trial have not been reported in follow-on publications.

COMBINATOR CURVE CONTROL

The current standard control strategy with a CPP is to determine a fixed *combinator curve*, which sets the relationship between the speed setting from the lever and both propeller pitch and engine speed reference (Vrijdag, 2009). Propeller pitch and engine speed are controlled in separate control loops, as illustrated in Figure 2.6. The combinator curve, shown in Figure 2.7, allows: the engine load to be reduced by reducing propeller pitch (area 1); propeller thrust to be controlled below minimum engine speed by reducing propeller pitch at minimum engine speed (area 2); and thrust to be reversed without reversing engine or gearbox (area 3). The associated static engine loading line for this combinator curve is presented in Figure 2.8.

The combinator curve as such determines the static operating point of the diesel engine and can be optimised for a number of criteria such as fuel efficiency, engine loading and cavitation. However, this average operating point also highly depends on the ship's state (loading, fouling, etc.) and the environmental conditions (wind and sea state). Accordingly, Vrijdag *et al.* (2008) argue that a single fixed combinator curve cannot ensure that engine operation will meet loading and cavitation requirements under all circumstances; they illustrate this with the practical example of a frigate. Figari *et al.* (2009) show that dynamically changing pitch as a function of weather conditions can significantly reduce fuel consumption and emissions, without fully addressing the control system design implications.

This limitation of a single combinator curve has partly been overcome by having a number of static combinator curves for different operating modes of the ship. For example, engine speed is kept low for fuel efficiency in 'transit' mode, and engine speed is maintained at a higher value for increased acceleration performance in 'manoeuvring'

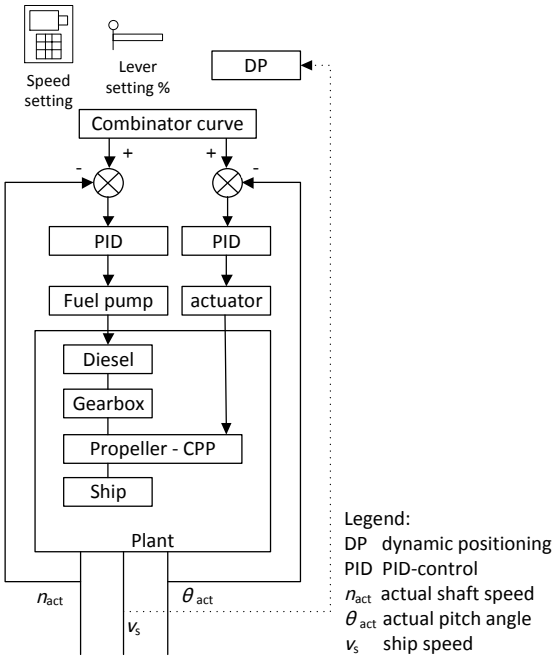

Figure 2.6: Control loop for mechanical propulsion with controllable pitch.

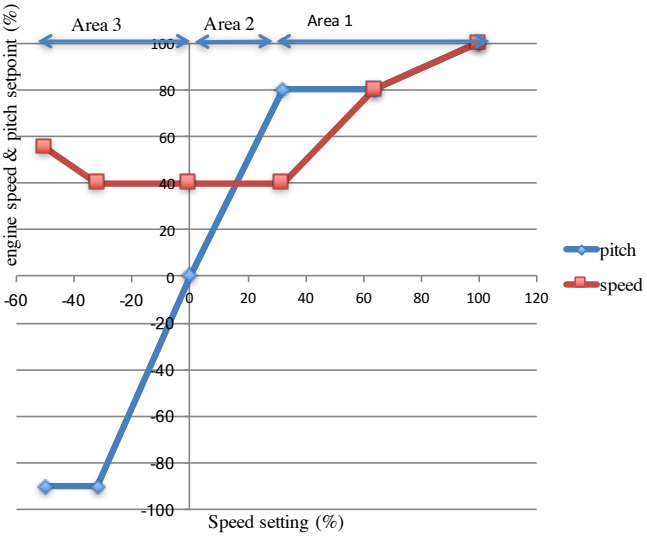

Area 1: reduce pitch to reduce engine load
Area 2: control propeller thrust below minimum engine speed by reducing pitch
Area 3: reverse thrust without reversing engine speed

Figure 2.7: Typical combinator curve.

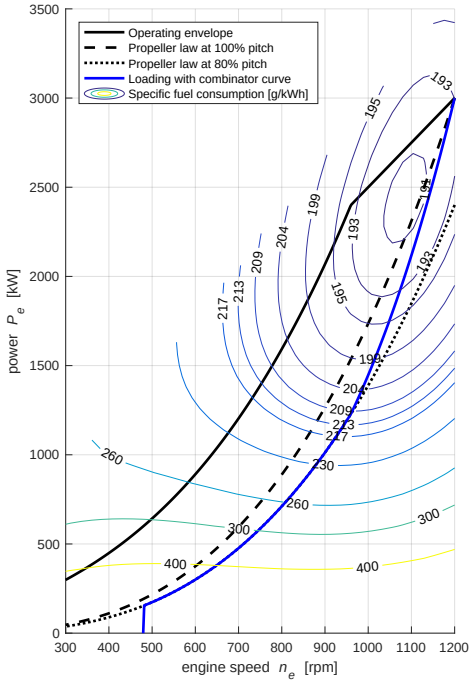

Figure 2.8: Engine loading with combinator curve control of Figure 2.7.

mode. However, this does not account for the impact of changes in ship's state and environmental conditions on the propeller curve, and therefore the plant performance can be poor in certain states and conditions.

COMBINATOR CURVE CONTROL WITH PITCH REDUCTION

Another strategy to prevent overloading has been to apply pitch reduction when the engine supersedes the *overloading criterion*, an alternative engine loading limit, comparable to the operating envelop introduced earlier. This approach has been applied to RNLN *M-class frigates* and *Canadian Patrol Frigates* (Guillemette *et al.* 1997; Vrijdag *et al.* 2008). Although this strategy effectively prevents overloading, it has a detrimental impact on propulsion performance, particularly on acceleration behaviour (Guillemette *et al.* 1997; van Spronsen *et al.* 2001) and cavitation inception (Vrijdag, 2009).

OPTIMAL SPEED AND PITCH H_∞ CONTROL

The speed regulation control strategy is responsible for the dynamic behaviour of the engine. Figure 2.9 shows the fluctuations of fuel rack position and shaft speed as a result of speed regulation as measured on a RNLN M-class frigate, from van Spronsen *et al.* (2001). In this specific case the engine suffers from overloading, which leads to increased maintenance cost.

To resolve this, van Spronsen *et al.* (2001) propose a control strategy that utilises the control inputs engine fuel rack and propeller pitch. They define the control objective

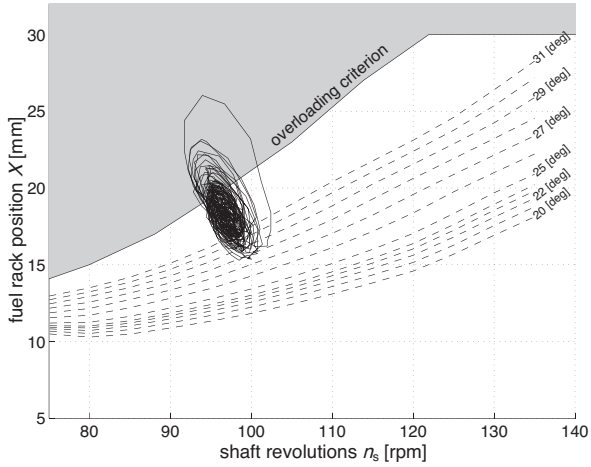

Figure 2.9: Dynamic overloading due to sea state plotted in the phase plane ©IFAC 2001 van Spronsen *et al.* (2001).

to minimise the effect of sea state on engine speed and maximise acceleration and deceleration performance. A constraint is defined to prevent the engine operating in the overloading region, i.e. torque superseding the overloading criterion. A schematic representation of the control loop is presented in Figure 2.10.

The proposed multiple input, multiple output H_∞ design achieves a promising control performance that prevents engine overloading while increasing acceleration performance. However, the control strategy is aimed at minimising engine speed fluctuation, and, therefore, causes significant fluctuation of fuel injection and propeller torque. This fluctuating fuel injection causes increased fuel consumption and fluctuating torque increases thermal loading and radiated noise. These effects of minimising engine speed fluctuation are undesirable, while, as argued before, shaft speed fluctuation does not have to be minimised.

EFFECTIVE ANGLE OF ATTACK CONTROL

Vrijdag, (2009) proposes a control strategy that reduces cavitation in operational conditions. With this control strategy, propeller pitch is governed to achieve the effective angle of attack at which the chance of cavitation occurring is minimal. This effective angle of attack in essence is the angle at which water flows into the propeller blade profile. The detailed definition is given in Vrijdag, (2009). Increasing engine speed to compensate for the reduced pitch due to the control strategy results in the requested virtual shaft, which is defined as follows:

$$n_{\text{virt}} = \frac{\theta - \theta_0}{\theta_{nom} - \theta_0} \cdot n \tag{2.1}$$

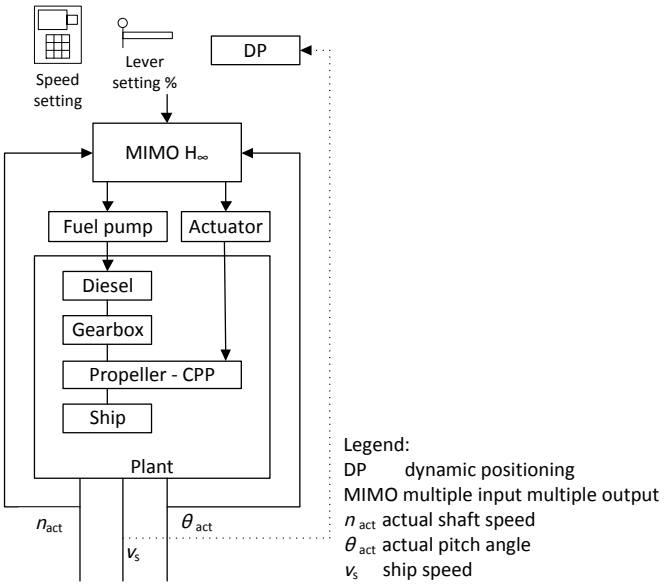

Figure 2.10: Control loop for optimal speed and pitch H_∞ control.

where n_{virt} is virtual shaft speed, θ is actual pitch angle, θ_0 is the pitch at which zero thrust is achieved, θ_{nom} is nominal pitch and n is actual shaft speed. The engine speed control loop is retained to allow testing on board a RNLN M-class frigate. The control loop is shown in Figure 2.11.

On board testing of the control strategy in combination with analysis of simulations has proven that this control strategy reduces cavitation time and -as a side effect- improves acceleration performance, without overloading the engine in trial conditions.

2.3. ELECTRICAL PROPULSION

ELECTRICAL propulsion has been around since the early 1900s. A short historical review of electrical propulsion is covered in Moreno *et al.* (2007). In the 1990s, electric propulsion received an enormous boost in the cruise ship industry and in capital naval ships (see Figure 1.1). A typical architecture of an electric propulsion system is depicted in Figure 2.12. Multiple diesel generator sets (1) feed a fixed frequency high voltage electrical bus (2). This bus feeds the electrical propulsion motor drive (5) and the hotel load (6), in most cases through a transformer (3). The electric propulsion motor drive consists of a power electronic converter (4) used to control shaft line speed and thus ship speed.

2.3.1. BENEFITS AND CHALLENGES OF ELECTRICAL PROPULSION

In the first place, electric propulsion is a fuel-efficient propulsion solution when the hotel load is a significant fraction of the propulsion power requirement and the operating profile is diverse, because the generator power can be used for both propulsion, through

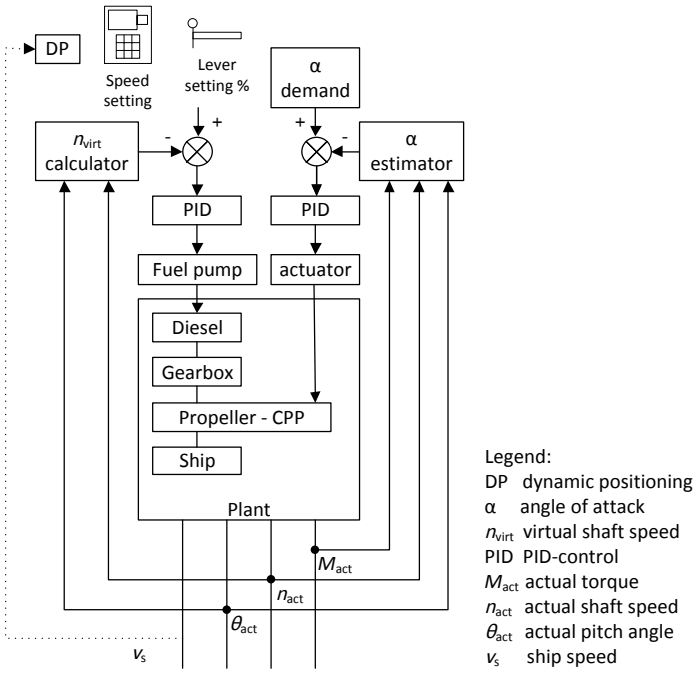

Figure 2.11: Control loop for effective angle of attack control.

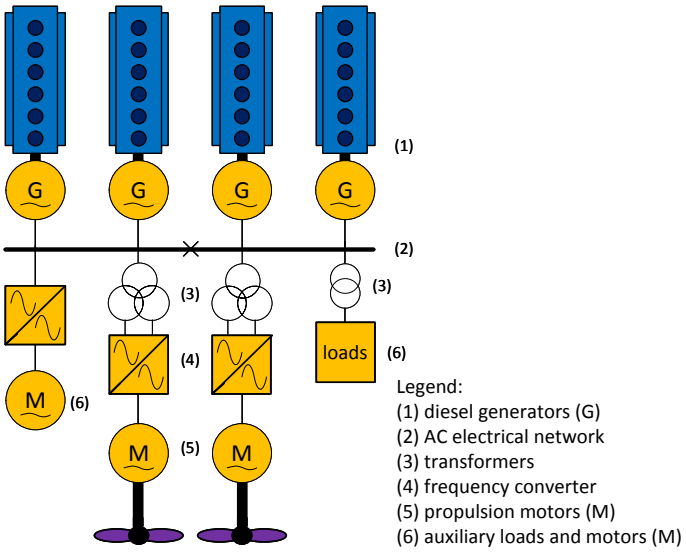

Figure 2.12: Typical electrical propulsion system layout.

the electric motors, and auxiliary systems (Vie, 1998). To achieve this, a power management system (PMS) matches the amount of running engines with the required combined propulsion and hotel load power. This control strategy ensures engines do not run inefficiently in part load and is often referred to as the *power station concept*.

Secondly, the NO_x emissions of electric propulsion are likely to be less than those of mechanical propulsion, because the propulsion power at full ship speed is, in most cases, split over more engines, which due to their lower individual power run at a higher speed. For example, a cruise ship with an electrical propulsion power of 20 MW per shaft typically has 5 diesel generators installed, running at 720 rpm, and a cruise ship with a mechanical propulsion plant of 20 MW per shaft typically has two main engines of 20 MW, each running at a maximum speed of 500 rpm with four-stroke diesel engines or 80 rpm with two-stroke engines. For Tier II, this would mean a cycle-averaged NO_x production of 9.7 g/kWh for the diesel generators used in electrical propulsion and of 10.5 or 14.4 g/kWh for the four-stroke or two-stroke diesel engines used in mechanical propulsion. Moreover, due to the power station concept of electrical propulsion, the diesel generators run closer to their design point, at which they typically produce less NO_x emissions or need less fuel-consumption-increasing NO_x abatement measures. Furthermore, they always run at rated speed, as opposed to mechanical propulsion engines, which run at reduced speed in part load, producing more NO_x due to the longer NO_x formation time, as illustrated in Figure 2.3.

The third advantage of electrical propulsion is the reduced maintenance load, as engines are shared between propulsion and auxiliary load and are switched off when they are not required.

Fourthly, electric propulsion can achieve reduced radiated noise due to the absence of a mechanical transmission path from the engine to the propeller. To this aim, the design of motor and power converter has to be optimised for minimal torque fluctuation. The impact of dynamic (operational) conditions on noise performance of electrical propulsion appears not to have been studied yet.

The fifth benefit of electric propulsion is its potential high availability, at least if the power and propulsion plant has been designed for this purpose.

On the contrary, electrical propulsion faces the following challenges:

- Due to the additional conversion stages in power converters and electric motors, electrical propulsion incurs increased losses. These losses lead to an increase in SFC, particularly near top speed of the ship.
- When running redundant engines to achieve high propulsion availability, which is required for sensitive DP operations, the engines run at low part load. This leads to poor fuel consumption and a lot of emissions.
- Most ships with electric propulsion use FPP, because electric motors with variable speed drives can provide maximum torque at every speed and run in reverse direction. Vrijdag, (2009) has shown that radiated noise due to cavitation increases under operational conditions when fixing propeller pitch and using speed control, which is the standard control strategy for electric motors. Therefore, cavitation potentially increases under operational conditions, particularly for electric

propulsion with fixed pitch propellers and speed control, as well as for mechanical propulsion with FPP.

- Because all loads experience the electrical network voltage and frequency, voltage and frequency swings under fault conditions can cause electrical systems to be switched off, thus reducing reliability and availability. Particularly in power systems with a high amount of variable speed drives, constant power load instability can occur. Sulligoi *et al.* (2016) describe this phenomenon, propose methods to analyse the risk with two modelling strategies and discuss mitigation strategies.

As before, the control strategy should be aimed at addressing these challenges. Alternatively, when the control strategy cannot sufficiently improve any of these performance criteria, another system architecture can be selected.

2.3.2. APPLICATION OF ELECTRIC PROPULSION

Even though the fuel savings attributed to the power station concept are mostly offset by the increased electrical losses, electric propulsion has been very successful in the cruise industry. This is mainly attributed to the robustness of the power station concept; failure of a diesel generator has hardly any impact on the operation of the vessel (Vie, 1998). Additionally, electrical propulsion allows flexibility in positioning machinery spaces, due to the absence of the shaft-line, which traditionally determines the engine room layout. Finally, the absence of the shaft-line also allows isolation of noise from the diesel engines, by installing diesel-generator sets on flexible, noise-isolating mountings.

Due to its success in the cruise ship industry, electric propulsion has also been applied in ferries, DP drilling vessels, cable layers, icebreakers, and capital naval vessels. A review of these applications and the associated developments in applied motor and converter technologies can be found in Moreno *et al.* (2007). The choice for electric propulsion on these vessels is mainly determined by their diverse operating profiles, as these lead to a large benefit for the power station concept.

The robustness of electrical propulsion has also contributed to its success in the offshore sector, because an electrical propulsion architecture allows redundant components such as generators, thrusters, and propulsors of different types to be added easily. This feature of electric propulsion is particularly important for DP to guarantee maintaining position in fault conditions. For example, running redundant engines as spinning reserve guarantees availability of sufficient power in failure conditions.

However, running extra engines causes part load operation and therefore lower efficiency and increased NO_x emissions, as illustrated in Figure 2.3. Moreover, the requirement for sufficient spinning reserve and sufficient installed power to maintain DP capability during the worst-case fault also drives installed power and thus investment cost. To overcome this, Wärtsilä offers a patented variant of the commercial standard AC architecture as depicted in Figure 2.13, in which the bus bars of two generator sets are galvanically isolated from each other with a phase shift transformer. This mitigates the need for phase shift propulsion transformers (used in conventional propulsion drives) and reduces the impact of a bus bar failure to 25% of installed power instead of 50% (Öster, 2010; Skaar *et al.* 2012).

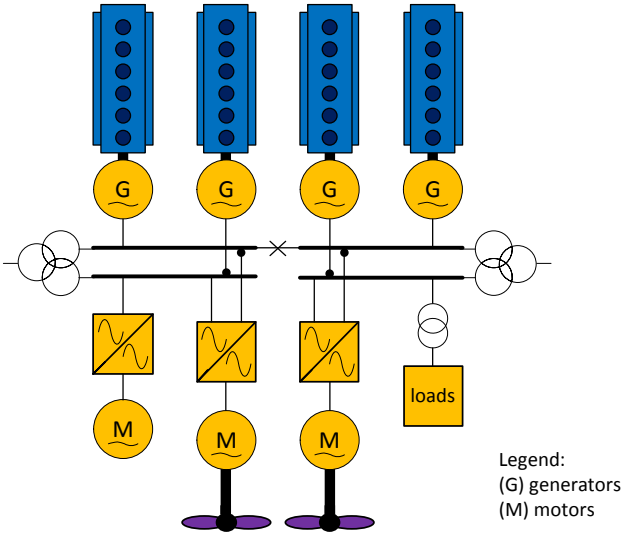

Figure 2.13: Electrical propulsion layout with separated phase shifted busbars.

The success of electrical propulsion in commercial ships and the drive to reduce running cost has prompted significant development programmes to enable electric propulsion for naval destroyers in the UK and US (Danan *et al.* 2005; Hodge *et al.* 1996, 1997, 1998, 1999, 2000, 2001, 2008; Mattick *et al.* 2005; O'Rourke, 2009). These development programmes were targeted to increase the power density with advanced technologies, consisting of new permanent magnet and high temperature super conducting motor technologies in order to fit electric propulsion in frigates and meet military requirements.

These development programmes have led to the application of electric propulsion in Royal Navy's *Type 45* destroyer (Loyd *et al.* 2003; Vanderpump *et al.* 2002) and *Queen Elizabeth* aircraft carriers (Sears *et al.* 2010), and in US Navy's *DDG-1000* destroyer (O'Rourke, 2009). In spite of development programmes for new motor technologies, these naval applications are still all based on the Advanced Induction Motor (AIM) with Pulse Width Modulation (PWM) frequency converter drives. This AIM drive is an advanced development of asynchronous motor technology. These naval applications consist of traditional fixed frequency high voltage AC generator sets with conventional control strategy, despite programmes to develop DC architectures. Therefore, the naval power and propulsion systems can also be represented by the typical propulsion system layout illustrated in Figure 2.12. However, their converters can be connected to the feeding bus without transformers. The absence of these transformers increases harmonics, which are mitigated by passive and active filters (Vanderpump *et al.* 2002).

2.3.3. CONTROL STRATEGIES FOR THE ELECTRICAL NETWORK

The control strategy for electrical propulsion architectures consists of two parts: the control of the electrical fixed frequency network aiming to provide robust power supply to

all electrical users, and the control of the propulsion aiming to drive the ship in a certain speed and direction.

VOLTAGE AND FREQUENCY CONTROL

The electric propulsion architectures nowadays consist of fixed frequency AC electrical networks. The frequency of the network is typically maintained by droop speed control in governors or by electric isochronous load sharing between governors. In the first case, with multiple generators in parallel, the droop in the governor controls the load sharing of active power between these generators. Similarly, the Automatic Voltage Regulator (AVR) maintains the required voltage and governs reactive load sharing between parallel-running generators. These control loops form the primary control level (Mahon, 1992).

The main disadvantage of fixed frequency networks is that the diesel generator always runs at its rated speed. Figure 4.3 shows that the specific fuel consumption of a typical engine running at reduced power and nominal speed is significantly higher than when the engine operates on the propeller curve under design conditions. A similar argument applies for CO_2 and other fuel-related emissions. However, NO_x emissions are typically lower when the engine runs on the generator line (see Figure 2.3). Furthermore, the centrifugal forces in the engine, and engine wear, are higher when the engine runs at rated speed in part load.

An alternative approach is a variable frequency electrical network as proposed in Simmonds, (2014). This can lead to fuel savings of approximately 5% for a typical diesel generator set. However, electrical equipment designed for variable frequency AC networks is only limitedly available. Moreover, additional power conversion would be required to provide power to constant frequency auxiliary loads, leading to increased conversion losses. Alternatively, a DC electrical network can be selected.

SECONDARY POWER MANAGEMENT CONTROL

The PMS performs secondary control, as depicted in Figure 2.14. It controls the speed and voltage setpoints as to maintain voltage and frequency within the operating limits of the system during system dynamics. For example, due to droop, the frequency of the electric network will reduce when load increases. Power management can (slowly) increase the setpoint to compensate for the droop and maintain the network frequency at 60 Hz. Moreover, during load changes the PMS provides automatic starting and stopping of generator sets and ensures online engines are not overloaded by limiting propulsion drives and other loads as necessary. Finally, the PMS can perform protection functions such as preventing blackout, switching off faulty system parts and reconfiguring the electrical network after blackout. These control actions typically are all rule-based (Karim *et al.* 2002) and can also be initiated by the operator. Specifically for ships with high availability requirements, such as DP vessels, the power management system is also responsible for ensuring sufficient spinning reserve is available.

The next sections cover advanced control strategies that can improve the function of the PMS to maintain voltage and frequency under fault conditions.

REAL-TIME MODEL BASED POWER MANAGEMENT

Amgai *et al.* (2014) propose using the *interaction balance principle* where sub models of the loads and power sources are used to calculate the optimum frequency setpoint for

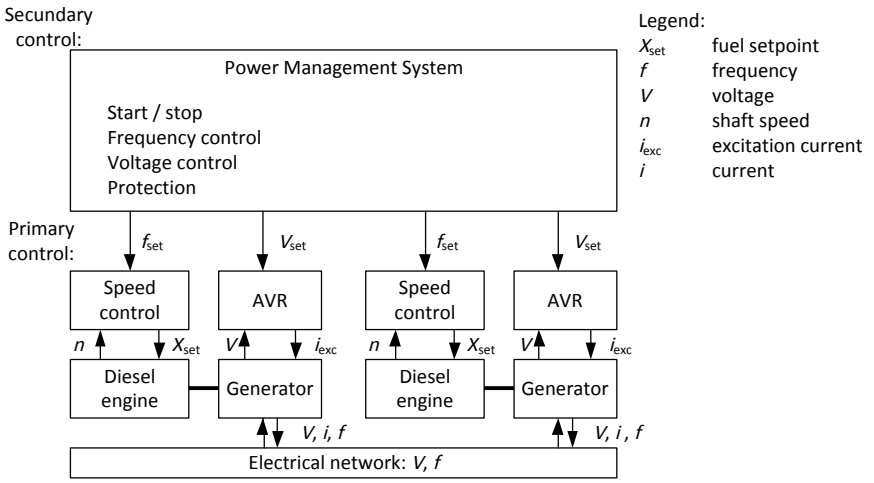

Figure 2.14: Typical layered control strategy for fixed frequency AC networks.

each power source that achieves the globally defined target frequency. The interaction balance principle can maintain system frequencies after generator blackout within the specified range while a system with speed governors without secondary control in the presented case drops below the specified minimum. However, a performance comparison with electric isochronous load sharing governors or central secondary control has not been undertaken.

POWER TRACKING

Seenumani *et al.* (2012) propose a multi time-scale approach for power tracking with two power sources with different dynamic properties. The work demonstrates that this approach can ensure fast and efficient power tracking due to its computational efficiency. However, the system architecture is highly simplified and constraints on engine loading appear not to have been applied, as the engine load increase is very steep in the presented results.

2.3.4. CONTROL STRATEGIES FOR PROPULSION CONTROL

The second part of control for electrical propulsion architectures is propulsion control. Propulsion control has to provide the ships thrust to propel the ship at a certain speed and, in the case of steerable thrusters, in a certain direction. Most electrical propulsion systems utilise fixed pitch propellers, because the electrical drive can run at every speed in forward and reverse direction and deliver full rated torque at every speed. As such, the speed of the ship can be fully controlled without the need for a controllable pitch propeller. The control strategy for the electric propulsion motor drive, therefore, is aimed to achieve the required shaft speed. Controlling the propulsion motor torque and flux by controlling the switching signals of the PWM converter fulfils this aim. The control strategy is schematically presented in Figure 2.15.

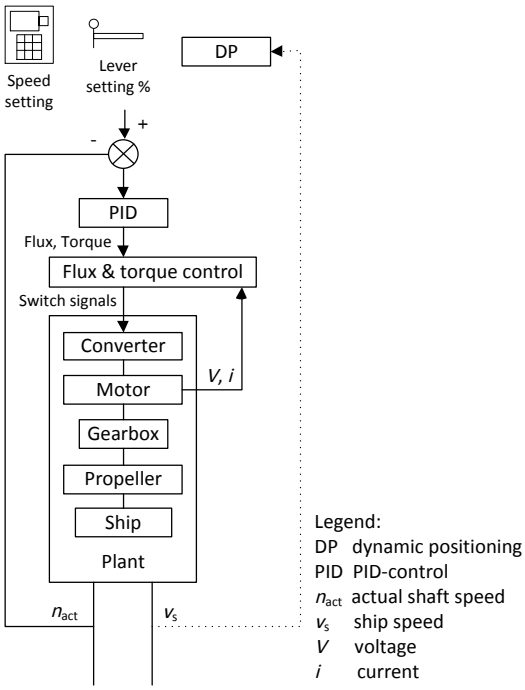

Figure 2.15: Typical schematic presentation of control strategy for electric drive.

Depending on how accurate this control needs to be, torque control using *Field Orientation*, *Direct Torque Control* or *Direct Self Control* can be applied. These torque control strategies are mostly used in combination with an outer speed control loop. An extensive description of these control-methods for induction motors and references to the associated literature can be found in Trzynadlowski, (2001). These modern control strategies can achieve almost instantaneous control of torque of the electric motor and, therefore, meet any requirement as defined for the drive. Furthermore, electric motors can provide full torque at every speed and can deliver above nominal torque for short time periods. Nevertheless, the diesel generator has to provide the load drawn from the electrical network. Thus, the speed of control directly influences the loading of the diesel generator and as such the diesel generator imposes restraints on the control of the electric motor.

TORQUE AND POWER CONTROL

While most electric propulsion drives use speed control, as illustrated in Figure 2.15, electric drives with torque and power control can significantly reduce thrust, torque and power fluctuations (Sorensen *et al.* 2009), as Faber, (1993) already concluded for mechanical propulsion. Sorensen *et al.* (2009) compare speed, torque and power control and conclude thrust losses in heavy seas are significantly reduced with both torque and power control. A combined torque and power controller demonstrates the most robust tracking performance in normal conditions. However, in extreme conditions due

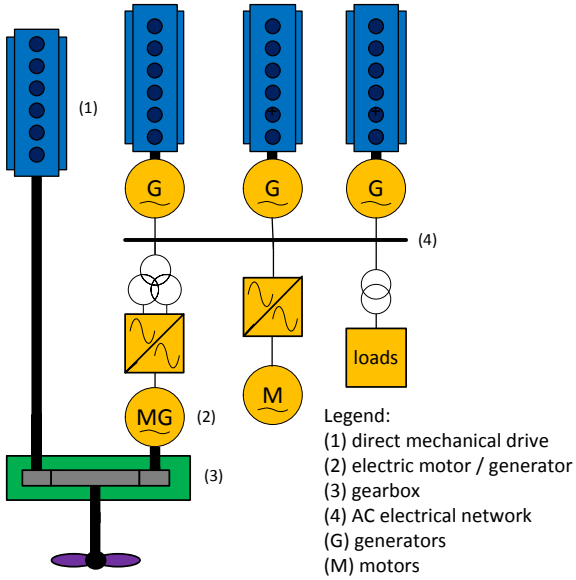

Figure 2.16: Typical hybrid propulsion system.

to heavy weather, the propeller can lift out of the water or endure ventilation. In these conditions, torque and power control can lead to propeller over-speed. Smogeli *et al.* (2008) propose two control strategies to prevent propeller over-speed: one that bounds the propeller speed with a PID control action and one that detects ventilation and subsequently reduces torque or power to reduce shaft speed to a value at which thrust loss does not occur any longer. While the first strategy prevents propeller over-speed, the second strategy achieves minimal thrust loss and highest propulsive efficiency. Similar to these strategies, Zhao *et al.* (2016) propose to reduce the shaft speed setting with a *speed modulation* control strategy when ventilation occurs, again, to reduce thrust loss.

2.4. HYBRID PROPULSION

WHEN the auxiliary load is only a fraction of the required propulsive power, the losses associated with the electrical conversion lead to increased fuel consumption for electric propulsion systems (McCoy, 2002). The extra electrical equipment also leads to increased weight, size and cost (Gemmell *et al.* 2014). Therefore, ships that frequently operate at low speed can benefit from a hybrid propulsion system (Castles *et al.* 2009; Sulligoi *et al.* 2012). In hybrid propulsion, a direct mechanical drive (1) provides propulsion for high speeds with high efficiency. Additionally, an electric motor (2), which is coupled to the same shaft through a gearbox (3) or directly to the shaft driving the propeller, provides propulsion for low speeds, thus avoiding running the main engine inefficiently in part load. This motor could also be used as a generator for electrical loads on the ships services electrical network (4). A typical layout for such a hybrid propulsion system is presented in Figure 2.16.

When the mechanical drive engine is running, this system allows generating capacity either from the electric generator or from the generating sets. Typically, rule-based control or the operator determines the generating capacity.

2.4.1. BENEFITS AND CHALLENGES OF HYBRID PROPULSION

Because hybrid propulsion is a combination of electrical and mechanical propulsion, it can benefit from the advantages of both, as discussed in Section 2.2 and 2.3. However, in order to achieve these benefits, a proper design (of the hybrid propulsion) is required and often a trade-off between these requirements has to be made. The control strategy allows an optimal trade-off and can use the extra degree of control by transferring electrical power from the mechanical drive to the electrical network and vice-versa. The main challenge for the hybrid propulsion design is to balance the trade-off between all requirements and design a control strategy to achieve this balance.

2.4.2. APPLICATION OF HYBRID PROPULSION

Typical applications of hybrid power and propulsion systems are naval frigates and destroyers (Castles *et al.* 2009; Sulligoi *et al.* 2012), towing vessels (Wijsmuller *et al.* 2007) and offshore vessels (Barcellos, 2013; MER, 2008). Castles *et al.* (2009) describe the economic benefits of a hybrid propulsion system for US Navy *DDG-51* class assuming rule-based control. The US Navy uses gas turbines as its prime movers, also for its ship services' generators. The part load specific fuel consumption of gas turbines is very poor, much worse than that of diesel engines. With gas turbines, hybrid propulsion thus can lead to significant fuel savings. Sulligoi *et al.* (2012) discuss the Italian Navy *FREMM* frigate configuration with diesel generators and a sprint gas turbine main engine. However, they do not discuss the economic benefits. Wijsmuller *et al.* (2007) compare the economic benefits of a number of hybrid-propulsion architectures for an emergency towing vessel. With the operational profile of this vessel, the engine power is 20% or less at 90% of its operational time. The most economical configuration for the given operational profile was hybrid propulsion with a large and small engine on each shaft, supporting medium patrol speeds (45% of the time) efficiently, and using electric propulsion for low speed patrol and loitering speeds (45% of the time). Finally, Barcellos, (2013) presents case studies in applying hybrid propulsion to offshore vessels. These studies show that the increased transit distance in combination with stringent availability requirements for DP operations suit hybrid propulsion very well. The mechanical propulsion plant can be optimised for efficient transit and the electrical plant for DP operation with high availability. Thus, fuel savings of more than 10% were achieved. The results from these studies support the assumption that hybrid propulsion is typically economical when the operational profile has distinct operating modes with a significant amount of time at low power. Similarly, Waard, (2015) found that hybrid propulsion provides economic benefits if the vessel sails a significant amount of time below 15% propulsive power, equivalent to 40% of its top speed.

2.4.3. CONTROL STRATEGIES FOR HYBRID PROPULSION

The current control strategies applied in practice and covered in literature for hybrid propulsion are based on two operating modes: mechanical drive and electrical drive.

First, the control strategies discussed in Section 2.3 apply to electric drive mode. Second, the control strategies as discussed in Section 2.2 apply to mechanical drive mode. In this mode, the electric machine can be switched off, used as an electric assist motor or used as a shaft generator. However, very few applications use the electric motor in parallel with the mechanical drive, as will be discussed next.

SHAFT GENERATOR CONTROL

The electric motor can run as a shaft generator if the prime mover has sufficient load margin. In the Italian Navy FREMM frigate configuration the engine driving the shaft is a gas turbine engine with a free power turbine. Due to the free power turbine maximum engine power is available at any shaft speed. Therefore, sufficient load margin is always available, unless the ship is sailing at top speed in off-design conditions. Thus, implementing the electric motor as a shaft generator is feasible for this configuration (Sulligoi *et al.* 2012). The control strategy applied to the converter of the shaft generator is speed and voltage droop control for the power generation plant side of the power converter. Moreover, the electric machine side of the converter uses field oriented control, which is adjusted for the current supplied by the power system side of the converter to maintain the DC voltage. These strategies combined prove to be successful in running a shaft generator and diesel generator in parallel, according to the work performed in Sulligoi *et al.* (2012). However, due to using speed and voltage droop control, the load dynamics are shared equally between the shaft generator and the diesel generator. This might not make optimum use of the gas turbine power that is available, as the gas turbine can handle load dynamics more easily than the diesel generator. Alternatively, running the diesel generator in speed droop control and the shaft generator in isochronous control would force the gasturbine to handle all dynamics. However, further research would be required to determine whether this could lead to a stable control strategy.

ELECTRIC MOTOR ASSIST

When the electric drive is designed to run in parallel with the mechanical drive, it can be used to increase the top speed of the ship and reduce the engine thermal loading and thus NO_x emissions. Topaloglou *et al.* (2016) propose a control strategy that uses the electric motor torque to reduce the main engine's air excess ratio λ, which indicates the amount of air available in the engine cylinder during combustion, and therefor is a measure of engine thermal loading. The proposed control strategy increases torque of the electric drive to maintain the reference λ value, which is a result of a static map as a function of engine torque, speed and charge pressure. During an acceleration manoeuvre simulated on the testbed of the National University of Athens, the proposed strategy achieves a 16% reduction in NO_x emissions and a 0.25 increase in minimum air excess ratio λ from 1.85 to 2.15, thus significantly reducing engine thermal loading during acceleration manoeuvres. Therefore, the proposed strategy clearly demonstrates the potential of performance improvement when the electric drive is used in parallel with the main diesel engine.

2.5. ELECTRICAL PROPULSION WITH HYBRID POWER SUPPLY

IN electrical propulsion with hybrid power supply, a combination of two or more types of power source can provide electrical power. We propose to classify power sources into:

- Combustion power supply, from diesel engines (1), gas turbines or steam turbines;
- Electrochemical power supply from fuel cells; or
- Stored power supply from energy storage systems (2) such as batteries, flywheels or super capacitors.

While extensive literature is available on the development of fuel cells, commercial application of electrochemical power supply in the maritime environment is limited. van Biert *et al.* (2016) provide a review of fuel cell systems for maritime applications, which includes an overview of maritime fuel cell research applications. Application of series production fuel cells on board has been limited to air independent propulsion on submarines, as the storage of the hydrogen fuel limits the amount of energy that can be produced without refuelling (Psoma *et al.* 2002; Sattler, 2000). Research now is focussed on more compact storage of hydrogen (Sattler, 2000), fuel cells with or without reformers that can use other fuels such as methanol, LNG or even diesel oil (Leites *et al.* 2012), and fuel cells combined with diesel engines or gasturbines to achieve high efficiencies while using more energy dense fuels (van Biert *et al.* 2016).

The development of stored power supply for automotive and power system application is an extensive research area. However, purely stored power supply on ships is limited to ferry *MV Ampère*, due to its limited range. The available energy storage technologies are categorised in Roskilly *et al.* (2015) and covered extensively in its references. Research into energy storage technology on board ships is significantly more limited and primarily focussed on the use of battery technologies (Dedes *et al.* 2012; Lan *et al.* 2015; Ovrum *et al.* 2015; Zahedi *et al.* 2014), although Lan *et al.* (2015) address sizing of a hybrid combination of combustion, photovoltaic (PV) and stored power supply. Specifically for handling pulsed loads on naval vessels, hybrid energy storage technology is required to supply up to 10 GW during microseconds bursts to high energy weapons. This hybrid energy storage combines high power density of ultra capacitors with high energy density of batteries (Lashway *et al.* 2016). In the remainder of this chapter, the main type of energy storage to be considered is the battery.

The idea to use battery energy storage for propulsion originates from the automotive industry, which increasingly uses batteries to store braking energy instead of dissipating it, to run the engine in a more efficient operating point, and to enable switching off the main engine, particularly when operating at no load or part load. A typical architecture of an electrical propulsion plant with hybrid power supply is shown in Figure 2.17. In this case, energy storage (2) is connected to the main distribution bus. However, energy storage can be connected at various locations of the electrical system:

- At the main high voltage bus bar through an AC/DC converter;
- At the LV bus bar through an AC/DC converter;
- Directly or through a DC/DC converter to the DC link of the propulsion converter.

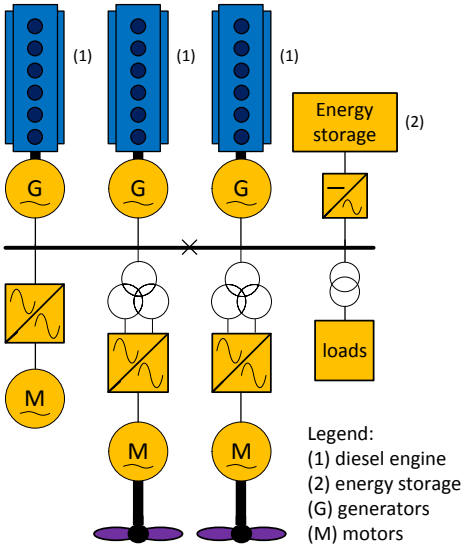

Figure 2.17: Typical electrical propulsion system with hybrid power supply.

2.5.1. BENEFITS AND CHALLENGES OF ELECTRICAL PROPULSION WITH HYBRID POWER SUPPLY

The benefits of applying stored and hybrid power supply in ship power and propulsion plants can be diverse:

- The energy storage can provide the required electrical power and enable switching off one or more engines when they would be running inefficiently at part load. The energy storage can then be recharged when the engine is running in an operating point with lower SFC and CO_2 and NO_x emissions. This can save fuel, reduce emissions, reduce noise, increase comfort and enable temporarily sailing without emissions, noise and vibrations from the engines (Zahedi *et al.* 2014).
- The battery can enable load levelling, by handling the power fluctuation. This results in constant loading of the engines, maintaining a more efficient operating point. Dedes *et al.* (2012) propose a hybrid propulsion configuration with hybrid power supply for dry bulk carriers and indicate this configuration could achieve significant savings in fuel consumption, CO_2 and NO_x emissions.
- The battery can enable peak shaving; the battery delivers power during periods where high power is required and recharges when less power is required. This strategy can run engines more efficiently and reduce installed power (Dedes *et al.* 2012).
- When the battery is recharged from the grid alongside, this can reduce fuel consumption and local emissions. However, the cost and emissions of power generation in the grid then has to be taken into account, although this power might be generated from renewable energy sources (Breijs *et al.* 2016; Volker, 2013).

- The battery can be used to store regenerated energy when braking on electric motors. In current electric propulsion plants, this energy is dissipated in braking resistors. However, the fuel savings due to storing braking energy from propulsion are limited because ships do not often have to stop quickly. On the other hand, significant energy can be regenerated in ships with heavy crane installations (Ovrum *et al.* 2015) and in offshore and drilling vessels with heave compensation.
- The battery can provide back-up power during a failure of combustion power supplies (diesel generators). This can omit the need for running extra diesel engines as spinning reserve and can potentially reduce the installed power on vessels with a requirement for a high availability of propulsion, for example DP vessels (Zahedi *et al.* 2014).

The battery in a hybrid power supply runs in parallel with generators. This leads to the following challenges:

- The control strategy needs to maximise the reduction in fuel consumption and emissions, by charging and discharging the battery at the right time.
- Load fluctuation on diesel engines increases fuel cost, emissions and maintenance load. Thus the control strategy should ideally share dynamic load between the battery and the diesel engine in such a way that the fuel cost, emissions and maintenance load of all power suppliers are minimised.
- The increase in purchase cost due to the installation of batteries needs to be minimised or offset by reduced installed power from diesel engines.

2.5.2. APPLICATION OF ELECTRICAL PROPULSION WITH HYBRID POWER SUPPLY

Batteries have only recently been applied in maritime applications, but their popularity is growing very quickly. For tugs and ferries, for example, the potential reduction of fuel consumption and emissions has led to investigation and application of electrical propulsion with hybrid power supply (Breijs *et al.* 2016; Volker, 2013). Batteries have also been used increasingly in offshore. However, most offshore applications have been equipped with a DC electrical network, to be covered in Section 2.7.

Volker, (2013) investigates the economic benefits of an electric propulsion system with hybrid power supply for towing vessels and ferries. Both case studies consider batteries for energy storage with rule-based control. The calculated fuel savings of the hybrid propulsion plant are marginal when the battery is not recharged from the shore grid. The results of studies like these, however, strongly depend on the operational profile. Moreover, no sensitivity studies have been performed.

Alternatively, the ferry *MV Hallaig* with electrical propulsion and hybrid power supply has demonstrated the potential of this architecture when using advanced control strategies. This ferry, delivered by IMTECH in 2014, is illustrated in Figure 2.18. Fuel savings of 35% were demonstrated during trials, caused by two effects. First the batteries were charged overnight, leading to 24% fuel savings. For this 24% fuel saving, electrical power from the grid was used, which has to be accounted for. However, using renewable energy for this power can significantly limit the environmental impact. Moreover, local

Figure 2.18: Ferry with electrical propulsion and hybrid power supply.

emissions in the operating environment of the ferry are reduced with this concept. The second part, 11% fuel savings, was attributed to optimising the use of the engine and the battery over the operating cycle of the ferry with the energy management system (Breijs *et al.* 2016; Caledonian Maritime Assets Limited, 2015; Rampen *et al.* 2014).

2.5.3. CONTROL STRATEGIES FOR ELECTRICAL PROPULSION WITH HYBRID POWER SUPPLY

Microgrids in the terrestrial grid often combine fossil-fuel power sources with renewable energy sources and energy storage and can thus be classified as a hybrid power supply. Therefore, literature on microgrid control strategies could provide useful insight into control of hybrid power supplies on ships. The control strategy for hybrid power supply consists of three levels: primary control, secondary control and tertiary control (Guerrero *et al.* 2011; Unamuno *et al.* 2015). Unamuno *et al.* (2015) classify primary control strategies into grid following and grid forming strategies, which are applicable to ships connected to the shore connection and at sea respectively; secondary strategies into centralised and non-centralised control; and tertiary strategies into centralised and distributed control strategies. Subsequently, they review and classify the strategies proposed in literature.

First, primary control has to achieve voltage and frequency stability. For completeness, Han *et al.* (2016) review and classify communication-based control strategies and droop-characteristic-based control strategies for inverter fed AC microgrids. However, generators on ships are connected to the grid directly, as opposed to most microgrid distributed generation (DG), which is often connected through frequency inverters (Han *et al.* 2016). Therefore, the primary control strategy is droop control, as discussed in detail in Olivares *et al.* (2014) and Zhang *et al.* (2010), and also proposed for shaft generator control on the grid side in Sulligoi *et al.* (2012) (Section 2.4.3). Moreover, this droop control strategy also achieves a scalable hierarchical control strategy for a multizone grid, as discussed extensively in Guerrero *et al.* (2011). Thus, the zonal distribution system can

be very robust for failures in grid sections, which is of particular interest for naval vessels, offshore ships and future autonomous vessels that require a high degree of availability and reliability (Geertsma *et al.* 2009; Hebner *et al.* 2016). To conclude, Sudhoff *et al.* (2015) describe a reduced scale naval DC microgrid that demonstrates such a zonal distribution system using droop control.

Secondly, secondary control strategies aim to correct the deviations in voltage and frequency, and balance demand and supply (Guerrero *et al.* 2011) (see also Section 2.3.3). Unamuno *et al.* (2015) classify secondary control for microgrids in centralised and non-centralised control. Ships power systems typically use centralised secondary control due to the limited size of the grid, although distributed control strategies might be considered for ships with very high continuity of power demands, such as naval ships, and might be an interesting enabler for future autonomous vessels (Geertsma *et al.* 2014, 2009; Visser *et al.* 2017).

When microgrids are connected to the grid, their tertiary control manages the active and reactive power flow to and from the main grid by centrally changing the global voltage and frequency settings of the microgrid as described by Guerrero *et al.* (2011). Unamuno *et al.* (2015) also review tertiary control strategies that use distributed management. These tertiary strategies only apply to the ships grid when connected to the shore connection and running at least one of its own power sources in parellel, which currently is not common practice. Alternatively, Shi *et al.* (2015) propose a distributed Energy Management System (EMS) that solves the optimal power flow problem of the microgrid both in island and grid-connected operation. They consider a cost function for the use of the battery that allocates cost to fast charging, switching between charging and discharging, and deep discharging. This strategy has a strong resemblance with energy management strategies used in automotive applications and can be applied to ship's hybrid power supplies.

The remainder of this section will discuss options for tertiary energy management of hybrid power supplies; to determine the power split between the different power sources. Sciarretta *et al.* (2014) discuss a comparison between various EMS strategies using a control benchmark. The strategies are classified as heuristic control strategies that are rule based and Equivalent Consumption Minimisation Strategies (ECMS) that solve an optimal control problem to minimise fuel consumption (Wirasingha *et al.* 2011). These strategies and the equivalent maritime strategies will be discussed next. Subsequently, control strategies that consider the future operating profile and uncertainties in their control problem (Haseltalab *et al.* 2016; Vu *et al.* 2015) and that are aimed at levelling the generator load based on the historic load profile will be covered (Ovrum *et al.* 2015).

HEURISTIC CONTROL STRATEGIES

In heuristic control strategies, logical rules determine the operating mode of the plant and the setting for the battery charge and discharge system. When the battery is applied to serve distinct operating modes, heuristic control strategies can achieve the aim of the design. For example, when a ship needs to be able to run silently or without emissions during certain periods, the engines can be switched off in this operating mode. Also fuel savings can be achieved with rule-based control, particularly when the operating profile consists of discrete, distinct operating modes.

An example of such a rule-based control strategy is described in Sciberras *et al.* (2012). This control strategy utilises the battery at low speeds for propulsion while shutting down the engine, and at high speed to electrically assist the engine. Sciberras *et al.* (2012) demonstrate that the amount of fuel saved by such a strategy depends on the battery capacity and thus system weight and cost. However, a comparison with a baseline without batteries lacks.

Another heuristic control approach is the map-based approach. In this approach multidimensional maps, whose entries are system parameters, determine the selection of the operating mode and the system settings. In the automotive industry this approach can achieve good fuel efficiency, although the Equivalent Consumption Minimisation Strategy (EMCS) outperforms heuristic control (Sciarretta *et al.* 2014). Map based heuristic control has not been covered in maritime applications or research yet to the best of our knowledge.

EQUIVALENT CONSUMPTION MINIMISATION STRATEGY

In the Equivalent Consumption Minimisation Strategy (ECMS), the optimum power management setpoints are calculated with an optimal control problem formulation that minimises the fuel consumption of the engine and the equivalent fuel consumption of the battery, which accounts for the fact that the battery needs to be recharged. In a comparison of various control strategies against a control benchmark of a hybrid electrical vehicle, various variants of the ECMS consumed the smallest amount of fuel when simulated over an unknown operating profile (Sciarretta *et al.* 2014). A schematic presentation of such a control strategy for hybrid power supply using ECMS is presented in Figure 2.19.

The energy management system of the hybrid ferry discussed in Section 2.5.2 uses an ECMS optimisation strategy. In this strategy, cost functions are defined for the fuel use of all power suppliers, including the battery. Load is shared between power supplies to minimise cost. Fuel savings of 10% due to the energy management system were demonstrated during operational trials (Breijs *et al.* 2016; Caledonian Maritime Assets Limited, 2015).

POWER MANAGEMENT THROUGH OPERATING LOAD ESTIMATION

Similarly, Vu *et al.* (2015) cover a power management scheme that determines the optimal power split based on a known future operating profile. This strategy uses the nonlinear optimisation approach to find the minimum of a cost function that accounts for fuel consumption and battery life. Furthermore, the strategy can also control discrete events such as the starting and stopping of multiple generators, as opposed to automotive strategies, which consider only a single engine. If the future operating profile is not known in advance, the strategy uses a novel load prediction scheme, which anticipates future load demand based on historical load demand data.

In a case study of an Electric Tug, Vu *et al.* (2015) show that the proposed strategy can achieve a 9% performance improvement for the combined cost function compared to a rule-based controller as described in Sciberras *et al.* (2012). This improvement is mainly due to the fact that the optimal power management scheme ensures the battery is at its minimum charge at the end of the operating cycle while the rule based controller aims to maintain maximum battery charge; the battery delivers 7% of the required energy for the

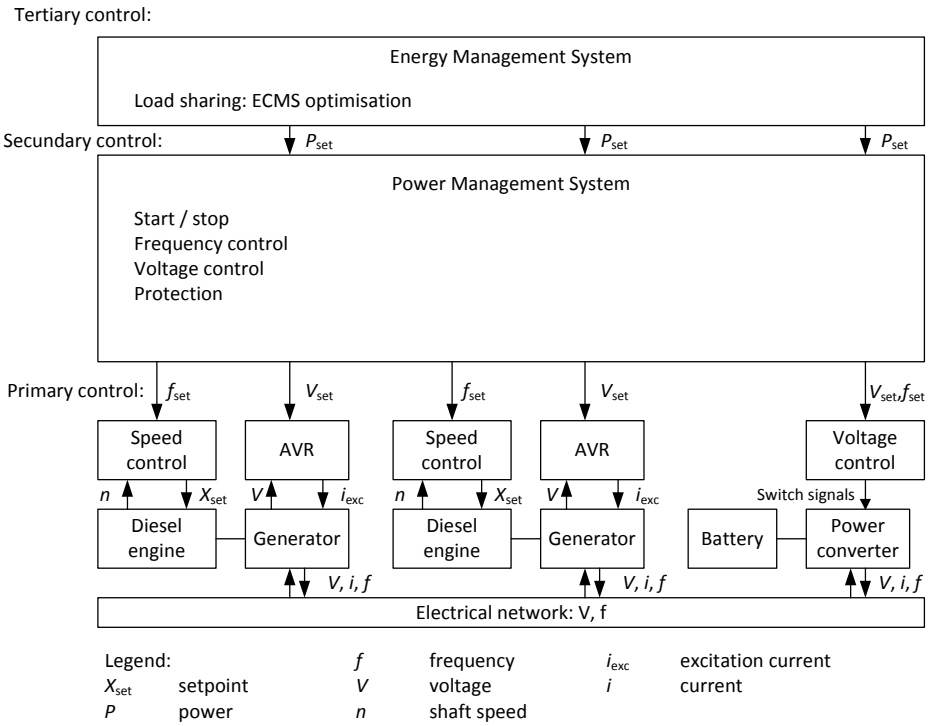

Figure 2.19: Control strategy for hybrid power supply with ECMS.

given operating profile, and the power flow optimisation accounts for 2% fuel consumption reduction. Finally, Haseltalab *et al.* (2016) propose an Energy Management strategy that uses Model Predictive Control to account for future power demand in the presence of uncertainty and environmental disturbances. They demonstrate the feasibility of this approach with a simulation study.

LOAD LEVELLING

When the engine operates close to the optimal working point from a fuel consumption perspective, load fluctuation due to fluctuating propulsion load (in high sea state) or other load disturbances, can cause increased fuel consumption. Then, providing (a percentage of) the fluctuating load from a battery can reduce the fuel consumption increase. Furthermore, dynamic engine loading can be reduced, potentially reducing engine wear. This strategy can particularly deliver fuel savings for transient loads like cranes or dredging pumps. For example, the fuel consumed during crane operation on a dry bulk vessel of 50,000 dwt can be reduced about 30% with the novel hybrid control strategy proposed in Ovrum *et al.* (2015). This energy management strategy aims to run the diesel generator at the average required power demand over the operating profile, looking at the historical power demand only, and uses battery charging and discharging

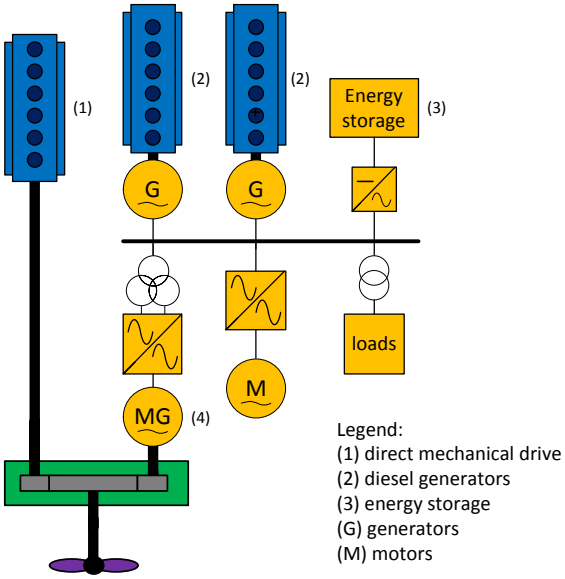

Figure 2.20: Typical hybrid propulsion system with hybrid power supply.

to supply the load transients. Moreover, the maximum rate of charging and discharging can be limited to reduce ageing of the battery.

2.6. HYBRID PROPULSION WITH HYBRID POWER SUPPLY

HYBRID propulsion with hybrid power supply utilises the maximum efficiency of direct mechanical drive (1) and the flexibility of a combination of prime mover(s) (2) and energy storage (3) for electrical supply. At low propulsive power an electric drive (4) is available to propel the ship and switch off the main engine (1). The machine providing electric drive can also be used as a generator. A typical architecture is illustrated in Figure 2.20.

Below, the application of this architecture will be covered and subsequently the control strategies for a hybrid propulsion system with hybrid power supply. An overview of control strategies that can be applied for hybrid propulsion has been covered in Section 2.4 and an overview of control strategies for systems with hybrid power supply in Section 2.5.

2.6.1. APPLICATION OF HYBRID PROPULSION WITH HYBRID POWER SUPPLY

Hybrid propulsion with hybrid power supply has first been researched extensively in harbour tugs. Following this research, Damen delivered the first tug with hybrid propulsion and hybrid power supply in 2014. An overview drawing of the vessel is shown in Figure 2.21.

Moreover, hybrid propulsion with hybrid power supply has been applied to the yacht *Savannah*, which Feadship launched in 2015 (Loon *et al.* 2016). To the best knowledge of

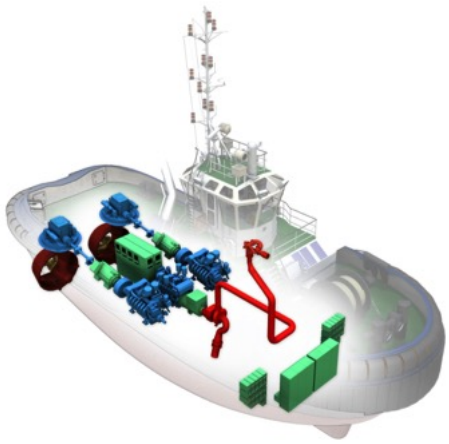

Figure 2.21: Overview drawing of hybrid harbour tug.

the author tugs and yachts are currently the only application in which the combination of hybrid propulsion and hybrid power supplies has been studied or implemented.

2.6.2. CONTROL STRATEGY FOR HYBRID PROPULSION WITH HYBRID POWER SUPPLY

The control strategies that have been investigated for hybrid propulsion with hybrid power supply will be covered in this section.

HEURISTIC CONTROL STRATEGY

Research at Delft University of Technology, suggests that hybrid propulsion with hybrid power supply can deliver significant savings in local emissions, partly by using energy from the batteries that are recharged with a shore connection (Drijver, 2013; Grimmelius *et al.* 2011; Koperen, 2009). These savings can be achieved with a heuristic rule based approach. In this approach the control mode of the plant is determined by the operating mode of the vessel (towing, high speed transit, low speed transit or standby) and the battery state of charge.

This approach can achieve positive results, because the operating modes of the plant lead to very distinct loading of the system. For example, in low speed transit or standby the main engine loading is very low and, therefore, switching off the engine stops the engine operating inefficiently. However, the amount of fuel and emission savings that can be achieved with a heuristic control strategy strongly depends on the operating profile of the ship and on the sizing of the components.

Furthermore, the hybrid propulsion configuration allows designs in which the main engines cannot deliver full bollard pull on their own. However, a design that for delivery

of full bollard pull depends on an electric motor or batteries potentially introduces reliability and safety risks. Thus, in current designs the main engine is sized to deliver full bollard pull without additional power from the electric motor.

EQUIVALENT CONSUMPTION MINIMISATION STRATEGY

In Grimmelius *et al.* (2011) the models required for an ECMS control strategy for hybrid propulsion with a battery as a single electrical power supply are introduced and the application on a tug as a test case is presented. The application does not include a comparison with a rule-based strategy so the benefits of the approach have not yet been established for the case study. Furthermore, practical applications tend to use diesel generators as well, further complicating the optimisation strategy. However, the models used in Grimmelius *et al.* (2011) only need minor additions to include a diesel generator power source.

2.7. ELECTRICAL PROPULSION WITH DC HYBRID POWER SUPPLY

ONE of the major drawbacks of electrical propulsion is that the fuel consumption of the engine in part load is higher for an engine running at fixed speed than for an engine running at variable speed (such as a direct drive engine). This was illustrated by the fuel consumption curves in Figure 4.3. This drawback of electrical propulsion has led to the concept of variable frequency electrical networks as discussed in Section 2.3. Application of variable frequency networks has been very limited, mostly because other consumers require fixed frequency power supply. However, DC distribution systems can also enable variable engine speed.

Historically, DC systems have been applied in specific applications such as submarines. However, fault protection and power system stability issues have limited their application. The continued development of power electronics (Hodge *et al.* 2008) and intelligent schemes to protect against faults (Butcher *et al.* 2009) and ensure power system stability (Herrera *et al.* 2017; Zadeh *et al.* 2013) have enabled more widespread application of DC systems. The most important reasons for applying DC systems are increased fuel efficiency when running generators in part load and reduced power conversion losses (Zahedi *et al.* 2014). A typical architecture of electrical propulsion with DC hybrid power supply is presented in Figure 2.22.

2.7.1. BENEFITS OF HYBRID DC POWER SUPPLY

The benefits of applying hybrid DC power supply to ships with electric propulsion are as follows:

- The DC architecture allows to run the diesel engine at variable speed, potentially leading to a reduction in fuel consumption, emissions, noise and engine mechanical and thermal loading.
- DC architectures are resilient to faults, because power electronics allow instantaneous control of electrical variables and electrical faults do not spread across the electrical network and disturb network voltage and frequency.

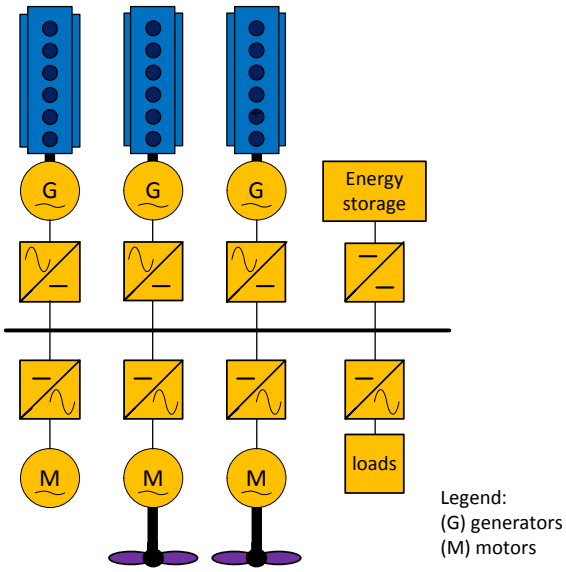

Figure 2.22: Electrical propulsion with DC hybrid power supply.

- The amount and size of switchgear potentially reduces when the power electronics in the system perform fault protection (Butcher *et al.* 2009).

Although DC architectures can provide significant benefits, the following challenges need to be resolved:

- All power sources and loads need to be connected to the DC network through power electronic converters. If a large amount of fixed frequency AC loads need to be fed, this can lead to a significant cost increase. However, if a significant amount of the total load is already fed through variable speed drives, DC architectures can lead to cost reduction (Parker *et al.* 2009).
- In order to enable DC architectures, fault protection needs to be resolved (Butcher *et al.* 2009).
- A coordinated control strategy is required to resolve stability issues and achieve optimal performance for the criteria listed in Section 3.1 (Herrera *et al.* 2017; Zadeh *et al.* 2013).

2.7.2. APPLICATION OF ELECTRICAL PROPULSION WITH HYBRID DC POWER SUPPLY

Traditionally, DC power supply systems have been applied in submarines in combination with large battery packs to enable air independent propulsion. More recently, the US Navy has also applied a DC distribution system to its DDG-1000 destroyers (Doerry *et al.* 1996; Naval Sea Systems Command (NSSC), 2007; O'Rourke, 2009). Similarly, the Royal Navy has considered DC power systems for its frigates in an extensive development programme, but has not implemented it yet (Butcher *et al.* 2009; Danan *et al.*

2005; Hodge *et al.* 1996, 1997, 1998, 1999, 2000, 2001, 2008; Mattick *et al.* 2005). Both these navies applied or considered DC power systems for their resiliency and to enable pulsed power loads. The designs contained a great amount of power electronic conversion equipment that was used to decouple voltage and frequency of different parts of the system, thereby achieving increased resilience. A key feature of these naval DC systems is their distributed nature.

DC electrical systems have been launched extensively in recent years in ferries and offshore vessels. Alewijnse delivered the DC power system of Offshore Supply Vessel MV Jaguar in 2012, Siemens delivered its first DC system with hybrid power supply on the Platform Supply Vessel MV Edda Ferd in 2013 and, finally, ABB delivered its first hybrid DC grid in 2013 on MV Dina Star. Other applications that utilise DC hybrid power supply systems are drilling ships, research vessels and wind farm support vessels. DC was also applied on the world's first large fully electrical vessel, a ferry in Norway; Siemens delivered the MF Ampere in 2015 with a DC grid only powered by batteries.

An attractive element that has led to the application of DC grids in offshore vessels is that their major electrical consumers use variable speed drives, which have a basic DC-architecture due to its DC-link. Examples of electrical consumers that can be fed from a shared DC-link are heavy-lifting cranes, variable speed propulsion and thruster drives, heavy pumps and compressors. Another feature of these DC grids in offshore vessels and ferries is their centralised design. The system comprises one or two DC switchboards. Further distribution of electrical power typically is AC from power converters. This ensures the stability and fault protection issues only have to be solved for a small local system, and requires only a limited amount of equipment that can switch DC fault currents. However, the continued development of DC systems and intelligent fault protection that reduces the requirement for switchgear is likely to lead to more distributed DC systems in the near future (Butcher *et al.* 2009).

Finally, DC hybrid power supply architectures appear very promising for luxury yachts, mainly to increase comfort, without losing performance. For these yachts the DC architecture allows easy integration of batteries and silent variable-speed electric drives (Bosich *et al.* 2013; Loon *et al.* 2016).

2.7.3. CONTROL STRATEGY FOR ELECTRICAL PROPULSION WITH DC POWER SUPPLY

This section covers the objectives of the control strategy for shipboard DC power systems and research into shipboard DC power system control.

PRIME MOVER FREQUENCY CONTROL

In DC power systems, the frequency of each generator can be selected independently of other generators as the AC voltage is rectified. As such, the speed-governing control loop is not used to achieve load sharing between generators in AC systems. This allows the engine speed to be optimised for any given criteria, such as minimised fuel consumption, optimal engine loading, minimised emission and minimised noise frequency.

Zahedi *et al.* (2014) propose a control strategy that governs engine speed to achieve minimal fuel consumption for the given load. In a simulation of an offshore support

vessel over seven operating modes, the DC system with variable engine speed resulted in 8% fuel savings compared to the conventional system discussed in Section 2.3.

LOAD SHARING

Load sharing in AC systems is achieved by frequency droop control, while the equivalent strategy for DC systems is voltage droop control (Zahedi *et al.* 2013). Therefore, by setting different values for voltage droop for different power sources in a DC system the power ripple can be unevenly split over the power sources. Thus, in a DC system with hybrid power supply, the share of dynamics taken up by the different types of power supply can be controlled.

OPTIMUM LOAD LEVELLING STRATEGY

Zahedi *et al.* (2014) propose an online optimisation strategy which utilises the battery first to run the generators at the optimum load from a fuel consumption point of view by applying a charge-discharge (CD) strategy and secondly to supply an optimum fraction of the power ripple. This CD strategy moves the operating point from an inefficient working point on k engines (k being the number of engines running to supply the required power) to a more efficient working point on k or $k-1$ engines at lower power, while discharging the battery, and, then, to another more efficient working point on k or $k+1$ engines at higher power, while charging the battery. This strategy thus does not aim to deplete the battery over the operating trajectory to recharge the battery from the grid.

This strategy requires determining the average power and power ripple. The average power and power ripple over a certain time interval or during an operating mode depend on future data as well. For online optimisation, these parameters are obtained filtering instantaneous values with experimentally derived time constants. In simulations, which use statistical values for a number of operating modes, the strategy results in 7% fuel savings. The results, however, strongly depend on the selection of time constants, which in practice might not be constant.

MODEL PREDICTIVE CONTROL FOR MULTIPLE CRITERIA

Park *et al.* (2015) propose real-time MPC to adjust the secondary control parameters, in the study case primary generator voltage droop, secondary generator power setpoint and propulsion motor power setpoint, to optimise for multiple performance attributes while maintaining power system component constraints. The primary control loops that the secondary control influences are voltage control for the primary power source and power control for the secondary power source and propulsion motor. The work consists of numerical simulations, real-time simulations and experiments on a testbed and demonstrates that real-time MPC is feasible and can be used for a control strategy that trades off conflicting performance requirements, both for known and unknown future operating conditions.

2.8. DISCUSSION AND SUMMARY

THIS chapter has categorised and reviewed the major current and future power and propulsion system architectures and their associated control strategies. This section provides an overview and discussion of the various power and propulsion architectures,

their benefits and trends for future applications, as well as a summary and discussion of available control strategies and their applicability to the various power and propulsion architectures.

2.8.1. POWER AND PROPULSION SYSTEM ARCHITECTURES

Table 2.1 summarises the benefits and drawbacks of the power and propulsion technologies covered in this chapter. Table 2.2 presents the applications of these power and propulsion architectures and illustrates the trends by listing potential future applications for these architectures.

In the '90s, the development of power electronics led to extensive application of electrical propulsion in order to overcome the poor part load efficiency and robustness of mechanical propulsion. This electric propulsion was first introduced in cruise ships. Capital naval ships, offshore vessels and other incidental applications followed promptly, as the hotel load for these ship types is a significant part of the total load.

Later, hybrid propulsion was introduced for vessels both operating a large proportion of time at design speed, and operating significant periods at low power, below 40% of their top speed, in order to maintain the very good efficiency at design speed. For example, warships and patrol vessels have increasingly utilised hybrid propulsion, just as tugs and offshore vessels.

More recently, the development of high power batteries in the automotive industry has enabled their use in shipping. At the expense of increased purchase and replacement cost, batteries can provide load levelling, efficient back-up power and a zero-noise-and-emission propulsion mode. Batteries have thus been increasingly applied in tugs, yachts, offshore vessels and ferries, due to the reducing cost of batteries, even though system complexity increases. Moreover, the opportunity to store regenerated energy is likely to lead to hybrid power supplies in drilling vessels and crane vessels in the near future. Furthermore, fuel consumption, emissions and installed power could be reduced for cargo ships as well, if batteries are used to level propulsion load fluctuation from heavy seas.

The use of purely stored power supply from batteries is limited to vessels that require a very short range, such as ferries like *MV Ampère*. Electrochemical power supply from fuel cells can be used for submarines that require a longer, but still limited range, with hydrogen stored in metal hydride cylinders.

Furthermore, the increase in the utilisation of power electronics in AC systems for main propulsion, thrusters, variable speed pumps, compressors and other drives has enabled the introduction of DC power systems. Initially, these DC power systems consisted of a number of drives with a shared DC bus. Subsequently, all loads were provided through power electronic converters. In such a configuration, a DC grid enables diesel generators to run at variable frequency, which reduces fuel consumption and engine maintenance. This reduction has prompted DC application in yachts, offshore vessels and ferries. Moreover, some naval vessels use electrical propulsion with DC hybrid power supplies to generate pulsed power for high energy weapons.

Initial research suggests DC power supply supported with energy storage can save 10 to 15% fuel, reduce CO_2 emissions and improve engine loading, at the cost of a slight increase in NO_x emissions, due to reducing engine speed in part load. These benefits could well lead to the application of DC hybrid power supplies for electric propulsion in

Table 2.1: Benefits and drawbacks of propulsion and power supply (PS) technologies.

Technol.	Benefit	Disadvantage	References
Mechanical propulsion	Low loss at design speed Low CO_2 and NO_x emissions at design speed Low conversion losses	Poor part load efficiency Mechanical transmission path of noise Low redundancy High NO_x at low speed	Fig 4.3 & 2.3, Ko *et al.* 2017 Guillemette *et al.* 1997; van Spronsen *et al.* 2001 Vrijdag *et al.* 2010 Baldi *et al.* 2014; Linden, 2017
Electrical propulsion	Robustness Match load with gener. Reduced NO_x emission at low speed High availability Potentially low noise	Const. generator speed Losses at design speed Risk of constant power load instability	Vie, 1998 Moreno *et al.* 2007 Sulligoi *et al.* 2016; Vanderpump *et al.* 2002 Fig 2.3
Hybrid propulsion	Low loss at design speed Robustness Matching load & engines at low speed Potentially low noise on electric drive	Const. generator speed System complexity	Wijsmuller *et al.* 2007 McCoy, 2002 Castles *et al.* 2009; Gemmell *et al.* 2014 Sulligoi *et al.* 2012; Waard, 2015
Electro-chemical PS	Air independant No harmfull emissions High efficiency and low noise	Limited range Safety Complex with reforming	Psoma *et al.* 2002 van Biert *et al.* 2016 Leites *et al.* 2012; Sattler, 2000
Stored DC PS	Air independant No harmfulle emissions and noise	Very limited range Safety	*MV Ampere*
Hybrid power supply	Load levelling Zero noise and emission Store regenerated energy Efficient back-up power Enabling pulsed power Reduced fuel cons. & emissions	Const. generator speed System Complexity Safety due to battery Battery cost	Dedes *et al.* 2012; Volker, 2013 Loon *et al.* 2016 Ovrum *et al.* 2015 Zahedi *et al.* 2014 Lashway *et al.* 2016 Breijs *et al.* 2016; Rampen *et al.* 2014; Vu *et al.* 2015 Fig 2.3, Topaloglou *et al.* 2016
DC power supply	Variable speed and load Optimal engine loading Red. noise and vibrations Red. fuel cons. and CO_2 Enabling pulsed power	System complexity Cost & losses from power electronics NO_x increase due to variable speed	Zahedi *et al.* 2014 Loon *et al.* 2016 Butcher *et al.* 2009 Hodge *et al.* 2008 Lashway *et al.* 2016

Table 2.2: Trends in application of propulsion (prop) and power supply (PS) architectures.

Archit.	Applications	Future applications	References
Mechanical propulsion	Tugs and yachts	Tugs and yachts	Baldi *et al.* 2014
	Naval vessels	Naval vessels	van Spronsen *et al.* 2001
	Cargo ships & crew suppliers	Cargo ships & crew suppliers	Vrijdag *et al.* 2010
Electrical propulsion	Cruise ships	Cruise ships	Moreno *et al.* 2007
	Capital naval vessels	Capital naval vessels	O'Rourke, 2009; Sears *et al.* 2010
	Offshore vessels		Vanderpump *et al.* 2002
	Drilling & crane vessels		Loyd *et al.* 2003; Vie, 1998
Hybrid propulsion	Tugs		Wijsmuller *et al.* 2007
	Warships and Patrol Vessels	Warships and Patrol Vessels	Castles *et al.* 2009; Sulligoi *et al.* 2012
	Long range offshore vessels		Barcellos, 2013; MER, 2008
Electroch. PS	Submarines	Submarines	Psoma *et al.* 2002
		Ferries	Sattler, 2000; van Biert *et al.* 2016
Hybrid PS	Tugs	Drilling vessels	Breijs *et al.* 2016
	Ferries	Crane vessels	Ovrum *et al.* 2015; Rampen *et al.* 2014; Volker, 2013
Hybrid propulsion & hybrid PS	Tugs	Tugs	Drijver, 2013; Koperen, 2009
	Yachts	Yachts	Grimmelius *et al.* 2011
		Cargo ships	Dedes *et al.* 2012
Electrical prop. & DC hybrid PS	Yachts	Cruise ship	Bosich *et al.* 2013
	Offshore vessels	Naval vessels	Zahedi *et al.* 2013
	Ferries	Drilling vessels	Zahedi *et al.* 2014
	Naval Vessels	Heavy crane vessels	*MV Jaguar, Edda Ferd, Dina Star*
		Dredgers	Doerry *et al.* 1996; O'Rourke, 2009
Hybrid prop. & DC hybrid PS	Yachts	Warships	Loon *et al.* 2016
		Patrol vessels	
		Tugs	
		Long range offshore vessels	

cruise ships, capital naval vessels, drilling vessels, crane vessels and dredgers in future. Furthermore, DC power supply seems equally applicable to hybrid propulsion architectures. Therefore, warships, patrol vessels, tugs and long-range offshore vessels appear promising applications for DC hybrid power supply with hybrid propulsion.

2.8.2. CONTROL STRATEGIES

Table 2.3 lists existing control strategies and their applicability to different power and propulsion systems. Furthermore, this table summarises the benefits of these control strategies.

The traditional method to control ship speed is to perform speed control for propulsion. The operator requests an engine or motor speed setting, which behaves linearly to ship speed, and the control system either injects fuel or switches power electronics to achieve this speed setting (Stapersma *et al.* 2009). However, in dynamic circumstances, due to wind and waves, this leads to load fluctuation that particularly burdens mechanical propulsion engines and leads to higher maintenance cost (Guillemette *et al.* 1997). To reduce engine torque fluctuation, torque or power control can be applied as demonstrated in Geertsma *et al.* (2016) and proven for electrical propulsion in Smogeli *et al.* (2008) and Sorensen *et al.* (2009).

Alternatively, the following three alternative methods for propulsion control with CPP can also reduce engine overloading. First, combinator curve control with CPP can reduce static engine loading and provide accurate manoeuvring. Unfortunately, the combinator curve is usually only designed for the propeller curve in design conditions. Overloading can still occur in off-design and dynamic conditions, and the working point of the diesel engine is not optimised for the specific operating conditions at a certain moment in time. Secondly, an $H\infty$ optimal controller can reduce dynamic engine loading and increase manoeuvrability (van Spronsen *et al.* 2001). Although this strategy significantly reduces dynamic engine loading and increases manoeuvrability, its performance is optimised for minimising speed fluctuation as opposed to minimising engine load fluctuation, which does more damage to the engine. Moreover, this strategy only allows one performance criterion to be optimised and, therefore, does not allow control that adapts to changing ship functions. Finally, the *angle of attack* control strategy governs propeller pitch to achieve the angle of attack on the propeller blade that minimises the risk of cavitation. Sea trials have demonstrated that this approach effectively reduces cavitation, improves manoeuvrability and reduces engine overloading (Vrijdag, 2009).

For AC and DC hybrid power supplies on ships, droop control is the most promising primary control strategy, due to its robustness and scalability, also for zonal distributed power supply. Secondary heuristic control strategies can achieve fuel consumption and emission reductions and a zero-emission operating mode. However, literature from maritime and automotive applications suggests that further fuel consumption and emission reductions can be achieved with a tertiary ECMS control strategy. Application of ECMS strategies on ships has demonstrated fuel consumption can be reduced with 5 to 10%. Further research is required to determine whether other important criteria can be improved with this strategy as well.

Finally, the application of DC power supplies has enabled running the generator at variable frequency, reducing fuel consumption, engine loading, emissions, noise and vi-

Table 2.3: Control strategies.

Control	Appl. architect.	Benefits	References
Speed control	Mechanical, electrical, and hybrid propulsion	Minimum speed fluct. Prevent over-speed Robust control strategy Relation with ship speed	van Spronsen *et al.* 2001 Guillemette *et al.* 1997 N. Xiros, 2002 Vrijdag, 2009; Vrijdag *et al.* 2010
Torque and power contol	Mechanical, electrical and hybrid propulsion	Reduced fuel cons. Improved thermal loading	Stapersma *et al.* 2004 Faber, 1993; Smogeli *et al.* 2008; Sorensen *et al.* 2009
Combinator control	Propulsion with CPP	Prevent static overload Accurate manoeuvring	Vrijdag *et al.* 2008 Geertsma *et al.* 2016; Stapersma *et al.* 2009
Optimal speed & pitch control	Propulsion with CPP	Reduced dynamic load Increased manouevrab.	van Spronsen *et al.* 2001 N. Xiros, 2002
Angle of attack contr.	Propulsion with CPP	Reduced noise Increased manoeuvrab.	Vrijdag, 2009 Vrijdag *et al.* 2010
Electric motor assist	Hybrid propulsion	Improved Manoeuvrab. Lower load & higher speed	Topaloglou *et al.* 2016
Frequency droop & isochronous control	AC power supply	Effective load sharing Splitting load dynamics	Karim *et al.* 2002; Mahon, 1992 Amgai *et al.* 2014; Seenumani *et al.* 2012
Heuristic control	AC & DC hybrid power supply	Different operating modes Zero emission mode	Sciberras *et al.* 2012 Karim *et al.* 2002
ECMS strategy	AC & DC hybrid power supply	Reduced fuel consumption and emissions Optimisation of other criteria	Shi *et al.* 2015; Vu *et al.* 2015 Grimmelius *et al.* 2011 Breijs *et al.* 2016; Rampen *et al.* 2014
Volt. droop load sharing	DC hybrid power supply	Splitting load dynamics Reduced engine loading	Sulligoi *et al.* 2012 Zahedi *et al.* 2013
Optimum load levelling	DC hybrid power supply	Reduced fuel consumption Engine Loading Noise and vibrations	Ovrum *et al.* 2015 Zahedi *et al.* 2013 Zahedi *et al.* 2014
Secondary MPC	Hybrid propulsion & hybrid power supply	Handle conflicting req. Handle unknown future conditions	Haseltalab *et al.* 2016 Grune *et al.* 2011; Park *et al.* 2015

brations. Various optimisation strategies, as the one proposed in Zahedi *et al.* (2014), can achieve significant improvements over various criteria and allow trade-offs between these criteria. Furthermore, MPC can be used for a control strategy that trades off conflicting performance requirements, both for known and unknown future operating profiles (Haseltalab *et al.* 2016; Park *et al.* 2015; Vu *et al.* 2015).

2.9. RESEARCH OPPORTUNITIES ON CONTROL STRATEGIES FOR SMART SHIPS

TECHNOLOGICAL advances in hybrid power and propulsion systems could meet the challenges for smart ships, as discussed in Section 2.1. However, in many cases, the control strategy is vital to improve and maximise performance. Further research into these control strategies is required, with a holistic approach, and in three directions:

- Control of the mechanical drive train for mechanical and hybrid propulsion architectures;
- Control of the electrical machine in hybrid propulsion architectures; and
- Control of hybrid power supplies for hybrid and electrical architectures.

2.9.1. CONTROL OF THE MECHANICAL DRIVE TRAIN

The control challenge of the mechanical drive train is twofold:

- Reduce the impact on engine fuel consumption, thermal and mechanical loading due to load fluctuation from waves and manoeuvring; and
- Control the CPP to optimise the static working point for fuel consumption, emissions, vibrations and static engine loading and the dynamic behaviour for cavitation noise, manoeuvrability and dynamic engine loading.

The review in this chapter has identified three potential strategies to resolve these challenges.

TORQUE CONTROL

Current control strategies for mechanical propulsion all rely on some form of speed control. Although disturbance attenuation can be reduced with advanced speed control strategies, results remain limited (Guillemette *et al.* 1997; van Spronsen *et al.* 2001; N. Xiros, 2002). Another approach is to regulate thrust with torque or power control. With this approach, disturbances would cause more shaft speed fluctuation, while oscillation in engine loading would be reduced. However, shaft speed fluctuation would remain limited as the mechanical propulsion plant has a strong self-regulating performance as demonstrated in Guillemette *et al.* (1997). Thus, the strategy could lead to better thermal loading and reduced fuel consumption, as was shown with limitedly validated models in Geertsma *et al.* (2016) for mechanical propulsion and with models and experiments in Sorensen *et al.* (2009) for electrical propulsion. On the other hand, the controller would have to maintain constraints on fuel injection, over- and under-speed and would require torque measurement. Vrijdag, (2009) described a test set-up on a RNLN M-class frigate,

which used accurate thrust measurement based on optical sensors that can measure shaft deflection up to nanometer accuracy. This thrust measurement, or an equivalent torque measurement device, could be used for this control strategy. For an architecture with hybrid power supplies, torque control would also allow a power setpoint to be used. Then, an optimisation strategy could calculate the optimum load share, in power, between various supplies, for example the main engine, a diesel generator and a battery.

ADAPTIVE COMBINATOR CONTROL

A CPP allows the static operating point to be moved to another point in the engine operating envelope, while maintaining the speed setting (see Figure 2.8). This would influence various performance criteria, such as fuel consumption, emissions, vibrations and static engine loading. A controller could be developed that defines the optimal pitch setting from the optimal static operating points resulting from the minimal weighted cost function of numerous criteria such as the ones mentioned above. However, in order to determine optimal pitch under operational conditions, the control strategy would have to account for uncertainty and for disturbances, most importantly due to waves. *Model Predictive Control* (MPC) can take both these effects into account (Haseltalab *et al.* 2016; Park *et al.* 2015; Vu *et al.* 2015). Furthermore, MPC could also be used to determine the optimum trajectory over a certain future time period, for example during an acceleration manoeuvre (Grune *et al.* 2011; Haseltalab *et al.* 2016; Negenborn *et al.* 2010).

ANGLE OF ATTACK AND TORQUE CONTROL

The *angle of attack* control strategy can demonstrably reduce cavitation and improve acceleration performance (Vrijdag, 2009), but the impact of the angle of attack control strategy on dynamic engine loading has not been investigated yet. However, the angle of attack strategy could be combined with torque control, to achieve stabilised torque and fuel injection. This combined control strategy could be used for a trade-off between various objectives, such as cavitation, manoeuvrability and dynamic engine loading. However, the impact of this control strategy on the static working point of the diesel engine needs to be investigated, because this working point determines fuel consumption, emissions, vibrations and static engine loading.

Furthermore, a trade-off could be made between dynamic performance improvements with the angle of attack control strategy and static performance improvements with adaptive combinator control. This could be achieved by adding the estimated angle of attack, as proposed by Vrijdag, (2009), as one of the performance indicators for the proposed Model Predictive Controller. Alternatively, this controller could impose constraints on the angle of attack, in order to prevent cavitation. For smart ships this constraint could, for example, only be imposed if cavitation noise has priority over other criteria.

2.9.2. CONTROL OF ELECTRICAL DRIVE IN HYBRID PROPULSION

Hybrid propulsion allows the electric motor to be used in parallel with the main engine, either with the motor providing torque in *electric motor assist mode* or with the motor operating as a generator in *power take-off mode*. Thus two control strategies could be developed for hybrid propulsion.

ELECTRIC MOTOR ASSIST

In most current applications or proposals for hybrid propulsion, the electrical machine is switched off during mechanical drive. Topaloglou *et al.* (2016) have demonstrated that electric motor assist can reduce the thermal loading on the propulsion diesel engine, with a control strategy that is aimed at reducing the air excess ratio of the main engine. A control strategy with the electric motor running in speed control and the engine supplying constant power in torque control, could potentially achieve this as well. Alternatively, a Model Predictive Controller providing torque setpoints for both the electric motor and the diesel engine with a performance indicator that heavily penalises torque fluctuations on the engine, might also achieve this. However, research would be required whether the computational speed of such an MPC strategy would be fast enough to keep the time period between discrete control actions small enough to maintain robust control.

Because AC electric generators always run at full speed, they could provide additional power more rapidly than the mechanically connected engine, as this engine runs on the propeller curve speed and has limited engine margin. Moreover, batteries could improve dynamic performance without increasing dynamic loading on the diesel generators. Thirdly, running the electric motor in electric assist mode could enable a reduced engine rating, particularly when maximum power is only required infrequently, as is the case on tugs.

In order to achieve reduced dynamic loading of the diesel generator, the optimised load sharing strategy with batteries could be used, as proposed in Zahedi *et al.* (2014). However, this approach can only be applied to DC power supplies. Alternatively in AC power supplies, the load sharing could be controlled by similarly optimising speed droop settings. Whether this could lead to a stable control strategy, which particularly also prevents overloading of any of the diesel generators, requires further research.

POWER TAKE-OFF

With the proposed shaft generator control strategy, the dynamics of load transients in the electrical systems are equally shared between diesel generator and shaft generator. Alternatively, if only the shaft generator or the diesel generator should handle the load transients, this could be achieved by running that generator(s) in isochronous mode and the other generator(s) in droop mode (see Section 2.3). In the configuration with a large propulsion gas turbine, load transients on the diesel generator could potentially be limited with this strategy. Moreover, hybrid power supplies could supply the load transients from batteries. However, further research would be required to determine whether this could lead to a stable and robust control strategy.

2.9.3. ENERGY MANAGEMENT OF HYBRID POWER SUPPLIES

Hybrid power supplies enable sharing the total instantaneous load between different types of power source, typically diesel engines and batteries. This is referred to as *energy management*. In particular, Equivalent Consumption Minimisation Strategies (ECMS) have shown to be a very promising energy management strategy.

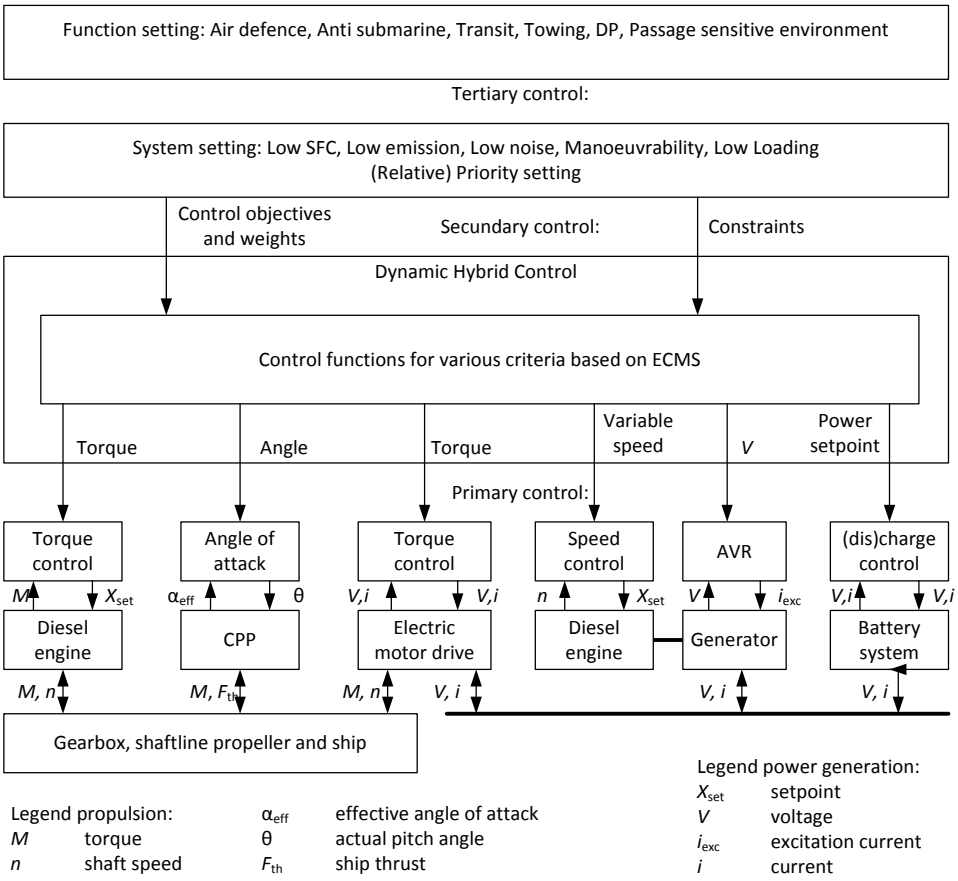

Figure 2.23: Schematic presentation of future integrated control strategy.

ECMS

In the automotive industry, the ECMS strategy has shown to achieve the best results in minimising fuel consumption over an unknown operating profile. Applying ECMS to power systems on ships has been proposed in Grimmelius *et al.* (2011). Moreover, application of ECMS on ferries and tugs has shown significant reduction in fuel consumption of 2% to 11% (Breijs *et al.* 2016; Vu *et al.* 2015).

ECMS WITH RECEDING HORIZON

When the distance or time of the remaining operating profile is known, the required final battery charge could be accounted for in the control problem with a reference state of charge that becomes smaller over time. This is referred to as the ECMS approach with receding horizon and could ensure the full battery capacity is used during the operating profile. Fuel consumption of this strategy, if well defined, could approach the optimal fuel consumption calculated with an off-line strategy, such as dynamic programming or the Euler-Lagrange optimal control formulation (Sciarretta *et al.* 2014).

ECMS STRATEGY FOR MULTIPLE PERFORMANCE CRITERIA

The ECMS approach has been developed to minimise fuel consumption. Many other criteria covered in Section 3.1, such as noise, vibrations, emissions or engine maintenance also primarily depend on the engine (and battery) operating point determined by the power setting of the power source. Therefore, similar cost functions as a function of power setting could be derived for these criteria as well and the overall optimal power setting could be determined from a weighted cost function over multiple criteria. Thus, using ECMS for multiple criteria could be a promising approach to improve performance over multiple functions for future smart ships.

2.9.4. INTEGRATED CONTROL APPROACH FOR FLEXIBLE MISSION CONTEXT

Ultimately, the control strategies proposed for further research should be combined. A schematic overview of the potential overarching control strategy for such an integrated system with hybrid propulsion and hybrid power supply feeding a DC power system is illustrated in Figure 2.23. This approach is similar to the approach proposed for microgrids in Guerrero *et al.* (2011) and discussed in Section 2.5.3. However, in this case we include the control of the mechanical drive and electrical drive and focus on the system dynamics in the gearbox, which is the system that mechanically connects the propulsion load and the main diesel engine and induction machine power sources. Significant research is required to establish the feasibility of such an integrated approach. In Chapter 4, 5 and 6, the holistic performance of primary and secondary control strategies as proposed in Section 2.9 is established with simulation studies for three case studies: a Patrol Vessel with mechanical propulsion and CPP, a frigate with hybrid propulsion and CPP, and a tug with hybrid propulsion and FPP, before proposing the integrated control strategy in Chapter 7 based on the results from the simulation studies.

2.10. CONCLUSIONS

THIS chapter has reviewed current and future power and propulsion system architectures and their associated control strategies for smart ships. The variety and complexity of these architectures poses an increasing amount of design choices to the ship and control system designer. In order to determine the optimal architecture, knowing the operational profile and the ship functions to be performed is essential. From the operating profile and ship functions, the candidate architectures for the ship can be established, based on the benefits and challenges for the various propulsion and power supply architectures in Table 2.1 and their application trends reported in Table 2.2, thus answering Research Question 1.

Based on the review in this chapter and its results in Table 2.1 and 2.2, we can derive the following general conclusions in answer to Research Question 1.

- Electrical propulsion is economically efficient and operationally effective when the mission and hotel loads are of a similar magnitude as the propulsion loads, for example in cruise ships, capital naval ships, and in offshore vessels that require the majority of its propulsive power for the dynamic positioning function. Then, the diesel generators can be switched on and off as required and alternately support all ship functions. However, if the propulsion load is significantly greater than

the electrical mission and hotel loads, then the conversion losses in the electrical propulsion drive increase fuel consumption and emissions while the electrical equipment drives up volume and weight.

- Hybrid propulsion is economically beneficial if the ship sails below 40% of its top speed a significant amount of time. This is applicable to ships that often perform the functions low speed sailing, patrolling or loitering, such as tugs, warships and patrol vessels and ships that often perform dynamic positioning such as offshore vessels and drilling and crane vessels. Hybrid propulsion, particularly in combination with hybrid power supply, can potentially also support ships sailing at constant speed in heavy weather conditions, as the direct drive main engine can then deliver constant torque while torque fluctuations are handled by the electric drive.
- Hybrid power supply is beneficial when the total electrical load has a great spread over time and can improve availability and reduce noise. The electrical load typically has a great spread over time for ships with functions that require large fluctuating loads, such as dredgers during dredging, heavy crane vessels during hoisting and lowering of loads and drilling vessels during drilling. The availability increase is of particular interest for ships that require high levels of dynamic positioning in order to safely perform functions such as loading and off-loading, performing maintenance on oil platform or windturbines and drilling. The potential low noise operation on the electrical drive is required for ship functions such as underwater warfare patrol for naval vessels and transit or operations in a noise restricted natural environment.
- Finally, DC power systems potentially bring down conversion losses and can run the generator at variable speed, reducing fuel consumption and associated emissions with up to 20%, for ship with electrical and hybrid propulsion, in particular when most electrical loads require variable speed drives for most of its functions. The increasingly electrically powered mission loads of naval vessels, for example rail gun and directed energy weapons, can also be more efficiently and effectively supported by DC power systems as they require pulsed loads, that can deteriorate both voltage and frequency stability of AC systems.

One of the most important aspects that determine whether the full potential of the selected architecture can be achieved in practice is the control strategy. As such, many intelligent control strategies have been investigated and applied in other applications such as the automotive industry and land based micro-grids. However, advanced control strategies have only most recently been investigated and applied in maritime applications, and only reductions in fuel consumption and emissions, of 15% to 35%, have been quantified for some cases, which is partly achieved by recharging batteries from the grid. Improvements in other criteria, such as propulsion availability, radiated noise and maintenance cost are crucial for effective hybrid power and propulsion systems as well. From the review of control strategies reported in literature as presented in Table 2.3, in answer to Research Question 2, we have identified three promising control strategies that utilise the degrees of freedom provided by the controllable pitch propeller (CPP), by the power split between the main engine and electric drive for hybrid propulsion, and

by the power split between the diesel generator and the energy storage in hybrid power supply.

This dissertation will address the three main control challenges identified in this chapter. First, Chapter 4 proposes a novel adaptive pitch control strategy for diesel mechanical and hybrid propulsion with controllable pitch propellers, which combines the angle of attack approach for propeller pitch control (Vrijdag *et al.* 2010) with slow integrating speed control for diesel engine fuel injection to achieve the identified advantages of torque control and to answer Research Question 5. Second, Chapter 5 proposes a novel parallel control strategy for hybrid propulsion with FPP or CPP that uses a combination of slow integrating speed control for the main engines and torque control for the electric drive, both for electric motor assist and power take-off, to answer Research Question 6. Third, Chapter 6 proposes a novel approach for the on-line solution of the charge depleting ECMS control problem for hybrid propulsion with hybrid power generation. This approach uses discrete variables for the various engines and operating modes, thus splitting the problem formulation in convex sub-problems, and combines branch and bound with convex optimisation. This approach is applied to an ECMS approach without and with operator load estimation. This ECMS approach can also be used to generate the torque setpoint for the parallel control strategy proposed in Chapter 5 and answers Research Question 7. Finally, Chapter 7 proposes the concept and design structure for autonomous control that can adapt the control system performance to changing ship functions, thus answering Research Question 8 and discusses the relation of the proposed autonomous control structure to the proposed control strategies: adaptive pitch control, parallel control for hybrid propulsion and energy management for hybrid power supply, based on the simulation studies in Chapter 4, 5 and 6.

3

POWER AND PROPULSION MODELLING AND PERFORMANCE QUANTIFICATION

A validated propulsion system model is required to evaluate performance of current state-of-the-art and future alternative propulsion systems and their control, and answer Research Question 3: 'What simulation model can be used to quantify MOEs fuel consumption, emissions, radiated noise, propulsion availability, manoeuvrability and maintainability due to engine mechanical and thermal loading?' To this end, this chapter proposes a propulsion model with a Mean Value First Principle (MVFP) diesel engine model that can be parameterised with publicly available manufacturer data and further calibrated with obligatory FAT measurements. This model predicts system performance within 5% of actual measurements during Factory Acceptance Tests (FAT) of the diesel engines and Sea Acceptance Tests (SAT) of a case study navy ship. Moreover, this chapter proposes measures of performance that objectively quantify the fuel consumption, acceleration rate, engine thermal loading and propeller cavitation during trial, design and off-design conditions in specified benchmark manoeuvres, within an hour simulation time, to answer Research Question 4: 'What benchmark manoeuvres and Measures of Performance (MOP) can quantify the MOEs listed above?'

The chapter is organised as follows: The propulsion system model is proposed in Section 3.2 and the control strategy in Section 3.3, to validate these models in Section 3.4 with FAT and SAT measurements. In Section 3.5, benchmark MOPs are proposed and the results with manoeuvring and transit mode of the proposed control strategy discussed. Finally, Section 3.6 concludes this chapter.

Parts of this chapter have been published in Applied Energy **206** (2017), Geertsma *et al.* (2017c), in Control Engineering Practice **76** (2018), Kalikatzarakis *et al.* (2018), in IFAC Proceedings Volumes **50(1)** (2017), Geertsma *et al.* (2017b) and in Applied Energy **228** (2018), Geertsma *et al.* (2018).

3.1. INTRODUCTION

THE control strategy for mechanical, electrical and hybrid propulsion requires a trade-off between various Measures of Effectiveness (MOEs) (Roedler *et al.* 2005), such as fuel consumption, manoeuvrability, engine thermal loading and, in some cases, cavitation noise (Grimmelius *et al.* 2000, 2001; van Spronsen *et al.* 2001; Vrijdag *et al.* 2010). While in some circumstances, such as a transit, the objective of the control strategy will be to sail at the lowest possible fuel consumption, in other circumstances, such as manoeuvring during dynamic positioning or entering and leaving port, the objective will be to provide maximum manoeuvrability. In either case, the engine should not be thermally overloaded. Furthermore, for military vessels and ships operating in an ecologically sensitive environment, limiting radiated noise through cavitation can be an important objective. Traditional control strategies, using fixed combinator curves and engine speed control, can achieve different trade-offs by defining 2 or more different operating modes: manoeuvring mode and transit mode (Geertsma *et al.* 2017a).

The assessment of the optimum trade-off for these propulsion architectures and their control strategies is a complex task. The optimum trade-off could be determined during sea trails at extremely high cost. Alternatively, propulsion system models could be used to investigate the control system settings at a much lower cost (Altosole *et al.* 2009; Campora *et al.* 2003; van Straaten *et al.* 2012). However, setting up these propulsion system models requires extensive data from the equipment manufacturers and no validated models are available in literature that can be calibrated with public manufacturer data, for example information available in engine project guides (MAN Diesel SE, 2008b). Moreover, the analysis of the trade-off requires a lot of expert knowledge and the Measures of Performance (MOPs)(Roedler *et al.* 2005) that should be considered in the control system design have not been clearly defined. Therefore, this chapter aims to provide a propulsion system model that can be calibrated with readily available equipment data and used to compare different propulsion system architectures and their control strategies, to define MOPs to analyse propulsion and control system performance in very limited simulation time, and to analyse the improvements advanced control strategy can potentially deliver.

This chapter first proposes a model including all subsystem models for hybrid propulsion with hybrid power generation, illustrated in Figure 3.1, as all architectures addressed in this thesis can be investigated with these subsystem models. Subsequently, a case study *Holland* class Patrol Vessel is used for the validation of the engine, gearbox, propeller and hull interaction. The typical propulsion system layout for a naval vessel, and for the case study Patrol Vessel, is shown in Figure 3.2.

Diesel mechanical propulsion systems have been modelled extensively, either with very complex diesel engine models, that require an extensive analysis of parameters and exhaustive calibration (Guan *et al.* 2014; Kyrtatos *et al.* 1994; Martelli, 2014; Schulten, 2005), or with look-up tables that are based on extensive measurements (Deleroi, 1995; van Straaten *et al.* 2012; Vrijdag, 2009). The propulsion system model proposed in this chapter is based on first principles and uses parameters obtained from publicly available manufacturers data, such as engine project guides (MAN Diesel SE, 2008b) and open water propeller diagrams (Dang *et al.* 2013; Kuiper, 1992). For good calibration of the engine turbocharger model, obligatory Factory Acceptance Test (FAT) data, in particular

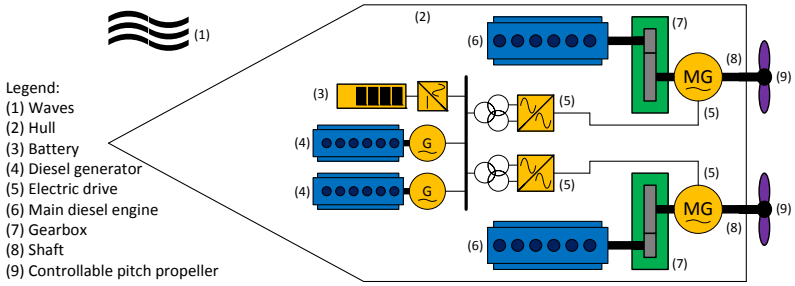

Figure 3.1: Typical hybrid propulsion with hybrid AC power supply system layout.

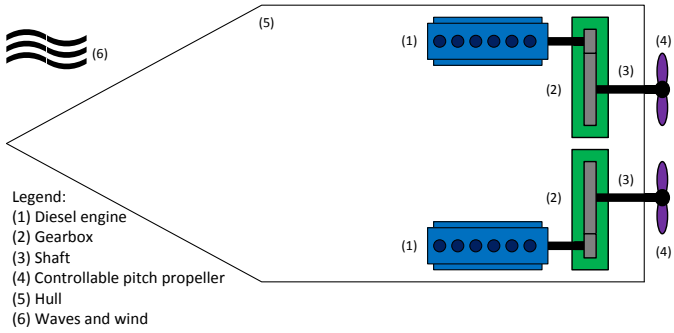

Figure 3.2: Typical mechanical propulsion system layout for a naval vessel from Geertsma *et al.* (2016).

turbocharger pressures and temperatures for multiple operating points, is required. The procedure to fit parameters, described in this chapter, requires FAT measurements only and do not require further heat release measurements or compressor and turbine maps, as opposed to most alternative models, which require an extensive amount of fitting parameters to achieve satisfactory performance prediction (Grimmelius *et al.* 2007; Hendricks, 1997). Because the model mimics the physical and thermodynamic behaviour, it can be used to evaluate the dynamic performance of diesel mechanical and hybrid propulsion of service vessels with special interest for fuel consumption, rate of acceleration, engine thermal loading and propeller cavitation.

The contribution of this chapter is threefold. First, the diesel engine model proposed in this chapter is the first Mean Value First Principle (MVFP) diesel engine model that can be calibrated based on FAT measurements, without compressor and turbine maps and extensive heat release measurements as proposed in Grimmelius *et al.* (2007) and Ding *et al.* (2012). Moreover, it provides accurate prediction of the required MOP across the operating envelope for comparative system and control studies, as demonstrated by the presented quantitative validation with the diesel engines FAT and the ships Sea Acceptance Trials (SAT) measurements. This diesel engine model can accurately predict engine performance because the six point Seiliger cycle, an accurate turbocharger model based on *Zinner* blowdown and the *Büchi* balance, and variable turbocharger efficiency, heat release efficiency and slip ratio have been added to the model proposed

in Miedema *et al.* (2002) to reflect the thermodynamic behaviour of modern highly turbocharged engines with large valve overlap *Miller* timing (Miller, 1947; Wang *et al.* 2008). Secondly, the total ship model validation provides new insight in the influence of a control strategy on holistic performance for various MOEs. Finally, we propose benchmark manoeuvres and MOPs to quantify fuel consumption, rate of acceleration, engine thermal loading and propeller cavitation, in order to evaluate performance improvements of conventional and advanced control strategies, and compare propulsion architectures against predefined MOPs.

3.2. SHIP PROPULSION SYSTEM MODEL

THE schematic representation of the hybrid propulsion with hybrid power supply model considered in this chapter is illustrated in Figure 3.3. We use the modular, hierarchical and causal modelling paradigm proposed in Colonna *et al.* (2007), in which the direction of the arrows illustrates the causality of the coupled effort and flow variables, for example main engine torque M_{me} with main engine speed n_{me}, electric machine torque M_{im} with electric machine speed n_{im}, propeller torque M_{p} with shaft speed n_{p} and propeller thrust T_{p} with ship speed v_{s}. Moreover, fuel injection setpoint X_{set}, pitch ratio setpoint $P_{\text{p,set}}$, induction machine torque setpoint $M_{\text{im,set}}$ or induction machine speed setpoint $n_{\text{im,set}}$ and battery current setpoint $i_{\text{bat,set}}$ represent control variables and wave orbital speed v_{w} and ship resistance function $R_{\text{v}}(v_{\text{s}})$ represents the disturbance due to waves. Because electrical network dynamics are not considered, the electrical network just balances supply and demand of all supply currents, from the electric drive in generator mode i_{fc}, the battery in discharge mode i_{bat} and the diesel generator i_{dg} and all load currents, from the electric drive in motor mode i_{fc}, the battery in charge mode i_{bat} and the auxiliary electrical loads i_{aux}. Finally, the operator can control ship speed by setting control input virtual shaft speed N_{virt} in rpm. The details of the sub-models are given below.

3.2.1. DIESEL ENGINE MODEL

Diesel engine models can be categorised by the level of dynamics that are considered and by the underlying physical detail, considering that the equation of motion and the associated state *engine speed* n_e are represented in the gearbox and shaft-line model, as follows:

- Zero order models represent the engines torque and fuel consumption with a purely mathematical equation derived from a number of measurement points (Shi *et al.* 2010) or from a look-up table. Either way, the dynamics of the turbocharger are not included. Because the thermal loading of the engine mainly depends on the charge pressure, these models are not suitable to predict the thermal loading of the engine.
- First order models contain a state variable representing either the turbocharger pressure or the turbocharger speed. These models can be based on complex underlying physical models (Miedema *et al.* 2002), on mathematical equations derived from a number of measurement points, or on look-up tables, which require

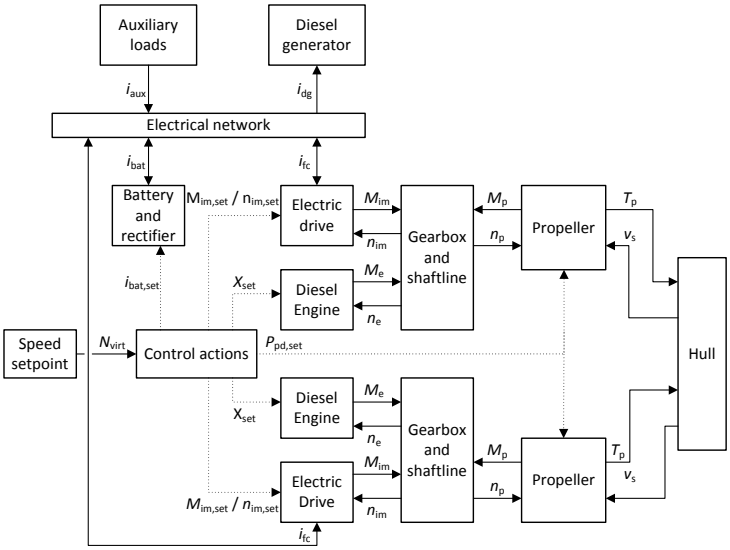

Figure 3.3: Schematic presentation of hybrid propulsion with hybrid power supply system for naval vessel showing causal coupling between models.

even more measurement points and therefore require extensive experimental data (Vrijdag, 2009, Ch. 2 pp. 16-19).

- High order Mean Value First Principle (MVFP) models include air and exhaust gas flow dynamics (Grimmelius *et al.* 2007; Guan *et al.* 2014; Nielsen *et al.* 2017a,b; Schulten *et al.* 2003) and require an extensive set of parameters and exhaustive calibration as shown in Ding, (2011). These models mostly use the filling and emptying approach for the inlet and exhaust receiver control volumes in combination with compressor and turbine maps and require extensive calibration parameters (Guan *et al.* 2014; Jensen *et al.* 1991). Schulten *et al.* (2003) use a gas exchange model and the six point Seiliger cycle to determine the exhaust gas conditions, while Guan *et al.* (2014) and Jensen *et al.* (1991) use a mathematical representation of the indicated efficiency and friction losses based on manufacturer data. When compressor and turbine maps are available, the novel approach presented in Guan *et al.* (2014) can extend these maps to the low speed region, thus predicting engine behaviour at low load, for example during slow steaming.

- Zero-dimensional crank angle models determine the thermodynamic state of the air and combustion gas in the cylinder during crank angle rotation for the closed cylinder process, assuming a single homogenous ideal gas in the cylinder (Kyrtatos *et al.* 1994), which can be combined with a heat release model using Wiebe functions (Ghojel, 2010) as proposed in Baldi *et al.* (2015), with a two-zone combustion model as proposed in Benvenuto *et al.* (2002) and Scappin *et al.* (2012) or with a multi-zone combustion model as proposed in Raptosasios *et al.* (2015). The approaches proposed in Scappin *et al.* (2012) and Raptosasios *et al.* (2015) can

also predict NO_x formation using the extended Zeldovich mechanism (Zeldovich, 1946), as they model the combustion process in sufficient detail.

- One-dimensional fluid dynamic models are used to predict the air flow, pressure and temperature along the flow path of the air, in the compressor, intercooler, inlet receiver, cylinder and exhaust system, including the turbine. Commercial software packages, such as GT-power and AVL Boost, estimate fluid properties along the flow, discretising the flow path, and can also address pressure waves. However, these packages require too much computational time to calculate the performance of an engine during a typical operational profile or ship manoeuvres (Millo *et al.* 2006; Pasini *et al.* 2016).
- Multi-zone combustion models (Raptosasios *et al.* 2015) and CFD combustion models (Pang *et al.* 2016) model the combustion process and the gas flow in the various engine components in three dimensions. While Raptosasios *et al.* (2015) demonstrate multi-zone combustion models with a zero-dimensional crank angle model can be used to predict NO_x production, CFD combustion models can be used to gain detailed insight into the processes of soot formation, NO_x formation, heat radiation and convective heat transfer in the cylinder during the combustion process (Pang *et al.* 2016). Nevertheless, the high computational burden of these models restricts their use for extensive propulsion system analysis for multiple MOEs that occur in different timescales.

This research focusses on the dynamic performance of the diesel engine, including the thermal loading of the engine, which can be represented by the air excess ratio, turbocharger entry temperature and exhaust valve temperature (Grimmelius *et al.* 2001; Sapra *et al.* 2017). Therefore, a MVFP has been chosen to model the diesel engine, based on the models used in Miedema *et al.* (2002). In order to improve the accuracy of the prediction of the engine parameters of interest, five significant improvements are included in the model.

First, an extensive measurement campaign performed in Barsingerhorn *et al.* (2015) demonstrated the turbocharger pressure was overestimated in the model of Miedema *et al.* (2002). Hence, we added a more accurate turbocharger model based on *Zinner* blowdown and the *Büchi* flow and power balance with a variable turbocharger efficiency, as proposed previously for a dual fuel engine in Mestemaker *et al.* (2014), a heat loss model for the turbocharger, and a third differential equation to reflect the delay in exhaust receiver pressure build-up due to receiver volume filling. Second, a fourth differential equation has been added to the model, representing the inertia of the fuel injection system and the ignition delay as proposed in Geertsma *et al.* (2016). Third, the six point Seiliger process has replaced the five point Seiliger process in order to more accurately predict the exhaust temperature and indicated efficiency, as proposed in Sui *et al.* (2017). Fourth, the heat release efficiency has been defined as a function of speed, to account for the longer exposure time of hot gas at lower engine speed. Finally, a variable slip ratio due to scavenging has been added, to accurately reflect the impact of *Miller* timing.

The resulting diesel engine model consists of the following sub-models: fuel pump, air swallow, heat release, Seiliger cycle, exhaust receiver and turbocharger, and mechanical conversion. In particular, the exhaust receiver and turbocharger model proposes a

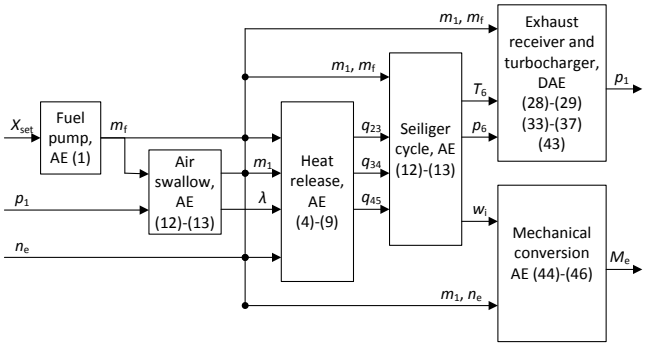

Figure 3.4: Schematic presentation of the diesel engine model and the interaction between its subsystems, consisting of Algebraic Equations (AE) or Differential and Algebraic Equations (DAE), from Geertsma *et al.* (2017c).

new modelling strategy based on *Zinner* blowdown, *Büchi* flow and power balance, the elliptic law (Dixon, 1998; Stapersma, 2010a) and a variable slip ratio assuming isentropic flow through a nozzle. The interaction of these sub-models and the equations representing their behaviour are shown in Figure 6.3.

FUEL PUMP

The fuel pump model represents the time delay caused by the inertia of the fuel pump actuator and the ignition delay, as proposed in Geertsma *et al.* (2016), as follows:

$$\frac{dm_f(t)}{dt} = \frac{m_{f,nom} X_{set}(t) - m_f(t)}{\tau_X}, \tag{3.1}$$

where $m_f(t)$ is the amount of fuel injected per cylinder per engine cycle in kg, t is time in s, $m_{f,nom}$ is the nominal amount of fuel injected per cylinder per engine cycle in kg, X_{set} is the fuel pump injection setpoint in % of nominal fuel injection and τ_X is the fuel injection time delay in s, which can be estimated with the time required for half a stroke, which is the maximum duration of combustion, as follows:

$$\tau_X = \frac{1}{4 n_{e,nom}}, \tag{3.2}$$

where $n_{e,nom}$ is the nominal engine speed in Hz. Fuel injection time delay in this model is assumed constant due to its small value, while a more accurate estimate could be achieved by using the actual engine speed. Furthermore, the nominal fuel injection $m_{f,nom}$ can be determined as follows:

$$m_{f,nom} = \frac{m_{bsfc,nom} P_{e,nom} k_e}{i_e n_{e,nom}}, \tag{3.3}$$

where $m_{bsfc,nom}$ is the nominal brake specific fuel consumption in kg/kWs, $P_{e,nom}$ is the nominal engine power in kW, k_e is the number of revolutions per cycle, which is 2 for a 4-stroke engine, and i_e is the number of cylinders of the engine.

AIR SWALLOW

The air swallow characteristics of the engine determine the air excess ratio λ, which represents the amount of air that is left after all fuel is combusted. This ratio is an important indicator for the thermal loading of the engine as discussed in Sapra *et al.* (2017) and can also be used to measure the effectiveness of Exhaust Gas Recirculation, as demonstrated in Asad *et al.* (2014) and Nielsen *et al.* (2017a). The scavenge efficiency of the engine can be assumed unity, because the model only considers 4 stroke engines with significant air slip (Stapersma, 2010b, Ch. 2 p. 55). Therefore, the air excess ratio matches the pseudo air excess ratio and can be defined as follows:

$$\lambda(t) = \frac{m_1(t)}{m_f(t)\sigma_f}, \tag{3.4}$$

where σ_f is the stoichiometric air fuel ratio of the fuel. Furthermore, the trapped mass at the start of compression in kg m_1 is determined by the charge air pressure p_1, using the ideal gas law, as follows:

$$m_1(t) = \frac{p_1(t)V_1}{R_a T_1}, \tag{3.5}$$

where V_1 is the cylinder volume at start of compression in m^3 and R_a is the gas constant of air in J/kgK. The volume V_1 is determined by the cylinder parameters as follows:

$$V_1 = \frac{\pi D_B^2 L_S r_c}{4(\varepsilon_c - 1)}, \tag{3.6}$$

where D_B is the bore diameter in m, L_S is the stroke length in m, ε_c is the geometric compression ratio, determined by the cylinder dimensions and r_c is the effective compression ratio, which is determined by the inlet valve timing and can be established as follows Stapersma, 2010c, Ch. 14, pp. 632-633:

$$r_c = (\varepsilon_c - 1)\, x_c + 1 \tag{3.7}$$

$$x_c = \frac{L_{IC}}{L_{BDC}} \tag{3.8}$$

$$L_{IC} = L_S\left(\frac{1}{\varepsilon_c - 1} + \frac{1}{2}\left((1 - \cos\alpha_{IC}) + \frac{1}{\lambda_{CR}}\left(1 - r_{tg}\right)\right)\right) \tag{3.9}$$

$$r_{tg} = \sqrt{1 - \lambda_{CR}^2 \sin^2\alpha_{IC}} \tag{3.10}$$

$$\lambda_{CR} = \frac{L_S}{2L_{CS}} \tag{3.11}$$

$$L_{BDC} = \frac{\varepsilon L_S}{\varepsilon - 1}, \tag{3.12}$$

where x_c is the compression stroke effectiveness factor, L_{IC} is the distance between the top of the cylinder and the piston crown, *cylinder space length L_p in Figure 3.5*, in m when the inlet valve closes, L_{BDC} is the cylinder space length in m when the cylinder is at bottom dead centre (BDC) position, L_{TDC} is the cylinder space length in m when the cylinder is at top dead centre (TDC) position, L_{CR} is the length of the crank rod in m, α_{IC} is the crank angle when the inlet valve closes, λ_{CR} is the length ratio of the crank rod to the crank shaft radius in m R_{CR} and r_{tg} is a trigonometric root used to split the equation.

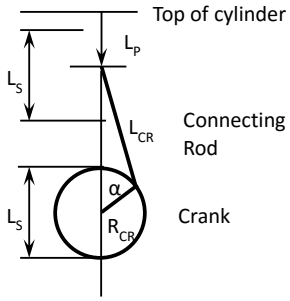

Figure 3.5: Schematic view of the geometry of cylinder, crank rod and crank shaft Stapersma, 2010c, Ch. 14, p. 632.

HEAT RELEASE

The heat release model represents the heat release during the isochoric, isobaric and isothermal combustion stages of the six point Seiliger proces. The released heat is assumed to be split between a constant volume segment q_{23} in kJ/kg, a constant pressure segment q_{34} in kJ/kg, and a constant temperature segment q_{45}, according to Schulten, (2005), as follows:

$$q_{23}(t) = X_{\mathrm{cv}}(t)\frac{m_{\mathrm{f}}(t)\eta_{\mathrm{q}}(t)\eta_{\mathrm{comb}}h^{\mathrm{L}}}{m_1(t)} \tag{3.13}$$

$$q_{34}(t) = (1 - X_{\mathrm{cv}}(t) - X_{\mathrm{ct}}(t))\frac{m_{\mathrm{f}}(t)\eta_{\mathrm{q}}(t)\eta_{\mathrm{comb}}h^{\mathrm{L}}}{m_1(t)} \tag{3.14}$$

$$q_{45}(t) = X_{\mathrm{ct}}(t)\frac{m_{\mathrm{f}}(t)\eta_{\mathrm{q}}(t)\eta_{\mathrm{comb}}h^{\mathrm{L}}}{m_1(t)}, \tag{3.15}$$

where X_{cv} is the portion of heat released at constant volume, X_{ct} is the portion of heat released at constant temperature, η_{q} is the heat release efficiency, η_{comb} is the combustion efficiency and h^{L} is the lower heating value of fuel at ISO conditions in kJ/kg. The combustion efficiency is considered a function of air excess ratio λ, according to Betz *et al.* (1986), but is unity within the engine operating limits. The nominal heat release efficiency η_{q} is estimated using nominal engine parameters and (3.5), (3.18)-(3.24) and (3.54)-(3.56). Furthermore, the percentage of heat lost is considered inversely related to engine speed in Hz n_{e}, as follows:

$$\eta_{\mathrm{q}}(t) = 1 - \left(1 - \eta_{\mathrm{q,nom}}\right)\frac{n_{\mathrm{e,nom}}}{n_{\mathrm{e}}(t)}. \tag{3.16}$$

For the energy management study in Chapter 6 a more accurate het loss model for the heat losses in the cylinder could also be implemented, as sufficient manufacturer data was available for calibration. Heywood *et al.* (1988) argue that several variables affect the magnitude of heat lost to the combustion chamber surfaces $\bar{Q}^{*}_{\mathrm{loss}}$ in J. The most important are engine speed, load and air excess ratio λ. After a thermodynamic analysis based on (Stapersma, 2010a,b,c,d), the following relation was derived (Kalikatzarakis,

2017):

$$\bar{Q}^{*}_{\text{loss}}(t) = w_1\left(-\frac{c_1}{\lambda^{*2}(t)} + 2\frac{c_1}{\lambda^{*}(t)} + c_2\right) + w_2\frac{p^{*0.7}_{max}(t)}{n^{*0.3}_{\text{me}}(t)}, \tag{3.17}$$

with $c_1, c_2 \in (0,1)$ $w_1, w_2 \in (0,1), \sum_{i=1}^{2} w_i = 1$, fitted parameters that can be calibrated with manufacturer data.

The constant volume portion of combustion X_{cv} is considered to increase linearly with engine speed at a negative rate $X_{\text{cv,grad}}$, and the constant temperature portion of combustion X_{ct} is considered to increase proportional to fuel injection, as follows:

$$X_{\text{cv}}(t) = X_{\text{cv,nom}} + \frac{n_{\text{e}}(t) - n_{\text{e,nom}}}{n_{\text{e,nom}}} X_{\text{cv,grad}} \tag{3.18}$$

$$X_{\text{ct}}(t) = X_{\text{ct,nom}}\frac{m_{\text{f}}(t)}{m_{\text{f,nom}}}, \tag{3.19}$$

where $X_{\text{ct,nom}}$ is the nominal constant temperature portion, and $X_{\text{cv,nom}}$ is the nominal constant volume portion, which can be estimated from the maximum cylinder pressure in the nominal working point $p_{\text{max,nom}}$ in Pa, which often is available in engine project guides, as follows:

$$X_{\text{cv,nom}} = \frac{c_{\text{v,a}}\, T_1\, r_{\text{c}}^{\kappa_{\text{a}}-1}\left(\frac{p_{\text{max,nom}}}{p_{\text{1,nom}}\, r_{\text{c}}^{\kappa_{\text{a}}}} - 1\right) m_{\text{1,nom}}}{\eta_{\text{q}}(t)\, m_{\text{f,nom}}\, h^{\text{L}}}, \tag{3.20}$$

where $c_{\text{v,a}}$ is the specific heat at constant volume of air in J/kgK, T_1 is the air temperature in the cylinder at the start of compression in K, κ_{a} is the specific heat ratio of air, $p_{\text{1,nom}}$ is the nominal charge air pressure in Pa and $m_{\text{1,nom}}$ is the nominal trapped mass at the start of compression in kg. Finally, the air temperature at start of compression T_1 in K is assumed constant and can be estimated according to Stapersma, 2010a, Ch. 6 p. 274, as follows:

$$T_1 = T_{\text{c}} + \varepsilon_{\text{inl}}\,(T_{\text{inl}} - T_{\text{c}}), \tag{3.21}$$

where T_{c} is the charge air temperature after the intercooler in K, ε_{inl} is the parasitic heat exchanger effectiveness of the heat exchange between inlet duct and the air and T_{inl} is the temperature of the inlet duct that heats the inducted air in K. Because the charge air temperature is fairly constant and the temperature is an estimate, all these temperatures are assumed constant.

SEILIGER CYCLE

The six stage Seiliger process consists of polytropic compression, isochoric combustion, isobaric combustion, isothermal combustion and polytropic expansion and can be used to determine the work produced during the closed cylinder process and establish the exhaust gas properties at the end of expansion (Stapersma, 2010b). Moreover, we assume the gas is a perfect gas with a homogeneous composition. This cycle is illustrated in Figure 3.6. The associated equations are summarised in Table 3.1 (Stapersma, 2010b, Ch. 3 p. 136-137), where V_{i}, p_{i} and T_{i} are the volume in m^3, pressure in Pa and temperature in K at state i, w_{ij} and q_{ij} are the specific work in kNm/kg and specific heat in kJ/kg

Table 3.1: Seiliger cycle equations Stapersma, 2010b, Ch. 3 pp.136-137.

Seiliger stage	**Volume** V	**Pressure** p	**Temperature** T	**Specific work** w	**Heat** q
Compression 1-2	$\frac{V_1}{V_2} = r_c$	$\frac{p_2}{p_1} = r_c^{\kappa_a}$	$\frac{T_2}{T_1} = r_c^{(\kappa_a - 1)}$	$w_{12} = \frac{R_a(T_2 - T_1)}{\kappa_a - 1}$	–
Isochoric combustion 2-3	$\frac{V_3}{V_2} = 1$	$\frac{p_3}{p_2} = a$	$\frac{T_3}{T_2} = a$	–	$q_{23} = c_{va}(T_3 - T_2)$
Isobaric combustion 3-4	$\frac{V_4}{V_3} = b$	$\frac{p_4}{p_3} = 1$	$\frac{T_4}{T_3} = b$	$w_{34} = R_a(T_4 - T_3)$	$q_{34} = c_{pa}(T_4 - T_3)$
Isothermal combustion 4-5	$\frac{V_5}{V_4} = c$	$\frac{p_4}{p_5} = c$	$\frac{T_5}{T_4} = 1$	$w_{45} = R_a T_4 \ln c$	$q_{45} = R_a T_4 \ln c$
Expansion 5-6	$\frac{V_6}{V_5} = \frac{r_{eo} r_c}{bc}$	$\frac{p_5}{p_6} = \left(\frac{r_{eo} r_c}{bc}\right)^{n_{exp}}$	$\frac{T_5}{T_6} = \left(\frac{r_{eo} r_c}{bc}\right)^{n_{exp}-1}$	$w_{45} = \frac{R_a(T_6 - T_5)}{(n_{exp} - 1)}$	–

produced during the process from state i to state j, a, b and c are the Seiliger parameters as defined in Stapersma, (2010b), $c_{p,a}$ is the specific heat at constant pressure for air in J/kgK, n_{exp} is the polytropic exponent for expansion, as polytropic expansion allows for jacket water cooling, and r_{eo} is the ratio of the volume at Seiliger point 6, when the exhaust valve opens, to point 1, when the inlet valve closes, which is determined by the exhaust valve opening angle α_{EO}, using (3.9), as follows:

$$r_{eo} = \frac{L_{EO}}{L_{IC}} \tag{3.22}$$

$$L_{EO} = L_S\left(\frac{1}{\varepsilon_c - 1} + \frac{1}{2}\left((1 - \cos\alpha_{EO}) + \frac{1}{\lambda_{CR}}(1 - r_{tg})\right)\right), \tag{3.23}$$

where L_{EO} is the is the cylinder space length when the exhaust valve opens. The total specific indicated work w_i in kJ/kg can then be determined from the work of the Seiliger stages in Table 3.1, as follows:

$$w_i = w_{12} + w_{34} + w_{45} + w_{56}. \tag{3.24}$$

EXHAUST RECEIVER AND TURBOCHARGER

The process of blow down after the exhaust valve opens, gas expelling during the exhaust stroke, and scavenging after the inlet opens can be represented by *Zinner* blowdown, as

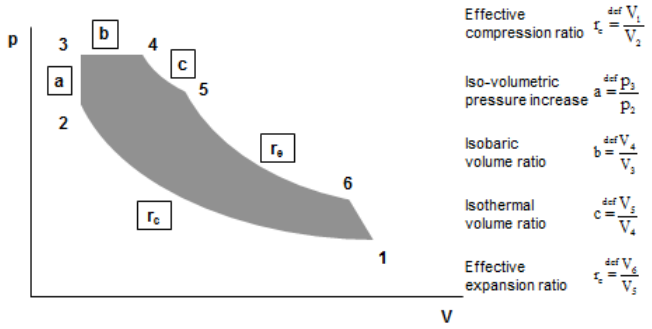

Figure 3.6: Typical six point Seiliger or dual cycle in pressure (p) - volume (V) plot, consisting of compression (1-2), isochoric combustion (2-3), isobaric combustion (3-4), isothermal combustion (4-5) and expansion (5-6), from Stapersma, (2010b).

proposed by Zinner, (1980) and extensively discussed in Stapersma, (2010a), as follows:

$$T_{\mathrm{bld}}(t) = \left(\frac{1}{n_{\mathrm{bld}}} + \frac{(n_{\mathrm{bld}} - 1)}{n_{\mathrm{bld}}} \frac{p_{\mathrm{d,s}}(t)}{p_6(t)} \right) T_6(t), \tag{3.25}$$

where T_{bld} is the *Zinner* blowdown temperature in K, n_{bld} is the polytropic expansion coefficient of the blowdown process, allowing for heat loss to the cylinder, exhaust valve and duct, and $p_{\mathrm{d,s}}$ is the equilibrium pressure in the exhaust receiver in Pa.

The resulting exhaust receiver temperature T_{d} in K after mixing of the air fuel mixture expelled from the cylinder and the scavenge air that slips through the cylinder, can be defined as follows Stapersma, (2010a):

$$T_{\mathrm{d}}(t) = \frac{c_{\mathrm{p,g}} T_{\mathrm{bld}}(t) \left(m_1(t) + m_{\mathrm{f}}(t)\right) + c_{\mathrm{p,a}} T_{\mathrm{slip}} s_{\mathrm{sl}}(t) m_1(t)}{c_{\mathrm{p,g}} \left(m_1(t) + m_{\mathrm{f}}(t)\right) + c_{\mathrm{p,a}} s_{\mathrm{sl}}(t) m_1(t)}, \tag{3.26}$$

where $c_{\mathrm{p,g}}$ is the specific heat at constant pressure for the exhaust gas in J/kgK, s_{sl} is the slip ratio of the scavenge process as defined in Stapersma, 2010a, Ch. 2 and T_{slip} is the temperature of the air slip during scavenging in K, which can be estimated using (3.21). The nominal slip ratio of the scavenge process $s_{\mathrm{sl,nom}}$ can be estimated from the total mass flow at nominal conditions $\dot{m}_{\mathrm{t,nom}}$ in kg/s, as follows:

$$s_{\mathrm{sl,nom}} = \frac{\dot{m}_{\mathrm{t,nom}} - \left(\dot{m}_{1,\mathrm{nom}} - \dot{m}_{\mathrm{f,nom}}\right)}{\dot{m}_{1,\mathrm{nom}}} \tag{3.27}$$

$$\dot{m}_{1,\mathrm{nom}} = \frac{p_{1,\mathrm{nom}} V_1 i_{\mathrm{e}} n_{\mathrm{e}}}{R_{\mathrm{a}} T_1 k_{\mathrm{e}}} \tag{3.28}$$

$$\dot{m}_{\mathrm{f,nom}} = m_{\mathrm{bsfc,nom}} P_{\mathrm{nom}}, \tag{3.29}$$

where $\dot{m}_{1,\mathrm{nom}}$ is the trapped mass flow of all cylinders at nominal conditions in kg/s and $\dot{m}_{f,\mathrm{nom}}$ is the nominal fuel mass flow in kg/s. Subsequently, the slip ratio can be represented as follows, as proposed in Stapersma, 2010a, Ch. 6:

$$s_{\mathrm{sl}}(t) = s_{\mathrm{sl,nom}} \frac{n_{\mathrm{e,nom}}}{n_{\mathrm{e}}(t)} \frac{m_{1,\mathrm{nom}}}{m_1(t)} \frac{p_1(t)}{p_{1,\mathrm{nom}}} \frac{\Psi_{\mathrm{sc}}(t)}{\Psi_{\mathrm{sc,nom}}} \tag{3.30}$$

$$\Psi_{\mathrm{sc}}(t) = \sqrt{\frac{2\kappa_{\mathrm{g}}}{\kappa_{\mathrm{g}}-1}} \sqrt{\left(\frac{p_{\mathrm{d}}(t)}{p_1(t)}\right)^{\frac{2}{\kappa_{\mathrm{g}}}} - \left(\frac{p_{\mathrm{d}}(t)}{p_1(t)}\right)^{\frac{\kappa_{\mathrm{g}}+1}{\kappa_{\mathrm{g}}}}}, \tag{3.31}$$

where κ_{g} is the specific heat ratio of the exhaust gas, $m_{1,\mathrm{nom}}$ is the trapped mass at nominal conditions in kg, which can be determined with (3.5), and Ψ_{sc} is the non-dimensional scavenge flow, assuming isentropic flow through a nozzle and choking above the critical pressure, as discussed extensively in Stapersma, (2010a). Moreover, the case study engine has a bypass valve to create additional flow around the cylinder to increase air flow in the turbocharger at low engine speed. This is represented by a bypass slip factor s_{byp} that is multiplied with the scavenge slip ratio s_{sc} to obtain the total slip ratio s_{sl}.

The pressure before the turbine is determined by the air swallow characteristics of the turbine. This model uses the elliptic law as derived in Dixon, 1998, Ch4. p. 122-124 and discussed in Stapersma, 2010a, Ch. 8 p. 363-410 to estimate the equilibrium pressure in the exhaust receiver $p_{\mathrm{d,s}}$ in Pa, as follows:

$$p_{\mathrm{d,s}}(t) = \sqrt{\frac{(s_{\mathrm{sl}}(t)\dot{m}_1(t) + \dot{m}_{\mathrm{f}}(t))^2 R_{\mathrm{g}} T_{\mathrm{d}}(t)}{\alpha_{\mathrm{Z}}^2 A_{\mathrm{eff}}^2} + p_{\mathrm{ex}}^2} \tag{3.32}$$

$$\dot{m}_1(t) = m_1(t) i_{\mathrm{e}} \frac{n_{\mathrm{e}}(t)}{k_{\mathrm{e}}} \tag{3.33}$$

$$\dot{m}_{\mathrm{f}}(t) = m_{\mathrm{f}}(t) i_{\mathrm{e}} \frac{n_{\mathrm{e}}(t)}{k_{\mathrm{e}}}, \tag{3.34}$$

where $\dot{m}_1$ is the trapped mass flow in kg/s, $\dot{m}_{\mathrm{f}}$ is the fuel mass flow in kg/s, R_{g} is the gas constant of the exhaust gas in J/kgK, α_{Z} is the *Zinner* turbine area decrease factor, which is assumed one for a contant pressure turbocharger, A_{eff} is the effective area of the turbine in m^2 and p_{ex} is the pressure after the turbocharger in Pa, which is assumed to be atmospheric pressure, neglecting exhaust pressure losses. The effective turbocharger area is estimated with (3.32) for nominal conditions. Substituting (3.25) in (3.26), (3.31) in (3.30), and (3.30) in (3.26) and (3.32), the quadratic system of Equations (3.26) and (3.32) can be solved explicitly.

We assume a time delay $\tau_{\mathrm{p,d}}$ for filling the exhaust receiver, because it measures a considerable volume. Thus, the pressure in the exhaust receiver p_{d} in Pa can be expressed as follows:

$$\frac{dp_{\mathrm{d}}(t)}{dt} = \frac{p_{\mathrm{d,s}}(t) - p_{\mathrm{d}}(t)}{\tau_{\mathrm{p,d}}}. \tag{3.35}$$

The equilibrium turbocharger pressure ratio $\pi_{\mathrm{com,s}}$, can be estimated from the pressure and temperature in the exhaust receiver from the *Büchi* equation (3.36) as discussed in Stapersma, 2010a, Ch. 8. The losses in the inlet duct, filter and air cooler are neglected. This leads to the following set of equations:

$$\pi_{\mathrm{com,s}}(t) = \left(1 + \delta_{\mathrm{f}}(t)\chi_{\mathrm{g}}\eta_{\mathrm{TC}}(t)r_{\mathrm{T,TC}}(t)\left(1 - \frac{1}{\pi_{\mathrm{tur}}(t)^{\left(\frac{\kappa_{\mathrm{g}}-1}{\kappa_{\mathrm{g}}}\right)}}\right)\right)^{\left(\frac{\kappa_{\mathrm{a}}-1}{\kappa_{\mathrm{a}}}\right)} \tag{3.36}$$

$$\pi_{\text{com,s}}(t) = \frac{p_{1,\text{s}}(t)}{p_{\text{amb}}} \tag{3.37}$$

$$\delta_{\text{f}}(t) = 1 + \frac{m_{\text{f}}(t)}{(1+s_{\text{sl}})\, m_1(t)} \tag{3.38}$$

$$r_{\text{T,TC}}(t) = \frac{T_{\text{d}}(t)}{T_{\text{amb}}} \tag{3.39}$$

$$\pi_{\text{tur}}(t) = \frac{p_{\text{d}}(t)}{p_{\text{ex}}}, \tag{3.40}$$

where δ_{f} is the fuel addition factor, χ_{g} is the ratio between the specific heats at constant pressure of the exhaust gas $c_{\text{p,g}}$ and of air $c_{\text{p,a}}$, η_{TC} is the turbocharger efficiency, $r_{\text{T,TC}}$ is the driving temperature ratio of the turbocharger, $p_{1,\text{s}}$ is the equilibrium turbocharger pressure at a static working point in Pa, p_{amb} and T_{amb} are the ambient pressure in Pa and temperature in K, because the inlet duct, filter and air cooler pressure losses are neglected and π_{tur} is the turbine pressure ratio. The variable turbocharger efficiency is represented with a quadratic function of charge pressure, as follows (Mestemaker *et al.* 2014):

$$\eta_{\text{TC}}(t) = a_\eta + b_\eta p_1(t) + c_\eta p_1^2(t), \tag{3.41}$$

where a_η, b_η and c_η are the polynomial coefficients of the turbocharger for estimating the turbocharger efficiency η_{TC}. The coefficients are estimated from the FAT load P_{FAT} in kW, speed n_{e} in rev/s, charge pressure p_1 in Pa and fuel consumption m_{bsfc} in g/kWh ,Table 3.1, and (3.3), (3.26), (3.32) and (3.36). The first order time delay of the turbocharger reaching equilibrium speed and pressure p_1 in Pa, due to it's inertia, is represented by a time delay τ_{TC}, as follows:

$$\frac{dp_1(t)}{dt} = \frac{p_{1,\text{s}}(t) - p_1(t)}{\tau_{\text{TC}}}. \tag{3.42}$$

The turbine exit temperature T_{ex} is determined from the exhaust receiver temperature T_{d}, using the isentropic turbine efficiency $\eta_{\text{tur,is}}$ and specific heat loss q_{hl} in kJ/kg, as follows:

$$T_{\text{ex,is}}(t) = T_{\text{d}}(t)\left(\frac{p_{\text{ex}}(t)}{p_{\text{d}}(t)}\right)^{\left(\frac{\kappa_{\text{g}}-1}{\kappa_{\text{g}}}\right)} \tag{3.43}$$

$$T_{\text{ex,id}}(t) = T_{\text{d}}(t) + \eta_{\text{tur,is}}(t)(T_{\text{ex,is}}(t) - T_{\text{d}}(t)) \tag{3.44}$$

$$T_{\text{ex}}(t) = T_{\text{ex,id}}(t) - \frac{q_{\text{hl}}(t)}{c_{\text{p,g}}}, \tag{3.45}$$

where $T_{\text{ex,is}}$ is the isentropic turbine exhaust temperature, and $T_{\text{ex,id}}$ is the ideal turbine exhaust temperature, including turbine losses without heat loss. The specific heat loss q_{hl} is considered to be linearly dependant on the temperature difference between the turbine entry temperature T_{d} and ambient temperature T_{amb} and linearly dependant on the reciproke of the mas flow $\dot{m}_{\text{t}}$, as Fourier's law dictates that heat loss depends on temperature flux and residence time, as follows:

$$q_{\mathrm{hl}}(t) = q_{\mathrm{hl,nom}} \frac{(T_{\mathrm{d}}(t) - T_{\mathrm{amb}})}{(T_{\mathrm{d,nom}} - T_{\mathrm{amb}})} \frac{\dot{m}_{\mathrm{t,nom}}}{\dot{m}_{\mathrm{t}}(t)}, \tag{3.46}$$

where $q_{\mathrm{hl,nom}}$ is the nominal specific heat loss determined from FAT measurements using [3.43-3.45] and the following equations for specific compressor and turbine work w_{com} and w_{tur}:

$$w_{\mathrm{com}}(t) = c_{\mathrm{p,a}}(T_{\mathrm{b}}(t) - T_{\mathrm{amb}}) \tag{3.47}$$

$$w_{\mathrm{tur}}(t) = \frac{w_{\mathrm{com}}(t)}{\delta_{\mathrm{f}}(t)\eta_{\mathrm{com,m}}} \tag{3.48}$$

$$w_{\mathrm{tur}}(t) = c_{\mathrm{p,g}}(T_{\mathrm{ex,id}}(t) - T_{\mathrm{d}}(t)), \tag{3.49}$$

where T_{b} is the temperature after the compressor in K and $\eta_{\mathrm{com,m}}$ is the mechanical turbocharger efficiency which is considered constant. The isentropic turbine efficiency $\eta_{\mathrm{tur,is}}$ is determined using a quadratic fit from FAT measurements as in [3.41] based on the following equations:

$$\eta_{\mathrm{tur,is}}(t) = \frac{T_{\mathrm{ex,id}}(t) - T_{\mathrm{d}}(t)}{T_{\mathrm{ex,is}}(t) - T_{\mathrm{d}}(t)} \tag{3.50}$$

$$\eta_{\mathrm{tur,is}}(t) = a_{\eta_t} + b_{\eta_t} p_1(t) + c_{\eta_t} p_1^2(t), \tag{3.51}$$

where a_{η_t}, b_{η_t} and c_{η_t} are the polynomial coefficients of the isentropic turbine efficiency. Finally, the exhaust valve temperature T_{ev} can be estimated using the heat transfer mechanism between the exhaust gasses and exhaust valve during blowdown and scavenging as proposed in Grimmelius *et al.* (2000), as follows:

$$T_{\mathrm{ev}}(t) = \frac{T_6(t) + r_{\mathrm{ht}}(t) T_1}{1 + r_{\mathrm{ht}}(t)} \tag{3.52}$$

$$r_{\mathrm{ht}}(t) = s_{\mathrm{sc}}(t)^{0.8} \left(\frac{T_1}{T_6(t)} \right)^{0.25} \left(\frac{\alpha_{\mathrm{EC}} - \alpha_{\mathrm{IO}}}{\alpha_{\mathrm{IO}} - \alpha_{\mathrm{EC}}} \right)^{0.2}, \tag{3.53}$$

where r_{ht} is the heat transfer ratio between heating during blowdown and cooling during scavenging, α_{IO} is the inlet valve opening angle, α_{EC} is the exhaust valve closing angle, and s_{sc} is the scavenge slip ratio without multiplication of bypass slip factor s_{byp} as the bypass flow does not cool the exhaust valve.

MECHANICAL CONVERSION

The conversion from indicated work in the cylinder to mechanical torque on the output shaft of the diesel engine leads to a torque loss M_{loss} in kNm that is represented with a linear loss model, as follows:

$$M_{\mathrm{e}}(t) = M_{\mathrm{i}}(t) - M_{\mathrm{loss}}(t) \tag{3.54}$$

$$M_{\mathrm{i}}(t) = \frac{w_{\mathrm{i}}(t) m_1(t) i_{\mathrm{e}}}{k_{\mathrm{e}} 2\pi} \tag{3.55}$$

$$M_{\mathrm{loss}}(t) = M_{\mathrm{loss,nom}} \left(1 + M_{\mathrm{loss,grad}} \frac{n_{\mathrm{e,nom}} - n_{\mathrm{e}}(t)}{n_{\mathrm{e,nom}}} \right), \tag{3.56}$$

where M_e is engine torque in kNm, M_i is the indicated torque in kNm, $M_{loss,nom}$ is the nominal torque loss in kNm and $M_{loss,grad}$ is the torque loss gradient. This approach assumes mechanical losses are independent of engine load, which is limitedly accurate. Alternatively, S. Chen *et al.* (1965) demonstrated that friction can be accurately modeled as a function of mean piston speed and mean effective pressure, which is directly related to the load. However, for this approach sufficient empirical data is required, which is not available for the case study in this Chapter.

For the energy management study in Chapter 6 sufficient calibration data was available to implement friction losses according to S. Chen *et al.* (1965). S. Chen *et al.* (1965) have experimentally established that mechanical losses due to friction M_{loss} in Nm can be derived from mean piston speed and mean effective pressure. By correlating (a) the mean piston speed with the rotational speed of the shaft n_{me} in Hz, and (b) the mean effective pressure with the maximum pressure of the Seiliger process p_{max} in Pa, friction losses can be estimated as follows[1]:

$$M^*_{loss}(t) = a + bp^*_{max}(t) + cn^*_{me}(t) + dn^{*2}_{me}(t), \tag{3.57}$$

with $a, b, c, d \in (0, 1)$ fitted parameters that can be calibrated with manufacturer data.

Finally, the first order equation of motion for engine rotation determines the engine speed, as mentioned at the start of this section. Because we consider the engine, gearbox, shaft-line and propeller to be rigidly coupled, the equation of motion for the rotation of this complete assembly is included in the gearbox and shaft-line model, as illustrated in Figure 3.10.

3.2.2. GEARBOX AND SHAFT-LINE MODEL

Literature on modelling of maritime gearbox losses is very limited, even though gearbox losses as a general subject has received renewed interest due to numerical modelling techniques (Concli *et al.* 2016). Models on maritime gearbox losses consist of either a complex thermal network model (Godjevac *et al.* 2016) or a simple gearbox loss function such as the ones in Geertsma *et al.* (2016), Godjevac *et al.* (2016), and Stapersma, (1994). While the thermal network model is based on non-dimensional heuristic estimation models for the various loss sources in the gearbox, it requires very detailed design information of the gearbox, which often is only available for the gearbox designer.

Godjevac *et al.* (2016) has shown that the linear torque loss model proposed in his work can accurately predict gearbox losses calculated with a thermal network model if calibrated correctly. However, Godjevac *et al.* (2016) proposes to use alternative parameters to predict the efficiency on the propeller curve and the generator (constant speed) line. Alternatively, we use values at both the propeller curve and the generator line to predict the gearbox torque losses across the full gearbox operating envelope. As a result, the gearbox torque loss M_l in Nm and the resulting gearbox output torque M_{gb} in Nm can be represented as follows:

$$M_l(t) = M_{l,nom}\left(a_{gb} + b_{gb}\frac{n_e(t)}{n_{e,nom}} + c_{gb}\frac{M_e(t)}{M_{e,nom}}\right) \tag{3.58}$$

[1] The superscript * denotes normalised values.

$$M_{\mathrm{l,nom}} = \frac{P_{\mathrm{l,nom}}}{n_{\mathrm{p,nom}}} \tag{3.59}$$

$$M_{\mathrm{gb}}(t) = M_{\mathrm{e}}(t)\, i_{\mathrm{gb}} - M_{\mathrm{l}}(t), \tag{3.60}$$

where $M_{\mathrm{l,nom}}$ is the nominal gearbox torque loss in Nm, a_{gb}, b_{gb} en c_{gb} are the gearbox loss function parameters, $P_{\mathrm{l,nom}}$ is the nominal gearbox loss power in W and $n_{\mathrm{p,nom}}$ is the nominal gearbox output shaft speed and thus the nominal propeller speed in rev/s. All these parameters can be determined from manufacturer data or from a thermal network model as proposed in Godjevac *et al.* (2016).

Apart from the gearbox losses, the shaft bearings cause additional losses. We assume these shaft-line losses M_{sl} in Nm to depend solely on the gearbox torque M_{gb} in Nm, as follows:

$$M_{\mathrm{sl}}(t) = \eta_{\mathrm{sl}} M_{\mathrm{gb}}(t), \tag{3.61}$$

where η_{sl} is the shaft line efficiency.

Finally, we represent the equation of motion for the engine, gearbox, shaft-line and propeller, which are assumed to be rigidly coupled, as follows:

$$\frac{d n_{\mathrm{p}}(t)}{d t} = \frac{M_{\mathrm{gb(t)}} - M_{\mathrm{sl(t)}} - M_{\mathrm{p}}(t)}{2\pi J_{\mathrm{tot}}} \tag{3.62}$$

$$J_{\mathrm{tot}} = J_{\mathrm{e}} i_{\mathrm{gb}}^2 + J_{\mathrm{gb}} + J_{\mathrm{sl}} + J_{\mathrm{p}} + J_{\mathrm{ew}}, \tag{3.63}$$

where n_{p} is the propeller and shaft-line speed in rev/s, J_{tot} is the total moment of inertia of the shaft and all connected rotating equipment reflected to propeller speed in kgm^2, J_{e} is the moment of inertia of the diesel engine in kgm^2, J_{gb} is the moment of inertia of the gearbox in kgm^2, J_{sl} is the moment of inertia of the shaft-line in kgm^2, J_{p} is the moment of inertia of the propeller in kgm^2 and J_{ew} is the moment of inertia of the entrained water in kgm^2.

3.2.3. PROPELLER MODEL

The first goal of the propeller model is to predict the thrust, torque and efficiency characteristics as a function of propeller pitch, and propeller and ship speed. We use the well established open water test results. In order to allow for reverse thrust, we use the four quadrant open water diagrams, which are widely available for typical propellers, for example in the Taylor and Gawn Series (Gawn, 1952; Taylor, 1933), the most widely used Wageningen B and Ka-series (Kuiper, 1992) and the recently developed Wageningen C- and D-series for Controllable Pitch Propellers (CPPs) (Dang *et al.* 2013, 2012).

In order to use the four quadrant open water diagrams, we first have to express the hydrodynamic pitch angle β in deg as a function of shaft speed n_{p} in rev/s, ship speed v_{s} in m/s and wakefield disturbance due to waves v_{w} in m/s, as follows:

$$v_{\mathrm{a}}(t) = v_{\mathrm{s}}(t)(1 - f_{\mathrm{w}}) + v_{\mathrm{w}}(t) \tag{3.64}$$

$$\beta(t) = arctan\left(\frac{v_{\mathrm{a}}(t)}{0.7\pi n_{\mathrm{p}}(t) D}\right), \tag{3.65}$$

where v_a is the advance speed of the water relative to the propeller in m/s, f_w is the wake fraction, which is considered constant and D is the propeller diameter in m.

The open water diagrams, which in the Wageningen C and D series have been made available in 40th order Fourier series, linearly truncated from the 31st harmonic to the 40th harmonic, provide the associated torque and trust coefficients C_Q and C_T as a function of propeller pitch to diameter ratio P_{pd} at 70% of the radius and the hydrodynamic pitch angle β in deg (Dang *et al.* 2013). The torque Q_p in Nm and thrust T_p in N are represented by the torque and thrust coefficients C_Q and C_T, as follows:

$$v_h(t) = \sqrt{v_a(t)^2 + \left(0.7\pi n_p(t) D\right)^2} \tag{3.66}$$

$$T_p(t) = C_T(t)\frac{1}{2}\rho v_h(t)^2 \frac{\pi}{4} D^2 \tag{3.67}$$

$$Q_p(t) = C_Q(t)\frac{1}{2}\rho v_h(t)^2 \frac{\pi}{4} D^3, \tag{3.68}$$

where v_h is the hydrodynamic velocity in m/s. In order to obtain the actual propeller torque M_p in Nm, the relative rotative efficiency of the propeller η_R, which is assumed constant, needs to be accounted for (Klein Woud *et al.* 2012):

$$M_p(t) = \frac{Q_p(t)}{\eta_R}. \tag{3.69}$$

Because we consider a CPP, the time delay between changing the pitch setpoint and the actual movement of the pitch needs to be accounted for. Grimmelius *et al.* (2006), Wesselink *et al.* (2006) and Godjevac *et al.* (2009) performed an extensive analysis on the non-linear behaviour of the forces in a CPP and in the CPP actuating mechanism and Altosole *et al.* (2012b), Martelli, (2014) and Martelli *et al.* (2014a) have derived a detailed non-linear model for the pitch actuation mechanism of a CPP and included this in a propulsion simulation model. However, in this study, we assume a first order system with time constant τ_P to represent the actuation delay due to friction, oil leakage, pressurising and inertia in the pitch actuation system, because Grimmelius *et al.* (2006) has shown a first order linear system can provide insight in the overall system behaviour as opposed to the behaviour of the CPP actuation mechanism and the associated wear. This leads to the following model equations:

$$\frac{dP_{pd}(t)}{dt} = \frac{P_{pd,set}(t) - P_{pd}(t)}{\tau_P}, \tag{3.70}$$

where $P_{pd,set}$ is the pitch ratio setpoint from the controller.

The second goal of the propeller model is to assess the influence of the control system strategy on the cavitation behaviour of the propeller. A wealth of research is available on the design of propellers and the use of cavitation tunnels and full scale measurements to determine the propeller cavitation behaviour and optimise its design. An extensive review on cavitation research is reported in Terwisga *et al.* (2007). More recently, application of Computational Fluid Dynamics (CFD) has allowed to optimise propeller design based on numerical analysis (Gaggero *et al.* 2014). However, for the purpose of dynamic simulation models, CFD is too detailed and computationally expensive.

Alternatively, Vrijdag, (2009) proposes to use the effective angle of attack α_{eff} in combination with an experimentally determined cavitation bucket of a propeller as a measure of the likelihood of cavitation occurring. The definition of the effective angle of attack α_{eff} and the reasoning behind this definition is extensively described in Vrijdag, (2009) and is as follows:

$$\alpha_{\text{eff}}(t) = \arctan\left(\frac{P_{\text{pd}}}{0.7\pi D}\right) - \arctan\left(\frac{c_1 v_{\text{a}}}{0.7\pi n_{\text{p}} D}\right) - \alpha_{\text{i}}, \tag{3.71}$$

where α_{i} is the shock free entry angle onto the leading edge of the propeller profile in deg, and c_1 is the *Vrijdag* coefficient to calibrate the effective angle of attack with the centre point of the cavitation bucket such that the cavitation bucket can be represented as two lines in the $\alpha_{\text{eff}} - \sigma_{\text{n}}$ phase plane. Vrijdag, 2009, Ch. 7 pp. 115-120 describes the procedure to determine c_1 and Vrijdag, 2009, Ch. 7 pp. 147-159 describes the schematic cavitation bucket in the $\alpha_{\text{eff}} - \sigma_{\text{n}}$ phase plane, with the cavitation number σ_{n} defined as follows:

$$\sigma_{\text{n}} = \frac{p_{\infty} - p_{\text{v}}}{1/2\rho n_{\text{p}}^2 D^2}, \tag{3.72}$$

where p_{∞} is the ambient water pressure at the center-line of the propeller in Pa and p_{v} is the vapour pressure of water at the ambient temperature in Pa. After experimentally determining the cavitation bucket, Vrijdag, (2009) has developed a control strategy that is aimed at maintaining the angle of attack near its optimum value and demonstrates its effectiveness in the $\alpha_{\text{eff}} - \sigma_{\text{n}}$ phase plane. This type of plot will be referred to as a *cavitation plot* in the remainder of this chapter.

3.2.4. HULL MODEL

The proposed model analyses ship motion only in surge direction, as opposed to more complex 6 degree of freedom models proposed in Schulten, (2005) and Martelli *et al.* (2014b). Therefore, the hull model needs to provide an estimate of the ships resistance R_{v} in N as a function of speed v_{s} in kts. The two most used methods to determine the ship resistance are the estimation of the ship resistance with semi-empirical methods such as Holtrop, (1984) and the measurement of the ship resistance in a towing tank test. For this study, tow test measurement were used that were corrected for environmental conditions and fouling (de Boer *et al.* 2011).

Subsequently, the equation of motion represents the ship manoeuvring dynamics in one degree of freedom, as follows:

$$\frac{dv_{\text{s}}(t)}{dt} = \frac{\left(k_{\text{p}} T_{\text{p}}(t) - \frac{R_{\text{v}}(v_{\text{s}}(t))}{1-f_{\text{t}}}\right)}{m}, \tag{3.73}$$

where k_{p} is the number of propellers, f_{t} is the thrust deduction factor, which is assumed constant and m is the ships mass in kg, neglecting the added mass due to the boundary layer.

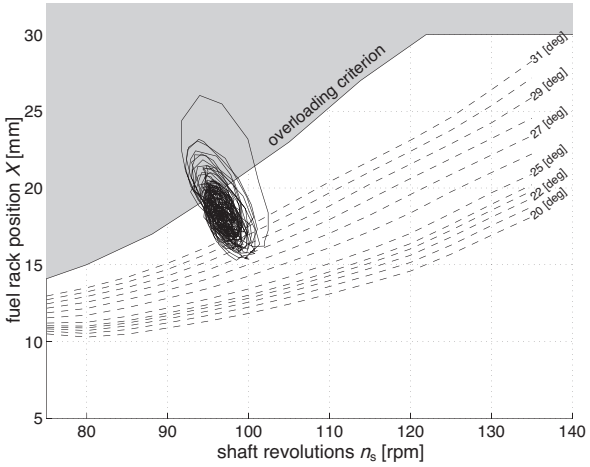

Figure 3.7: Engine speed and fuel rack measurements of diesel direct propulsion in Sea State 6 head waves, plotted in the phase plane, with constant pitch lines in degrees (deg), violating the engine overloading criterion ©IFAC 2001 van Spronsen *et al.* (2001).

3.2.5. WAVE MODEL

Waves can cause serious disturbances on the loading of diesel engines when a ship sails in high sea states, particularly when the engine runs in speed control. van Spronsen *et al.* (2001) have documented measurements on a *Karel Doorman* class frigate sailing in head waves in Sea State 6, which is the worst case scenario within normal operations according to typical design specifications. These measurements, shown in Figure 3.7, clearly illustrate how the disturbance of waves can cause engine overloading.

The wave model takes two disturbances into account: the added resistance due to sea state, wind speed, fouling and displacement and the disturbance on the average speed of the water entering the propeller (Geertsma *et al.* 2016). Additional effects, such as variances in the mean wake speed as a result of the pitching motion of the ship (Taskar *et al.* 2016) or oblique inflow into the propeller (Amini *et al.* 2012) are neglected. The main cause of the disturbance on engine loading is the fluctuating wake speed of the water flowing into the propeller, as previously discussed in Geertsma *et al.* (2016). The orbital movement of water causes a disturbance on the average speed of the water entering the propeller, an exponential distribution of water speed along the depth of the propeller and an oblique inflow. In this study, we are interested in the significant disturbance of the wave orbital movement on the propeller loading, due to the significant wave height. We therefore consider the wake speed relative to the propeller center v_w in m/s, as follows (Gerritsma, 1989; Gerritsma *et al.* 1972):

$$v_{\mathrm{w}}(t) = \zeta \omega_{\mathrm{wv}} e^{k_{\mathrm{w}} z} \cos\left(\alpha_{\mathrm{wk}}(t)\right) \tag{3.74}$$

$$\frac{d\alpha_{\mathrm{wk}}(t)}{dt} = k_{\mathrm{w}} v_s(t) + \omega_{\mathrm{wv}} \tag{3.75}$$

$$k_{\mathrm{w}} = \frac{\omega_{\mathrm{wv}}^2}{g}, \tag{3.76}$$

where ζ is the significant wave amplitude in m, ω_{wv} is the wave radial frequency in rad/s, k_{w} is the wave number in 1/m, z is the water depth in m at the propeller center, α_{wk} is the angle of the vertical wave movement at the propeller centre in rad, and g is the standard gravity in m/s^2.

The resulting model consists of a system of differential and algebraic equations with state variable angle of the vertical wave movement α_{wk}, input ship speed v_{s} in m/s, and output wake speed disturbance due to waves v_{wk} in m/s. The summarising equations are as follows:

$$\frac{d\alpha_{\mathrm{wk}}(t)}{dt} = f_{18}\left(\alpha_{\mathrm{wk}}(t), v_{\mathrm{s}}(t)\right) \tag{3.77}$$

$$v_{\mathrm{wk}} = f_{19}(t)\left(\alpha_{\mathrm{wk}}(t)\right). \tag{3.78}$$

3.2.6. INDUCTION MACHINE AND FREQUENCY CONVERTER

Induction machine models can be categorised in three categories: equivalent circuit models, state-space models and partial or complete finite element models (Singh *et al.* 2016). Because we are interested in the control of the induction machine, including the transients in machine field and torque, we use a fifth-order state-space induction machine model as proposed in Ong, (1998). Furthermore, we assume balanced supply voltage and thus neglect the zero sequence current. In order to reduce the simulation time, we model the flux equations in the synchronously rotating reference frame aligned with the rotor flux, leading to stationary flux vectors and a zero q component of the rotor field, while Ong, (1998) uses the stationary reference frame.

First, the following state equations represent the dynamic behaviour of the stator and rotor flux linkages:

$$\Psi_{\mathrm{qs}}^{\mathrm{e}}(t) = \omega_{\mathrm{b}} \int_0^t \left(u_{\mathrm{qs}}(t) + \frac{r_{\mathrm{s}}}{x_{\mathrm{s}}} \left(\Psi_{\mathrm{mq}}^{\mathrm{e}}(t) - \Psi_{\mathrm{qs}}^{\mathrm{e}}(t) \right) - \frac{\omega_{\mathrm{e}}(t)}{\omega_{\mathrm{b}}} \Psi_{\mathrm{ds}}^{\mathrm{e}}(t) \right) dt \tag{3.79}$$

$$\Psi_{\mathrm{ds}}^{\mathrm{e}}(t) = \omega_{\mathrm{b}} \int_0^t \left(u_{\mathrm{ds}}(t) + \frac{r_{\mathrm{s}}}{x_{\mathrm{s}}} \left(\Psi_{\mathrm{md}}^{\mathrm{e}}(t) - \Psi_{\mathrm{ds}}^{\mathrm{e}}(t) \right) + \frac{\omega_{\mathrm{e}}(t)}{\omega_{\mathrm{b}}} \Psi_{\mathrm{qs}}^{\mathrm{e}}(t) \right) dt \tag{3.80}$$

$$\Psi_{\mathrm{qr}}^{\mathrm{e}}(t) = \omega_{\mathrm{b}} \int_0^t \left(\frac{r_{\mathrm{r}}}{x_{\mathrm{r}}} \left(\Psi_{\mathrm{mq}}^{\mathrm{e}}(t) - \Psi_{\mathrm{qr}}^{\mathrm{e}}(t) \right) - \frac{\omega_{\mathrm{e}}(t) - \omega_{\mathrm{r}}(t)}{\omega_{\mathrm{b}}} \Psi_{\mathrm{dr}}^{\mathrm{e}}(t) \right) dt \tag{3.81}$$

$$\Psi_{\mathrm{dr}}^{\mathrm{e}}(t) = \omega_{\mathrm{b}} \int_0^t \left(\frac{r_{\mathrm{r}}}{x_{\mathrm{r}}} \left(\Psi_{\mathrm{md}}^{\mathrm{e}}(t) - \Psi_{\mathrm{dr}}^{\mathrm{e}}(t) \right) + \frac{\omega_{\mathrm{e}}(t) - \omega_{\mathrm{r}}(t)}{\omega_{\mathrm{b}}} \Psi_{\mathrm{qr}}^{\mathrm{e}}(t) \right) dt \tag{3.82}$$

$$\omega_{\mathrm{e}}(t) = \omega_{\mathrm{r}}(t) - \frac{r_{\mathrm{r}} \omega_{\mathrm{b}} i_{\mathrm{qr}}^{\mathrm{e}}(t)}{\Psi_{\mathrm{dr}}^{\mathrm{e}}(t)} \tag{3.83}$$

$$\rho_{\mathrm{e}}(t) = \int_0^t \omega_{\mathrm{e}}(t) dt, \tag{3.84}$$

where $\Psi_{\mathrm{qs}}^{\mathrm{e}}$ is the quadrature component of the stator flux linkage per second in the rotating reference frame in V, ω_{b} is the base frequency in rad/s, u_{qs} is the quadrature component of the stator voltage in V, r_{s} is the stator resistance in Ω, x_{s} is the stator self-

inductance in Ω, Ψ^{e}_{mq} is the quadrature component of the mutual flux linkage per second in the rotating reference frame in V, ω_e is the frequency of the rotating reference frame in rad/s, Ψ^{e}_{ds} is the direct component of the stator flux linkage per second in the rotating reference frame in V, u_{ds} is the direct component of the stator voltage in V, Ψ^{e}_{md} is the direct component of the mutual flux linkage per second in the rotating reference frame in V, Ψ^{e}_{qr} is the quadrature component of the rotor flux linkage per second in the rotating reference frame in V, r_r is the rotor resistance in Ω, x_r is the rotor self-inductance in Ω, ω_r is the electrical rotor speed in rad/s, Ψ^{e}_{dr} is the direct component of the rotor flux linkage per second in the rotating reference frame in V and ρ_e is the angle of the rotating reference frame relative to the a phase of the stator. The electrical rotor speed ω_r is determined by the induction machine shaft speed ω_i, as follows:

$$\omega_r = P_{pp}\omega_i, \tag{3.85}$$

where P_{pp} is the number of pole pairs of the electric machine.

Second, the relationship between the mutual flux and the stator and rotor flux can be represented, as follows:

$$\Psi^{e}_{mq}(t) = x_M\left(\frac{\Psi^{e}_{qs}(t)}{x_{ls}} + \frac{\Psi^{e}_{qr}(t)}{x_{lr}}\right) \tag{3.86}$$

$$\Psi^{e}_{md}(t) = x_M\left(\frac{\Psi^{e}_{ds}(t)}{x_{ls}} + \frac{\Psi^{e}_{dr}(t)}{x_{lr}}\right) \tag{3.87}$$

$$\frac{1}{x_M} = \frac{1}{x_m} + \frac{1}{x_{ls}} + \frac{1}{x_{lr}}, \tag{3.88}$$

where x_M is the equivalent inductance in Ω and x_m is the mutual inductance in Ω. CHECK difference x_r and x_{lr} in ONG!

Third, the quadrature and direct stator and rotor current in the synchronously rotating reference frame i^{e}_{qs}, i^{e}_{ds}, i^{e}_{qr} and i^{e}_{dr} can be represented by the following equations:

$$i^{e}_{qs}(t) = \frac{\Psi^{e}_{qs}(t) - \Psi^{e}_{mq}(t)}{x_{ls}} \tag{3.89}$$

$$i^{e}_{ds}(t) = \frac{\Psi^{e}_{ds}(t) - \Psi^{e}_{md}(t)}{x_{ls}} \tag{3.90}$$

$$i^{e}_{qr}(t) = \frac{\Psi^{e}_{qr}(t) - \Psi^{e}_{mq}(t)}{x_{lr}} \tag{3.91}$$

$$i^{e}_{dr}(t) = \frac{\Psi^{e}_{dr}(t) - \Psi^{e}_{md}(t)}{x_{lr}}. \tag{3.92}$$

The phase values of the currents can then be obtained using Park's transformation (Ong, 1998, Ch. 5 p. 142). These current values are used as feedback for the controller.

Finally, the electromagnetic torque M_{em} produced in the induction machine can be described as follows:

$$M_{em}(t) = \frac{3P_{pp}}{2\omega_b}\left(\Psi^{e}_{ds}(t)i^{e}_{qs}(t) - \Psi^{e}_{qs}(t)i^{e}_{ds}(t)\right). \tag{3.93}$$

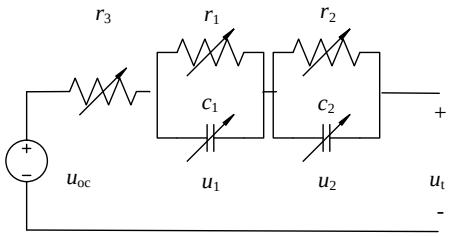

Figure 3.8: Battery equivalent circuit.

This dissertation investigates the mechanical dynamics of parallel control of hybrid propulsion, and does not intend to study the dynamics of the electrical network. Because the response time of modern frequency drives is in the order of ms and the mechanical dynamic response is in the order of 0.1 s, we assume the induction machine is fed with an ideal voltage source. The frequency converter is thus modelled as an ideal voltage source providing the requested voltage and frequency to the induction machine.

3.2.7. BATTERY

The battery model is used to evaluate the battery dynamics and in particular the relationship between the open cell voltage and the state of charge (SOC). Although in this dissertation we assume the state of charge feedback to the Energy Management Strategy is accurate, the used battery model could also be used to investigate SOC estimation schemes and the impact of inaccurate SOC estimation on EMS performance. Therefore, the battery is represented by a 2nd order electrical equivalent circuit model, given in Figure 3.8, as proposed in Tian *et al.* (2014). Equivalent circuit models with one resistor and two resistor-capacitor elements provide a good trade-off between model complexity and accuracy in describing voltage dynamics of a lithium-ion battery (Hu *et al.* 2012; Tian *et al.* 2014). In the proposed model, the open circuit voltage (u_{oc}) in V, capacitors (c_i) in F and resistors (r_i) in Ohm, are functions of the state of charge (SOC), as follows (Erdinc *et al.* 2009; Gao *et al.* 2002):

$$u_{oc}(S_{OC}(t)) = v_1 e^{-v_2 S_{OC}(t)} + v_3 + v_4 S_{OC}(t) + v_5 {S_{OC}}^2(t) + v_6 {S_{OC}}^3(t) \tag{3.94}$$

$$r_i(S_{OC}(t)) = \alpha_{i,1} e^{-\alpha_{i,2} S_{OC}(t)} + \alpha_{i,2}, \quad i = 1,3 \tag{3.95}$$

$$c_i(S_{OC}(t)) = \beta_{i,1} e^{-\beta_{i,2} S_{OC}(t)} + \beta_{i,2}, \quad i = 1,2. \tag{3.96}$$

The constants $\vec{\mathbf{v}} = (v_1, ..., v_6) \in \mathbb{R}^6$ and arrays $\mathbf{A} = (\alpha_{i,j}) \in \mathbb{R}^{3x2}, \mathbf{B} = (\beta_{i,j}) \in \mathbb{R}^{2x2}$ constitute the model's parameters.

The circuit behaviour is described as follows:

$$\frac{d}{dt} u_i(t) = -\frac{u_i(t)}{c_i r_i} + \frac{i_{bat}(t)}{c_i}, i = 1,2 \tag{3.97}$$

$$u_t(t) = u_{oc}(t) - \sum_{i=1}^{2} u_i(t) - r_3 i_{bat}(t). \tag{3.98}$$

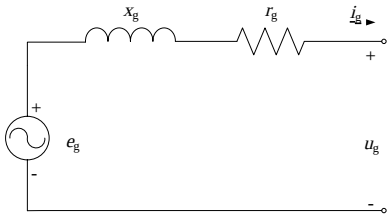

Figure 3.9: Synchronous generator per-phase equivalent circuit.

The performance of any energy management strategy strongly depends on accurate SOC estimation, because the use of the battery is constrained by a minimum SOC to limit battery degradation, and adaptive strategies adapt the use of the battery as a function of the SOC. However, accurate SOC estimation remains challenging, because SOC can not be directly measured and is influenced by parameters such as battery temperature and battery ageing (Hu *et al.* 2012; Tian *et al.* 2014; Waag *et al.* 2014). While the Ampere-hour (Ah) counting method is the simplest method, it is susceptible to accumulated SOC drift due to current measurement errors and requires recalibration with other methods, such as estimation based on open cell voltage (OCV) (F. Zheng *et al.* 2016) or model based estimation (Tian *et al.* 2014). A comprehensive review of SOC estimation techniques and other battery management system functions is available in Waag *et al.* (2014). For this dissertation, we neglect measurement inaccuracies and therefore use Ah counting to estimate SOC, as follows:

$$S_{\mathrm{OC}}(t) = S_{\mathrm{OC}}(t_0) + \int_{t_0}^{t} -\frac{i_{\mathrm{bat}}(t)}{Q_{\mathrm{bat}}} dt. \tag{3.99}$$

3.2.8. DIESEL-GENERATOR SET

This dissertation does not consider the electrical network dynamics since they do not influence fuel consumption (Patel, 2012). As such, simplified models have been developed for the components of the diesel-generator (DG) set, which assume constant voltage and allow us to omit the Automatic Voltage Generator (AVR). A PI controller represents the governor of the DG, and a quadratic relation between torque and injected fuel per cycle has been assumed for the DG, as proposed in Shi *et al.* (2010) and omitting the dependency on engine speed as the DG runs at constant speed. A steady-state model, based on the per-phase equivalent circuit of Figure 3.9 has been used for the synchronous generator. Its state is estimated from the required network current, which is converted into torque demand towards the DG.

First, the instantaneous per-phase voltage u_{gen}, is derived as follows:

$$u_{\mathrm{gen,nom}}(t) = \frac{u_{\mathrm{line}}(t)}{\sqrt{3}} \tag{3.100}$$

$$\omega_{\mathrm{gen,el,nom}}(t) = \omega_{\mathrm{dg,nom}}(t) \frac{P_{\mathrm{pp}}}{2} \tag{3.101}$$

$$u_{\text{gen}}(t) = u_{\text{gen,nom}}(t)\frac{\omega_{\text{gen,el}}(t)}{\omega_{\text{el,nom}}(t)} = u_{\text{gen,nom}}(t)\frac{\omega_{\text{dg}}(t)}{\omega_{\text{dg,nom}}(t)}. \tag{3.102}$$

Subsequently, power input to the generator P_{gen} and electrical power to the network P_{el} in W are determined as follows:

$$P_{\text{gen,el}}(t) = 3u_g(t)i_g(t)\cos\left(f_p\right) \tag{3.103}$$

$$P_{\text{gen,loss}}(t) = \underbrace{P_{\text{gen,nom}}\, c_f}_{\text{Friction Losses}} + \underbrace{\left|i_g(t)\right|^2 r_g}_{\text{Copper Losses}} \tag{3.104}$$

$$P_{\text{gen}}(t) = P_{\text{gen,el}}(t) + P_{\text{gen,loss}}(t) \tag{3.105}$$

$$M_{\text{gen}}(t) = \frac{P_{gen}(t)}{\omega_{\text{dg}}(t)}. \tag{3.106}$$

Finally, the generator dynamics balancing power provided by the generator diesel P_{dg} and power provided to the generator P_{gen}, and the speed governor are represented as follows:

$$m_{\text{f,dg}}(t) = K_P\left(\omega^*_{\text{dg,set}} - \omega_{\text{dg}}(t)^*\right) + K_I\int_0^t\left(\omega^*_{\text{dg,set}} - \omega_{\text{dg}}(t)^*\right)dt \tag{3.107}$$

$$M^*_{\text{dg}} = \left(1 - a(1-m^*_{\text{f}}) + b(1-m^*_{\text{f}})^2\right) \tag{3.108}$$

$$\frac{d\omega_{\text{dg}}}{dt} = \frac{M_{\text{dg}} - M_{\text{gen}}}{2\pi I_{\text{dg}}}, \tag{3.109}$$

with $a, b, c \in (0,1)$ fitted parameters.

3.2.9. AUXILIARY LOADS

The electrical network needs to supply the load for the frequency converters for the induction machines (IMs) when in motoring mode, the battery when in charging mode and all auxiliary electrical loads. While these auxiliary loads fluctuate during tug operations, in this dissertation we do not consider the effect of the auxiliary load and consider this load constant. The relationship between the auxiliary load power P_{aux} and the auxiliary current i_{aux} for the three phase electrical network is defined as follows:

$$P_{\text{aux}}(t) = 3u_{\text{gen}}(t)i_{\text{aux}}(t)\cos\left(f_{\text{p}}\right). \tag{3.110}$$

3.2.10. MECHANICAL PROPULSION SYSTEM MODEL

For the validation of the interaction between the propulsion engine, gearbox, propeller and hull, this chapter uses the direct drive mechanical propulsion system of a *Holland* class Patrol Vessel. The schematic presentation of the direct drive propulsion system is illustrated in Figure 3.10.

In summary, the mechanical propulsion system model consists of 4 sub-models with a system of Differential and Algebraic Equations (DAEs) and the wave sub-model with an Algebraic Equation (AE), with the relations shown in Figure 3.10. The model consists of

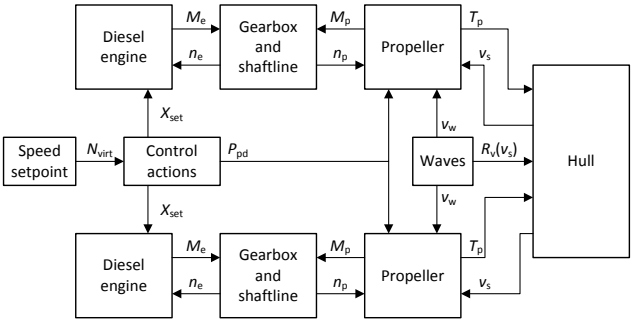

Figure 3.10: Schematic presentation of direct drive propulsion system for naval vessel showing causal coupling between models.

6 state variables: fuel injection per cylinder per cycle m_f, charge pressure p_1, exhaust receiver pressure p_d, propeller speed n_p, propeller pitch P_{pd} and ship speed v_s. The overall system is thus composed of the diesel engine DAEs (3.1), (3.4), (3.5), (3.13)-(3.19), Table 3.1,(3.22)-(3.26) and (3.30)-(3.56), the gearbox DAEs (3.58) and (3.60)-(3.62), the propeller DAEs (4.7)-(3.70), the hull DAE (3.73), and the wave AE (3.74).

3.3. CONVENTIONAL CONTROL

3.3.1. CONTROL OBJECTIVES

THE objective for the conventional control strategy is to represent the control system implemented on the case study, the *Holland* class patrol vessel. The control objectives for this baseline control strategy, used to validate the propulsion system model, are:

- Provide requested virtual shaft speed n_{virt} as defined in Vrijdag *et al.* (2010):

$$n_{virt}(t) = \frac{P_{pd}(t) - P_{pd,0}}{P_{pd,nom}} - P_{pd,0} n_p, \tag{3.111}$$

  where $P_{pd,0}$ is the pitch ratio at which zero thrust is achieved and $P_{pd,nom}$ is the nominal pitch ratio.
- Prevent engine overloading in design conditions by limiting the telegraph position acceleration rate, limiting the pitch increase rate as a function of virtual shaft speed and reducing pitch when the engine margin is too small.
- Provide high manoeuvrability within engine overloading limitations in manoeuvring mode for design conditions.
- Provide high propulsion efficiency within engine overloading limitations in transit mode for design conditions.

3.3.2. CONTROL SYSTEM DESIGN

An extensive review on the control strategies used for mechanical propulsion is covered in Chapter 2 and is available in Geertsma *et al.* (2017a). While some alternative strategies

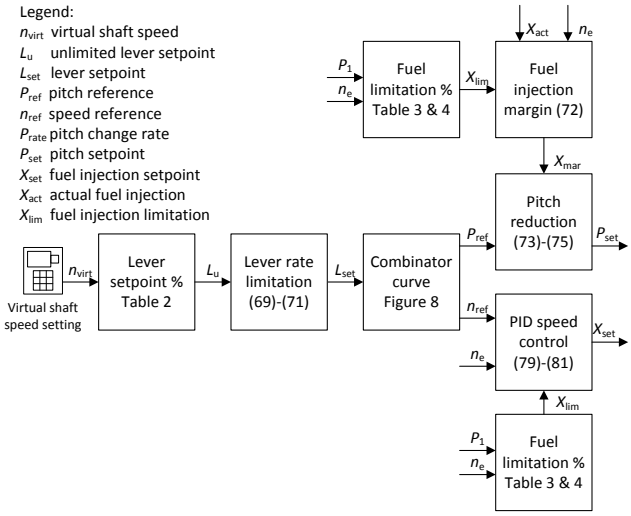

Figure 3.11: Schematic representation of baseline control strategy for diesel mechanical propulsion with CPP.

have been proposed, the basic principle for control of mechanical propulsion with CPPs remains speed control of the engine in combination with one or two fixed combinator curves (Guillemette *et al.* 1997; van Spronsen *et al.* 2001; N. Xiros, 2002). The schematic representation of the baseline control strategy used for validation is given in Figure 3.11.

The virtual shaft speed setpoint $n_{\text{virt,set}}$ in Hz is converted in an unlimited lever setpoint L_u in % with linear interpolation, according to Table 3.2. Subsequently, the increase rate of the lever setpoint is limited to limit engine thermal loading, as follows:

$$L_u(t) - L_{set}(t-\Delta T) > R_{L+}\Delta T: \quad L_{set}(t) = L_{set}(t-\Delta T) + R_{L+}\Delta T \tag{3.112}$$

$$R_{L-} \leq L_u(t) - L_{set}(t-\Delta T) \leq R_{L+}: \quad L_{set}(t) = L_u(t) \tag{3.113}$$

$$L_u(t) - L_{set}(t-\Delta T) < R_{L-}\Delta T: \quad L_{set}(t) = L_{set}(t-\Delta T) + R_{L-}\Delta T, \tag{3.114}$$

where L_{set} is the setpoint after rate limitation in %, ΔT is the time step over which the rate is limited, R_{L+} is the maximum increase rate of the lever setpoint and R_{L-} is the maximum decrease rate of the lever setpoint.

The relationship between the lever setpoint L_{set} and the propeller pitch and engine speed references P_{ref} and n_{ref} is expressed in the combinator curves for manoeuvring mode and transit mode, as illustrated in Figure 3.12. The fuel injection limitations X_{lim} in % as a function of charge pressure p_1 in Pa and engine speed n_e in rev/s are represented in Table 3.3 and 3.4.

The pitch is reduced when the fuel injection margin X_{mar} is below $X_{mar,min}$ in order to prevent thermal overloading and the pitch increase rate R_{P+} is limited according to

Table 3.2: Unlimited lever setpoint L_u as a function of virtual shaft speed setpoint $n_{virt,set}$.

virtual shaft speed	rpm	0	84	128	186	230
unlimited lever setpoint	%	0	25	50	95	100

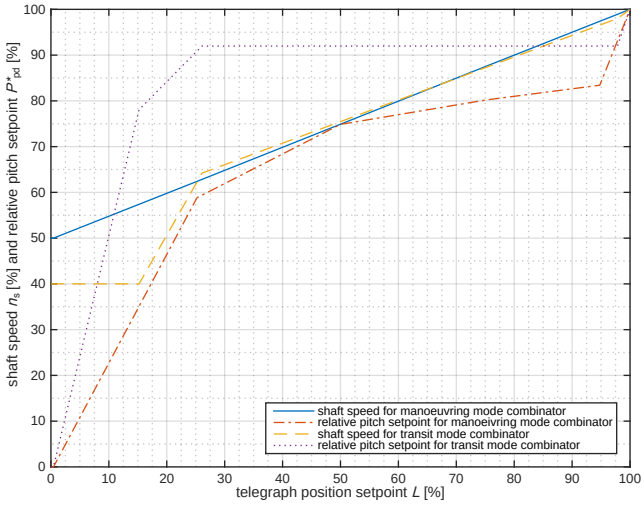

Figure 3.12: Combinator curves for baseline control strategy in manoeuvring and transit modes.

Table 3.3: Fuel injection limitation X_{lim} as a function of charge pressure p_1.

absolute charge pressure	kPa	0	100	300	350	400	500
fuel injection limitation	%	42	42	103	109	115	115

Table 3.4: Fuel injection limitation X_{lim} as a function of engine speed n_e.

engine speed	rpm	400	500	500	700	800	900	1000
fuel limitation	%	40	46	55	67	84	105	105

Table 3.5: Pitch increase rate R_{P+} as a linear interpolation function f_1 of virtual shaft speed n_{virt}.

virtual shaft speed	rpm	0	40	77	153	190	230	240
pitch increase rate	%/s	3	2	1	1	0.5	0.2	0.2

the linear relationship f_1 shown in Table 3.5, as follows:

$$X_{mar} = X_{lim} - X_{set} \tag{3.115}$$

$$X_{mar} < X_{mar,min}\% : R_{P+} = R_{Pr} \tag{3.116}$$

$$X_{mar} \geq X_{mar,min}\% : R_{P+} = f_1(n_{virt}), \tag{3.117}$$

where X_{set} is the fuel injection setpoint for the fuel pump in % and n_{virt} is the actual virtual shaft speed in Hz. Subsequently, the pitch setpoint P_{set} is represented by the following equations:

$$P_{ref}(t) - P_{set}(t - \Delta T) > R_{P+}\Delta T : \\ P_{set}(t) = P_{set}(t - \Delta T) + R_{P+}\Delta T \tag{3.118}$$

$$R_{P-} \leq P_{ref}(t) - P_{set}(t - \Delta T) \leq R_{P+} : \\ P_{set}(t) = P_{ref}(t) \tag{3.119}$$

$$P_{ref}(t) - P_{set}(t - \Delta T) < R_{P-}\Delta T : \\ P_{set}(t) = P_{set}(t - \Delta T) + R_{P-}\Delta T, \tag{3.120}$$

where R_{P-} is the maximum decrease rate of the pitch setpoint.

The controller algorithm for the engine speed control that provides the fuel injection setpoint X_{set} is as follows:

$$X_{PID}(t) = K_P\left(\frac{n_{ref}(t)}{100} - \frac{n_e(t)}{n_{e,nom}}\right) + \\ K_I\int_0^t\left(\frac{n_{ref}(t)}{100} - \frac{n_e(t)}{n_{e,nom}}\right)dt \tag{3.121}$$

$$X_{PID}(t) \leq X_{lim}(t) : X_{set}(t) = X_{PID}(t) \tag{3.122}$$

$$X_{PID}(t) > X_{lim}(t) : X_{set}(t) = X_{lim}(t), \tag{3.123}$$

where X_{PID} is the unlimited fuel injection setpoint, K_P is the proportional gain and K_I is the reset rate. The control parameters are listed in Table 3.6.

3.3.3. CONTROL SYSTEM TUNING

The settings of the control parameters in Table 3.2, 3.3, 3.4, 3.5 and 3.6 and Figure 3.12 have been determined through extensive dynamic simulations (de Boer *et al.* 2011). Because the relationship between the control parameters and the propulsion system MOEs is not very clear and depends on the operational conditions, the tuning requires weeks of analysing simulation time traces. Moreover, while the risk of thermal overloading has

Table 3.6: Control parameters in manoeuvring mode (MAN) and transit mode (TRAN).

Propulsion mode	**MAN**	**TRAN**
proportional gain K_P	2	2
reset rate K_I	0.5	0.5
maximum lever increase rate R_{L+}	1.5 %/s	0.75 %/s
maximum lever decrease rate R_{L-}	-3 %/s	-1.5 %/s
pitch reduction rate R_{Pr}	-1.89 %/s	-1.89 %/s
minimum injection margin $X_{mar,min}$	16.5%	16.5%
maximum pitch reduction rate R_{P-}	-10 %/s	-10 %/s

been eliminated, manoeuvrability, cavitation noise and fuel consumption might suffer from the conservative settings. However, the lack of MOPs to quantify system performance, has limited a thorough analysis of the trade-off between the various MOEs.

3.4. VALIDATION OF PROPULSION SYSTEM MODEL

WE use the terminology for model qualification, verification and validation as proposed in Schlesinger *et al.* (1979). The model qualification, the analysis to obtain the conceptual model, and the conceptual model itself have been described in Section 3.2. We have performed the model verification per subsystem, as proposed in Vrijdag, (2009), for each of the subsystem models by varying the input parameters and comparing the response with analytical results (see Figure 3.16 and 3.19).

Validation procedures with statistical analysis for a complex multidisciplinary simulation model have been described in Du *et al.* (2002), Schulten *et al.* (2007), Vrijdag *et al.* (2007), Vrijdag, (2009) and Vrijdag, (2014). Schulten *et al.* (2007) quantify the uncertainty of the static model results by estimating the parameter uncertainty and running the simulation model for the extremes of the 95% confidence interval for the full model. Alternatively, Du *et al.* (2002) propose to estimate the parameter uncertainty and subsequently determine the sensitivity of the sub-model either mathematically with Taylor approximations or numerically with infinitesimally small disturbances. Subsequently, the total ship model uncertainty can be established with linearisation by first order Taylor approximations. Vrijdag *et al.* (2007) compare these two methods with a case study and conclude the method proposed in Du *et al.* (2002) is more efficient while delivering comparable results. Subsequently, the validity of the model can be determined by comparing the model result interval with the confidence interval of measurements (Schulten *et al.* 2007). Another widely used method, Monte Carlo simulation, has been applied to a propulsion system model in Vrijdag, (2014). While this method can handle non-linearities, as opposed to the method in Du *et al.* (2002), it does not provide insight in system behaviour. The main drawback of all these approaches is that the outcome of the statistical analysis strongly depends on the estimated parameter uncertainty and that other types of uncertainty are not addressed.

In our case, we want to establish how well we can predict the behaviour of a propulsion plant in uncertain operational conditions based on the model and its calibration with Factory Acceptance Test (FAT) data and determine how we can use this model to quantify the performance of the system and its control strategy for various MOEs. Subsequently, we want to use it to analyse the influence of the control strategy on the performance of the system as a whole quantified through a number of MOPs. Therefore, in this section we carry out quantitive validation with measurements of the ship in real operational conditions during the ships SAT.

3.4.1. DIESEL ENGINE MODEL VALIDATION

The diesel engine models proposed in this dissertation, or earlier versions proposed in Miedema *et al.* (2002) and Geertsma *et al.* (2016), have not been validated in previous work. Therefore, this section first discusses the parametrisation and calibration of the model, based on the approach described in Vrijdag, (2009). Subsequently, a quantitative validation wil be discussed using the full FAT data.

The parameters used in the diesel engine model have been obtained from four sources. Most engine parameters are available from the engine project guide and operating manual (MAN Diesel SE, 2008a,b). Furthermore, some parameters have been estimated based on diesel engine theory (Stapersma, 2010a,b) or general physics theory. Finally, FAT results have given the remaining parameters, for calibration of the turbocharger efficiency as a function of the charge pressure, heat loss as a function air flow and turbocharger entry temperature and heat release as a function of engine speed. The diesel engine parameters and their source have been summarised in Table 3.7.

The model is run at the FAT speed and power settings with the parameters from Table 3.7. The results in Figure 3.13, 3.14 and 3.15 show that the FAT measurements for specific fuel consumption, charge air pressure, combustion pressure, fuel injection and exhaust receiver temperature are within 5% of the model predictions. The turbocharger exit temperature is also reasonably predicted with the model, although the deviation at 25% load is slightly higher at 8%.

The FAT measurement data only consists of a limited amount of operating points in the full engine operating envelope, along the propeller curve. Full validation of the model requires measurements across all operating points of the engine. Therefore, a more extensive measurement campaign is recommended for further model validation. Alternatively, using measurements form Platform Management System logging of operational vessels can provide data for further validation analysis.

For completeness, Figure 3.16 shows the specific fuel consumption and the air excess ratio over the complete operating envelope of the engine. When comparing this with the specific fuel consumption of a typical high speed engine in Figure 3.18, as published in van Straaten *et al.* (2012), the model results are within 5 % down to 10 % load of the engine. The minimum air excess ratio within the engine operating envelope is 1.4. This value can serve as a minimum air excess ratio that needs to be maintained in dynamic conditions.

Figure 3.17 shows the exhaust valve temperature and the exhaust receiver temperature, and therefore the entry temperature of the turbine. The trend of the exhaust valve temperature exactly matches the trend of the air access ratio, as previously demonstrated

Table 3.7: Diesel engine parameters from project guide (PG), physics theory (P), FAT data (F) or estimate (E).

Diesel engine parameter description	**value**	**source**
nominal engine power $P_{e_{nom}}$	5400 kW	PG
nominal engine speed $n_{e_{nom}}$	16.7 rev/s	PG
number of cylinders i_e	12	PG
number of revolutions per cycle k_e	2	PG
bore diameter D_B	0.28 m	PG
stroke length L_S	0.33 m	PG
crank rod length L_{CR}	0.64063	PG
crank angle after TDC, inlet closure α_{IC}	224 °	PG
crank angle after TDC, exhaust open α_{EO}	119 °	PG
nominal spec. fuel consumption $m_{bsfc_{nom}}$	198 g/kWh	PG
heat release efficiency η_q	0.886	PG
geometric compression ratio ε_c	13.8	PG
total nominal mass flow $\dot{m}_{t_{nom}}$	10.5 kg/s	PG
cylinder volume at state 1 V_1	0.0199 m^3	PG
nominal pressure at state 1 $p_{1_{nom}}$	4.1e^5 Pa	PG
maximum cylinder pressure $p_{max_{nom}}$	188e^5 Pa	PG
temperature after the intercooler T_c	323 K	PG
temperature of the inlet duct T_{inl}	423K	E
parasitic heat exchanger effectiveness ε_{inl}	0.05	E
fuel injection time delay τ_X	0.015 s	E
turbocharger time constant τ_{TC}	5 s	E
exhaust receiver time constant τ_{p_d}	0.01 s	E
gas constant of air R_a	287 J/kgK	P
specific heat at constant volume of air $c_{v,a}$	717.5 J/kgK	P
specific heat at const. pressure of air $c_{p,a}$	1005 J/kgK	P
specific heat at const. p of exhaust gas $c_{p,g}$	1100 J/kgK	P
isentropic index of air κ_a	1.4	P
isentropic index of the exhaust gas κ_g	1.353	P
lower heating value of fuel h^L	42700 J/kg	PG
stoichiometric air to fuel ratio σ_f	14.5	PG
polytropic exponent for expansion n_{exp}	1.38	E
polytropic exponent for blowdown n_{bld}	1.38	E
nominal mechanical efficiency $\eta_{m_{nom}}$	0.90	E
constant volume portion gradient $X_{cv_{grad}}$	-0.4164	F
constant temperature portion $X_{ct_{nom}}$	0.4	E
turbocharger factor a_η	-3.29e^{-12}	F
turbocharger factor b_η	-2.52e^{-6}	F
turbocharger factor c_η	0.2143	F
ambient pressure p_{amb}	1e^5 Pa	PG
ambient temperature T_{amb}	318 K	PG

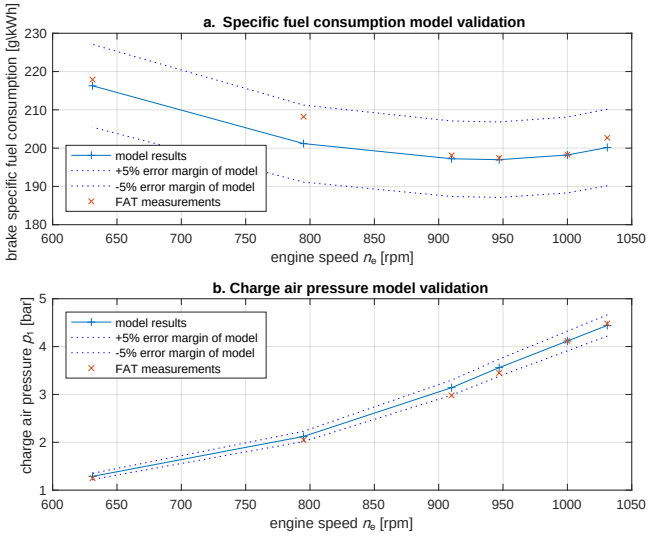

Figure 3.13: Diesel engine model validation with FAT results for specific fuel consumption and charge air pressure.

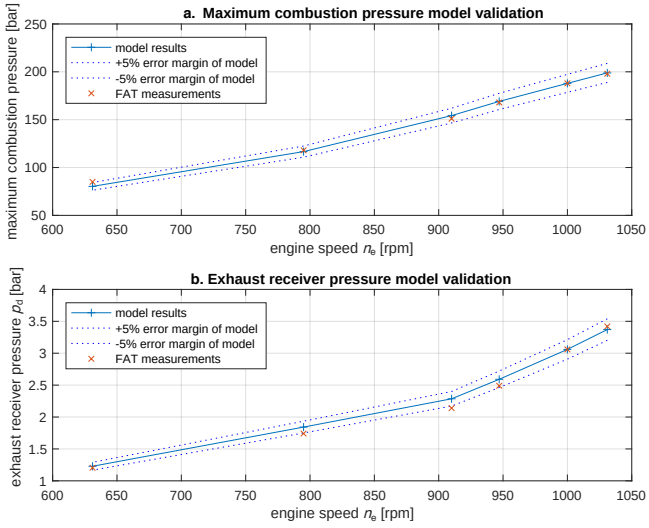

Figure 3.14: Diesel engine model validation with FAT results for specific fuel consumption and charge air pressure.

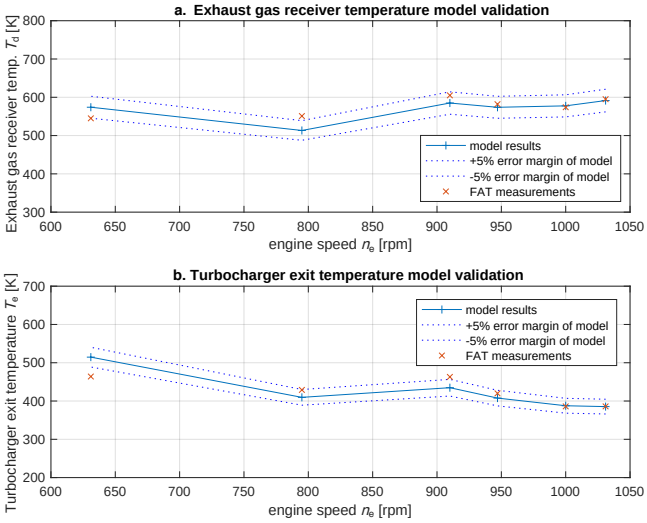

Figure 3.15: Diesel engine model validation with FAT results for maximum combustion and exhaust receiver pressure.

with modelling and experiments in Sapra *et al.* (2017). This suggests that the air access ratio can serve as a good indicator for engine thermal loading. Although the trend of the exhaust receiver temperature shows an even bigger discontinuity at 900 rpm, the speed below which the cylinder bypass valve opens and provides extra cooling air to the exhaust receiver, the exhaust receiver temperature is also strongly influenced by the air access ratio.

3.4.2. GEARBOX MODEL VALIDATION

The gearbox loss model parameters a_{gb}, b_{gb} and c_{gb} and the nominal gearbox loss $P_{l,nom}$ in W were obtained from a linear fit through three data points of the gearbox manufacturer data and are presented in Table 5.4. When inspecting the results from the gearbox loss model in Figure 3.19 and comparing them with the losses obtained from the manufacturers data over the full torque and speed envelop, we establish that the obtained values are within 1%, confirming the visual impression that the gearbox power losses exhibit a quadratic relationship with engine speed.

3.4.3. PROPELLER MODEL VALIDATION

Available propeller models and data series have been discussed in Geertsma *et al.* (2016) and an extensive review is available in Carlton, (2012). In this dissertation we use the Wageningen CD series, which represent 'contemporary and practical CPP designs' (Dang *et al.* 2012). Moreover, the 5 blade propellers in this series represent CPP design 'aimed at applications for the navies'Dang *et al.* (2012) and the design compromise was focused on 'better cavitation performance for high pitch and large blade ara ratios ' (Dang *et al.*

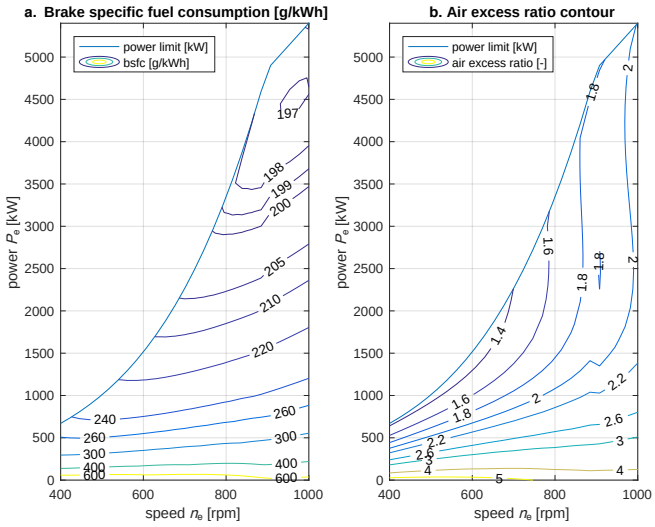

Figure 3.16: Diesel engine model specific fuel consumption and air excess ratio results in complete operating envelope of the engine.

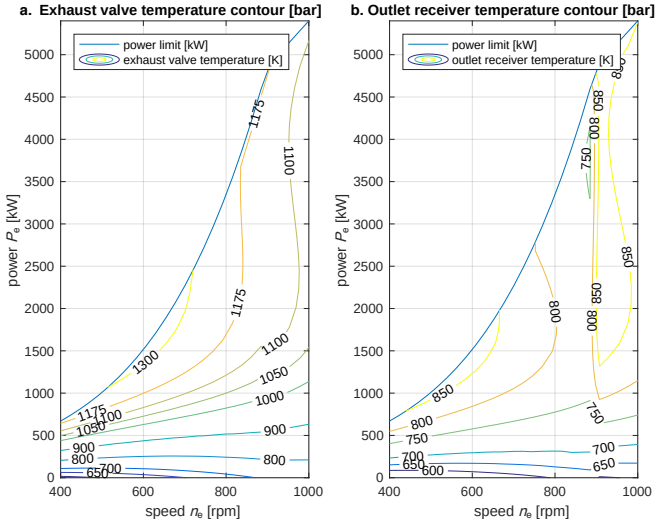

Figure 3.17: Diesel engine model exhaust vale and exhaust receiver temperature results in complete operating envelope of the engine.

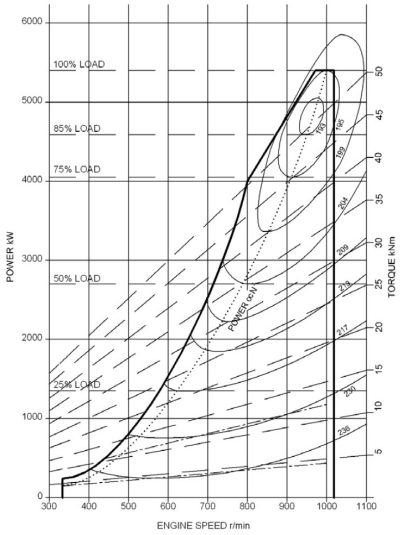

Figure 3.18: Specific fuel consumption of typical high speed engine from van Straaten *et al.* (2012).

Table 3.8: Gearbox parameters.

gearbox loss parameter a_{gb}	0
gearbox loss parameter b_{gb}	0.75
gearbox loss parameter c_{gb}	0.25
gearbox nominal power loss $P_{l_{nom}}$ in kW	109
gearbox speed reduction ratio i_{gb}	4.355
nominal propeller speed $N_{p_{nom}}$ in rpm	230
total inertia J_t in kgm^2	4600

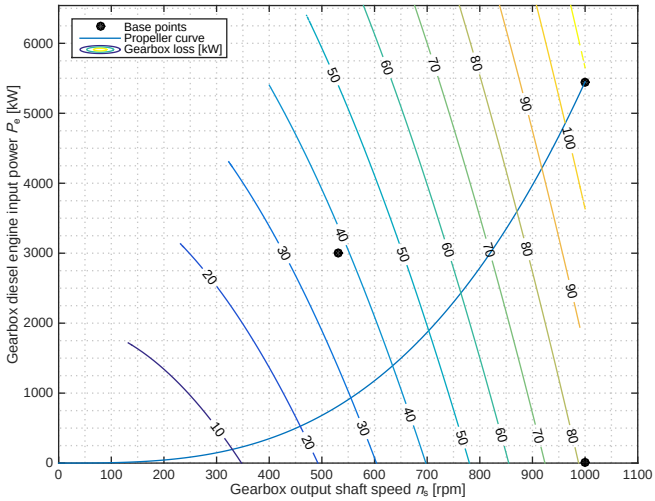

Figure 3.19: Gearbox loss model contour plot with the three data points used for the linear fit and the propeller curve.

Table 3.9: Propeller parameters.

wake fraction w	0.08
relative rotative efficiency η_R	1
propeller diameter D in m	3.2
design pitch ratio at 0.7R P_d	0.8
nominal pitch ratio at 0.7R P_{nom}	1.18
pitch ratio for zero thrust P_0	0.068
first order pitch actuation delay τ_P	1.67
Vrijdag coefficient c_1	0.7
shock free entry angle α_i	0

2012). We use the Wageningen C5-60 propeller, which has been made available to the partners in the Joint Industry Project on developing the Wageningen C- and D-series for Controllable Pitch Propellers (CPPs). This propeller has a similar open water diagram to the propeller fitted to the *Holland class* patrol vessel. The propeller parameters are presented in Table 5.5.

Because the Wageningen C5-60 propeller is not yet publicly available, this chapter does not present the model results of this propeller separately. Clearly, the model uses the results of the open water tests, which is a well accepted method to model propeller thrust and torque within the assumptions of a homogenous advance speed, perpendicular flow into the propeller and quasi static performance. However, the modelling strategy

Table 3.10: Hull and wave model parameters in trial, design and off-design condition.

Condition	trial	service	off-design
ship mass m in 10^3kg		3800	
number of propellers m		2	
thrust deduction factor t		0.155	
propeller center depth z in m		6.5	
wave amplitude ζ in m	0	1	2.5
wave frequency ω in rad/s	-	0.966	0.628
wave number k	-	0.095	0.0402

and software code needs to be verified. For verification purposes we refer to the results of the C4-40 propeller presented in Geertsma *et al.* (2016), which can be compared with the results presented in Dang *et al.* (2013). Moreover, for an uncertainty analysis of the method used to determine the Wageningen C- and D-series propellers, we refer to Dang *et al.* (2012).

3.4.4. HULL AND WAVE MODEL VALIDATION

The ship resistance and the wave model parameters very strongly depend on the conditions in which the ship operates. In order to investigate the effect of varying conditions we consider three typical conditions. Trial condition is defined as Sea State 0, wind speed of 3 m/s and no fouling. Service condition is defined as Sea State 4, wind speed of 11 m/s, head seas and wind and 6 months out of dock fouling. Off-design condition is defined as Sea State 6, wind speed of 24 m/s, head seas and wind and 6 months out of dock fouling. The parameters that represent these conditions are shown in Table 3.10 and Figure 3.20.

The validation of resistance test results is routinely performed by organisations such as MARIN, who have performed the resistance test. However, the total ship model validation demonstrates that the model's resulting ship speed corresponds with the tow tank test results. The verification of the behaviour of the propulsion plant in waves is performed with the total ship model based on ship measurements.

3.4.5. TOTAL SHIP MODEL VALIDATION

The total ship model consist of the mechanical propulsion system model described in Section 3.2 and of the control strategy described in Section 3.3. The parameters and validation of these models have been discussed in the previous Sections. The aim of this Section is to quantitatively validate the dynamic behaviour of the total ship model including the conventional control strategy. To this end, we compare the simulation results of an acceleration manoeuvre with the actual measurements of the same acceleration manoeuvre performed during the SAT's of *HNLMS Holland*, shown in Figure 3.21. Even though the available measurements are limited, the available measurements deliver good confidence in the model credibility. Moreover, we compare the behaviour of the propulsion plant sailing at constant speed in waves with earlier measurements per-

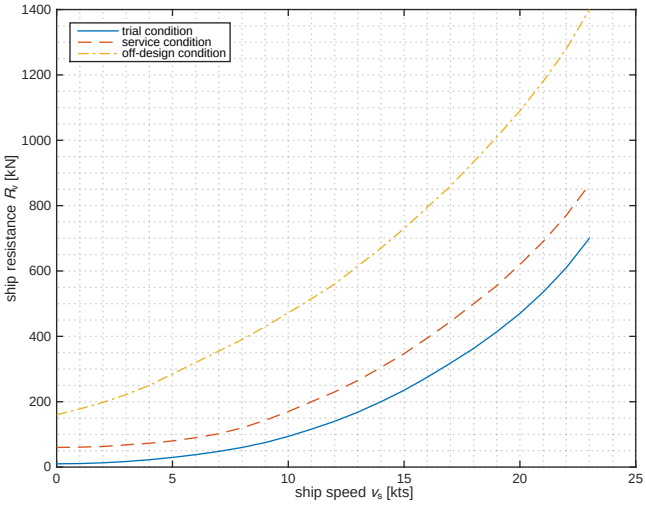

Figure 3.20: Ship resistance from model tests corrected for environmental conditions and fouling in trial, service and off-design condition.

Figure 3.21: *Zr. Ms. Holland.*

formed on a *Karel Doorman* class frigate in Sea State 6 as reported in van Spronsen *et al.* (2001).

ACCELERATION MANOEUVRE

The results of the acceleration manoeuvre from zero ship speed and a virtual shaft speed of 0 rpm to a setpoint of 230 rpm virtual shaft speed at time t = 30s are presented in Figure 3.22, 3.23 and 3.24. The model results during the manoeuvre for fuel injection,

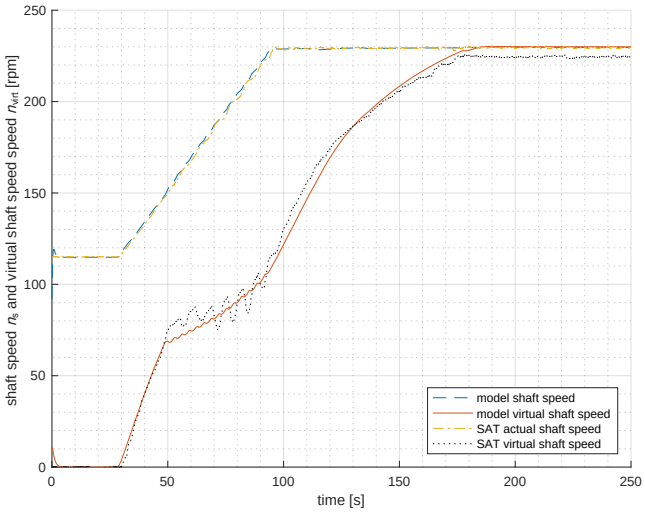

Figure 3.22: Total ship model validation with SAT results for shaft speed and virtual shaft speed.

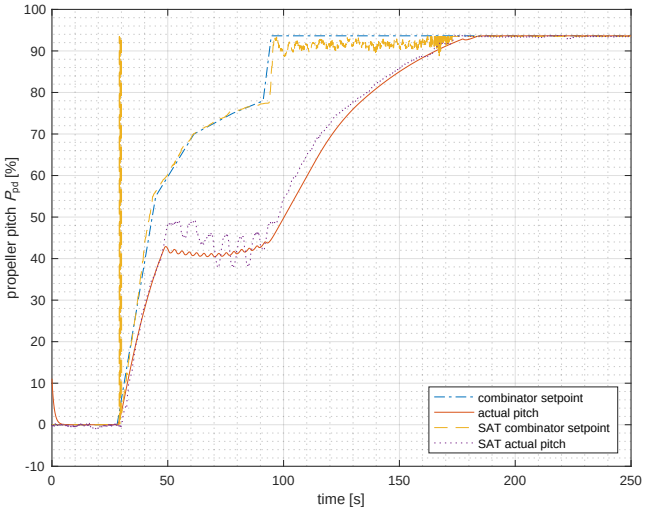

Figure 3.23: Total ship model validation with SAT results for engine loading and margin.

shaft speed and virtual shaft speed stay within 5% of the measurements. The pitch has a larger deviation, but this is caused by the different open water diagram of the actual propeller compared to the C5-60 propeller that was used in the model.

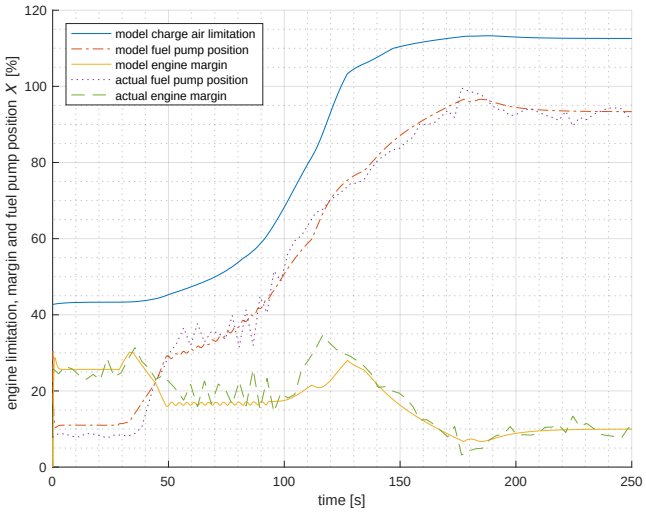

Figure 3.24: Total ship model validation with SAT results for propellor pitch and propeller pitch setpoints.

The following main differences between the model results and the measurements can be identified:

- The model fuel pump position is approximately 2.5% higher than the measured fuel pump position at the start of the manoeuvre when the diesel engine load is below 10%. The results in Figure 3.16 and 3.18 show the overestimated fuel consumption of the model causes this difference. This can possibly be resolved with more accurate modelling of the heat losses during expansion and blowdown after performing a more extensive measurement campaign on an engine, as discussed in Section 3.4.1.
- The response of the actual pitch has a time variant dead time of maximum 2 s on top of the linear delay. This delay is mainly caused by the counter balance valve as described in detail in Wesselink *et al.* (2006). Wesselink *et al.* (2006) propose to either remove the counter balance valve or maintain the control pressure of the counter balance valve if a fast pitch actuation is required to support an *angle of attack* control strategy as proposed in Vrijdag *et al.* (2010). Then, a pitch actuation bandwidth of 0.6 Hz can be achieved. Alternatively, the nonlinear effects could be included in the model as proposed in Wesselink *et al.* (2006), Altosole *et al.* (2012b) and Martelli *et al.* (2014a) or the nonlinear effects could be neglected and the pitch actuation bandwidth of the model could be reduced to 0.15 Hz, leading to $\tau_P = 6.7$.
- The actual engine margin between $t = 105$s and $t = 130$s is significantly higher than the predicted engine margin. Because the charge pressure has not been logged the actual cause of this difference cannot be accurately determined. A possible cause is the non-linear behaviour of the pitch actuation. However, the propeller

Table 3.11: Changed propulsion model parameters to simulate a typical frigate, similar to *Karel Doorman* class at 100 rpm virtual shaft speed.

Parameter	value
Propeller diameter in m	4.2
Propeller pitch ratio at 100 rpm	1.2
Gearbox ratio	7.3

pitch and engine loading of the model and the measurements in this time bracket do behave similarly. Therefore, the predicted performance of the total system model stays within 5% of the actual measurements.

- The combinator setpoint signal measured during the SAT exhibits what appears to be a high amount of signal noise. The signal is supposed to be constant at 93.5%, which is the final pitch setpoint associated with the virtual shaft speed of 230 rpm. Moreover, the signal features a spike at t=30s, before following the expected ramp. The cause of this noise is unknown but does not appear to influence the overall system response.

In summary, this quantitative validation demonstrates that the model predicts the total propulsion system behaviour within 5%.

SAILING IN HEAVY SEAS

Measurements of sailing in heavy seas of the patrol vessel are not available. The only available measurements of a similar ship sailing in heavy seas have been reported in Vrijdag, (2009) and van Spronsen *et al.* (2001). van Spronsen *et al.* (2001) report the measurements of a *Karel Doorman* class frigate in Sea State 6 and the results of these measurements are shown in Figure 3.7.

To use these measurements for verification of the modelling strategy, we have changed the model parameters to reflect the main parameters of a typical frigate. The parameters used are shown in Table 3.11. For the hull and wave model parameters off-design conditions are assumed, as the reported results have been obtained in Sea State 6. Moreover, the pitch reduction strategy was not used in this simulation, because during the measurements no pitch reduction strategy was included in the control strategy and overloading actually occurred. Figure 3.25 shows the results at 100 rpm virtual shaft speed of the propulsion system model that is modified to reflect a *Karel Doorman* class frigate.

The results in Figure 3.25 demonstrate that the average magnitude of the disturbance of the engine speed and fuel injection due to the waves is predicted well: the fuel rack position fluctuates between 15 and 22 mm, with a nominal fuel rack position of 30 mm. The irregular effects of waves that clearly appear in the measurements in Figure 3.7, are neglected in the model. Therefore, the propulsion system model does not predict the extreme values of the disturbance due to waves, but predicts the effect due to the significant wave height (Gerritsma, 1989).

An accurate statistical analysis of the uncertainty of the model cannot be performed with these measurements, because the sea state only roughly determines the range of

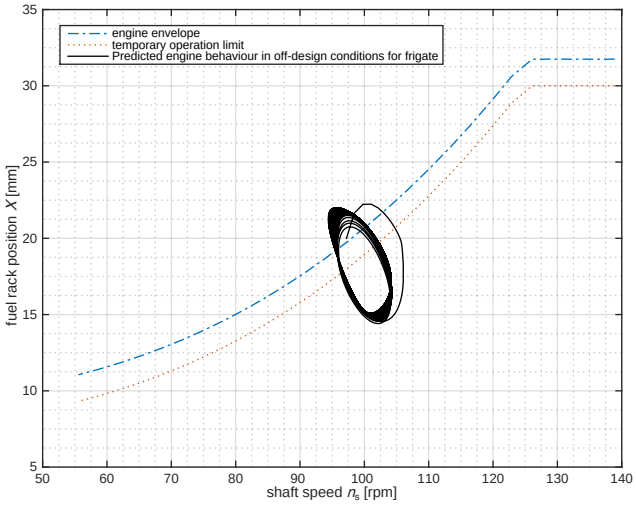

Figure 3.25: Total ship model validation of simulated M-frigate at 100 rpm in Sea State 6.

the wave height. For example, Sea State 6 is defined as a significant wave height between 4 and 6 m. More accurate loggings or measurements of the actual wave height would be required as input data for an accurate statistical analysis.

3.5. MEASURES OF PERFORMANCE

VARIOUS standardised operating profiles have been determined in the automotive field to evaluate and compare MOPs of energy management strategies for hybrid electric vehicles, such as the world-harmonised light-duty vehicle test cycle (WLTC) and the new European driving cycle (NEDC) (Ko *et al.* 2017). Moreover, a control benchmark simulation model exists for these control strategies (Sciarretta *et al.* 2014). These standards have not yet been defined for the evaluation of ship control strategies. Altosole *et al.* (2012a, 2017) propose the *slam start* and *crash stop* manoeuvres to evaluate control strategy performance during the most extreme acceleration and deceleration manoeuvres. While these manoeuvres are very valid to evaluate the feasibility of control strategies, they do not quantify MOEs, such as fuel consumption and engine loading, during regular operational conditions. Theotokatos *et al.* (2015) map performance and emission parameters of a ship propulsion system in the engine operating envelope, but do not extend the analysis to measure ships effectiveness, for example expressing fuel consumption in ton/mile.

The aim of this dissertation is to evaluate MOEs fuel consumption, rate of acceleration, engine thermal loading and propeller cavitation with a validated model and obtain insight into the influence of the control strategy on holistic system performance. For this purpose, we propose the following benchmark manoeuvres:

- Sail at constant speed in trial, design and off-design conditions;
- Accelerate from 0 to 15 kts with the slam start manoeuvre: increasing the lever setpoint to maximum virtual shaft speed at once (Altosole *et al.* 2012b).
- Accelerate from 0 to 5, 5 to 10 and 10 to 15 kts in design conditions with an intermediate sprint. The intermediate sprint manoeuvres are performed by increasing the virtual shaft speed from the setting corresponding to the initial ship speed to the setting corresponding to the final ship speed.

Moreover, we propose the following MOPs, obtained from these benchmark manoeuvres:

- Fuel consumption per mile for trial, design and off-design conditions, presented as a function of ships speed during sailing at constant speed, as previously proposed in Klein Woud *et al.* 2012, Ch12, pp. 482-483;
- Acceleration time for speed increases from 0 to 5, 5 to 10, 10 to 15 and 0 to 15 kts in design conditions;
- Average air excess ratio at constant speed for trial, design and off-design conditions, presented as a function of ship speed. This performance criterion serves as an indicator for engine thermal loading during constant speed sailing due to the average temperature;
- Minimum air excess ratio during speed increases from 0 to 5, 5 to 10, 10 to 15 and 0 to 15 kts in design conditions. This performance criterion serves as an indicator for engine thermal loading due to acceleration manoeuvres;
- Air excess ratio fluctuation at constant speed for design and off-design conditions, presented as a function of ship speed. This performance criteria serves as an indicator for thermal stresses in the engine caused by waves due to temperature fluctuation;
- Cavitation plot of acceleration manoeuvres from 5 to 10 and 10 to 15 kts in design conditions.

The MOPs of the baseline propulsion model and control system are shown in Figures 4.29, 4.30, 4.31, 4.7, 4.8, Table 3.12 and Table 3.13. These simulation results have been obtained with MATLAB Simulink R2016b software on a PC with Intel Core i7 processor and 16 GB memory. The required time to run all simulations to obtain these MOPs is 1 hour.

3.5.1. DISCUSSION

We can now compare the performance of the transit mode, with a combinator curve with relatively high pitch, low engine speed and slow acceleration rates for pitch and engine speed, with the performance of the manoeuvring mode, with a combinator curve with relatively low pitch, high engine speed and fast acceleration rates for pitch and engine speed and observe the following:

- The combinator curve of the transit mode achieves 30% less fuel consumption at 5 kts, 10% less fuel consumption at 10 kts and 2% less fuel consumption at 15 kts

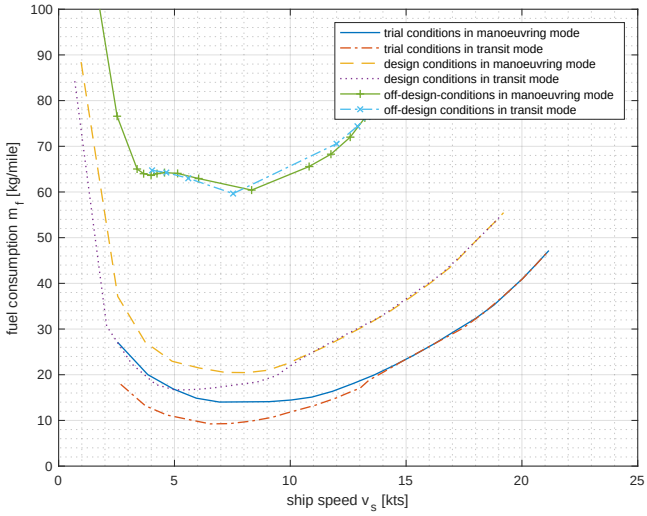

Figure 3.26: Fuel consumption plot as a function of ships speed for various conditions in manoeuvring and transit mode.

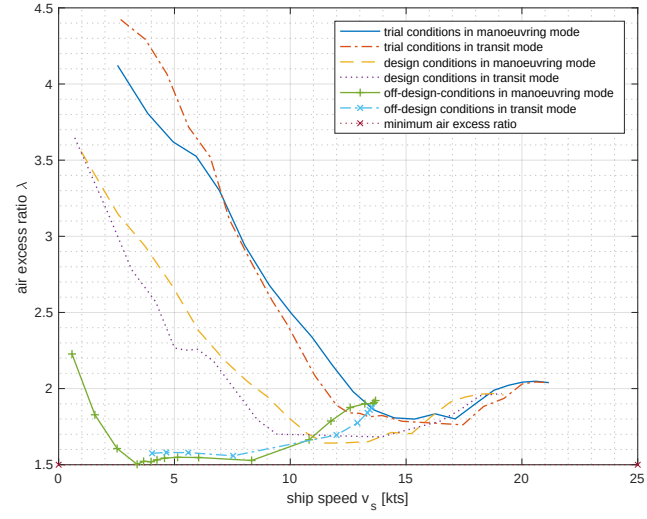

Figure 3.27: Air excess ratio plot as a function of ships speed for various condition in manoeuvring and transit mode.

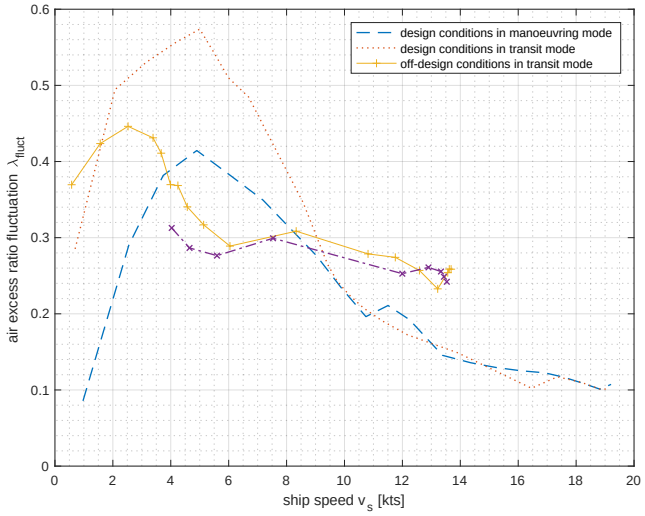

Figure 3.28: Air excess ratio fluctuation plot as a function of ships speed for design and off-design conditions in manoeuvring and transit mode.

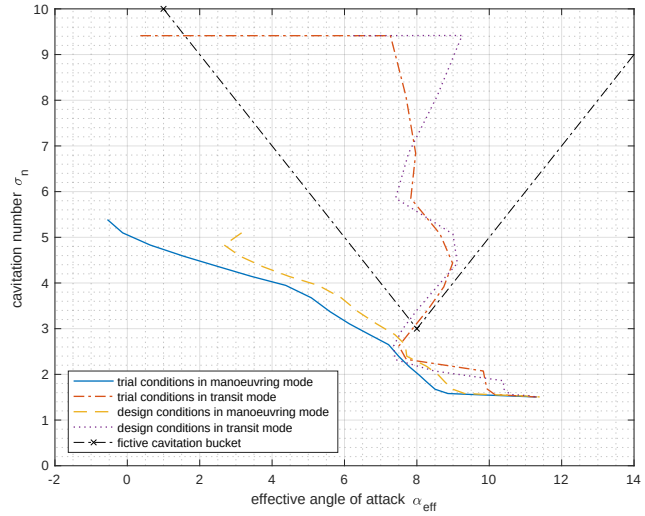

Figure 3.29: Cavitation plot from low speed to maximum speed for various conditions in manoeuvring and transit mode.

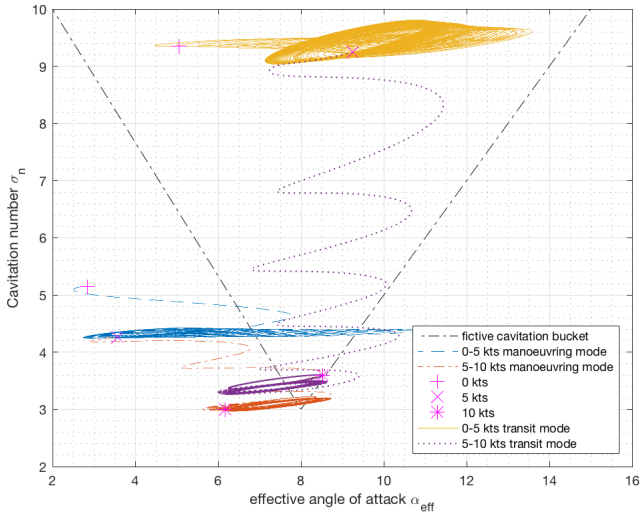

Figure 3.30: Cavitation plot for acceleration manoeuvres at design condition in manoeuvring and transit mode.

Table 3.12: Acceleration time, minimum air excess ratio and maximum angle of attack during acceleration in manoeuvring mode (design condition).

Criterion	**0-5 kts**	**5-10 kts**	**5-15 kts**	**0-15 kts**
Acceleration time (s)	100	114	80	100
Air excess ratio	1.77	1.65	1.65	1.75
Angle of attack (deg)	9.6	10.6	12.6	12.2

Table 3.13: Acceleration time, minimum air excess ratio and maximum angle of attack during acceleration in transit mode (design condition).

Criterion	**0-5 kts**	**5-10 kts**	**5-15 kts**	**0-15 kts**
Acceleration time (s)	384	845	152	170
Air excess ratio	1.67	1.63	1.64	1.76
Angle of attack (deg)	12.8	11.1	12.4	10.7

compared to the manoeuvring mode. The increased fuel consumption of the manoeuvring mode is mainly caused by the reduced open water efficiency of the propeller due to the reduced pitch. Further reducing fuel consumption can possibly be achieved by further increasing the pitch during transit mode when the engine loading allows this, in trail and design conditions. In off-design conditions, however, the difference in fuel consumption disappears, because the pitch reduction enforces the same reduced pitch for the transit mode to prevent overloading of the engine.

- The air excess ratio at constant speed in manoeuvring mode is 0.1 to 0.3 higher than in transit mode, at low speeds when the pitch reduction mechanism is not limiting pitch. This lower air excess ratio leads to a significantly lower thermal loading of the engine, of approximately 30 to 90 K. This is caused by the lower pitch and higher engine revolutions and enables using higher acceleration rates for pitch and engine speed without thermally overloading the engine. Due to these high acceleration rates the acceleration time of the ship is in average 2 times faster in manoeuvring mode than in transit mode.
- In order to investigate the methodology of using the cavitation plot to assess the cavitation performance, we define a fictive cavitation bucket that matches the propeller and is centred at an angle of attack of 8 degrees. However, the shown cavitation buckets for these propeller have not been determined through measurement and are only shown to give some indication of the control strategy influence on cavitation behaviour. With this fictive cavitation bucket, the combinator curve of the transit mode falls within this bucket up to a speed of 10 kts for static conditions and only slightly violates the cavitation bucket during acceleration manoeuvres up to the same speed. Alternatively, the low pitch of the manoeuvring mode causes it to significantly violate the cavitation bucket. The cavitation plots for constant speed sailing and acceleration manoeuvres are both positioned outside the typical cavitation bucket.

In conclusion, the MOPs can be used to quickly and quantitatively asses the performance of a control strategy and its parameters. Moreover, these benchmark manoeuvres and performance criteria can be used to compare performance of alternative control strategies, but also of alternative propulsion configurations.

3.6. CONCLUSIONS AND RECOMMENDATIONS

AFTER having established candidate architectures and control strategies for a particular ship type and its function based on the literature review in Chapter 2 or a quantitive mathematical model (Georgescu *et al.* 2018, 2017), thus answering Research Questions 1 and 2, a method is required to objectively and quickly quantify and assess the effectiveness of the system architecture and control strategy for diesel mechanical and hybrid propulsion systems and answer Research Question 3 and 4. This chapter has proposed a new diesel propulsion system model that can be parameterised with available manufacturer data. This model is based on a previous Mean Value First Principle (MVFP) model and has been improved to reflect modern turbocharger and Miller-timing behaviour based on advanced diesel engine theory. Subsequently, we have validated the

MVFP diesel engine model with measurements in factory conditions and in operational conditions at sea with a case study naval vessel. The predictions of the diesel engine model are within 5% of most measurement values, including the exhaust gas receiver temperature T_d, which will be used to quantify engine thermal loading in combination with the air excess ratio λ and the exhaust valve temperature T_{ev}.

The baseline control strategy for mechanical propulsion with fixed combinator curves, acceleration limitations and pitch reduction strategy has been described. We have shown that this strategy can prevent engine overloading effectively while achieving conservative manoeuvrability, acceleration and cavitation behaviour. Quantitative validation has demonstrated that the propulsion system model credibly predicts propulsion system behaviour within 5% accuracy. Moreover, the wave model behaviour in Sea State 6 has been verified with the propulsion system model with modified parameters that reflect a frigate. The results of this model were found to match measurements on a frigate in Sea State 6. Moreover, we have proposed models for the induction machine and frequency converter for hybrid propulsion and simple models for the diesel generator, battery and auxiliary loads for hybrid power supply. Thus, we have answered Research Question 3 by proposing a simulation model for mechanical and hybrid propulsion and hybrid power generation, that can be used to to quantify MOEs fuel consumption, emissions, radiated noise, propulsion availability, manoeuvrability and maintainability due to engine mechanical and thermal loading.

Finally, this chapter has proposed benchmark manoeuvres and associated measures of performance (MOPs) to quantify the performance of the propulsion plant on the following measures of effectiveness (MOEs): fuel consumption, rate of acceleration, engine thermal loading and propeller cavitation, thus answering Research Question 4. These MOPs and the propulsion system model have been used to evaluate the performance of two operating modes of the conventional control strategy. Analysing these two control modes previously either required days of sea trials, or weeks of analysing various simulation time traces. Alternatively, the proposed MOPs can be determined within an hour of simulation time. Depending on the particular control strategy and operating conditions, fuel savings up to 30%, thermal loading reduction of 90 K and reductions of 50% in acceleration time can be achieved.

In Chapter 4, the model proposed in this chapter is used to evaluate an adaptive pitch control strategy that aims to reduce fuel consumption and emissions, improve the ships manoeuvrability and reduce cavitation noise while preventing engine overloading compared to the conventional control strategy for the case study *Holland* class Patrol Vessel, to answer Research Question 5. Adding the induction motor model, as proposed in Section 3.2.6 and Geertsma *et al.* (2017b) will allow to evaluate the performance of hybrid propulsion plants with CPP as well. Chapter 5 uses the proposed model and MOEs to propose and evaluate the performance of a parallel control strategy that uses the adaptive pitch control strategy proposed in Chapter 4 in combination with torque control of the electric drive, to answer Research Question 6. Finally, Chapter 6 uses the models proposed in this Chapter to evaluate novel Energy Management strategies for hybrid propulsion with hybrid power supply, to answer Research Question 7.

4

ADAPTIVE PITCH CONTROL FOR MECHANICAL AND HYBRID PROPULSION

Shipping urgently needs to reduce its impact on the environment, both due to CO_2, NO_x and particulate matter (PM) emissions and due to underwater noise. On the other hand, multifunction ships such as offshore support vessels, anchor handling and towing vessels, naval vessels and wind farm construction and support vessels require fast and accurate manoeuvring and need highly reliable systems to support reduced or no crew. Diesel mechanical propulsion with controllable pitch propellers provides high efficiency and low CO_2 emissions, but has traditionally been poor in manoeuvrability, can suffer from thermal overloading due to manoeuvring and requires significant measures to meet NO_x and PM emission regulations. The control strategy of diesel mechanical propulsion with fixed combinator curves is one of the causes of the poor manoeuvrability, thermal overloading and cavitation noise during manoeuvring, such as slam start and intermediate acceleration manoeuvres. This chapter proposes an adaptive pitch control strategy with slow integrating speed control that can reduce fuel consumption, CO_2, NO_x and PM emissions and underwater noise, can improve acceleration performance, can limit engine loading and can prevent engine under- and overspeed, thus answering Research Question 5: 'What control strategy can be used for controllable pitch propellers to provide the best possible performance against an adaptive trade-off between the various conflicting MOEs listed in Section 1.2?'

This chapter is organised as follows: After the introduction in Section 4.1, Section 4.2 proposes the adaptive pitch control strategy and establishes its settings for the case study Holland *class Patrol Vessel; Section 4.3 evaluates the control strategy and compares its performance with the baseline control strategy of the case study Patrol Vessel as introduced in Chapter 3; and finally, Section 4.4 presents the main conclusions.*

Parts of this chapter have been published in Applied Energy **228** (2018), Geertsma *et al.* (2018).

4.1. INTRODUCTION

CHAPTER 3 quantifies a savings potential for pitch control of up to 30% at certain speeds and operating modes for vessels with diesel mechanical propulsion and high manoeuvrability requirements, at the expense of slow acceleration and increased engine thermal loading. How these fuel savings can be achieved while also accelerating fast and limiting engine thermal loading will be addressed in this chapter.

4.1.1. LITERATURE REVIEW

The most applied control strategy for pitch control is the use of a fixed relationship between the setpoint: lever position or virtual shaft speed; and the control actions: propeller pitch ratio and engine speed (Geertsma *et al.* 2017a; Klein Woud *et al.* 2012; Martelli, 2014; Martelli *et al.* 2017). The optimum propeller pitch ratio and gearbox ratio is then determined for the design point of the propulsion plant, according to the matching procedure proposed in Stapersma, (2005) or, alternatively, in Coraddu *et al.* (2011). Figari *et al.* (2009) demonstrate that fuel consumption and emissions can be reduced by dynamically changing pitch, when sea, wind and loading conditions change, without fully addressing control system design. Vrijdag *et al.* (2008) conclude that one combinator curve cannot achieve optimal cavitation performance while maintaining engine loading limitations across all operating conditions, due to variations in weather, ship loading and hull fouling. Therefore, Vrijdag *et al.* (2010) propose a control strategy that maintains an optimum inflow angle of the water onto the propeller blade, *angle of attack*, in the pitch control region of the combinator, and demonstrates the feasibility of this approach in sea trials. The sea trials, in combination with simulation studies, also demonstrate that the engines are not thermally overloaded and acceleration performance improves significantly (Vrijdag, 2009; Vrijdag *et al.* 2007, 2009). The impact on fuel consumption of the ship and the influence of the primary engine speed control strategy on system dynamics were not addressed.

While engine speed control is used as a standard for propulsion engines due to its robust control and under- and overspeed protection, as discussed in Chapter 2 (Geertsma *et al.* 2017a), speed control does lead to significant and potentially damaging load disturbances in waves (Faber, 1993; Guillemette *et al.* 1997; Stapersma *et al.* 2004, 2009; van Spronsen *et al.* 2001). Alternative speed control strategies, such as H_∞ state feedback control (N. Xiros, 2002), optimal speed feedback using speed signal amplification (Guillemette *et al.* 1997), multivariable adaptive extremum engine control (Mizuno *et al.* 2010) and Multiple Input and Multiple Output (MIMO) optimal speed and pitch H_∞ control (van Spronsen *et al.* 2001), can all reduce the load fluctuation, but still aim to reject disturbance of engine speed due to waves with fuel injection control action. While a multivariable control scheme utilising a variable geometry turbocharger can improve manoeuvrability while maintaining smoke emission constraints, as proposed in Stefanopoulou *et al.* (2000), this requires a diesel engine with variable geometry turbocharger. Similarly, adaptive feedforward control of exhaust gas recirculation can reduce emissions in large diesel engines, but only if equipped with exhaust gas recirculation (Nielsen *et al.* 2017a).

Alternatively, Sorensen *et al.* (2009) found that, for electric propulsion, primary control based on torque, power or combined torque-and-power control all gave less thrust,

torque and power variance in waves than speed control, while accurately following thrust commands. While a slight increase in shaft speed fluctuation was observed, the stable nature of the propulsion system ensured shaft speed oscillations remained acceptable. For extreme situations, such as propeller emergence, thrust loss estimation and anti-spin thruster control can be added to prevent overspeed and thrust loss (Bakkeheim *et al.* 2008; Smogeli *et al.* 2008; Sorensen, 2005). Similarly, Coraddu *et al.* (2013) demonstrated with both simulation model experiments and free running model tests that torque and power control leads to lower load fluctuation in turns. Moreover, Blanke *et al.* (2007) demonstrated in a tow-tank test environment that the propeller efficiency in moderate waves increases with up to 2% for torque control compared to speed control, due to the variation in advance speed from waves. Similarly, torque or power control for propulsion diesel engines has been reported by Blanke *et al.* (1990), Faber, (1993), and Geertsma *et al.* (2016). Both Faber, (1993) and Blanke *et al.* (1990) discuss how power control can lead to reduced loading and thermal fluctuations on propulsion diesel engines, but neither quantify the variance reduction or demonstrate the feasibility. Geertsma *et al.* (2016) propose torque control and demonstrate torque control can eliminate thermal loading fluctuation due to waves and significantly reduce cylinder peak temperatures. However, practical feasibility and implementation with pitch control were not addressed.

4.1.2. AIM AND CONTRIBUTION

While shipping urgently has to reduce its environmental impact due to emissions and underwater noise, many ship types, such as offshore vessels, interterminal transport vessels, windturbine construction and support vessels, ferries, and naval vessels also require fast and accurate manoeuvring and reduced maintenance to support reduced maintenance and autonomous shipping (Kretschmann *et al.* 2017; H. Zheng *et al.* 2017a). This chapter investigates how much fuel consumption and emissions can be reduced with the novel *adaptive pitch control* strategy, while also improving straight line manoeuvring performance and limiting engine thermal loading. Moreover, settings that minimise risk of propeller cavitation for this control strategy are proposed.

The novelty of this work is threefold: First, we propose a novel adaptive pitch control strategy for diesel mechanical and hybrid propulsion with controllable pitch propellers, which combines the angle of attack approach for propeller pitch control (Vrijdag *et al.* 2010) with slow integrating speed control for diesel engine fuel injection. Secondly, we demonstrate how this approach can be used in a control strategy that works across the speed range of the ship to reduce fuel consumption and CO_2 emissions and increase acceleration performance, while consistently limiting engine thermal loading. Finally, we quantify performance improvement with the proposed control strategy for a case study patrol vessel compared to the current baseline control strategy.

4.2. ADAPTIVE PITCH CONTROL STRATEGY

THE adaptive pitch control strategy aims to achieve many control objectives with essentially the same control actions as the baseline pitch control strategy. These control actions are propeller pitch ratio setpoint and fuel pump injection setpoint: $u(t) = [P_{\text{p,set}}, X_{\text{set}}]$. While the baseline control strategy uses measured system outputs propeller

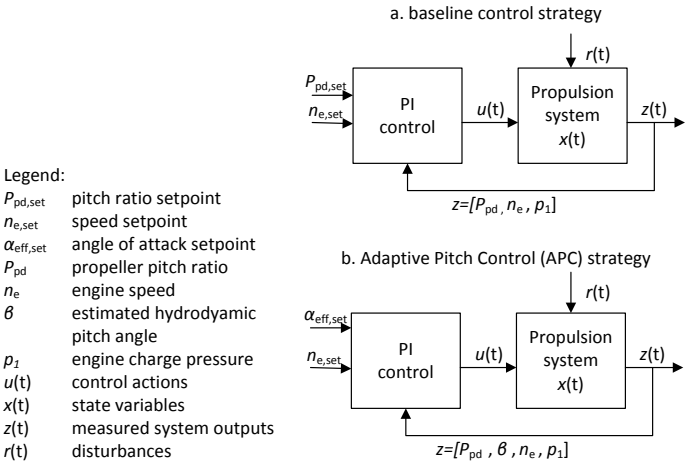

Figure 4.1: Simplified representation of baseline control strategy and proposed adaptive pitch control strategy for diesel mechanical propulsion with CPP.

pitch ratio P_{pd} and engine speed n_e, the adaptive pitch control strategy additionally uses the estimated hydrodynamic pitch angle: $z(t) = [P_{\text{pd}}, n_{\text{e}}, \beta]$. The comparison of the simplified representation of both feedback control strategies is presented in Figure 4.1. The following section extensively discusses the control objectives and how the proposed adaptive pitch control strategy achieves highly improved and near optimal performance for these objectives, within the physical limitations of the propulsion system components.

4.2.1. CONTROL OBJECTIVES

The control objective for the adaptive pitch control strategy is to optimise for the Measures of Effectiveness (MOEs) fuel consumption, manoeuvrability, engine thermal loading and, in some cases, cavitation noise, while providing the requested virtual shaft speed. In order to quantify the performance against these MOEs, we use the Measures of Performance (MOPs) (Roedler *et al.* 2005) proposed in Chapter 3 (Geertsma *et al.* 2017c). The control objectives derived from these MOPs are:

1. Provide requested virtual shaft speed n_{virt} as defined in (3.111) (Vrijdag *et al.* 2010).
2. Maintain operation within the cavitation bucket for the widest possible operating conditions.
3. Minimise fuel consumption across the ship speed profile and for all operating conditions.
4. Maintain engine air excess ratio λ within predefined limits. We will investigate system performance against a number of minimum values of the air excess ratio λ.
5. Prevent engine overspeed and under-speed.

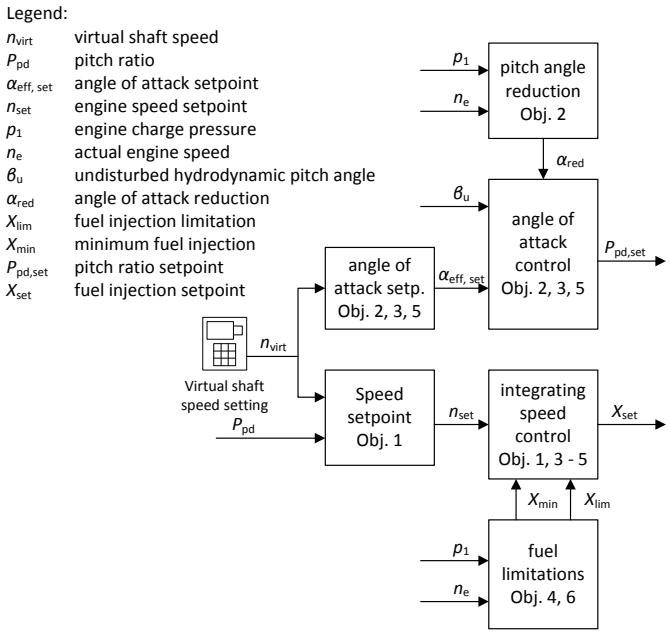

Figure 4.2: Schematic representation of proposed adaptive pitch control strategy for diesel mechanical propulsion with CPP.

The proposed control strategy is presented schematically in Figure 4.2. Next, we will discuss the proposed control laws and constraints, and how they achieve the control objectives.

VIRTUAL SHAFT SPEED

The first control objective is to provide the requested virtual shaft speed as defined in (3.111). In the conventional control strategy, this is achieved with fixed combinator curves, as shown in Figure 3.12. While the proposed adaptive pitch control strategy changes pitch based on operating conditions, the speed setpoint needs to be adjusted to compensate pitch changes. Therefore, the speed setpoint is determined from the actual pitch, as previously proposed in Vrijdag *et al.* (2010), as follows:

$$n_{set}(t) = \frac{P_{\mathrm{pd,nom}} - P_{\mathrm{pd},0}}{P_{\mathrm{pd}}(t) - P_{\mathrm{pd},0}} n_{\mathrm{virt,set}}(t). \tag{4.1}$$

MAINTAIN OPERATION WITHIN THE CAVITATION BUCKET

After experimentally determining the propeller cavitation bucket, Vrijdag, (2009) has developed a control strategy that is aimed at maintaining the optimum inflow angle of the water onto the propeller blade, the angle of attack, near its optimum value. Experiments demonstrate the effectiveness of this strategy in the $\alpha_{\mathrm{eff}} - \sigma_{\mathrm{n}}$ phase plane, which will be referred to as a cavitation plot in the remainder of this chapter. This effective angle of attack α_{eff}, is defined as follows:

$$\alpha_{\text{eff}}(t) = \arctan\left(\frac{P_{\text{pd}}(t)}{0.7\pi}\right) - \arctan\left(\frac{c_1 v_{\text{a}}(t)}{0.7\pi n_{\text{p}}(t) D_{\text{p}}}\right) - \alpha_{\text{i}}, \tag{4.2}$$

where α_{i} is the shock free entry angle onto the leading edge of the propeller profile in deg, and c_1 is the coefficient to calibrate the effective angle of attack with the centre point of the cavitation bucket such that the cavitation bucket can be represented as two lines in the $\alpha_{\text{eff}} - \sigma_{\text{n}}$ phase plane. Vrijdag, 2009, Ch. 7, pp. 115-120 describes the procedure to determine c_1 and Vrijdag, 2009, Ch. 7, pp. 147-159 describes the schematic cavitation bucket in the $\alpha_{\text{eff}} - \sigma_{\text{n}}$ phase plane, with the cavitation number σ_{n} defined as follows:

$$\sigma_{\text{n}}(t) = \frac{p_\infty - p_{\text{v}}}{1/2 \rho_{\text{sw}} \left(n_{\text{p}}(t)\right)^2 D_{\text{p}}^2}, \tag{4.3}$$

where p_∞ is the ambient water pressure at the center-line of the propeller in Pa, p_{v} is the vapour pressure of water at the ambient temperature in Pa, ρ_{sw} is seawater density in kg/m^3, and D_{p} is the propeller diameter in m.

The proposed control strategy forms the basis for the control strategy proposed in this chapter. While the implementation of the angle off attack strategy in Vrijdag, (2009) was aimed at minimising cavitation, the work already concluded that this control strategy improves acceleration behaviour and prevents the loss of ship speed due to pitch reduction when preventing engine loading. This chapter aims to quantify the benefits of the adaptive pitch control strategy and proposes an integrated control strategy aimed at achieving all control objectives mentioned above. The angle off attack setpoint $\alpha_{\text{eff, set}}$ can be defined as a function of the virtual shaft speed, but in this case is taken constant and determines the normalised pitch control setpoint $P^*_{\text{pd, set}}$, as follows:

$$P^*_{\text{pd,set}}(t) = \frac{0.7\pi \tan\left(\theta_{\text{set}}(t) - \theta_{\text{red}}(t)\right) + P_{\text{pd,0}}}{P_{\text{pd,nom}} - P_{\text{pd,0}}} \tag{4.4}$$

$$\theta_{\text{set}}(t) = \alpha_{\text{eff,set}} + \alpha_{\text{i}} + \arctan\left(c_1 \tan\left(\beta(t)\right)\right) \tag{4.5}$$

$$\beta(t) = arctan\left(\frac{v_{\text{a}}(t)}{0.7\pi n_{\text{p}}(t) D_{\text{p}}}\right) \tag{4.6}$$

$$v_{\text{a}}(t) = v_{\text{s}}(t)(1 - f_{\text{w}}) + v_{\text{w}}(t), \tag{4.7}$$

where θ_{set} is the pitch angle setpoint in rad, θ_{red} is the pitch angle setpoint reduction in rad, β is the hydrodynamic pitch angle in rad, v_{a} is the advance speed of the water relative to the propeller in m/s, and f_{w} is the wake fraction, which is considered constant.

While the actual hydrodynamic pitch angle cannot be directly measured, we assume this value is available. In Vrijdag, (2009) a method is proposed to derive the hydrodynamic pitch angle by measuring thrust and using the inverse of the four quadrant open water diagram. Moreover, a pitch angle reduction term θ_{red} is added, which is proportional to the margin of the unlimited fuel injection setpoint to the fuel injection limitations, as follows:

$$\theta_{\text{red}}(t) = P_\theta X_{\text{mar}}(t) \tag{4.8}$$

$$0 \leq \theta_{\text{red}}(t) \leq \theta_{\text{red,max}}, \tag{4.9}$$

where P_θ is the proportional pitch angle reduction gain, X_{mar} is the fuel injection margin as defined in (4.16) and $\theta_{\text{red, max}}$ indicates the maximum value of the pitch angle reduction.

When the control objective to minimise acceleration time is also strived for, the air excess ratio limitation of the engine causes pitch reduction. Subsequently, the angle of attack is not maintained at its optimum value. In a separate low cavitation mode the air excess ratio limitation is prevented by limiting the fuel injection increase rate limitation, $R_{\text{X,cav}}$.

MINIMISE FUEL CONSUMPTION

The operating points of four components determine the fuel consumption of a direct mechanical propulsion plant with controllable pitch propeller: the diesel engine, the gearbox, the shaft-line and the propeller, as we consider the ship resistance of the hull as a given fact for this study. The speed and fuel injection of the diesel engine, in combination with the charge pressure, determine the specific fuel consumption of the engine. The speed and torque of the shaft-line and gearbox determine their losses, which are relatively small and will not be considered for the control strategy. Finally, the propeller open water efficiency is determined by the operating point of the propeller, governed by ship speed, wake-field disturbance from waves and propeller speed and pitch. Moreover, automotive and maritime research has shown that quasi static behaviour to a large extent determines the fuel consumption of cars and ships (Sciarretta *et al.* 2014; Shi, 2013; Shi *et al.* 2010), although Blanke *et al.* (2007) have demonstrated the engine control strategy can utilise the varying inflow velocity to increase the propeller efficiency in moderate seas, as will be addressed in Section 4.2.1.

The operating point at which the diesel engine consumes the minimum amount of fuel for a given power can be established from the specific fuel consumption contour plot, shown for the case study diesel engine in Figure 4.3. At the lowest fuel consumption for a given power, the gradient of the specific fuel consumption is zero. The theoretical cube law propeller curve with a design point at full speed at 90% of rated power is also shown in Figure 4.3. On this propeller curve, the fuel consumption is very close to its lowest value for a give power, as the gradient of the specific fuel consumption is close to zero. Moreover, the diesel engine project guide recommends operating the diesel engine on this propeller curve, as the margin to the engines power limit is sufficient (MAN Diesel SE, 2008b).

Similarly, the control objective to operate the engine at or close to the operating point defined by the theoretical propeller curve also leads to the highest possible open water efficiency of the propeller, as the open water efficiency typically is highest at the highest possible pitch and the operating envelope of the engine does not allow increasing pitch, and thus the load, above the theoretical propeller curve. For engines with wide operating envelopes, alternative control strategies might lead to lower fuel consumption. One such strategy can reduce fuel consumption in part load by up to 7%, by using hybrid propulsion with power take-off for a sequentially turbocharged diesel engine, as discussed in Geertsma *et al.* (2017d). In conclusion, the second resulting control objective is to operate the engine at or close to the operating point defined by the theoretical propeller curve with a design point at 90% rated power and the engine speed that provides the required virtual shaft speed.

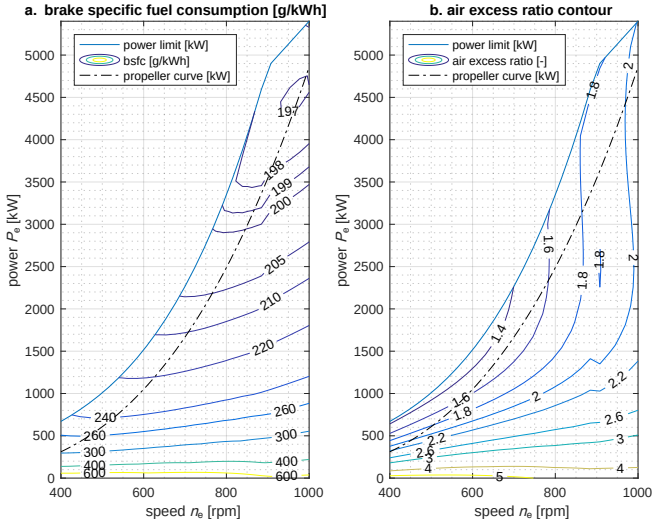

Figure 4.3: Specific fuel consumption and air excess ratio contour plot in engine operating envelope with theoretical cube law propeller curve.

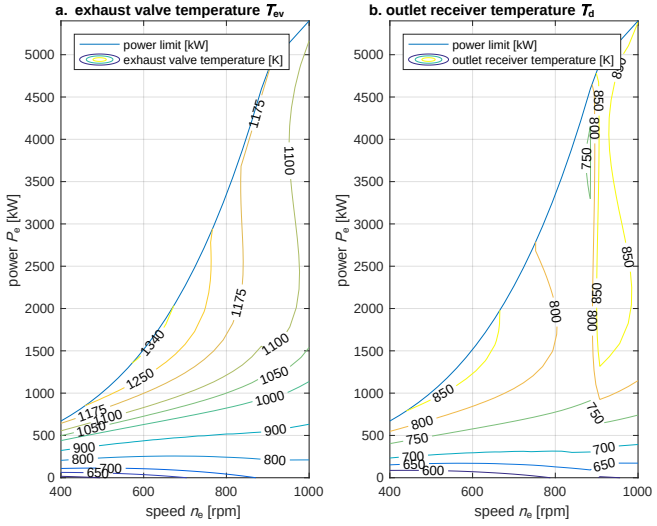

Figure 4.4: Exhaust valve and receiver temperature plot in engine operating envelope with theoretical cube law propeller curve.

This control objective can be achieved by governing control action propeller pitch ratio setpoint $P_{\text{pd,set}}$ and can be translated in maintaining a constant propeller torque coefficient K_{Q}, which is defined as (Klein Woud *et al.* 2012):

$$K_{\text{Q}}(t) = \frac{Q_{\text{p}}(t)}{\rho_{\text{sw}} \left(n_{\text{p}}(t)\right)^2 D_{\text{p}}^4}, \tag{4.10}$$

where Q_{p} is the open water propeller torque in kNm, and D_{p} is the propeller diameter in m.

However, control objectives 3, 4 and 6 benefit from maintaining a constant effective angle of attack α_{eff}, instead of a constant pitch or propeller torque coefficient K_{Q}. Moreover, for the case study Patrol Vessel, with a nearly cubed resistance curve due to its low Froude number, maintaining a constant angle of attack also leads to operating the propeller at an almost constant propeller torque coefficient K_{Q} and at or close to the theoretical propeller curve. Therefore, the propeller pitch ratio setpoint $P_{\text{p,set}}$ is controlled to maintain the angle of attack at its setpoint value $\alpha_{\text{eff,set}}$, as defined in (4.4) and (4.5).

MAINTAIN ENGINE AIR EXCESS RATIO

The engine air excess ratio, the relative amount of air that is left after complete combustion of all fuel, is an important indicator for engine thermal loading, as demonstrated in Grimmelius *et al.* (2000), Grimmelius *et al.* (2001), Sapra *et al.* (2017), Geertsma *et al.* (2017c), and Figure 4.3 and 4.4. While the air excess ratio contour plot in Figure 4.3 illustrates the air excess ratio in stationary conditions, the air excess ratio during dynamic conditions, such as acceleration and wave induced disturbances, can be significantly lower or higher due to the turbocharger lag. In this section, we will first address wave induced disturbances and propose integrating speed control to resolve these and then propose a fuel injection constraint that maintains the air excess ratio at a minimum value during acceleration.

Geertsma *et al.* (2016) have demonstrated that engine torque control as opposed to engine speed control can completely eliminate thermal loading fluctuation due to disturbance from waves. Moreover, Blanke *et al.* (2007) have demonstrated with model experiments that torque control can lead to 2% fuel consumption reduction in moderate seas by utilising the varying inflow velocity onto the propeller blade, thus increasing the propeller efficiency. However, the first control objective is to provide the requested virtual shaft speed and torque control would require an additional torque sensor, that might be less reliable than speed sensing. Therefore, we propose to use integrating speed control, without a proportional gain on the speed error, similar to the slow integrating speed control strategy that Rubis *et al.* (1986) proposed for gas turbine mechanical propulsion, due to its good performance in heavy waves. Slow integrating speed control exhibits a similar dynamic behaviour in waves as torque control and, in combination with (4.1), also provides the requested virtual shaft speed. Thus, the following control algorithm is proposed to achieve slow integrating speed control:

$$X_{\text{I}}(t) = K_{\text{I,ic}} \int_0^t \left(\frac{n_{\text{set}}(t)\, i_{\text{gb}}}{n_{\text{e,nom}}} - \frac{n_{\text{e}}(t)}{n_{\text{e,nom}}} \right) dt, \tag{4.11}$$

where X_I is the fuel injection setpoint from integrating speed control, $K_\mathrm{I,ic}$ is the reset rate for slow integrating speed control, i_gb is the gearbox reduction ratio, and $n_\mathrm{e,nom}$ is the nominal engine speed in Hz.

During an acceleration the charge pressure will lag at a lower value due to the turbocharger inertia, which causes a higher thermal loading than in stationary conditions. In order to prevent thermal overloading, the objective thus is to maintain the air excess ratio at a minimum value. This can be achieved by first limiting the fuel pump position based on the charge pressure and secondly reducing the angle of attack setpoint when the fuel pump position is limited. The fuel pump position limitation is defined as follows, as derived from Geertsma *et al.* 2017c, Eq. (4) and (5):

$$X_{\mathrm{lim},\lambda}(t) = \frac{p_1(t) V_1}{R_\mathrm{a} T_1 \sigma_\mathrm{f} m_\mathrm{f,nom} \lambda_m i n}, \tag{4.12}$$

where $X_{\mathrm{lim},\lambda}$ is the fuel injection limitation to limit the air acces ratio λ in % of nominal fuel injection $m_\mathrm{f,nom}$, V_1 is the cylinder volume at the start of compression in m^3, R_a is the gas constant of air in J/kgK, T_1 is the temperature at the start of compression in K and σ_f is the stoichiometric air fuel ratio of the fuel.

Another important parameter to limit engine thermal loading is the rate of increase of exhaust valve temperature dT_ev/dt during an acceleration, which is mainly determined by the rate of increase of torque and therefore fuel injection X. In order to limit this rate of increase, the proposed adaptive pitch control strategy incorporates a fuel injection increase rate limitation $R_\mathrm{X,therm}$ to prevent thermal overloading due to a high dT/dt. Moreover, in order to prevent cavitation due to running into the air excess ratio limitation, a second setting for this rate is determined for the low cavitation mode: the torque increase rate limitation for reduced cavitation $R_\mathrm{X,cav}$.

MINIMISE ACCELERATION TIME

The objective to minimise acceleration time is restricted by the objective to prevent engine thermal overloading (van Spronsen *et al.* 2001) and thus by the objective to maintain engine air excess ratio. In traditional control strategies this is achieved by limiting the rate of the increase in engine speed during an acceleration manoeuvre, as demonstrated in Geertsma *et al.* (2016), and discussed in Chapter 3. Vrijdag *et al.* (2010) has demonstrated, through a combination of simulation and validation, that the acceleration behaviour improves due to the proposed angle of attack control strategy with an acceptable engine thermal loading. In essence, the acceleration manoeuvre is faster, because the pitch is increased more slowly during the acceleration manoeuvre, leading to higher engine speed. Geertsma *et al.* (2017c) have demonstrated that indeed a reduced pitch during an acceleration manoeuvre increases engine speed and reduces engine thermal loading, because the turbo charger pressure and thus the air excess ratio increases faster at higher engine speeds. In the proposed slow integrating speed control strategy, according to (4.11), speed increase rate limiters are not required, as will be demonstrated in the results of this chapter. Therefore, the setting of the reset rate K_I determines the speed of acceleration and needs to be determined in a trade-off between acceleration behaviour and engine thermal loading during an acceleration.

PREVENT ENGINE OVERSPEED AND UNDER-SPEED

Slow integrating speed control as defined in (4.11) introduces the risk of engine over-speed or under-speed due to disturbances, as integrating speed control follows the speed setpoint significantly slower than an aggressive PI controller. To prevent engine over-speed, the following fuel limitation is introduced:

$$X_{\text{lim,os}}(t) = \frac{n_{\text{e,max}} - n_{\text{e}}(t)}{n_{\text{e,nom}}} P_{\text{os}}, \tag{4.13}$$

where $X_{\text{lim,os}}$ is the fuel injection limitation to prevent overspeed, $n_{\text{e,max}}$ is maximum engine speed, and P_{os} is the overspeed limitation gain. Similarly, the following minimum fuel injection X_{min} prevents engine under-speed:

$$X_{\text{min}}(t) = \frac{n_{\text{e,min}} - n_{\text{e}}(t)}{n_{\text{e,nom}}} P_{\text{us}}, \tag{4.14}$$

where $n_{\text{e,min}}$ is minimum engine speed, and P_{us} is the under-speed limitation gain. Moreover, the fuel injection limitation and the fuel injection margin X_{mar} are defined as:

$$X_{\text{lim}}(t) = \max\left(X_{\text{lim,os}}(t), X_{\text{lim},\lambda}(t)\right) \tag{4.15}$$

$$X_{\text{mar}}(t) = X_{\text{I}}(t) - X_{\text{lim}}(t)., \tag{4.16}$$

where X_{lim} is the fuel injection limitation in %. Finally, the fuel injection is limited between the minimum fuel injection X_{min} and the fuel injection limitation X_{lim}, as follows:

$$X_{\text{I}}(t) < X_{\text{min}} : X_{set}(t) = X_{\text{min}} \tag{4.17}$$

$$X_{\text{min}}(t) \leq X_{\text{I}}(t) \leq X_{lim}(t) : X_{set}(t) = X_{\text{I}}(t) \tag{4.18}$$

$$X_{\text{I}}(t) > X_{lim}(t) : X_{set}(t) = X_{lim}(t). \tag{4.19}$$

With a traditional combinator curve, reducing pitch at low speed settings while maintaining minimum engine speed prevents engine under-speed. When applying the adaptive pitch control strategy the pitch should also be constrained to the value associated with minimum engines speed, as follows:

$$P^*_{\text{pd,max}}(t) = \frac{n_{\text{virt,set}}(t)\, i_{\text{gb}}}{n_{\text{e,mins}}} \tag{4.20}$$

$$P_{\text{pd,set}}(t) = P_{\text{pd,0}} + \max\left(P^*_{\text{pd,max}}(t), P^*_{\text{pd,set}}(t)\right)\left(P_{\text{pd,nom}} - P_{\text{pd,0}}\right), \tag{4.21}$$

where $n_{\text{e,mins}}$ is the minimum engine speed setpoint.

Finally, when pitch is limited to prevent engine under-speed, engine speed should be kept constant at minimum engine speed $n_{\text{e,min}}$. In this region slow integrating speed control can lead to excessive speed fluctuation, which will be limited by the under-speed fuel injection limitation described in (4.14). Nevertheless, in this region engine speed is better kept constant by applying traditional fast PI speed control, as described in Geertsma *et al.* (2017c), as follows:

$$X_{PI}(t) = K_P\left(\frac{n_{ref}(t)}{100} - \frac{n_e(t)}{n_{e_{nom}}}\right) + K_I\int_0^t\left(\frac{n_{ref}(t)}{100} - \frac{n_e(t)}{n_{e_{nom}}}\right)dt, \tag{4.22}$$

where X_{PI} is the unlimited fuel injection setpoint for speed control, K_P is the proportional gain and K_I is the reset rate. PI speed control replaces slow integrating speed control when the engine speed setpoint is less or equal to minimum engine speed $n_{\text{e,min}}$ with a hysteresis of 2.5%. Effectively, PI gain scheduling (Astrom *et al.* 2001) is applied in this case with a clear switching value, when the engine speed setpoint is at its minimum value with a hysteresis of 2.5 % to prevent repetitious switching between the gain values. While repetitious switching is prevented by using the speed setpoint as switching variable, alternatively, a continuous function for the proportional gain P could be derived, as used in pitch control with gain scheduling for wind turbines (Ren *et al.* 2016).

4

4.2.2. CONTROLLER SETTINGS

With the traditional control strategy, many of the control parameters require extensive tuning as discussed in Section 3.3.3 and de Boer *et al.* (2011) and van Straaten *et al.* (2012). The resulting parameters of the traditional control strategy are listed in Table 3.6. Alternatively, the proposed control strategy primarily requires limitations for physical parameters and a number of gains. The only parameters that require tuning are the gain and reset rate for speed control at minimum engine speed $K_{\text{P,sc}}$ and $K_{\text{I,sc}}$, and the reset rate for slow integrating speed control $K_{\text{I,ic}}$.

Various tuning strategies for PI control are discussed in literature (Astrom *et al.* 2001; Stapersma *et al.* 2017; Vrijdag *et al.* 2017; N. I. Xiros, 2014). While Astrom *et al.* (2001) provide an overview of tuning strategies, N. I. Xiros, (2014) proposes an improved PID tuning method for marine engine speed regulation to meet sensitivity H_∞ requirements. However, the stability of the system does not require stringent engine speed disturbance rejection criteria, as demonstrated in Geertsma *et al.* (2016) and we aim to minimise torque fluctuations. Moreover, the reset rate for slow integrating speed control $K_{\text{I,ic}}$ physically primarily influences the rate of temperature increase dT_{ev}/dt during an acceleration and therefore is tuned to achieve gradual dT_{ev}/dt. Moreover, the influence of the gain and reset rate for speed control K_{p}&K_{i} on the behaviour in waves can be investigated with linearised propulsion system models as proposed in Stapersma *et al.* (2017) and Vrijdag *et al.* (2017). The parameters in this chapter were based on this approach and the results in this chapter demonstrate the stability of the used settings. The resulting control parameters for the proposed adaptive pitch control strategy are listed in Table 4.1.

4.3. RESULTS

4.3.1. SIMULATION EXPERIMENTS

THE simulation experiments for the case study *Holland* class Patrol Vessel in this chapter aim to compare the proposed control strategy with the baseline control strategy of the actual vessel, which has been used for the validation of the simulation model in Chapter 3. We use two types of straight line manoeuvres to establish the Measures of

Table 4.1: Control parameters for the proposed adaptive pitch control strategy

Control parameter	**Value**
effective angle of attack setpoint $\alpha_{\text{eff,set}}$ in deg	10.5
reset rate slow integrating speed control $K_{\text{I,ic}}$	0.2
proportional gain speed control $K_{\text{P,sc}}$	2
reset rate speed control $K_{\text{I,sc}}$	0.5
minimum engine speed $n_{\text{e,min}}$	350 rpm
maximum engine speed $n_{\text{e,max}}$	1050 rpm
under-speed limitation gain P_{us}	8
overspeed limitation gain P_{os}	22
fuel injection rate for thermal loading $R_{\text{X,thermal}}$	1.67%
fuel injection rate for cavitation $R_{\text{X,cav}}$ in %	0.42%
conservative air excess ratio limitation λ_{min}	1.6
regular air excess ratio limitation λ_{min}	1.45

Performance (MOP): sailing at constant speed and two acceleration manoeuvres, as follows:

- Sailing at constant speed is used to establish the fuel consumption, air excess ratio and exhaust valve temperature as a function of ship speed;
- The slam start manoeuvre proposed in Altosole *et al.* (2017) is used to establish the shortest possible acceleration time from 0 kts to 15 kts ship speed, by setting the virtual shaft speed to the maximum value at the start of the manoeuvre; and
- Intermediate sprints are used to establish MOPs during regular acceleration. For intermediate sprints, the virtual shaft speed setting is increased from the setting that provides the starting ship speed to the setting that achieves the speed at the end of the manoeuvre.

These benchmark manoeuvres can be used to demonstrate that the proposed control strategy meets the objectives described in Section 4.2.1. Moreover, we have performed the proposed benchmark manoeuvres to establish the Measures of Performance (MOPs) proposed in Chapter 3.

As reported in Geertsma *et al.* (2017c), 'the ship resistance and the wave model parameters very strongly depend on the conditions in which the ship operates'. In this chapter, we consider the following two typical conditions:

- Trial condition, defined as Sea State 0, wind speed of 3 m/s and no fouling.
- Design condition, defined as Sea State 4, wind speed of 11 m/s, head seas and wind and 6 months out of dock fouling.

The parameters that represent these conditions are shown in Table 3.10 and Figure 3.20, in Chapter 3.

Table 4.2: Control strategies, modes and settings evaluated in simulation experiments reported in Section 4.3.

Control strategy name	**mode**	**increase rate R_{L+} or R_X**	**air excess ratio λ_{min}**
baseline speed control	manoeuvre	R_{L+} = 1.5%/s	
baseline speed control	transit	R_{L+} = 0.75%/s	
adaptive pitch control (APC)	fast APC	$R_{X,therm}$ = 1.67%/s	$\lambda_{min} = 1.45$
adaptive pitch control (APC)	APC with limited air excess ratio λ	$R_{X,therm}$ = 1.67%/s	$\lambda_{min} = 1.6$
adaptive pitch control (APC)	slow APC to prevent cavitation	$R_{X,cav}$ = 0.42%/s	$\lambda_{min} = 1.6$

The simulation results have been obtained with MATLAB Simulink R2016b software on a PC with Intel Core i7 processor and 16 GB memory. The simulation to establish the slam start and intermediate sprint accelerations requires 6s simulation time in trial conditions and 77s in design conditions. Both these simulations cover 9000s, or 2.5h simulated time. The difference in simulation time is caused by the dynamics introduced by waves, limiting the maximum step time for design conditions. The simulation to establish the static operating point for design conditions over 22 virtual shaft speeds, allowing stabilisation of each operating point for 1000s, takes 256s for 22000s simulated time. In conclusion, the simulation requires approximately 1/100s simulation time for 1s simulated time in design conditions.

4.3.2. EVALUATED CONTROL STRATEGIES

In the simulation experiments, the baseline transit and manoeuvre mode control strategies, as described in Chapter 3, are compared with the adaptive pitch control strategy as described in Section 4.2, with various settings as reported in Table 4.1. An overview of the 5 control strategies, their modes and settings used for the evaluation in Section 4.3 is listed in Table 5.7.

4.3.3. EVALUATION OF CONTROL OBJECTIVES

VIRTUAL SHAFT SPEED

The first control objective is to provide the requested virtual shaft speed. This objective is one of the key reasons to employ traditional speed control, as feedback control on speed can robustly handle the uncertainty associated with weather conditions, ships course relative to the wind and waves, hull fouling and ships displacement. Figures 4.5 and 4.6 present the results of the intermediate acceleration from 0 kts to 5 kts, 5 kts to 10 kts, 10 kts to 15 kts and 15 kts to maximum speed for trial conditions and for design conditions, reflecting two very different conditions and thus the described uncertainty.

The baseline control strategy provides the requested shaft speed unless pitch is reduced to prevent overloading, as described in Section 3.3. While engine speed control robustly maintains engine speed at the requested speed from the combinator curve, the pitch reduction strategy reduces pitch and therefore virtual shaft speed. Therefore, in

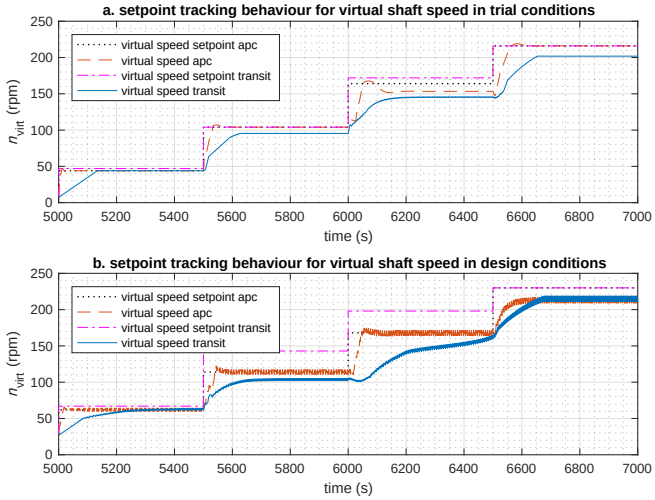

Figure 4.5: Setpoint tracking behaviour for virtual shaft speed n_{virt} in trial and design conditions for baseline transit control and adaptive pitch control with limited air excess ratio.

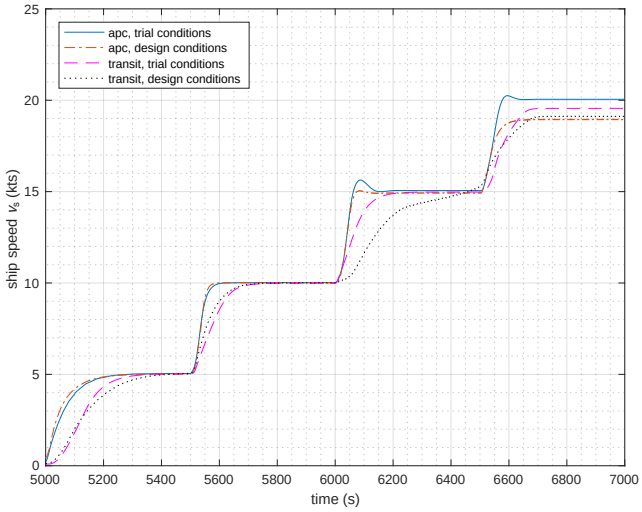

Figure 4.6: Ship speed during intermediate sprint acceleration in trial and design conditions for baseline transit control and adaptive pitch control with limited air excess ratio.

conditions with a high ship resistance, such as design conditions, the traditional control strategy does not actually provide the requested virtual shaft speed, as shown in Figure 4.5. Actually, even in trial conditions, at certain engine speed the requested virtual shaft speed is not achieved. The operator can achieve the required ship speed by requesting a higher virtual shaft speed than the virtual shaft speed required for that ship speed, which is clearly demonstrated by the high virtual speed setpoint of 200 rpm required to achieve 15 kts ship speed with baseline transit control in design conditions in Figure 4.5b. The maximum speed in transit mode is different to the maximum speed in manoeuvre mode as the amount of pitch reduction is different due to the different combinator curves and thus engine speed between transit and manoeuvre mode.

The proposed adaptive pitch control strategy, in this case with limited air excess ratio, follows the virtual shaft speed setpoint accurately, because higher or lower pitch than nominal pitch is compensated with a proportional decrease or increase in speed setpoint due to (4.1). Only if the air excess ratio limitation λ is higher than the air excess ratio on the theoretical propeller curve, for this engine higher than 1.50, the virtual shaft speed will not reach its setting as the air excess ratio limitation is not compensated by increased engine speed. Slow integrating speed control responds more slowly to changes in engine speed and therefore ship speed, leading to a slight overshoot in virtual shaft speed during acceleration, as shown in Figure 4.5. However, this overshoot only leads to an overshoot in ship speed of 0.3 kts, and only in light trial conditions. During design conditions, when the engine margin is smaller, constant ship speed is only reached when the virtual shaft speed overshoot has already stabilised. Therefore, this overshoot is acceptable, also because it leads to significantly faster acceleration. The robust virtual shaft speed following capability under large uncertainties is a significant advantage of the proposed adaptive pitch control compared to the baseline strategy, that does not accurately follow the virtual shaft speed setpoint, and this behaviour is achieved with simple feedback control as opposed to complex algorithms as proposed in Haseltalab *et al.* (2017a).

MAINTAIN OPERATION WITHIN THE CAVITATION BUCKET

While the propeller of the patrol vessel has not been designed for low noise operation, the angle of attack at the design point of the propeller is too high for low cavitation behaviour. However, for the evaluation of the control objective to maintain operation within the cavitation bucket, we assume the cavitation bucket is centred around the angle of attack at the design point, which could be achieved at a lower angle of attack with a similar propeller with a larger diameter. Therefore, the objective of the control strategy is to maintain the angle of attack centred around the design angle of attack: 10.5 deg.

The cavitation plots at constant speed for trial and design conditions in Figures 4.7 and 4.8 demonstrate that the adaptive pitch control strategy maintains the effective angle of attack at the desired angle of 10.5 degrees, irrespective of the uncertainties in weather conditions, while the effective angle of attack of the baseline transit and manoeuvre mode strongly depends on weather conditions and is not kept constant for varying ship speed. Moreover, during intermediate sprints, shown in the cavitation plots in Figure 4.9 and 4.10, the effective angle of attack is maintained centred around the desired value of 10.5, as opposed to the baseline transit mode plot shown in Figure 4.11. The fluctuation in angle of attack, caused by waves, does not increase with the adaptive pitch control strategy compared to the fluctuation in angle of attack with a constant

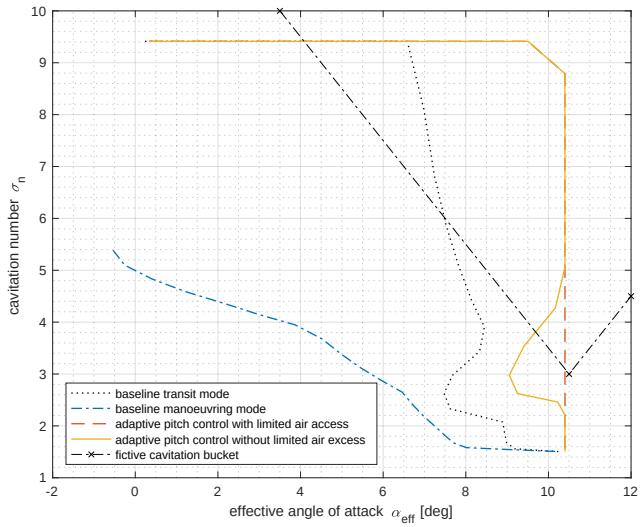

Figure 4.7: Cavitation plot from low speed to maximum speed for trial conditions in manoeuvring and transit mode and with adaptive pitch control with and without limited air excess ratio.

pitch angle in the baseline control strategies, confirming the adaptive pitch control strategy does not lead to instability.

However, the adaptive pitch control strategy with limited air excess ratio during acceleration does reduce pitch during the acceleration, as shown in Figure 4.12, and then the angle of attack reduces during the manoeuvre, as shown in Figure 4.9. This can be resolved by reducing the fuel injection increase rate to a lower value, $R_{X,cav}$. Then the pitch reduces only to maintain the angle of attack centred around 10.5 deg as shown in Figure 4.12 and 4.10, leading to a lower rate of increase of engine speed and slower acceleration as shown in Figure 4.13.

MINIMISE FUEL CONSUMPTION

The control objective to minimise fuel consumption during constant speed sailing is achieved when the engine runs on the theoretical propeller curve as argued in Section 4.2.1. The fast adaptive pitch control strategy achieves operating points and ellipses on the theoretical propeller curve at various ship speeds for transit and design conditions, as shown in Figure 4.14. Alternatively, in Figure 4.15 the baseline transit control strategy operates well below the theoretical propeller curve, mainly due to its conservative settings to prevent engine overloading under any circumstances 3.3.3. Moreover, the baseline transit control strategy operates further away from the theoretical propeller curve during design conditions than during trial conditions. The orientation of the ellipses due to speed and torque fluctuation from waves changes due to slow integrating speed control: the torque fluctuations reduce to minimal values at the cost of a slight increase in speed fluctuations as shown in Figure 4.14, compared to the more vertical ellipses in

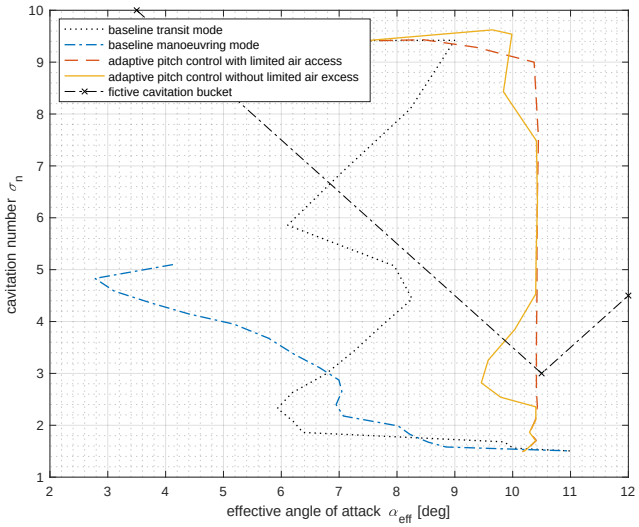

Figure 4.8: Cavitation plot at constant speed from low speed to maximum speed for baseline transit and manoeuvre mode and for adaptive pitch control with (1.6) and without (1.45) limited air excess ratio in design conditions.

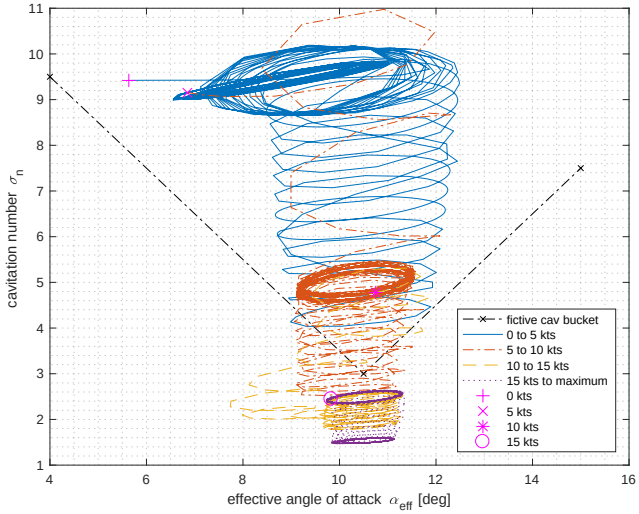

Figure 4.9: Cavitation plot in design conditions during intermediate sprints from 0 to 5 kts, 5 to 10 kts, 10 to 15 kts, and 15 kts to maximum ship speed, for adaptive pitch control with limited air excess ratio (1.6) and a fuel injection increase rate to only prevent thermal overloading $R_{X,therm}$.

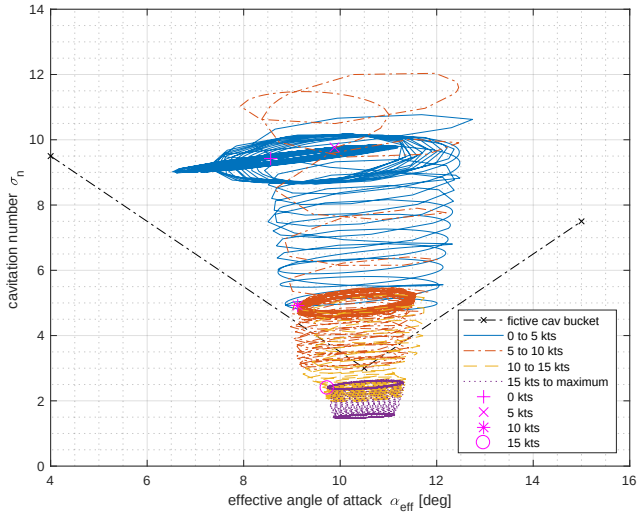

Figure 4.10: Cavitation plot in design conditions during intermediate sprints from 0 to 5 kts, 5 to 10 kts, 10 to 15 kts, and 15 kts to maximum ship speed, for slow adaptive pitch control to prevent cavitation $R_{X,cav}$.

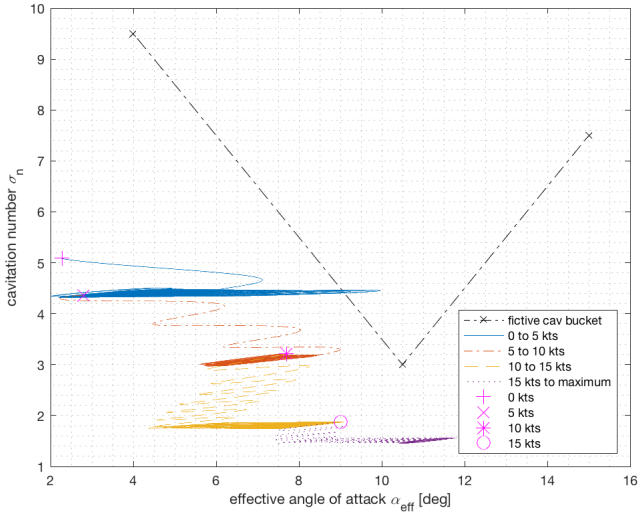

Figure 4.11: Cavitation plot in design conditions during intermediate sprints from 0 to 5 kts, 5 to 10 kts, 10 to 15 kts, and 15 kts to maximum ship speed with baseline transit mode.

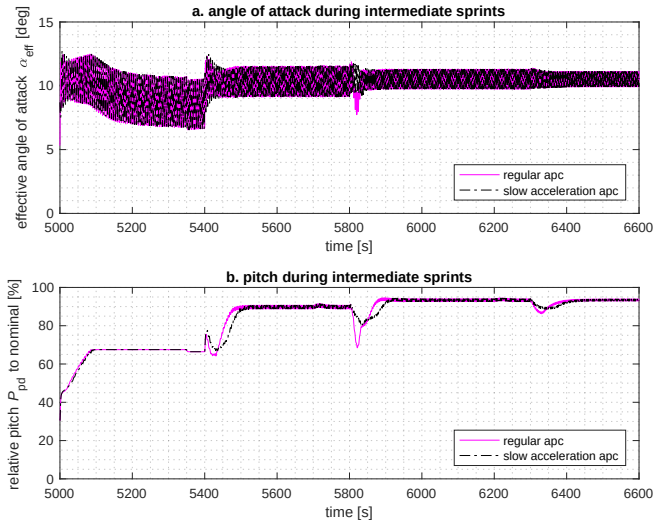

Figure 4.12: Angle of attack and pitch during intermediate sprints in design conditions from 0 to 5 kts, 5 to 10 kts, 10 to 15 kts, and 15 kts to maximum ship speed comparing adaptive pitch control with limited air excess ratio (1.6) and fuel injection increase rate $R_{X,therm}$, with slow adaptive pitch control with fuel injection increase rate $R_{X,cav}$.

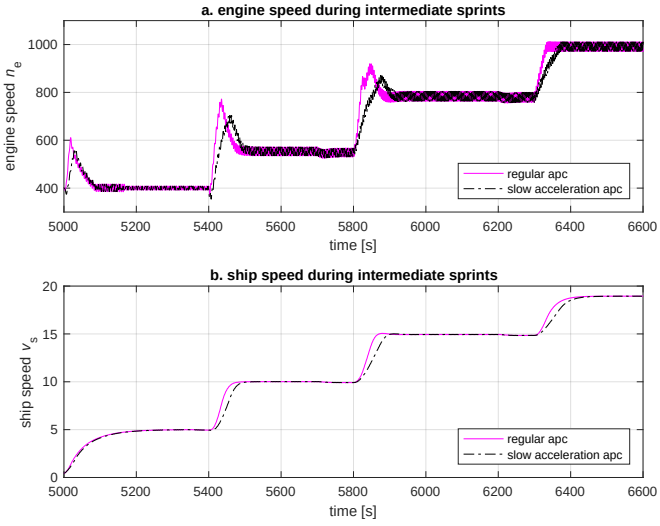

Figure 4.13: Engine and ship speed during intermediate sprints in design conditions from 0 to 5 kts, 5 to 10 kts, 10 to 15 kts, and 15 kts to maximum ship speed comparing adaptive pitch control with limited air excess ratio (1.6) and fuel injection increase rate $R_{X,therm}$, with slow adaptive pitch control with fuel injection increase rate $R_{X,cav}$.

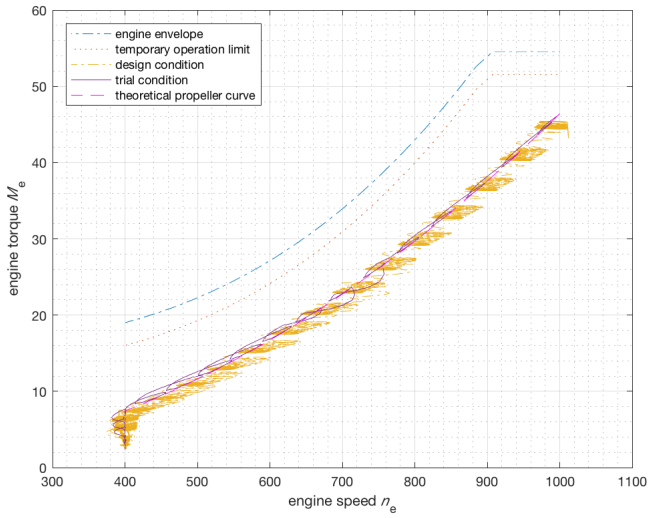

Figure 4.14: Constant ship speed operation from low speed to maximum speed in engine operating envelope for fast adaptive pitch control strategy (with air excess ratio limitation $\lambda_{\text{lim}} = 1.45$) in trial and design conditions.

4.15, almost eliminating fluctuating air excess ratio and temperatures as shown in Figure 4.21. Thus, we can conclude the adaptive pitch control strategy at constant ship speed compensates the uncertainty in weather conditions robustly and runs the engine at its most efficient operating point with sufficient margin to the engine operating envelope.

While the efficiency during acceleration does not heavily impact the fuel consumption over the operating profile of the ship, the efficiency during acceleration is also an indicator for acceleration performance. Therefore, Figure 4.16 and 4.17 present the propeller open water efficiency and the effective engine efficiency during intermediate sprints and the slam start acceleration. During these accelerations, the engine efficiency and propeller efficiency are consistently higher for the fast adaptive pitch control strategy than for the baseline manoeuvre strategy. This has two reasons: first, the pitch in adaptive pitch control is higher and therefore the propeller operates at a higher open water efficiency; secondly, engine speed and engine load increase faster during acceleration, thus operating the engine at higher efficiency, because the adaptive pitch control strategy retracts pitch during the acceleration procedure to maintain the effective angle of attack, as shown in Figure 4.18 and 4.19.

The approach to minimise fuel consumption works very well with the proposed angle of attack approach, because fuel consumption is close to its minimum for a constant angle of attack for this particular engine. Nevertheless, if an engine has a different specific fuel consumption plot or if the trade-off between quasi-static NO_x emissions and fuel consumption should be taken into account, still an optimum quasi-static relationship between engine speed and torque could be established, which can be either translated into a relationship between shaft speed n_p and effective angle of attack α_{eff}

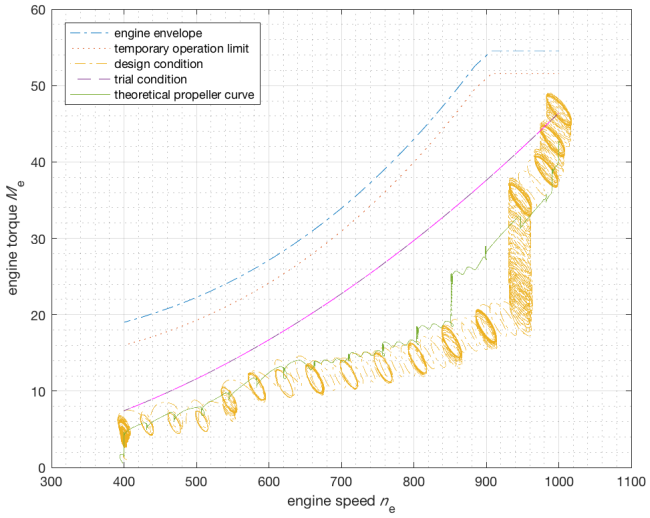

Figure 4.15: Constant ship speed operation from low speed to maximum speed in engine operating envelope for baseline transit control strategy in trial and design conditions.

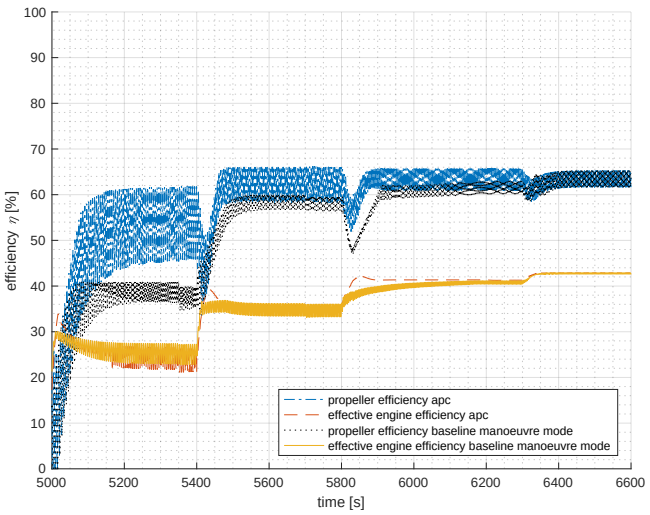

Figure 4.16: Propeller open water efficiency and effective engine efficiency during intermediate accelerations from 0 to 5 kts, 5 to 10 kts, 10 to 15 kts, and 15 kts to maximum ship speed in design conditions for baseline manoeuvre mode and adaptive pitch control.

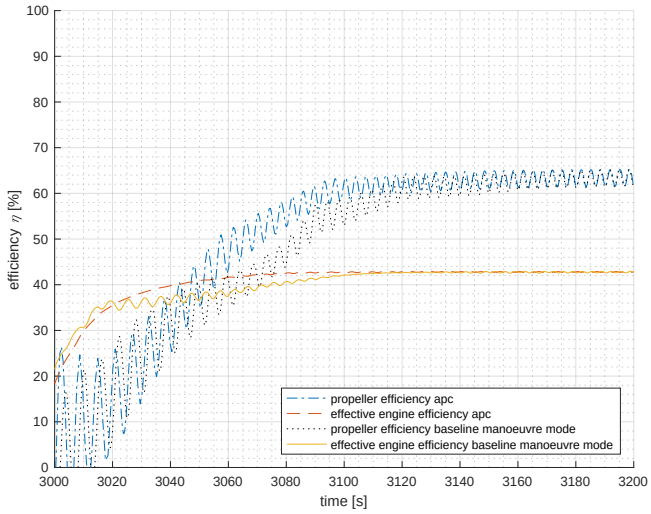

Figure 4.17: Propeller open water efficiency and effective engine efficiency during slam start acceleration from 0 kts to maximum ship speed in design conditions for baseline manoeuvre mode and fast adaptive pitch control.

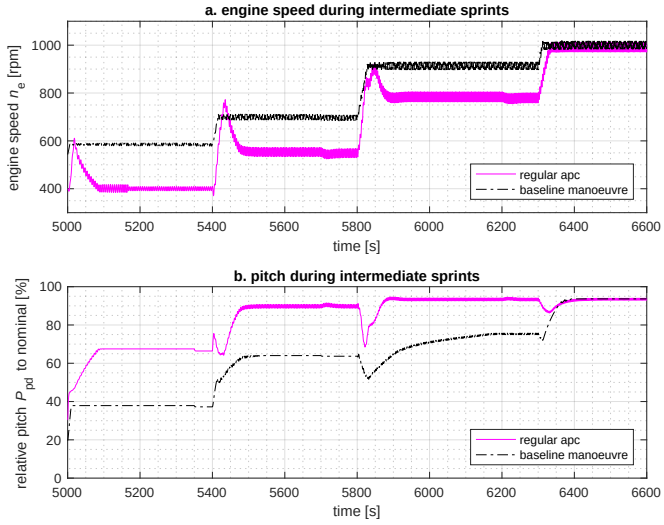

Figure 4.18: Engine speed and pitch during intermediate accelerations from 0 to 5 kts, 5 to 10 kts, 10 to 15 kts, and 15 kts to maximum ship speed in design conditions for baseline manoeuvre mode and fast adaptive pitch control.

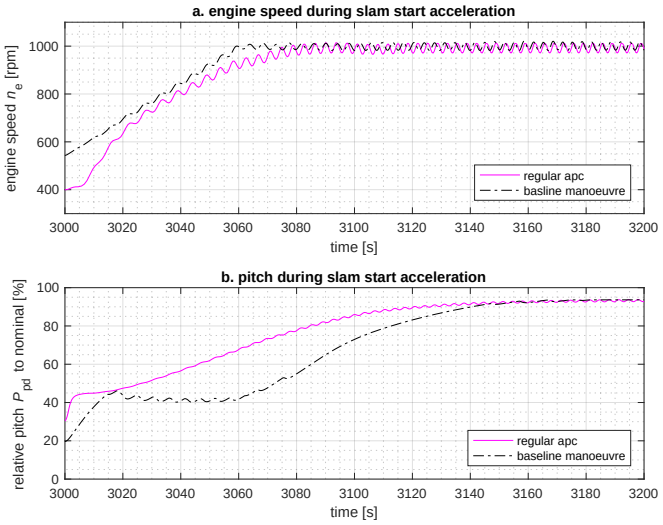

Figure 4.19: Engine speed and pitch during slam start acceleration from 0 kts to maximum ship speed in design conditions for baseline manoeuvre mode and fast adaptive pitch control.

or shaft speed n_p and propeller torque coefficient K_Q. The input for the development of the setting for this approach are static specific fuel consumption or NO_x emission maps, such as Figure 4.3, Figure 2.3, or Figure 1 to 3 in Nuesch *et al.* (2014). Nuesch *et al.* (2014) practically demonstrate NO_x emissions can be addressed with a quasi-static approach, as opposed to particulate matter (PM) emissions, which are sensitive to turbo charger lag and primarily benefit from a smooth torque trajectory, one of the benefits of the proposed slow integrating speed control strategy. Moreover, the static PM emission map in Figure 2 in Nuesch *et al.* (2014) shows that PM emissions for that specific automotive diesel engine appears near its minimum around the theoretical propeller curve. Therefore, future work could be aimed at confirming the expectation that the proposed adaptive pitch control strategy with slow integrating torque control also has a positive influence on PM emissions, and at investigating the trade-off between fuel consumption and NO_x emissions.

MAINTAIN ENGINE AIR EXCESS RATIO

Figure 4.20 and 4.21 demonstrate that the proposed control strategy maintains the air excess ratio within the predefined limits, either above the minimum value of 1.45 or above the value of 1.6. When the air excess ratio λ_{min} is kept at a higher value, the temperatures during the slam start and intermediate acceleration are significantly lower. The baseline manoeuvre mode maintains even higher air excess ratios during all manoeuvres and therefore maintains lower temperatures, but that is caused by the very conservative settings to prevent overloading in heavy off-design conditions. In the nominal operating point on the theoretical propeller curve at 700 rpm and 1650 kW, the air excess ratio also is 1.35 and the exhaust valve temperature 1350 K. Therefore, an air excess ratio of 1.45

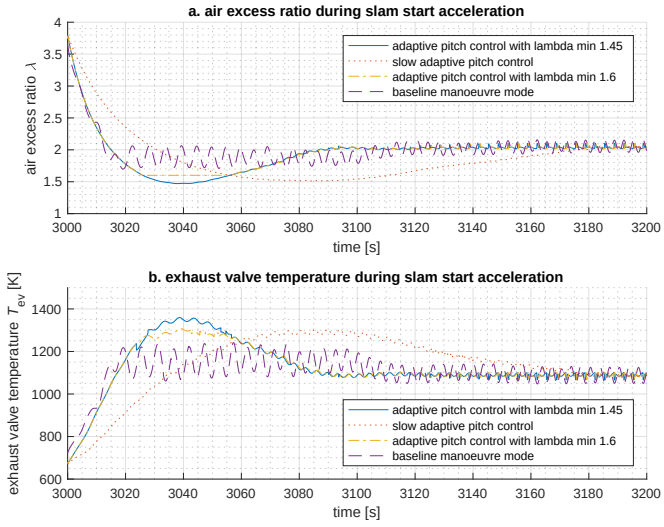

Figure 4.20: Air acces ratio and exhaust valve temperature during slam start acceleration from stationary to maximum speed for adaptive pitch control strategy with various settings and baseline manoeuvre mode in design conditions.

and an exhaust valve temperature of 1350 K should not lead to engine thermal overloading.

In almost all manoeuvres the maximum exhaust valve temperature remains below 1350 K, suggesting that the proposed control strategy with a minimum air excess ratio does not lead to thermal overloading. However, during the intermediate sprint from 10 to 15 kts the maximum cylinder temperature peaks to 1400K, while the air excess ratio λ is maintained at a minimum value of 1.45. During this acceleration, engine speed ranges from 600 to 800 rpm, the range in which the air acces ratio is lowest and exhaust valve temperature highest during static conditions. Nevertheless, the higher temperature during this manoeuvre compared to other manoeuvres with the same minimum air acces ratio proves that the exhaust valve temperature is not directly dependant on the in-cylinder air excess ratio λ.

Close inspection of the simulation results shows that during this acceleration, the charge pressure lags, causing a reduced scavenge flow and therefore reduced exhaust valve cooling. This dependency of scavenge flow on charge pressure is clear from (3.30) and (3.31) in Chapter 3 and the relationship between scavenge flow and exhaust temperature is expressed in (3.52) in Chapter 3. While further research would be required to establish whether this would indeed lead to thermal overloading of the engine, an alternative maximum fuel injection value as a function of charge pressure p_1 slightly more conservative than (4.12), could be used to reduce thermal loading during this specific case. Then, the relationship would either have to be experimentally established or have to be determined with the simulation model used in this chapter using the engine model in isolation and fixing the charge pressure model input.

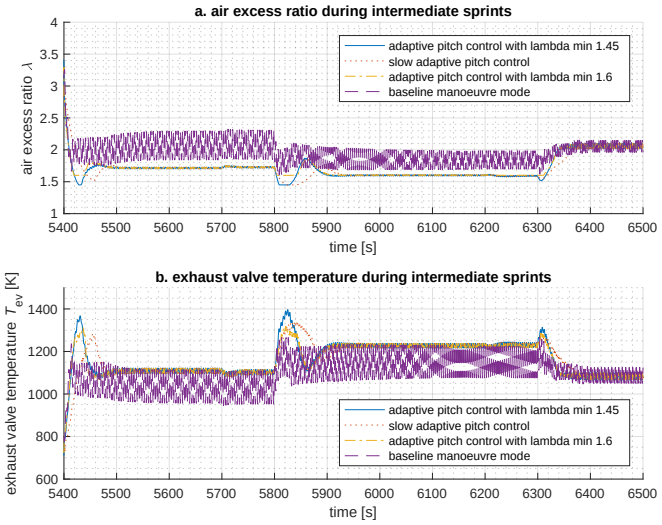

Figure 4.21: Air acces ratio and exhaust valve temperature during intermediate sprints from 0 to 5 kts, 5 to 10 kts, 10 to 15 kts and 15 kts to maximum speed for adaptive pitch control strategy with various settings and baseline manoeuvre mode in design conditions.

Alongside the maximum temperature that is reached during acceleration, the rate of change of the exhaust valve temperature dT_{ev}/dt during an acceleration is also important for thermal stresses in the engine. Figure 4.20 and 4.21 illustrate that for the adaptive pitch control strategy the average rate of change of the exhaust valve temperature dT_{ev}/dt during the initial phase of the acceleration is similar to the baseline manoeuvre mode, but that the fluctuation due to waves does not occur for the adaptive pitch control strategy, due to the slow integration speed control. Moreover, close to the peak temperature, when the thermal stresses are highest, the increase rate of the temperature reduces, again without the fluctuation due to waves. While further research would be necessary to accurately determine the thermal stresses caused by the two control strategies, Figure 4.20 and 4.21 suggest the behaviour of the adaptive pitch control strategy is more gradual and therefore less likely to cause thermal overloading.

MINIMISE ACCELERATION TIME

The control objective to minimise acceleration time is a trade-off with the control objective to prevent engine thermal overloading. In order to reduce engine thermal loading during an acceleration manoeuvre, charge pressure needs to increase as fast as possible as a higher charge pressure provides a higher air excess ratio and scavenge flow increases at higher charge pressures. Increasing charge pressure during an acceleration can be best achieved by increasing engine speed and thus air flow in the engine. However, the fuel injection limitation of the baseline control strategy and the air acces ratio limitation of the proposed strategy limit the fuel injection during the acceleration manoeuvre and therefore the torque available for acceleration. Reducing pitch during the acceleration

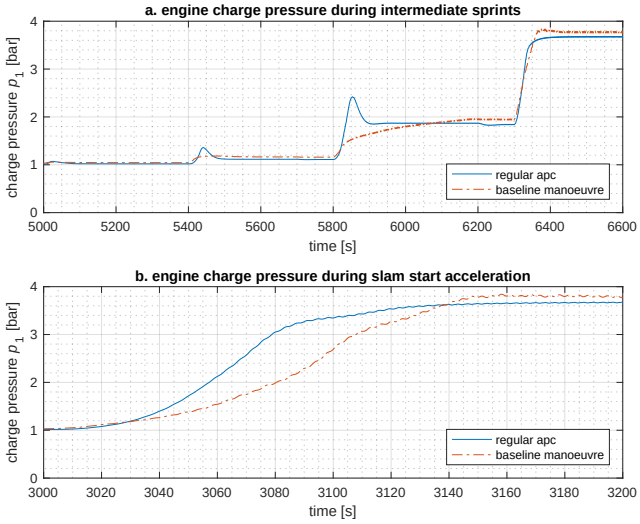

Figure 4.22: Charge air during intermediate sprints from 0 to 5 kts, 5 to 10 kts, 10 to 15 kts, and 15 kts to maximum ship speed and slam start acceleration for baseline manoeuvre control and adaptive pitch control (apc) in design conditions.

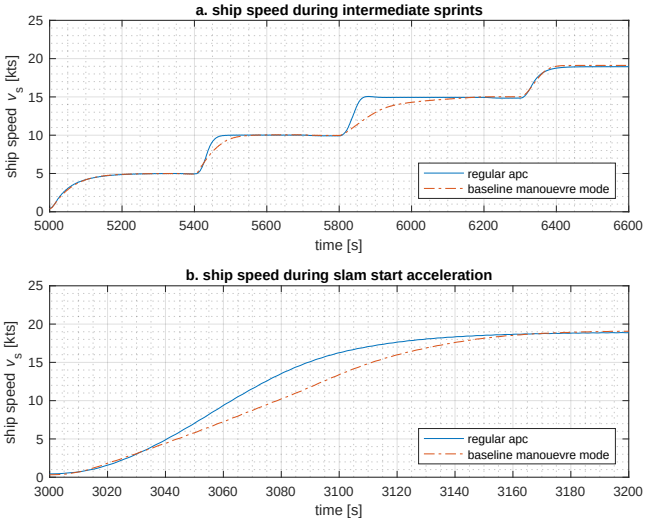

Figure 4.23: Ship speed during intermediate sprints from 0 to 5 kts, 5 to 10 kts, 10 to 15 kts, and 15 kts to maximum ship speed and slam start acceleration for baseline manoeuvre control and adaptive pitch control (apc) in design conditions.

manoeuvre, which is an indirect effect of the effective angle of attack control strategy, helps increasing engine speed during an acceleration manoeuvre due to (3.111).

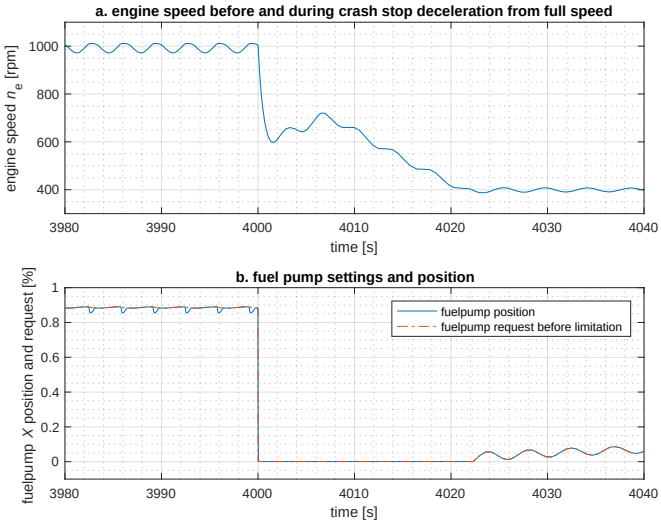

Figure 4.24: Engine speed and fuel pump request and position during sailing at maximum speed and crash stop deceleration with fast adaptive pitch control in design conditions.

Figure 4.18 demonstrates how, with fast adaptive pitch control, engine speed is increased during intermediate sprints due to pitch reduction, well above the engine speed after reaching constant speed, and Figure 4.22 shows that this engine speed increase leads to a faster increase in charge pressure than during an intermediate sprint with the baseline manoeuvre mode. During a slam start acceleration with adaptive pitch control, engine speed and charge pressure do rise faster than with the baseline manoeuvre mode, but the increase in engine speed then is limited by the air excess ratio limitations due to the turbocharge lag, as shown in Figure 4.19 and 4.22. Acceleration is 32% faster with fast adaptive pitch control than with the baseline manoeuvre, as shown in Figure 4.23, but a further increase in engine speed during the acceleration might enable even faster acceleration.

If the propulsion engines would be supported by an electric machine in a hybrid propulsion configuration, as proposed in Geertsma *et al.* (2017b) and Topaloglou *et al.* (2016), engine speed potentially could be increased even more, further reducing the effect of the turbocharger lag and reducing acceleration time. Geertsma *et al.* (2017b) shows that a combination of speed control on the induction machine and torque control of the main engine would reduce acceleration time by 40% compared to acceleration time without the electric machine, when a fixed combinator curve is used. Chapter 5 evaluates how much acceleration time can be further reduced with the combination of the proposed adaptive pitch control strategy and parallel control of an electric drive and propulsion diesel engine.

PREVENT ENGINE OVERSPEED AND UNDER-SPEED

The control objective to prevent engine over- and under-speed is achieved by hard over- and under-speed limitations defined in (4.13) and (4.14) and by switching from slow integrating speed control (4.11) to fast *PI* speed control (4.22). Figure 4.24 shows that fuel injection is limited during speed fluctuations in design conditions at the maximum virtual shaft speed setting, limiting engine overspeed to below 1050 rpm. Moreover, it shows how during the crash stop deceleration, (Altosole *et al.* 2012b, 2017), engine under-speed is prevented by switching to fast *PI* speed control (4.22), and how the fuel rack limitation that prevents engine under-speed is not even used during the crash stop manoeuvre. While slow integrating speed control does cause a 50 % increase in speed fluctuation due to heavy seas, from 30 rpm to 45 rpm, as illustrated in Figure 4.9 and 4.10, engine speed stability is maintained in all conditions.

4.3.4. BEHAVIOUR IN WAVES AND TURNS

The results in all operating envelopes shown, Figure 4.14, 4.15, 4.25, 4.26, 4.27 and 4.28, demonstrate that the adaptive pitch control strategy reduces the torque fluctuations due to waves, because slow integrating speed control attenuates torque fluctuations at the cost of a slight increase in engine speed fluctuations. Moreover, the adaptive pitch control strategy aims to maintain the angle of attack constant and tries to compensate the wake speed fluctuations from waves. However, due to the slow response of pitch actuation, the angle of attack during waves is not kept constant. While faster pitch actuation might enable the adaptive pitch control strategy to better maintain a constant angle of attack during high frequency wake fluctuations, we expect that the adaptive pitch control strategy can compensate for the relative slow wake speed fluctuations due to turns, particularly in stabilised conditions, as reported in Coraddu *et al.* 2013, Figure 3. Moreover, the method to establish the angle of attack as described in Vrijdag, (2009) also uses the assumption of constant propeller characteristics, which Coraddu *et al.* (2013) suggests also to hold for estimating the effect in turns, even though effects such as non-uniform wake distribution and oblique propeller inflow due to turns will have an impact on the accuracy of this assumption. Therefore, future work should be performed, first with simulation models and subsequently with model or full scale trials, to establish whether the adaptive pitch control strategy can also maintain the angle of attack in turns, thus reducing cavitation noise and increasing propeller and propulsion efficiency.

4.3.5. MEASURES OF PERFORMANCE

The MOPs of the proposed adaptive pitch control strategy with and without a limited air excess ratio can now be compared with the MOPs of the transit and manoeuvre mode of the baseline control strategy as discussed in Geertsma *et al.* (2017c). The fuel consumption plot for trial and design conditions, the air excess ratio plot for trial conditions, the cavitation plots for trial and design conditions and the angle of attack plot for trial conditions are shown in Figures 4.29, 4.30, 4.31, 4.7, 4.8 and 4.32, for the three control strategies. Moreover, the acceleration time, minimum air excess ratio and maximum angle of attack of the transit and manoeuvre mode of the baseline control strategy and the proposed adaptive pitch control strategy with a limited air excess ratio are presented in Table 5.8.

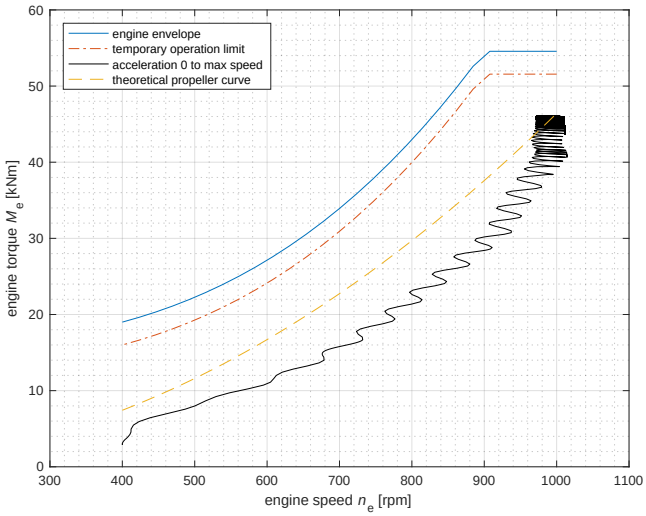

Figure 4.25: Slam start acceleration from stationary to maximum speed in engine operating envelope for fast adaptive pitch control strategy with air excess ratio limitation $\lambda_{\text{lim}} = 1.45$ in trial and design conditions.

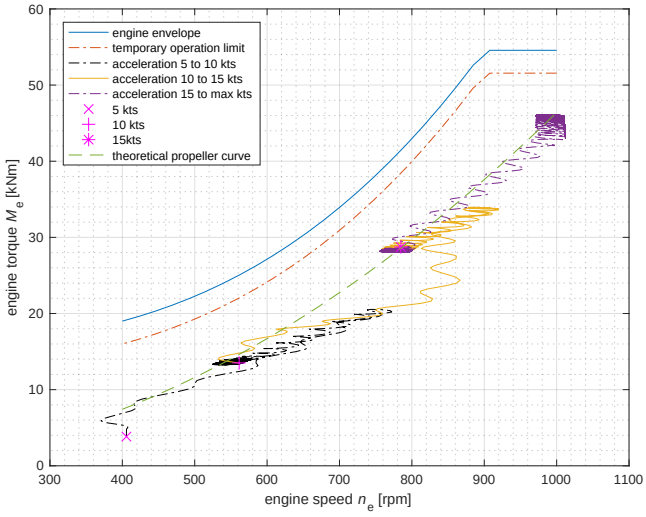

Figure 4.26: Intermediate sprints in design conditions from 0 to 5 kts, 5 to 10 kts, 10 to 15 kts, and 15 kts to maximum ship speed in engine operating envelope for fast adaptive pitch control strategy with air excess ratio limitation $\lambda_{\text{lim}} = 1.45$ in trial and design conditions.

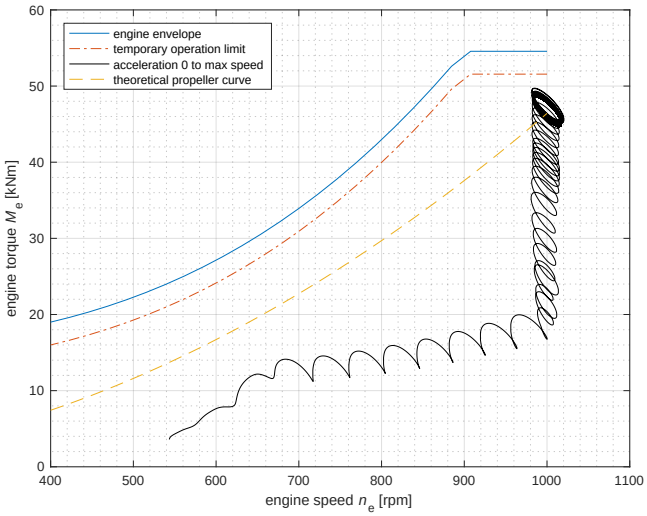

Figure 4.27: Slam start acceleration from stationary to maximum speed in engine operating envelope for baseline manoeuvre control strategy in trial and design conditions.

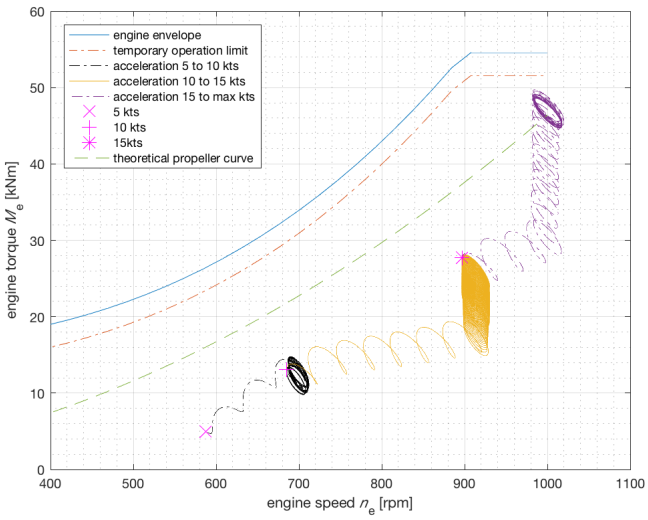

Figure 4.28: Intermediate sprints in design conditions from 0 to 5 kts, 5 to 10 kts, 10 to 15 kts, and 15 kts to maximum ship speed in engine operating envelope for baseline manoeuvre control strategy in trial and design conditions.

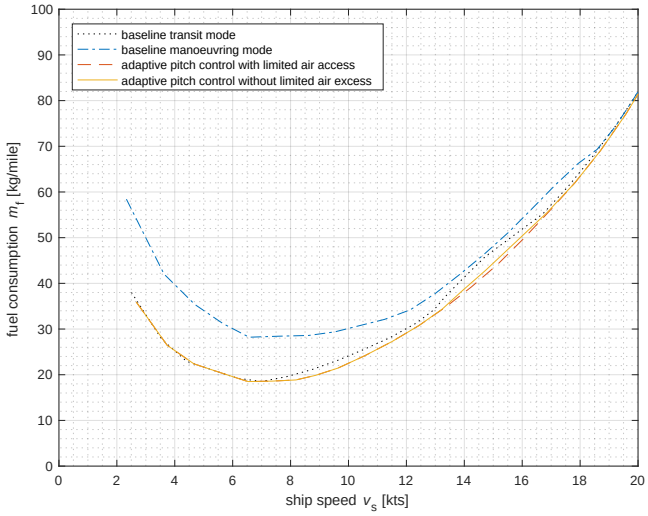

Figure 4.29: Fuel consumption plot as a function of ships speed for trial conditions in manoeuvring and transit mode and with adaptive pitch control with and without limited air excess ratio.

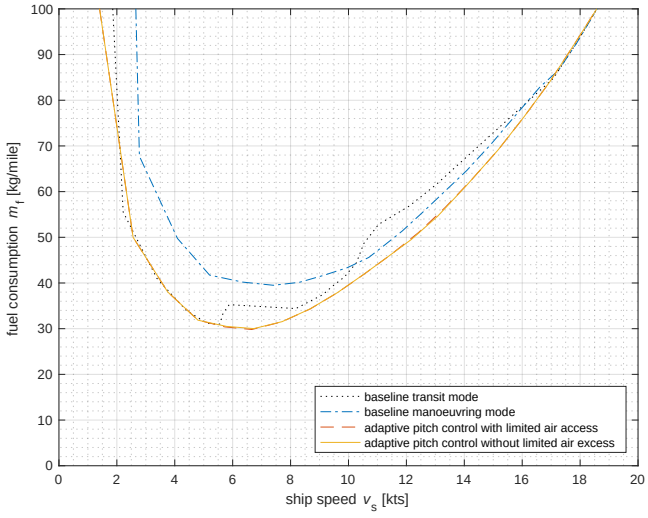

Figure 4.30: Fuel consumption plot as a function of ships speed for design conditions in manoeuvring and transit mode and with adaptive pitch control with and without limited air excess ratio.

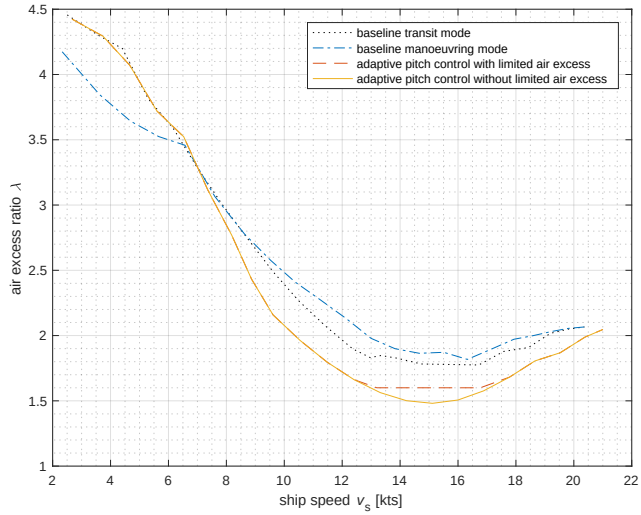

Figure 4.31: Air excess ratio plot as a function of ships speed for trial conditions in manoeuvring and transit mode and with adaptive pitch control with and without limited air excess ratio.

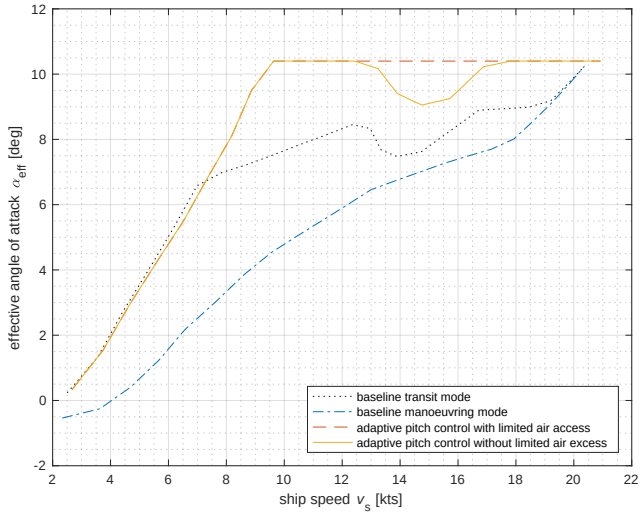

Figure 4.32: Angle of attack plot from low speed to maximum speed for trial conditions in manoeuvring and transit mode and with adaptive pitch control with and without limited air excess ratio.

Table 4.3: Acceleration time, minimum air excess ratio and maximum angle of attack during acceleration with baseline control in manoeuvring (man) and transit (tran) mode compared with the proposed adaptive pitch control (apc) strategy (design condition).

Control strategy	**tran**	**man**	**apc**	**slow apc**
Acceleration time (s): 0-5 kts	418	332	325	329
Acceleration time (s): 5-10 kts	253	154	87	98
Acceleration time (s): 10-15 kts	452	382	64	96
Acceleration time (s): 0-15 kts	203	111	89	139
Air excess ratio: 0-5 kts	2.43	2.50	1.93	2.07
Air excess ratio: 5-10 kts	1.68	1.66	1.45	1.51
Air excess ratio: 10-15 kts	1.69	1.62	1.45	1.45
Air excess ratio: 0-15 kts	1.75	1.70	1.47	1.51
Angle of attack (deg): 0-5 kts	13.6	10.0	12.5	12.7
Angle of attack (deg): 5-10 kts	10.9	9.0	12.3	12.5
Angle of attack (deg): 10-15 kts	10.8	9.1	11.4	11.7
Angle of attack (deg): 0-15 kts	10.3	11.1	12.5	12.7

From the comparison of the MOPs, we can draw the following conclusions:

- The adaptive pitch control strategy reduces fuel consumption in design conditions by 5% to 15% compared to the baseline transit mode in the ship speed range from 6 to 15 kts, and by 5% to 30% compared to the baseline manoeuvre mode in the speed range up to 15 kts. This is achieved by running the engine at the theoretical propeller curve on the associated air excess ratio. When the air excess ratio is limited at 1.6, in the engine speed range from 600 to 800 rpm the engine torque is actually limited at a value below the theoretical propeller curve, causing a slight increase in fuel consumption of up to 2%, because the air excess ratio at 700 rpm on the propeller curve is 1.5, as shown in Figure 4.3. Nevertheless, this would be a very conservative setting as the theoretical propeller curve lies well within the operating envelope of the engine.
- The adaptive pitch control strategy reduces acceleration time from 0 to 15 kts with the slam start procedure by 32% compared to the baseline manoeuvre mode and by 63% compared to the transit mode, while consistently maintaining the air excess ratio at a minimum value of 1.6. For an intermediate acceleration from 10 to 15 kts, acceleration time reduces by 84%. While faster acceleration can be achieved by using the slam start procedure (Altosole *et al.* 2017), requesting maximum virtual start speed in stead of the virtual shaft speed associated with 15 kts, the adaptive pitch control strategy does provide a more consistent acceleration time, also for intermediate acceleration, without thermally overloading the engine.
- During acceleration the angle of attack is kept around the design value of 10.5 deg, as shown in Figures 4.7, 4.8, 4.9 and 4.10. The wake flow fluctuation causes the

angle of attack to fluctuate with a similar amplitude as with the baseline control strategy.

In summary, the adaptive pitch control strategy accelerates much faster and much more consistently than the baseline manoeuvre mode, while also reducing fuel consumption significantly, without thermally overloading the engine and reducing cavitation risk for a propeller designed for low cavitation. Moreover, the control strategy does not need operator input to switch between fuel efficient or manoeuvrable operation.

4.4. CONCLUSIONS

THIS chapter has proposed the *adaptive pitch control* strategy for diesel mechanical or hybrid propulsion with slow integrating speed control and used the simulation models and Measures of Performance proposed in Chapter 3 to answer Research Question 5, thus demonstrating the following:

- Adaptive pitch control (APC) robustly follows the requested virtual shaft speed, as the adaptive pitch setpoint is compensated by a speed setpoint correction;
- APC operates the propeller around its effective angle of attack. With current slow hydraulic pitch actuation systems the response is too slow to attenuate the wake flow disturbance due to waves, in particular due to the counter balance valve. However the average angle of attack during manoeuvring remains close to the desired value;
- APC reduces fuel consumption and has the potential to improve NO_x, as the angle of attack setpoint can be used to run the engine at a predetermined operating curve, in this case the theoretical propeller curve. The operating curve can be selected based on the trade-off between the static CO_2 and NO_x emission maps. Moreover particulate matter (PM) emissions are reduced due to the smooth torque trajectory due to slow integrating speed control;
- APC maintains the air excess ratio λ at its required minimum value, thus limiting engine thermal loading. Varying the minimum air excess ratio depending on the ship function allows engine thermal loading to be adapted to the ships function. While the air excess ratio in dynamic conditions is not an exact indicator for engine thermal loading, alternatively a map based charge pressure could be used;
- APC reduces acceleration time particularly during intermediates sprints, due to its consistent acceleration behaviour; and
- APC robustly prevents engine over- and under-speed.
- For the case study patrol vessel, the adaptive pitch control strategy reduces fuel consumption by 5% to 15% compared to the baseline transit mode in the ship speed range from 6 to 15 kts, and reduces acceleration time from 0 to 15 kts with the slam start procedure by 32% compared to the baseline manoeuvre mode and by 84% for an intermediate acceleration from 10 to 15 kts, without thermally overloading the engine.

With the proposed adaptive control strategy and these additional improvements, the freedom of control provided by controllable pitch propeller can be optimally utilised to

contribute to the urgently required reduction of the environmental impact of shipping, both due to emissions and noise, without operator input. Moreover, the improvements in acceleration performance and reduction in engine thermal loading ensure the ships can be used for its increasingly diverse tasks without operator input and with minimum time in port for maintenance, thus supporting more autonomous operation.

5

PARALLEL CONTROL FOR HYBRID PROPULSION

Multifunction ships, naval vessels in particular, need to reduce fuel consumption while maintaining manoeuvrability. Hybrid propulsion that runs a main diesel engine and electric drive in parallel can achieve this. However, a parallel control strategy needs to be developed. In this chapter, we propose a novel parallel control strategy in combination with the adaptive pitch control strategy proposed in Chapter 4 and use the simulation model of a hybrid propulsion system, introduced in Chapter 3 to investigate the performance of the proposed parallel control strategy for hybrid propulsion on multifunction ships, and answer Research Question 6: 'What control strategy can be used for the power split between the propulsion engine and electric drive in hybrid propulsion to provide the best possible performance against an adaptive trade-off between the various conflicting MOEs? '

The chapter is organised as follows: After the introduction in Section 5.1, we describe the hybrid propulsion system of the frigate and introduce the dynamic model in Section 5.2. Subsequently, we describe the two proposed control strategies, parallel adaptive pitch control in Section 5.3 and parallel electric speed control in Section 5.4, and the baseline strategy in Section 5.5. In Section 5.6, we present the comparison of these strategies with the baseline strategy. In Section 5.7, we summarise the conclusions.

Parts of this chapter have been published in IFAC Proceedings Volumes **50(1)** (2017), Geertsma *et al.* (2017b) and in Proceedings of IEEE ESTS (2017), Geertsma *et al.* (2017d).

5.1. INTRODUCTION

ELECTRIC propulsion has gained enormous interest in the cruise ship industry in the '90s (Vie, 1998), because it allows to match the connected power generating capacity with total power demand of the vessel. Since then, electric propulsion has also been successfully applied in ferries, DP drilling vessels, cable layers, icebreakers, tugs, capital naval vessels, and even in naval combatants (Hodge *et al.* 2008; Loyd *et al.* 2003; Moreno *et al.* 2007). However, the significant conversion losses in the generators, transformers, frequency converters and electric machines lead to poor propulsion efficiency at full load. Thus, electric propulsion has only been applied on ships with a very broad operating profile and a significant portion of hotel load compared to the propulsion load.

Alternatively, hybrid propulsion achieves high efficiencies with direct drive diesel engines or gas turbines at high speed, while allowing for a similar flexibility to select the electric power generating capacity for electric propulsion and hotel load at low ship speeds, as discussed in Chapter 2, (Geertsma *et al.* 2017a). This concept is particularly suitable for vessels that in some operating modes require a large propulsion load and in other operating modes require a propulsion load that is of the same magnitude as the ships services (Waard, 2015). For example, hybrid propulsion has been applied to naval frigates and destroyers (Castles *et al.* 2009), towing vessels (Breijs *et al.* 2016), offshore vessels (Barcellos, 2013), and yachts (Loon *et al.* 2016).

In most current applications of hybrid propulsion, the ship either operates in direct mechanical mode or in electrical mode. These applications do not yet achieve the full potential of the hybrid propulsion concept. First, when the main engine is running, the electric drive can very efficiently generate electric power, and the diesel generators can thus be shut down. Secondly, the electric motor can assist the main diesel engine, for example to improve acceleration performance, reduce thermal loading of the main engine or increase top speed. However, to run the main engine and electric drive in parallel, an advanced control strategy is required.

5.1.1. LITERATURE REVIEW

Parallel control of a combustion engine and an electric drive has been a field of extensive study for automotive applications and initially focused on reducing fuel consumption and emissions (Ambuhl *et al.* 2007; Chasse *et al.* 2011; Guardiola *et al.* 2014; Musardo *et al.* 2005; Paganelli *et al.* 2002, 2000; Sciarretta *et al.* 2004, 2014; Sivertsson *et al.* 2015). Initially, research focussed on minimising fuel consumption over typical driving cycles, trying to approach the potential minimum fuel consumption established with offline solutions (Chasse *et al.* 2011; Sciarretta *et al.* 2014) with online energy management strategies based on the Equivalent Consumption Minimisation Strategy (ECMS) (Paganelli *et al.* 2002, 2000; Sciarretta *et al.* 2004). This ECMS approach assigns an equivalent cost to the use of the battery which can be updated based on the state of charge of the battery (Ambuhl *et al.* 2007) or an estimation about operating conditions (Musardo *et al.* 2005) and can also be applied in a map-based approach (Sivertsson *et al.* 2015). Later studies also aimed to discharge the battery over the operating profile, in order to minimise fuel consumption and recharge the batteries from renewable energy from the grid (Guardiola *et al.* 2014). These studies confirmed that fuel consumption can be estimated sufficiently accurately with a quasi-static approach (Sciarretta *et al.* 2014) and are mainly

concerned with determining the optimum power split between the combustion engine and electric drive, typically fed from a battery.

In recent work, also other criteria than fuel consumption are considered in order to determine the optimum power-split (Jauch *et al.* 2016, 2018; Johannesson *et al.* 2015; Maamria *et al.* 2017). In Maamria *et al.* (2017) the temperature of the engine and catalyst are included in the optimisation algorithm as extra state variables. This allows taking into account the effect of the engine and catalyst temperature on pollutant emissions and prevents the engine to cool down too much, thus causing excessive emissions. As the thermal inertia of the engine and catalyst is large, a quasi-static approach suffices. Alternatively, Jauch *et al.* (2016, 2018) design a model and controller to address drivability. They use a feedforward control filter and feedback controller with disturbance observer to achieve the desired response to the accelerator during a dynamic acceleration manoeuvre. The work suggests this controller can be combined with an ECMS strategy to achieve the optimal fuel consumption as well. Finally, Johannesson *et al.* (2015) attempt to improve both fuel consumption and drivability over a known future operating profile with model predictive control for hybrid long haul trucks, for example also trying to reduce unnecessary gear shifting.

While these automotive studies provide useful insights on energy management strategies for fuel consumption of ships (Breijs *et al.* 2016; Kalikatzarakis *et al.* 2018; Scibberas *et al.* 2015; Sciberras *et al.* 2012; Vu *et al.* 2015; Yuan *et al.* 2016), the dynamic problem for ships is very different. First, the operator of a ship does not directly operate the torque request with the accelerator, but requests a lever setpoint which is translated into a combination of shaft speed and pitch setpoints, or a virtual shaft speed, defined in (3.111), as proposed in Vrijdag *et al.* (2010). Secondly, the inertia of the ship means that phenomena like jerk and kick, (Jauch *et al.* 2018) are not relevant for ship acceleration. The main challenge for acceleration of ships is to accelerate the ship as fast as possible without overloading the engines (Altosole *et al.* 2017; Geertsma *et al.* 2017c; Guillemette *et al.* 1997; van Spronsen *et al.* 2001), or causing excessive NO_x, smoke or Particulate Matter (PM) emissions (Nielsen *et al.* 2017a, 2018; Papalambrou *et al.* 2017; Topaloglou *et al.* 2016). Similarly, during turns, loss of speed should be limited while also preventing engine overloading (Coraddu *et al.* 2013), even during machinery failure (You, 2018).

Parallel control strategies in which the electric drive supports the main engine during acceleration have been proposed in literature for ships with fixed pitch propellers (FPP) (Dedes *et al.* 2012; Nielsen *et al.* 2017a,b, 2018; Papalambrou *et al.* 2017; Topaloglou *et al.* 2016). Topaloglou *et al.* (2016) propose a power-split controller that aims to maintain the air excess ratio λ at a specified value imposed by a lookup table. In an experimental setup, they enforce a load-step, representing ship propulsion with an FPP, while they aim to control the air excess ratio. During the load step the air excess ratio dips, but subsequently the controller improves the air excess ratio by applying torque to the electric drive. For the same experimental setup as in Topaloglou *et al.* (2016), Papalambrou *et al.* (2017) use Model Predictive Control (MPC) to control the power split. Again, the controller improves the air excess ratio significantly, but the initial dip in air excess ratio λ remains due to the fast speed controller of the engine. Nielsen *et al.* (2017b, 2018) deal with the problem of smoke formation during acceleration for an engine with exhaust gas recirculation. Nielsen *et al.* (2017b) propose an adaptive feedforward controller for ex-

haust gas recirculation and Nielsen *et al.* (2018) propose two extended fuel limiters to limit fuel injection during acceleration, one using an oxygen sensor and another using the control oriented model proposed in Nielsen *et al.* (2017a). The simulation experiments and experimental validation demonstrate that the combination of the feedforward controller with the fuel limiter using the control oriented model almost completely eliminates smoke formation during acceleration, while maintaining manoeuvrability. As smoke formation is strongly related to the air-excess ratio, their feedforward control strategy with limiters does manage to maintain the air-excess ratio. Finally, Dedes *et al.* (2012) demonstrates how hybrid propulsion with hybrid power supply can also significantly reduce fuel consumption for cargo ships, by eliminating loading transients and running the main engines near its optimum working point. The additional power from the electric drive can also prevent main engine overloading in adverse weather, in particular on commercial vessels, due to the trend to reduce engine rating to meet EEDI guidelines and these vessels' fixed pitch propellers (Dedes *et al.* 2012; Kouroutzis *et al.* 2016).

Control of propeller pitch and parallel control of the engine and electric drive for ships with controllable pitch propellers (CPP) have been studied in Geertsma *et al.* (2016, 2017b,d). Geertsma *et al.* (2016) propose to use torque control to control ship speed and shows that acceleration time can be reduced for ships with CPP by reducing pitch during acceleration. However, this preliminary study does not propose a robust control strategy. Geertsma *et al.* (2017b,d) propose to use speed control for the electric drive in combination with torque control for the main engine and their simulation experiments demonstrate this can lead to a significant reduction in acceleration time, because the electric drive speed setpoint can be ramped up more quickly than the main engine speed setpoint. Chapter 4 proposes the adaptive pitch control strategy for diesel mechanical propulsion, which uses slow integrating speed control and thus exhibits the benefits of torque control. The simulation study in this chapter demonstrates adaptive pitch control can improve intermediate acceleration significantly, but the acceleration performance to maximum speed is still limited due to turbocharger lag.

5.1.2. AIM AND CONTRIBUTION

Hybrid propulsion provides efficient propulsion at high speed and power and allows sharing hotel load and electric propulsion at low speeds for ships with diverse operating speed. Studies on ships with FPP have shown hybrid propulsion can also be used to reduce emissions and smoke formation during acceleration and constant speed sailing and to reduce fuel consumption. This chapter aims to investigate what performance improvement hybrid propulsion can provide when used in a configuration with controllable pitch propellers with adaptive pitch control and slow integrating speed control for MOEs fuel consumption, emissions, maoeuvrability and thermal loading.

This chapter addresses the following novelties: First, a novel Parallel Adaptive Pitch Control (PAPC) strategy is proposed, which combines slow integrating speed control of the main engine with torque control of the electric drive and which can be used with adaptive pitch control. Second, the performance trade-off for hybrid propulsion between fuel consumption, acceleration time for slam start and intermediate sprints, cavitation noise and engine thermal loading for hybrid propulsion with the proposed control

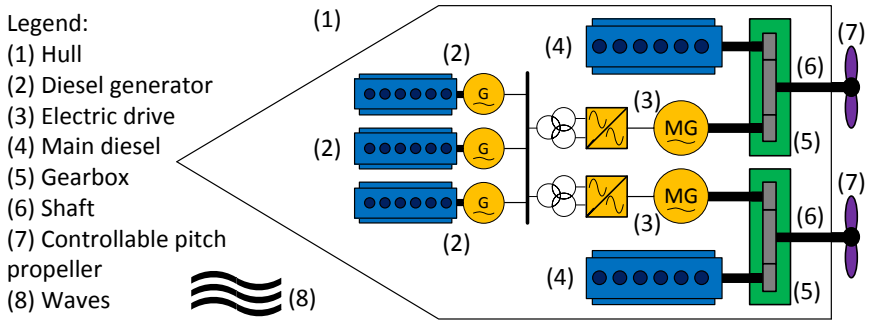

Figure 5.1: Typical hybrid propulsion system layout for a naval vessel.

strategy is analysed and compared with the hybrid electrical speed control strategy with torque control for the diesel engine, as proposed in Geertsma *et al.* (2017b,d) and with 3 other baseline control strategies.

5

5.2. SYSTEM DESCRIPTION

IN this chapter, we consider hybrid propulsion that propels a frigate with two shafts, each consisting of one diesel engine, one electric drive, a gearbox, a shaft and a controllable pitch propeller (CPP), as illustrated in Figure 5.1. Figure 5.1 also shows the electrical network that feeds the electrical drive, but the electrical network dynamics are not considered in this dissertation. The model representation of the hybrid propulsion components and their interaction are shown in Figure 5.2. In order to investigate the performance of the propulsion plant in adverse weather conditions, the influence of waves on the advance speed of the propeller is modelled as a disturbance. The models of the diesel engine, induction machine and its frequency converter, gearbox, shaft-line, propeller, hull and waves have been described in Chapter 3, (Geertsma *et al.* 2017c). We use the simulation models and benchmark manoeuvres described in Chapter 3 to compare the performance of the proposed Parallel Adaptive Pitch Control (PAPC) strategy with a number of alternative baseline control strategies, including the Parallel Electric Speed Control Strategy (PESC) proposed in Geertsma *et al.* (2017b) and Geertsma *et al.* (2017d). The subsequent sections will discuss the proposed PAPC and alternative baseline control strategies.

5.3. PARALLEL ADAPTIVE PITCH CONTROL

THE Parallel adaptive pitch control (PAPC) strategy aims to further improve the Measures of Effectiveness (MOEs) fuel consumption and emissions, further reduce engine thermal loading and improve manoeuvrability, compared to the Adaptive Pitch Control strategy without using the parallel electric drive. Thus, PAPC can use the torque from the induction machine through the voltage setpoints for the frequency converter to improve these MOPs, resulting in the control actions propeller pitch ratio setpoint, fuel pump injection setpoint and voltage setpoints, as follows: $u(t) = [P_{\text{p,set}}, X_{\text{set}}, v^s_{\text{ds,set}}, v^s_{\text{qs,set}}]$. The simplified representation of the proposed control strategy is shown in Figure 5.3b.

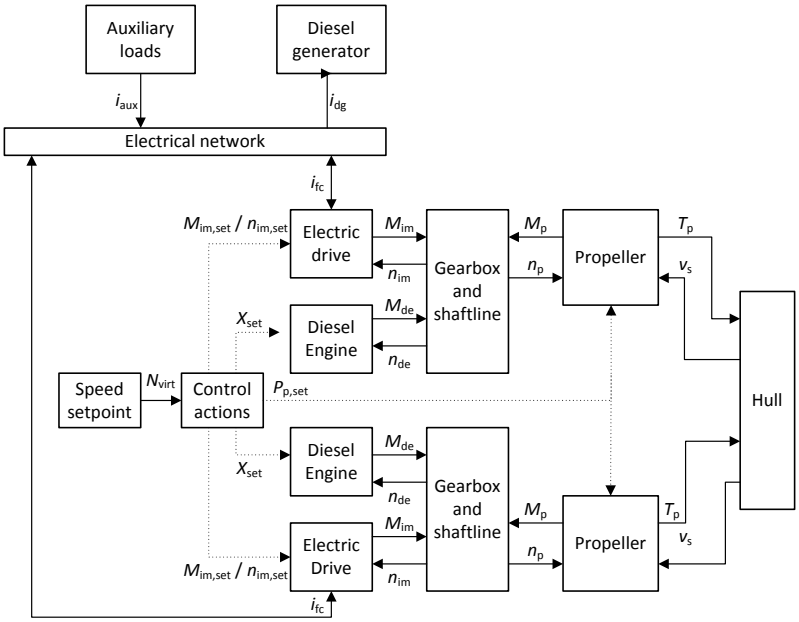

Figure 5.2: Schematic presentation of hybrid propulsion system for naval vessel showing coupling between models.

Legend:

$P_{pd,set}$	propeller pitch ratio setpoint
$M_{e,set}$	engine torque setpoint
$n_{im,set}$	induction machine speed setpoint
$\alpha_{eff,set}$	angle of attack setpoint
$n_{e,set}$	engine speed setpoint
$M_{im,set}$	induction machine torque setpoint
P_{pd}	propeller pitch ratio
M_e	engine torque
p_1	engine charge pressure
n_{im}	Shaft line and induction machine speed
i_{qs}^s	quadrature stator current, stationary
i_{ds}^s	direct stator current, stationary
n_e	engine speed
β	hydrodyamic pitch angle
$u(t)$	control actions
$x(t)$	state variables
$z(t)$	measured system outputs
$r(t)$	disturbances

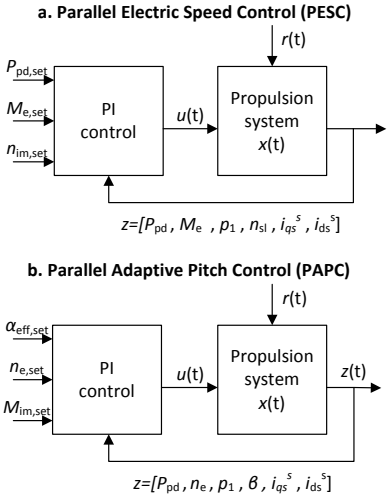

Figure 5.3: Simplified representation of Parallel Electric Sped Control (PESC) and proposed Parallel Adaptive Pitch Control strategy for hybrid propulsion with CPP.

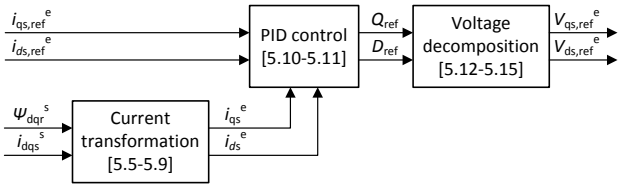

Figure 5.4: Schematic representation of direct field oriented control strategy.

5.3.1. CONTROL OBJECTIVES AND DESIGN

In the Parallel Adaptive Pitch Control (PAPC) control strategy, the secondary control objectives are to assist diesel engine main propulsion to achieve higher ship speeds, increase acceleration and reduce engine thermal loading and emissions influenced by engine dynamics, such as Particulate Matter (PM) and smoke (Nielsen *et al.* 2018; Nuesch *et al.* 2014), while maintaining the primary objective to provide the requested virtual shaft speed. These secondary objectives are particularly aimed at the slam start acceleration during which acceleration of adaptive pitch control only improved slightly due to the turbocharger lag, as discussed in Chapter 4.

We maintain Adaptive Pitch Control (APC) as presented in Chapter 4 and provide additional torque to the shaft line with the electric motor. The electric motor torque is controlled with direct field oriented control as proposed by Blaschke, (1974) and Hasse, (1969) and covered in depth in Sudhoff *et al.* (1998), Trzynadlowski, (2001) and Ong, (1998). Figure 5.4 illustrates the schematic representation of the field oriented control strategy used in this study. The quadrature and direct stator current references in the synchronously rotating reference frame $i^{e}_{qs,ref}$ and $i^{e}_{ds,ref}$ in A are determined from the torque and direct rotor flux references $M_{em,ref}$ in Nm and $\Psi^{e}_{dr,ref}$ in V, as follows:

$$i^{e}_{qs,ref}(t) = \frac{2}{3P_{pp}} \frac{(x_{lr} + x_m)}{x_m} \frac{M_{em,ref}(t)\omega_b}{\Psi^{e}_{dr,ref}(t)} \tag{5.1}$$

$$i^{e}_{ds,ref}(t) = \frac{1}{x_m} \Psi^{e}_{dr,ref}(t). \tag{5.2}$$

The actual quadrature and direct current in the synchronously rotating reference frame i^{e}_{qs} and i^{e}_{ds} in A can be determined from the measured stator current $[i^{s}_{ds}\ i^{s}_{qs}]$ and mutual flux $[\Psi^{s}_{md}\ \Psi^{s}_{mq}]$ in V, as follows:

$$\Psi^{s}_{qr}(t) = \frac{x_r + x_m}{x_m} \Psi^{s}_{mq}(t) - x_r i^{s}_{qs}(t) \tag{5.3}$$

$$\Psi^{s}_{dr}(t) = \frac{x_r + x_m}{x_m} \Psi^{s}_{md}(t) - x_r i^{s}_{ds}(t) \tag{5.4}$$

$$|\Psi^{s}_{r}(t)| = \sqrt{\Psi^{s}_{dr}(t)^2 + \Psi^{s}_{qr}(t)^2} \tag{5.5}$$

$$\cos\rho_e(t) = \frac{\Psi^{s}_{dr}(t)}{|\Psi^{s}_{r}(t)|} \tag{5.6}$$

$$\sin\rho_{\mathrm{e}}(t) = \frac{\Psi^{\mathrm{s}}_{\mathrm{qr}}(t)}{|\Psi^{\mathrm{s}}_{\mathrm{r}}(t)|} \tag{5.7}$$

$$i^{\mathrm{e}}_{\mathrm{qs}}(t) = i^{\mathrm{s}}_{\mathrm{qs}}(t)\cos\left(\rho_{\mathrm{e}}(t)\right) - i^{\mathrm{s}}_{\mathrm{ds}}(t)\sin\left(\rho_{\mathrm{e}}(t)\right) \tag{5.8}$$

$$i^{\mathrm{e}}_{\mathrm{ds}}(t) = i^{\mathrm{s}}_{\mathrm{qs}}(t)\sin\left(\rho_{\mathrm{e}}(t)\right) - i^{\mathrm{s}}_{\mathrm{ds}}(t)\cos\left(\rho_{\mathrm{e}}(t)\right). \tag{5.9}$$

Subsequently, PID control is applied to obtain the quadrature and direct references Q_{ref} and D_{ref}, as follows:

$$Q_{\mathrm{ref}}(t) = K_{\mathrm{PT}}\left(i^{\mathrm{e}}_{\mathrm{qs,ref}}(t) - i^{\mathrm{e}}_{\mathrm{qs}}(t)\right) + K_{\mathrm{IT}}\int_0^t \left(i^{\mathrm{e}}_{\mathrm{qs,ref}}(t) - i^{\mathrm{e}}_{\mathrm{qs}}(t)\right) dt \tag{5.10}$$

$$D_{\mathrm{ref}}(t) = K_{\mathrm{PD}}\left(i^{\mathrm{e}}_{\mathrm{ds,ref}}(t) - i^{\mathrm{e}}_{\mathrm{ds}}(t)\right) + K_{\mathrm{ID}}\int_0^t \left(i^{\mathrm{e}}_{\mathrm{ds,ref}}(t) - i^{\mathrm{e}}_{\mathrm{ds}}(t)\right) dt, \tag{5.11}$$

where K_{PT}, K_{IT}, K_{PD} and K_{ID} are the gains and reset rates, which have been determined by manual tuning, as defined in Table 5.1. Finally, the decoupling equations, as discussed in Ong, 1998, Ch. 9, pp. 448, are used to obtain the direct and quadrature voltage references $v^{\mathrm{s}}_{\mathrm{qs,ref}}$ and $v^{\mathrm{s}}_{\mathrm{qs,ref}}$, as follows:

$$v^{\mathrm{e}}_{\mathrm{qs,ref}}(t) = Q_{\mathrm{ref}}(t) + \frac{x_{\mathrm{s}}\omega_{\mathrm{e}}(t)}{\omega_{\mathrm{b}}} i^{\mathrm{e}}_{\mathrm{ds}}(t) + \frac{x_{\mathrm{m}}}{x_{\mathrm{r}}+x_{\mathrm{m}}}\frac{\omega_{\mathrm{e}}(t)}{\omega_{\mathrm{b}}}\Psi^{\mathrm{e}}_{\mathrm{dr,ref}}(t) \tag{5.12}$$

$$v^{\mathrm{e}}_{\mathrm{ds,ref}}(t) = D_{\mathrm{ref}}(t) + \frac{x_{\mathrm{s}}\omega_{\mathrm{e}}(t)}{\omega_{\mathrm{b}}} i^{\mathrm{e}}_{\mathrm{qs}}(t) + \frac{x_{\mathrm{m}}}{(x_{\mathrm{r}}+x_{\mathrm{m}})\,\omega_{\mathrm{b}}}\frac{\mathbf{d}\Psi^{\mathrm{e}}_{\mathrm{dr,ref}}(t)}{\mathbf{d}t} \tag{5.13}$$

$$v^{\mathrm{s}}_{\mathrm{qs,ref}}(t) = v^{\mathrm{e}}_{\mathrm{qs}}(t)\cos\left(\rho_{\mathrm{e}}(t)\right) + v^{\mathrm{e}}_{\mathrm{ds}}(t)\sin\left(\rho_{\mathrm{e}}(t)\right) \tag{5.14}$$

$$v^{\mathrm{s}}_{\mathrm{ds,ref}}(t) = -v^{\mathrm{e}}_{\mathrm{qs}}(t)\sin\left(\rho_{\mathrm{e}}(t)\right) + v^{\mathrm{e}}_{\mathrm{ds}}(t)\cos\left(\rho_{\mathrm{e}}(t)\right). \tag{5.15}$$

The phase values of the voltage can then be obtained using Clarke's transformation (Ong, 1998, Ch. 5 p. 142). These phase voltages serve as the reference values for the frequency converter, which is assumed to be an ideal voltage source.

In this study, the control strategy was modelled in the synchronously rotating reference frame, like the induction machine in Geertsma *et al.* (2017b). While in a real system the actual quadrature and direct current in the synchronously rotating reference frame $i^{\mathrm{e}}_{\mathrm{qs}}$ and $i^{\mathrm{e}}_{\mathrm{ds}}$ can be determined from flux and stator current measurements as discussed in Geertsma *et al.* (2017b), we directly use the quadrature and direct current in the synchronously rotating reference frame from the simulation model. Thus, simulation time is significantly reduced, due to the absence of fluctuating sine wave signals. This can be allowed, because we are not interested in the effects of noise and inaccuracy of the measurements.

The relative torque setpoint for torque control $M_{\mathrm{em,set}}$ in % is a function of the virtual shaft speed and is shown in the combinator curve in Figure 5.5. We only apply additional torque from the electric drive above 90 rpm virtual shaft speed $N_{\mathrm{virt,set}}$, because engine fuel consumption is near its optimum value without additional electric drive torque. Moreover, intermediate sprint acceleration is already fast due to adaptive pitch control, and the optimum angle of attack for cavitation is achieved without additional torque, as discussed in Chapter 3. When additional torque is applied, the angle of attack for the propeller also needs to be increased in order to align the matching of

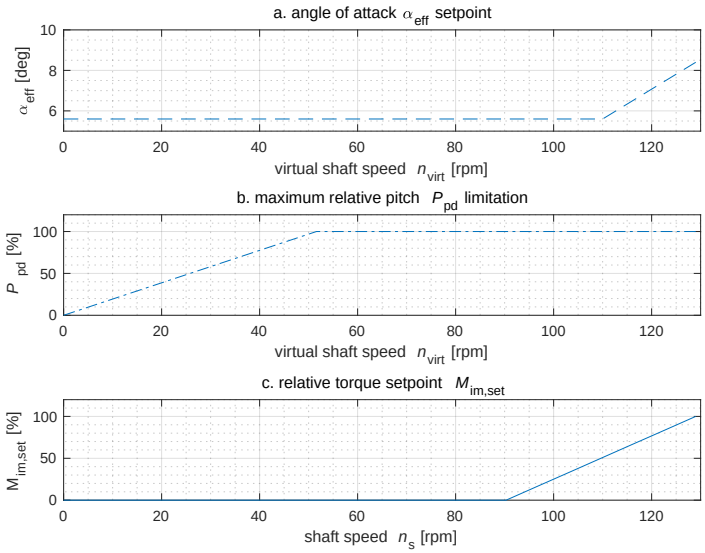

Figure 5.5: Combinator curve for hybrid propulsion with Parallel Adaptive Pitch Control (PAPC) control strategy.

the propeller with the total torque of the main engine and electric drive and maintain operation on the theoretical propeller curve. The resulting combinator curve with the effective angle of attack setpoint as a function of actual shaft speed, the maximum pitch angle to prevent engine under-speed and the electric drive torque as a function of virtual shaft speed is shown in Figure 5.5. In future work, the torque setpoint applied in the PAPC control strategies could be established with more advanced optimised power split control strategies as proposed for ship application in Chapter 6 and in Kalikatzarakis *et al.* (2018), Grimmelius *et al.* (2011) and Breijs *et al.* (2016) and for automotive applications in Sciarretta *et al.* (2014), Koot *et al.* (2005) and Silvas *et al.* (2015) and many other works.

5.4. PARALLEL ELECTRIC SPEED CONTROL

PARALLEL electric speed control (PESC) was proposed in Geertsma *et al.* (2017b) and Geertsma *et al.* (2017d) for hybrid propulsion, using speed control for the electric drive and torque control for the main engine. Because the increase rate of the speed setpoint for the electric drive can be higher than that of the diesel engine, which is limited by its turbocharger lag, this initial study demonstrated acceleration times can be improved significantly. The disadvantage of this strategy is that the engine control strategy would need to change when switching from pure mechanical propulsion to parallel hybrid propulsion, as soon as the electric drive is used in parallel with the main engine. Nevertheless, this control strategy provides a good benchmark for fast acceleration.

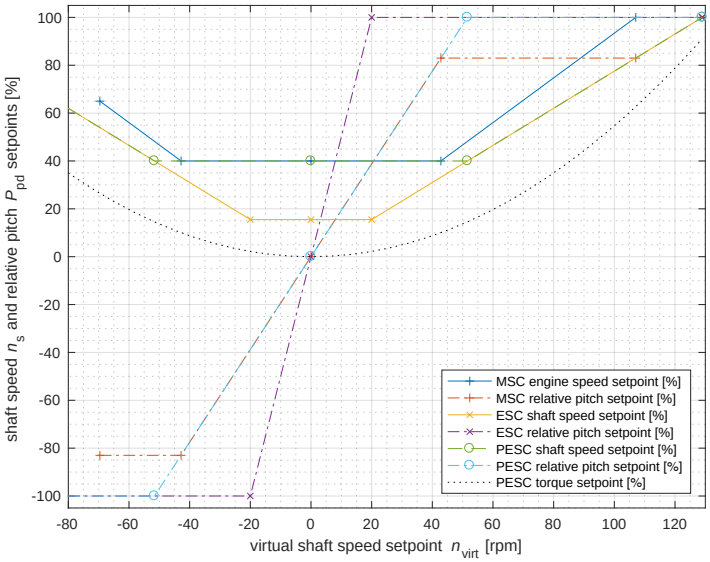

Figure 5.6: Combinator curve for diesel mechanical and hybrid propulsion for baseline Mechanical Speed Control (MSC), Electrical Speed Control (ESC) and Parallel Electric Speed Control (PESC) control strategies.

In this control strategy, the primary objective again is to propel the ship at the requested virtual shaft speed, with the following secondary objectives:

- Increase acceleration by utilising electric motor torque.
- Reduce engine thermal loading and thermal loading fluctuation by running the engine at constant torque.

The electric drive now utilises speed control, by adding an extra speed control loop in front of the torque controller, as follows:

$$M_{\text{im,ref}}(t) = K_{\text{PS}}\left(\frac{\omega_{\text{ref}}(t)-\omega_{\text{i}}(t)}{\omega_{\text{nom}}}\right) + K_{\text{IS}}\int_0^t\left(\frac{\omega_{\text{ref}}(t)-\omega_{\text{i}}(t)}{\omega_{\text{nom}}}\right)dt, \tag{5.16}$$

where $M_{\text{im,ref}}$ is the induction machine torque setpoint in %, ω_{ref} is the reference speed for the induction machine as defined in the combinator curve shown in Figure 5.6, and ω_{i} is the induction machine shaft speed in rad/s.

Furthermore, the diesel engine is controlled with a torque control loop, as previously proposed in Geertsma *et al.* (2016) and Geertsma *et al.* (2017b) and illustrated in Figure 5.7. The fuel pump setpoint $X_{\text{set}}(t)$ is derived from the engine torque setpoint $M_{\text{e,ref}}$, as follows:

$$X_{\text{set,2}}(t) = K_{\text{PT}}\left(\frac{M_{\text{e,ref}}(t)}{M_{\text{e,nom}}} - \frac{M_{\text{e}}(t)}{M_{\text{e,nom}}}\right) + K_{\text{IT}}\int_0^t\left(\frac{M_{\text{e,ref}}(t)}{M_{\text{e,nom}}} - \frac{M_{\text{e}}(t)}{M_{\text{e,nom}}}\right)dt, \tag{5.17}$$

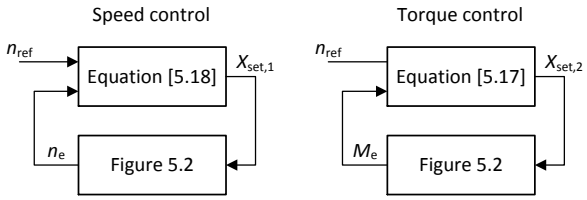

Figure 5.7: Control loop for mechanical propulsion for speed control and torque control.

Table 5.1: Speed and torque control parameters

	induction machine	**diesel engine**
proportional gain speed K_{PS}	10	2
reset rate speed K_{IS}	0.02	0.5
proportional gain torque K_{PT}	1	0.1
reset rate torque K_{IT}	0.2	2
proportional gain field K_{PD}	1	
reset rate field K_{ID}	0.5	
acceleration rate dn_{max}	1.5 rev/s	0.75 rev/s

where $M_{\text{e,nom}}$ is the nominal engine torque in kNm and the engine torque setpoint $M_{\text{e,ref}}$ is a function of the virtual shaft speed and is shown in the combinator curve in Figure 5.6.

5.5. BASELINE SPEED CONTROL STRATEGIES

5.5.1. MECHANICAL SPEED CONTROL STRATEGY

IN the baseline Mechanical Speed Control (MSC) strategy the main diesel engine provides propulsion. The primary control objective is to provide propulsion at the requested virtual shaft speed n_{virt} in rpm. The relationship between the virtual shaft speed setpoint, the engine speed setpoint and pitch ratio setpoint is determined in the combinator curve as discussed in Martelli, (2014) and Geertsma *et al.* (2016). This combinator curve should ensure the static operating points of the engine in design conditions have sufficient margin to the engine operating envelope. The combinator curve used in the baseline control strategy is illustrated in Figure 5.6. Please note that the nominal pitch ratio P_{nom} for the baseline control strategy is lower (83%) than the pitch ratio for the parallel control strategies (100%), because the available power at maximum shaft speed is only nominal engine power. Moreover, the matching of the propeller with the hybrid propulsion plant was performed with total available power of the diesel engine and the electric drive, according to the matching procedure proposed in Stapersma, (2005).

The primary control strategy for the baseline controller is engine speed control, using the speed setpoint from the combinator curve. The schematic representation of diesel

engine speed control is shown in Figure 5.7. The controller algorithm is defined as follows:

$$X_{\text{set},1}(t) = K_{\text{PS}}\left(\frac{n_{\text{ref}}(t)}{100} - \frac{n_{\text{e}}(t)}{n_{\text{nom}}}\right) + K_{\text{IS}}\int_0^t \left(\frac{n_{\text{ref}}(t)}{100} - \frac{n_{\text{e}}(t)}{n_{\text{nom}}}\right) dt, \tag{5.18}$$

where X_{set} is the fuel pump setpoint in %, K_{PS} is the proportional gain for speed control, K_{IS} is the reset rate for speed control, n_{ref} is the reference speed in % and n_{nom} is the nominal engine speed in rev/s.

In order to prevent thermal overloading of the diesel engine, the acceleration rate can be limited as proposed in Vrijdag *et al.* (2010). With a virtual shaft speed acceleration rate of 0.75 rev/s, engine loading is retained within the operating envelope, as will be shown in Section 5.6. The resulting speed control parameters are listed in Table 5.1. In all control strategies the behaviour of the pitch controller and the associated hydraulic circuit is simplified with a first order time delay as described in Geertsma *et al.* (2016). Alternative modelling strategies that account for the delays due to the non-linearities in CPP system behaviour, as discussed in Godjevac *et al.* (2009), are proposed in Wesselink *et al.* (2006), Martelli, (2014) and Martelli *et al.* (2014a).

5

5.5.2. ELECTRIC SPEED CONTROL STRATEGY

The Electric Speed Control Strategy (ESC) in electric mode aims to provide fuel-efficient, silent propulsion and consists of a combinator curve that determines shaft speed and propeller pitch setpoints from the requested virtual shaft speed, PID control on shaft speed for the electric drive, and feedforward control for propeller pitch. Thus, the torque reference setpoint for the direct field oriented control described in Section 5.3 is established through PID control, according to (5.16). The increase rate of propeller pitch is limited to reflect the maximum pitch change rate of the hydraulic actuation system. The increase rate of the electric drive limits dynamic loading of the power generation system. The PID parameters have been determined by trial and error, using *Ziegler-Nichols* Ziegler *et al.* (1942). The control parameters are listed in Table 5.1 and the combinator curve is illustrated in Figure 5.6.

5.6. RESULTS

5.6.1. SIMULATION EXPERIMENTS

THE simulation experiments for the case study frigate in this chapter aim to compare the proposed Parallel Adaptive Pitch Control (PAPC) strategy with various alternative baseline control strategies. Similar to Chapter 4, sailing at constant speed and two acceleration manoeuvres, all in a straight line, are used to establish the Measures of Performance (MOP). The slam start acceleration manoeuvre determines the fastest possible acceleration from 0 to 24 kts ship speed (Altosole *et al.* 2017). When the slam start manoeuvre starts, the maximum virtual shaft speed is selected to accelerate as fast as possible. To establish acceleration during intermediate sprints, the virtual shaft speed setting is raised from the value representing initial ship speed to the value that provides the target ship speed. These Measures of Performance (MOPs) are thus established with the benchmark manoeuvres proposed in chapter 3 (Geertsma *et al.* 2017c). The results

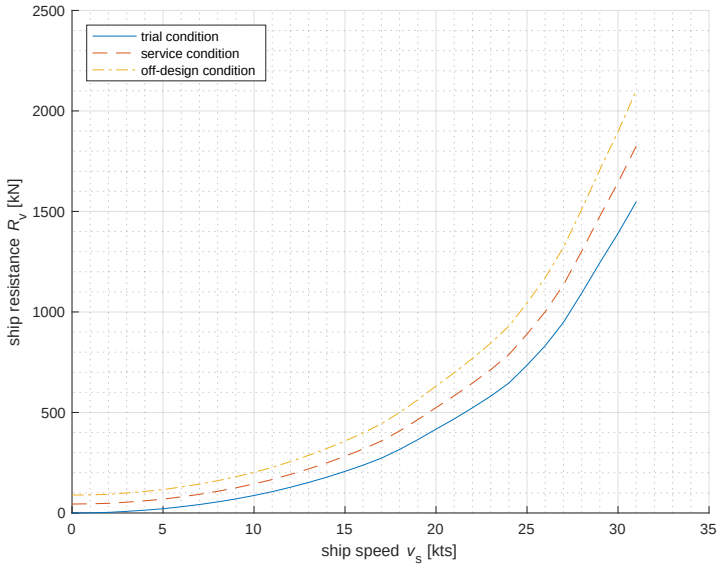

Figure 5.8: Ship resistance from model tests corrected for environmental conditions and fouling in trial, service and off-design condition.

in the followings sections have been established with simulations in MATLAB Simulink R2016b software on a PC with Intel Core i7 processor and 16 GB memory.

The model parameters used for the hybrid diesel-electric propulsion model are presented in Table 5.2 for the diesel engine, in Table 5.3 for the induction machine, in Table 5.4 for the gearbox, in Table 5.5 for the propeller and in Table 5.6 for the hull. Similar to chapter 4, we consider the following two typical conditions:

- Trial condition, defined as Sea State 0, wind speed of 3 m/s and no fouling.
- Design condition, defined as Sea State 4, wind speed of 11 m/s, head seas and wind and 6 months out of dock fouling.

These conditions are reflected in the parameters in Table 5.6 and Figure 5.8.

The resulting static operation of the main diesel engines is presented in Figure 5.9 and 5.10. Figure 5.9 demonstrates that the theoretical propeller law is close to the lowest fuel consumption of the engine and maintains sufficient margin to the temporary operating limit. Moreover, the lowest in-cylinder air excess ratio λ during static operation within the temporary operating limit is just below 1.4 and on the theoretical propeller curve 1.45. Figure 5.10 shows that during static operation the isothermal lines for the exhaust valve temperature in the operating envelop coincide with the lines of constant air excess ratio. Moreover the maximum exhaust valve temperature is approximately 1340 K. Therefore, we aim to operate the engine on the theoretical propeller curve for minimum fuel consumption and emission and accept a minimum air excess ratio of 1.45 and maximum exhaust valve temperature of 1340 K.

Table 5.2: Frigate case study diesel engine model parameters.

nominal engine power $P_{e_{nom}}$	9100 kW
nominal engine speed $n_{e_{nom}}$	16.7 rev/s
number of cylinders i_e	20
number of revolutions per cycle k_e	2
bore diameter D_B	0.28 m
stroke length L_S	0.33 m
crank rod length L_{CR}	0.64063
crank angle after TDC, inlet closure α_{IC}	224 °
crank angle after TDC, exh open α_{EO}	119 °
nominal spec. fuel cons. $m_{bsfc_{nom}}$	189 g/kWh
heat release efficiency η_q	0.915
geometric compression ratio ε_c	13.8
total nominal mass flow $\dot{m}_{t_{nom}}$	17.26 kg/s
cylinder volume at state 1 V_1	0.0199 m^3
nominal pressure at state 1 $p_{1_{nom}}$	4.52e^5 Pa
maximum cylinder pressure $p_{max_{nom}}$	206e^5 Pa
temperature after the intercooler T_c	323 K
temperature of the inlet duct T_{inl}	423K
parasitic heat exch effectiveness ε_{inl}	0.05
fuel injection time delay τ_X	0.015 s
turbocharger time constant τ_{TC}	5 s
exhaust receiver time constant τ_{p_d}	0.01 s
gas constant of air R_a	287 J/kgK
specific heat at constant vol of air c_{v-a}	717.5 J/kgK
specific heat at const. press of air c_{p_a}	1005 J/kgK
specific heat at const. p of exhaust c_{p_g}	1100 J/kgK
isentropic index of air κ_a	1.4
isentropic index of the exhaust gas κ_g	1.353
lower heating value of fuel h^L	42700 J/kg
stoichiometric air to fuel ratio σ_f	14.5
polytropic exponent for expansion n_{exp}	1.38
polytropic exponent for blowdown n_{bld}	1.38
nominal mechanical efficiency $\eta_{m_{nom}}$	0.90
constant volume portion grad $X_{cv_{grad}}$	-0.4560
constant temperature portion $X_{ct_{nom}}$	0.4
turbocharger factor a_η, b_η, c_η	-5.13e^{-12},-3.99e^{-6},0.092
ambient pressure p_{amb}	1e^5 Pa
ambient temperature T_{amb}	318 K

Table 5.3: Induction machine parameters

pole pairs P	5
nominal voltage V	3150 V
base speed ω_{b}	66.5 rad/s
mutual reactance x_m	10.30 Ω
stator self reactance x_s	0.534 Ω
rotor self reactance x_r	0.2522 Ω
stator resistance r_s	0.0630 Ω
rotor resistance r_r	0.0552 Ω
nominal power P_{nom}	3000 kW

Table 5.4: Gearbox parameters

gearbox loss parameter a_{gb}	0.0269
gearbox loss parameter b_{gb}	0.7254
gearbox loss parameter c_{gb}	0.2454
gearbox nominal power loss $P_{\mathrm{l_{nom}}}$ in kW	484 (4%)
gearbox speed reduction ratio i_{gb}	7.752
nominal propeller speed $n_{\mathrm{p_{nom}}}$ in rpm	129

Table 5.5: Propeller parameters

wake fraction w	0.09
relative rotative efficiency η_{R}	1
propeller diameter D in m	4.8
design pitch ratio at 0.7R P_{d}	1.4
nominal pitch ratio at 0.7R P_{nom}	1.8
pitch ratio for zero thrust P_0	0.238
first order pitch actuation delay τ_{P}	1.67
Vrijdag coefficient c_1	1
shock free entry angle α_{i}	0.0524

Table 5.6: Hull model parameters.

ship mass m in 10^3kg	5200
number of propellers m	2
thrust deduction factor t	0.155

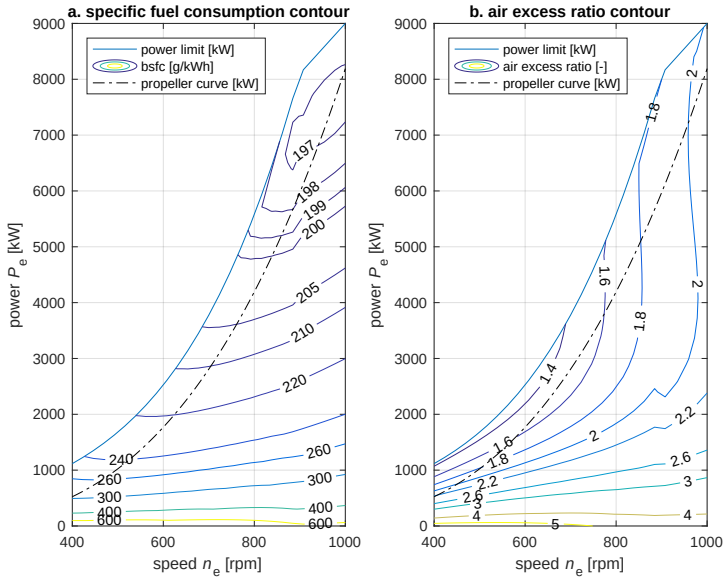

Figure 5.9: Specific fuel consumption and air excess ratio contour plot in engine operating envelope of main diesel engine with theoretical cube law propeller curve.

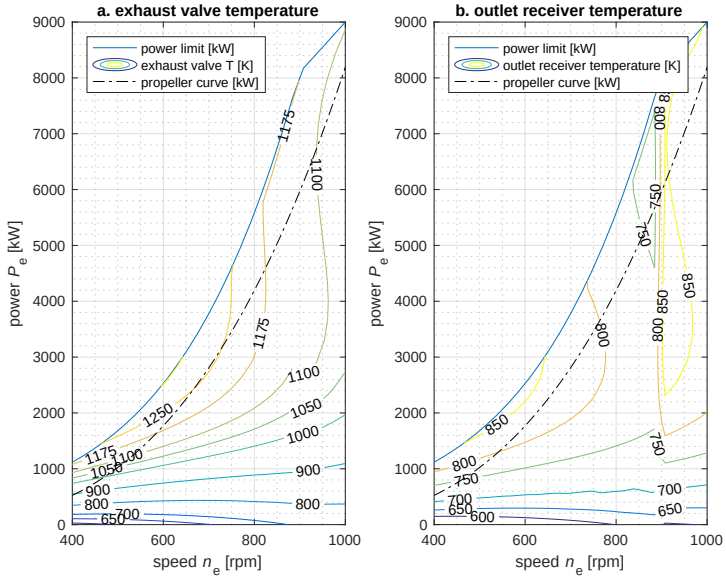

Figure 5.10: Exhaust valve and receiver temperature plot in engine operating envelope of main diesel engine with theoretical cube law propeller curve.

Table 5.7: Control strategies, modes and settings evaluated in simulation experiments reported in Section 5.6.

Control strategy name	**Drive**	**increase rate R_{L+} or R_X**	**air excess ratio λ_{min}**
Mechanical Speed Control (MSC)	Diesel engine	R_{L+} = 0.56%/s	
Electric Speed Control (ESC)	Electric drvie	R_{L+} = 10%/s	
Adaptive Pitch Control (APC)	Diesel engine	$R_{X,therm}$ = 0.83%/s	λ_{min} = 1.45
Parallel ESC (PESC)	Engine & electric drive	R_X = 3.33%/s	
Parallel APC (PAPC)	Engine & electric drive	$R_{X,cav}$ = 0.83%/s	λ_{min} = 1.45
Slow parallel APC (slow PAPC)	Engine & electric drive	$R_{X,cav}$ = 0.28%/s	λ_{min} = 1.45
Fast parallel APC (fast PAPC)	Engine & electric drive	$R_{X,cav}$ = 1.67%/s	λ_{min} = 1.6

5.6.2. EVALUATED CONTROL STRATEGIES

In the simulation experiments, the proposed Parallel Adaptive Pitch Control (PAPC) strategy, as described in Section 5.3, is compared with the Parallel Electric Speed Control strategy as described in Section 5.4, and three control strategies that do not use the main engine and electric drive in parallel: Mechanical Speed Control (MSC), Electrical Speed Control (ESC) and Adaptive Pitch Control (APC) as proposed in Chapter 4. An overview of the 5 control strategies, their modes and settings used for the evaluation in Section 5.6 is listed in Table 5.7. We will first discuss the constant speed sailing in order to compare the fuel consumption of the various control strategies and assess their static operating points in the engine envelope., and then assess the acceleration manoeuvres in order to establish whether the Parallel Adaptive Pitch Control Strategy (PAPC) indeed achieves the stated secondary objectives.

5.6.3. CONSTANT SPEED SAILING

The fuel consumption plots as a function of ship speed for constant speed sailing for Parallel Adaptive Pitch Control (PAPC) and the four alternative control strategies are shown in Figure 5.11. In design conditions all control strategies achieve a similar fuel consumption, apart from the electrical speed control strategy at low ship speeds, up to 15 kts. At these low ship speeds, the electric speed control (ESC) strategy maintains full propeller pitch, while all control strategies that use the main diesel engine, either in parallel or separately, need to reduce pitch to maintain minimum engine speed, 400 rpm, below 10 kts ship speed. This pitch reduction leads to a strong reduction in angle of attack, as shown in Figure 5.12. Due to the pitch reduction, the propeller open water efficiency significantly drops, as illustrated in Figure 5.13. Moreover, below 15 kts ship speed engine power is low, causing an increasing specific fuel consumption for all strategies that run the engine, Figure 5.14, while the power station concept for electric propulsion maintains its specific fuel consumption by switching engines off when load is reduced, which is represented by the assumption of constant specific fuel consumption for the diesel generators. The diesel generator specific fuel consumption (SFC) in Figure 5.14 includes the generator losses but excludes the induction machine losses.

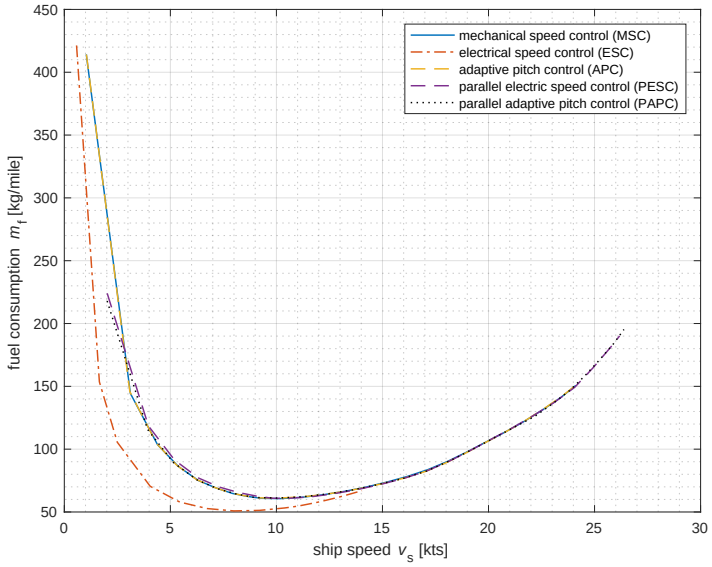

Figure 5.11: Fuel consumption plot as a function of constant ship speed for design conditions for Parallel Adaptive Pitch Control (PAPC) and various alternative control strategies.

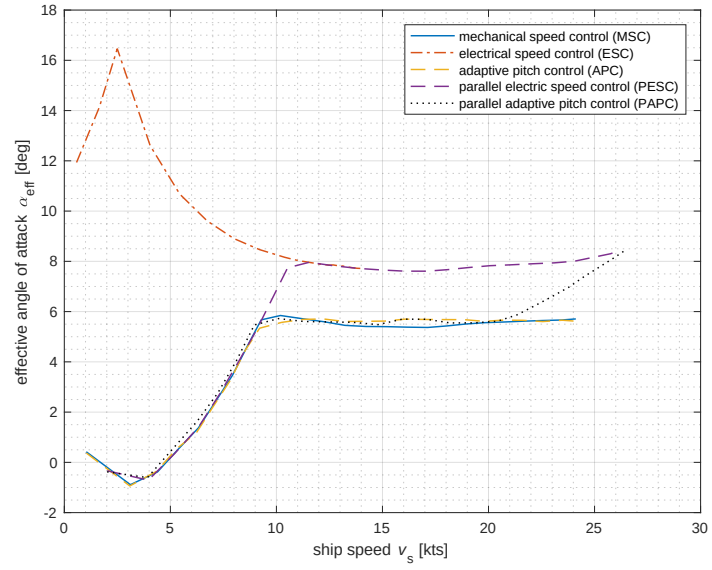

Figure 5.12: Effective angle of attack as a function of constant ship speed for design conditions for Parallel Adaptive Pitch Control (PAPC) and various alternative control strategies.

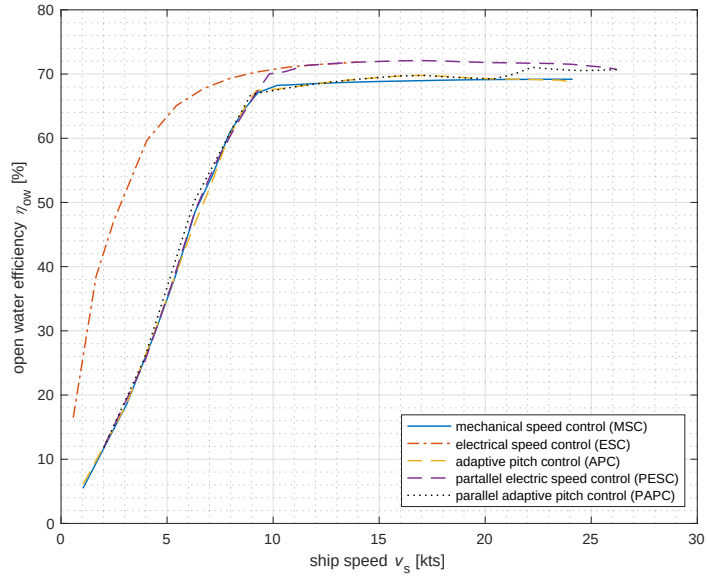

Figure 5.13: Propeller open water efficiency as a function of constant ship speed for design conditions for Parallel Adaptive Pitch Control (PAPC) and various alternative control strategies.

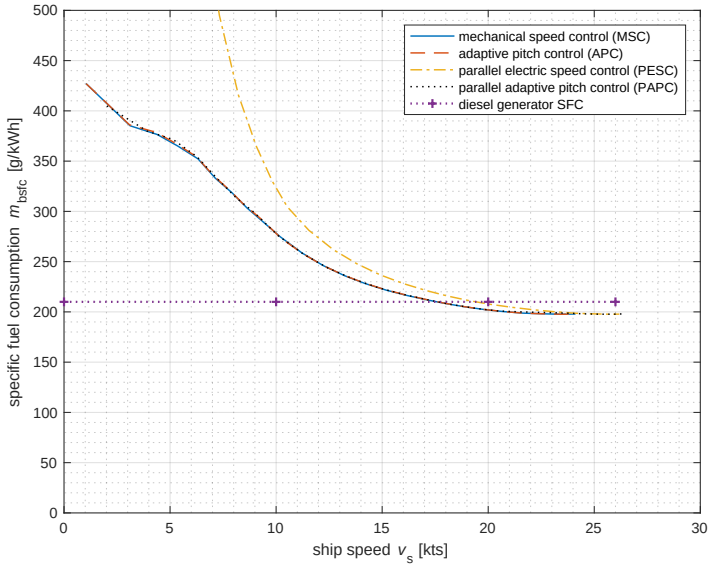

Figure 5.14: Specific fuel consumption for the main diesel engine as a function of constant ship speed for design conditions for Parallel Adaptive Pitch Control (PAPC) and various alternative control strategies.

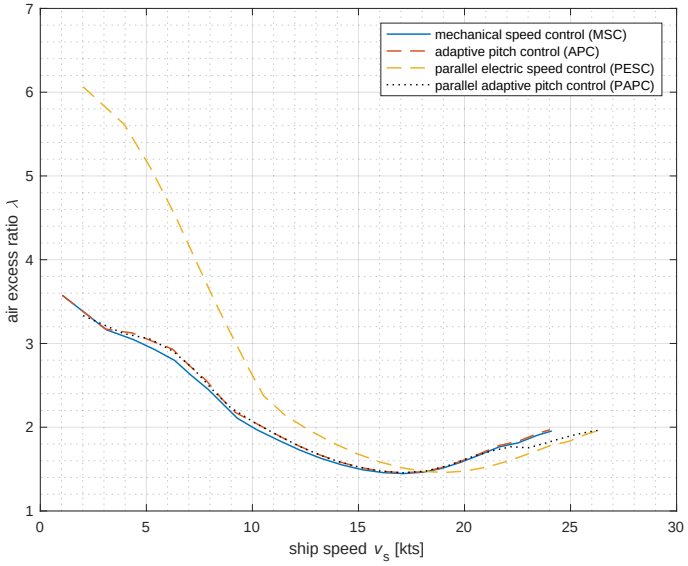

Figure 5.15: Air excess ratio as a function of constant ship speed for design conditions for Parallel Adaptive Pitch Control (PAPC) and various alternative control strategies.

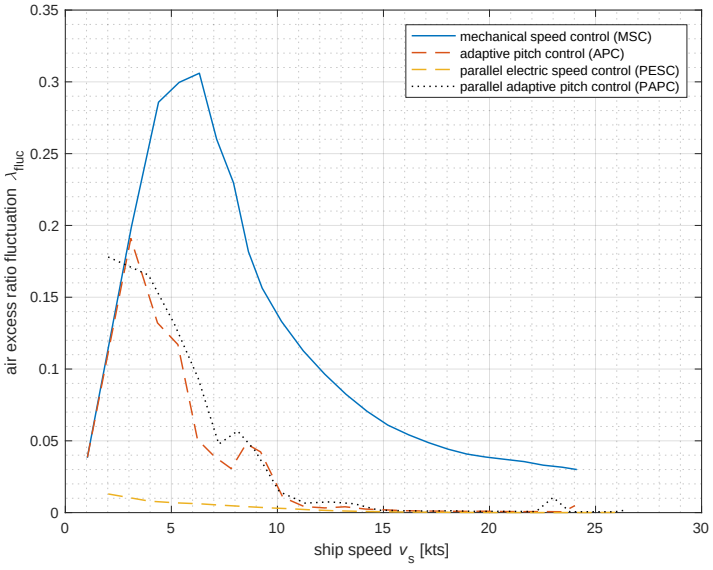

Figure 5.16: Air excess ratio fluctuation due to waves as a function of constant ship speed for design conditions for Parallel Adaptive Pitch Control (PAPC) and various alternative control strategies.

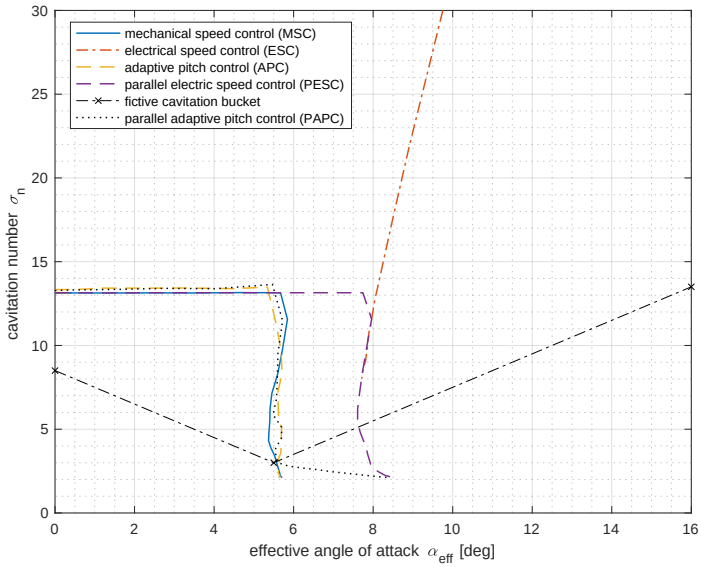

Figure 5.17: Cavitation plot during constant speed sailing in design conditions for Parallel Adaptive Pitch Control (PAPC) and various alternative control strategies.

For constant speed sailing, the average air excess ratio λ has a similar behaviour for all control strategies, as in this condition the combinator curves are matched for the theoretical propeller curve with 90% loading at full speed of the engine, as shown in Figure 5.15. With PESC, the main engine provides less power at the same ship speed across the speed range of the ship, as the electric drive provides an equal share of the total power. Alternatively, with PAPC the electric drive provides additional power from 22 to 26 kts. When the electric drive provides additional power, with PAPC above 22 kts, the effective angle of attack is increased to provide more thrust at the same shaft speed, leading to maximum pitch and an angle of attack of 8.5 deg at maximum ship speed, as shown in Figure 5.12. With ESC, pitch is 1.8, it's maximum value, across the combinator curve, until 15 rpm of the shaft, and with PESC until minimum engine speed at 40 rpm of the shaft. This leads to a high angle of attack for PESC and ESC control strategies, as shown in Figure 5.12 and 5.17 and a slightly higher open water efficiency, as shown in Figure 5.13. Figure 5.16 shows the air excess ratio fluctuation is high with Mechanical Speed Control (MSC). Above 15 kts, APC and PAPC eliminate air excess ratio fluctuation and thus thermal loading fluctuation. Below 15 kts, APC and PAPC use engine speed control and therefore thermal loading fluctuation increases, while for ESC thermal loading fluctuation of the diesel engine is eliminated completely.

The cavitation plot in Figure 5.17 demonstrates how APC maintains the effective angle of attack at 5.5 degrees. While MSC in design conditions also operates close to the optimal angle of attack, this would not be the case for trial or off-design conditions as discussed in Chapter 4. The PAPC strategy also maintains the effective angle of attack

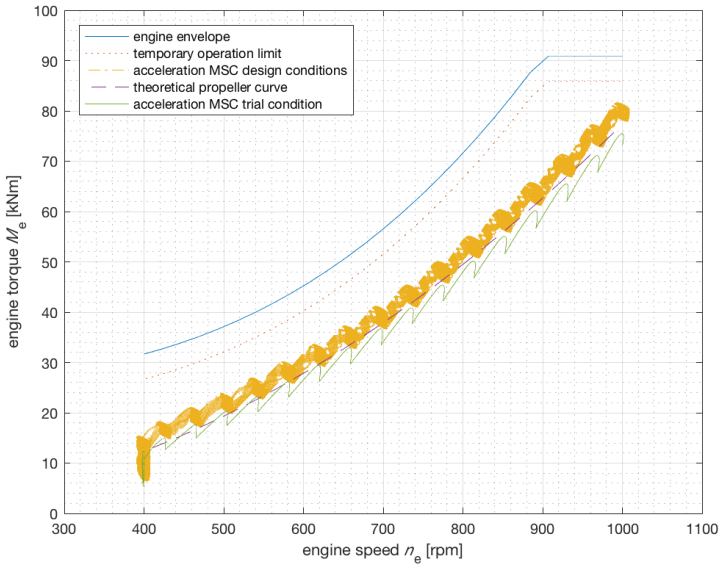

Figure 5.18: Constant ship speed operation from low speed to maximum speed in engine operating envelope for mechanical speed control (MSC) strategy in trial and design conditions.

close to its optimal value, up to 20 kts ship speed. At higher ship speed the angle of attack is gradually increased in order to provide full power and thrust with parallel hybrid propulsion and achieve 26 kts top speed, as shown in Figure 5.12.

Figure 5.18, 5.19 and 5.20 demonstrate the static operating points of the Mechanical Speed Control strategy (MSC), Parallel Electric Speed Control (PESC) and Parallel Adaptive Pitch Control (PAPC) strategy in the operating envelope of the engine for trial and design conditions. The MSC operates near the theoretical propeller curve in design conditions, as the combinator curve in Figure 5.6 was designed for design conditions. However, in trial conditions the engine is significantly less loaded, so the engine is not running at its optimal operating point. Due to the large propulsion power for a frigate compared to the case study Patrol Vessel in Chapter 3 and 4, the influence of weather conditions is smaller. Also, the MSC controller is significantly less conservative than the controller of the case study *Holland* class Patrol Vessel, in order to investigate the impact of the control strategy without pitch reduction and conservative combinator curves. The PESC control strategy both in design and trial conditions operates close to the theoretical propeller curve and appears to be least influenced by disturbances as the electric drive handles the disturbances due to its speed control. Finally, the PAPC control strategy operates close to the theoretical propeller curve up to 800 rpm engine speed. Above 800 rpm engine speed, the operating points. follow the theoretical propeller curve les accurately for two reasons: the simple linear combinator curve for angle of attack and electric motor assisting torque of Figure 5.5 and the pitch limitation of 1.8 which limits pitch at top speed in trial conditions. Both these aspects could be addressed by more

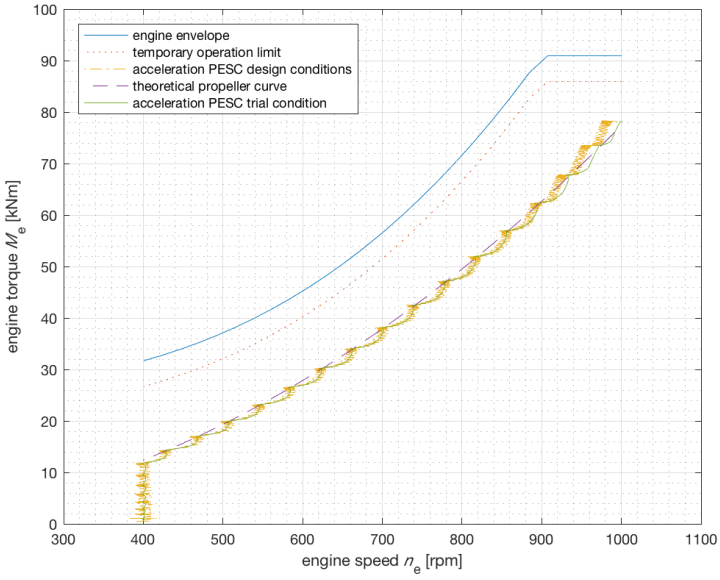

Figure 5.19: Constant ship speed operation from low speed to maximum speed in engine operating envelope for parallel electric speed control (PESC) strategy in trial and design conditions.

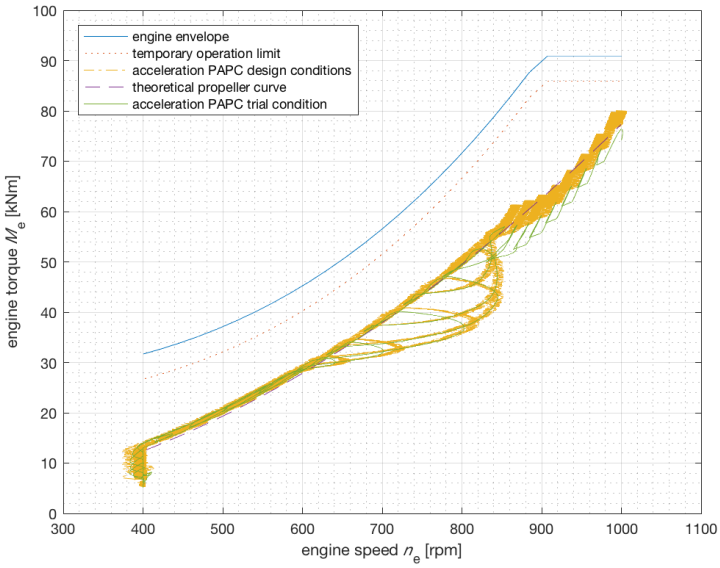

Figure 5.20: Constant ship speed operation from low speed to maximum speed in engine operating envelope for parallel adaptive pitch control (PAPC) strategy in trial and design conditions.

Table 5.8: Acceleration time, minimum air excess ratio, maximum exhaust valve temperature (T) and maximum angle of attack during intermediate sprints (IS) from 0 to 10, 10 to 20 and 20 to 24 [kts], and slam start (SS) from 0 to 24 and 0 to 26 [kts] acceleration with mechanical speed control (MSC), adaptive pitch control (APC), parallel electric speed control (PESC) and parallel adaptive pitch control (PAPC) control in design condition.

Control strategy	**MSC**	**APC**	**PESC**	**PAPC**	**PAPC slow**	**PAPC fast**
Acceleration time t IS (s): 0-10 kts	269	69	185	59	92	46
Acceleration time t IS (s): 10-20 kts	138	72	101	74	154	54
Acceleration time t IS (s): 20-24 kts	77	120	64	32	51	25
Acceleration time t SS (s): 0-24 kts	204	192	70	86	184	67
Acceleration time t SS (s): 0-26 kts	-	-	113	117	269	98
Air excess ratio λ IS: 0-10 kts	1.58	1.45	2.52	1.45	1.47	1.45
Air excess ratio λ IS: 10-20 kts	1.24	1.45	0.98	1.45	1.45	1.45
Air excess ratio λ IS: 20-24 kts	1.53	1.55	1.26	1.67	1.71	1.62
Air excess ratio λ SS: 0-24 kts	1.27	1.45	1.28	1.60	1.69	1.52
Exhaust temp. T_{ev} IS [K]: 0-10 kts	1104	1376	845	1378	1286	1444
Exhaust temp. T_{ev} IS [K]: 10-20 kts	1443	1390	1674	1386	1453	1453
Exhaust temp.T_{ev} IS [K]: 20-24 kts	1305	1301	1546	1238	1278	1278
Exhaust temp. T_{ev} SS [K]: 0-24 kts	1455	1377	1531	1286	1367	1367
Angle of attack α_{eff} IS [deg]: 0-10 kts	11.6	7.6	22.3	7.6	7.6	7.6
Angle of attack α_{eff} IS [deg]: 10-20 kts	9.6	7.6	15.5	8.0	7.9	8.3
Angle of attack α_{eff} IS [deg]: 20-24 kts	7.3	6.6	10.8	8.6	8.2	8.9
Angle of attack α_{eff} SS [deg]: 0-24 kts	9.1	7.5	14.9	9.2	9.2	9.2

accurate matching and by choosing the design pitch at a lower value than the pitch limitation.

5.6.4. ACCELERATION MANOEUVRES

The Measures of Performance (MOP) as defined in Chapter 3 for the intermediate sprint (IS) and slam start (SS) straight line acceleration manoeuvres with the four control strategies are presented in Table 5.8. Moreover, the operating trajectory of the engine in the phase plane operating envelope of the diesel engine for the mechanical speed control (MSC), parallel electric speed control (PESC), adaptive pitch control (APC) and parallel adaptive pitch control (PAPC) control strategies are shown in Figure 5.21, 5.23, 5.22, and 5.24 for these manoeuvres. Finally, Figure 5.27, 5.29, 5.28, and 5.30 show the intermediate sprints (IS) from 0 to 10, 10 to 20 and 20 to 24 kts in the cavitation plot.

MECHANICAL SPEED CONTROL

The baseline mechanical speed (MSC) control strategy, in Table 5.8, shows long acceleration times compared to all other control strategies, but at the same time exhibits extremely low values for the air excess ratio λ, in particular during the intermediate sprint

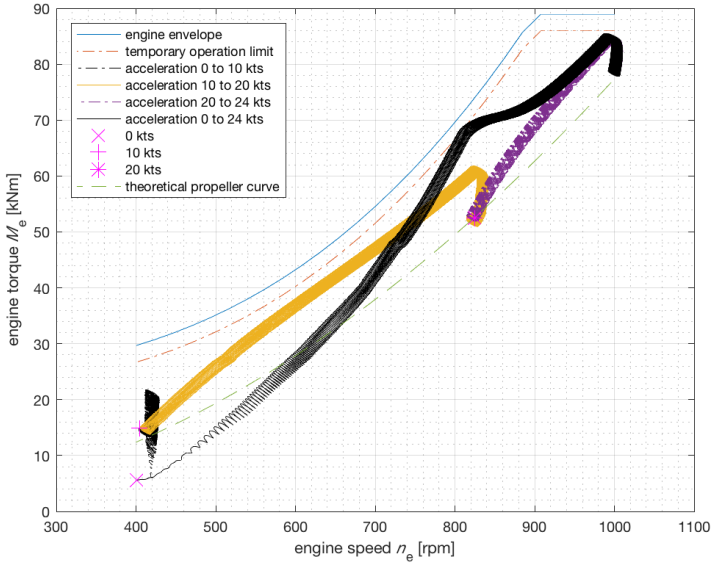

Figure 5.21: Slam start (SS) from 0 to 24 kts and intermediate sprints (IS) from 0 to 10, 10 to 20 and 20 to 24 kts in engine operating envelope for mechanical speed control (MSC) strategy in design conditions.

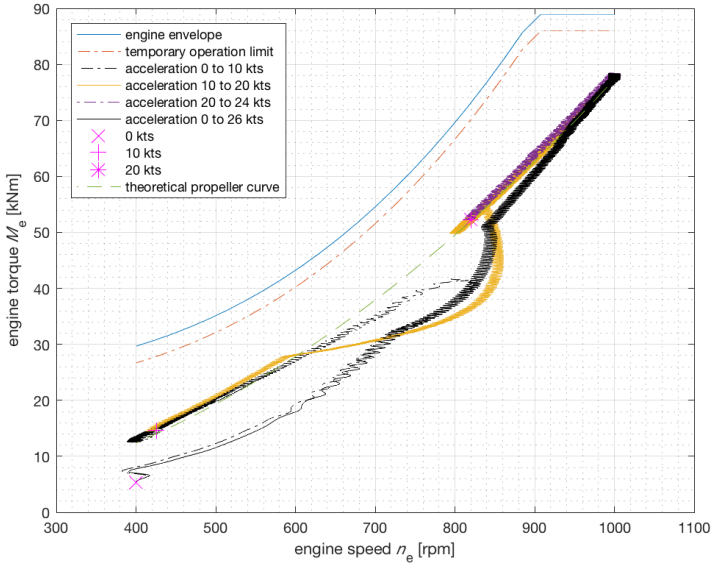

Figure 5.22: Slam start (SS) from 0 to 24 kts and intermediate sprints (IS) from 0 to 10, 10 to 20 and 20 to 24 kts in engine operating envelope for adaptive speed control (APC) strategy in design conditions.

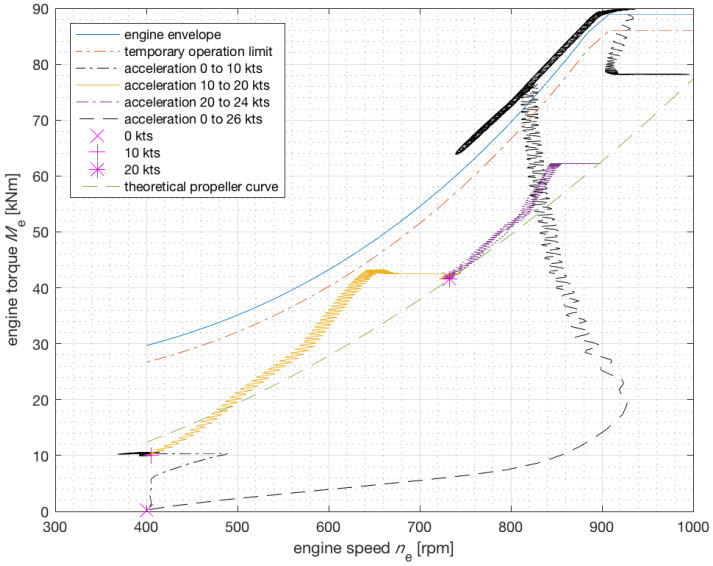

Figure 5.23: Slam start (SS) from 0 to 24 kts and intermediate sprints (IS) from 0 to 10, 10 to 20 and 20 to 24 kts in engine operating envelope for parallel electric speed control (PESC) strategy in design conditions.

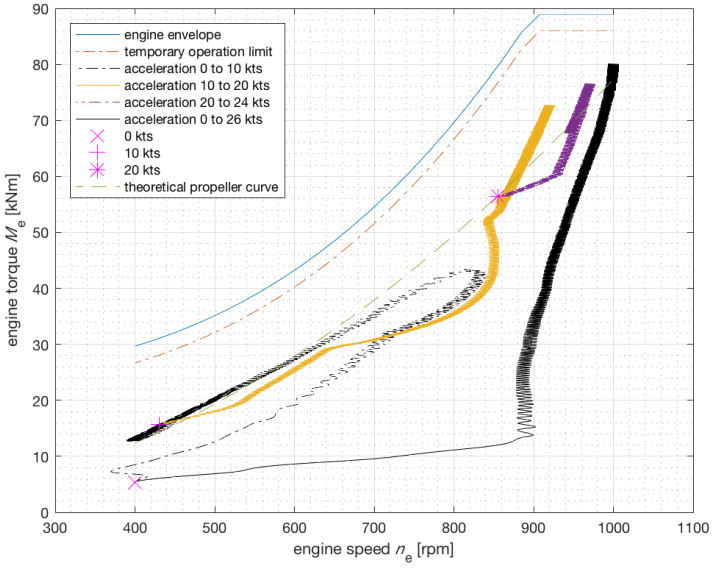

Figure 5.24: Slam start (SS) from 0 to 24 kts and intermediate sprints (IS) from 0 to 10, 10 to 20 and 20 to 24 kts in engine operating envelope for parallel adaptive speed control (PAPC) strategy in design conditions.

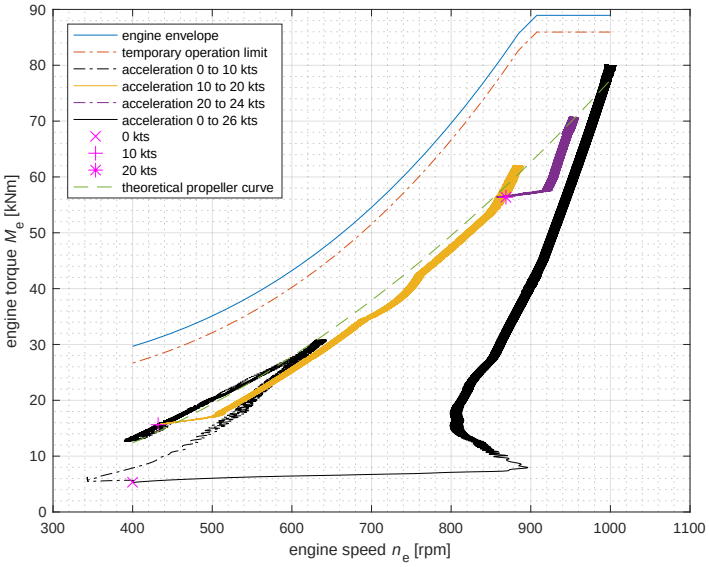

Figure 5.25: Slam start (SS) from 0 to 24 kts and intermediate sprints (IS) from 0 to 10, 10 to 20 and 20 to 24 kts in engine operating envelope for slow parallel adaptive speed control (slow PAPC) strategy in design conditions.

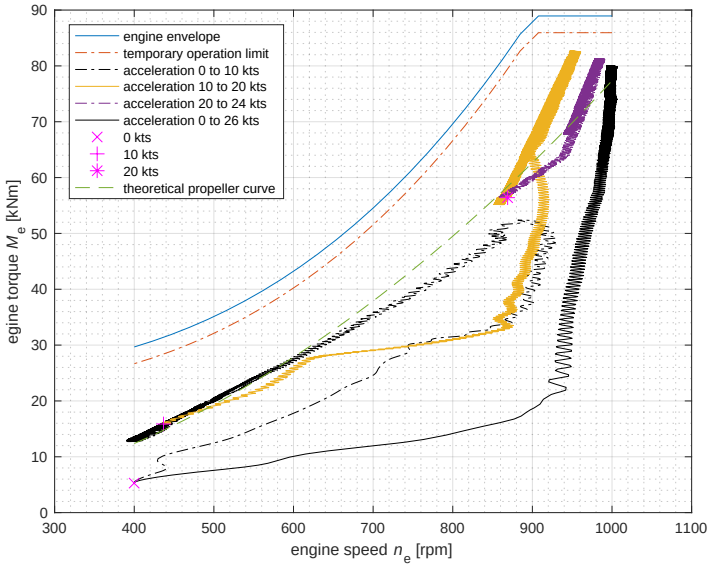

Figure 5.26: Slam start (SS) from 0 to 24 kts and intermediate sprints (IS) from 0 to 10, 10 to 20 and 20 to 24 kts in engine operating envelope for fast parallel adaptive speed control (slow PAPC) strategy in design conditions.

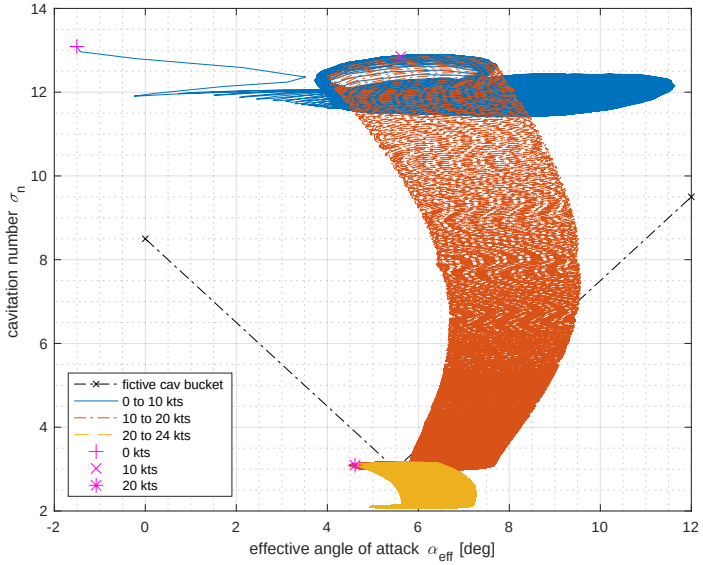

Figure 5.27: Intermediate sprints (IS) from 0 to 10, 10 to 20 and 20 to 24 kts in cavitation plot for mechanical speed control (MSC) strategy in design conditions.

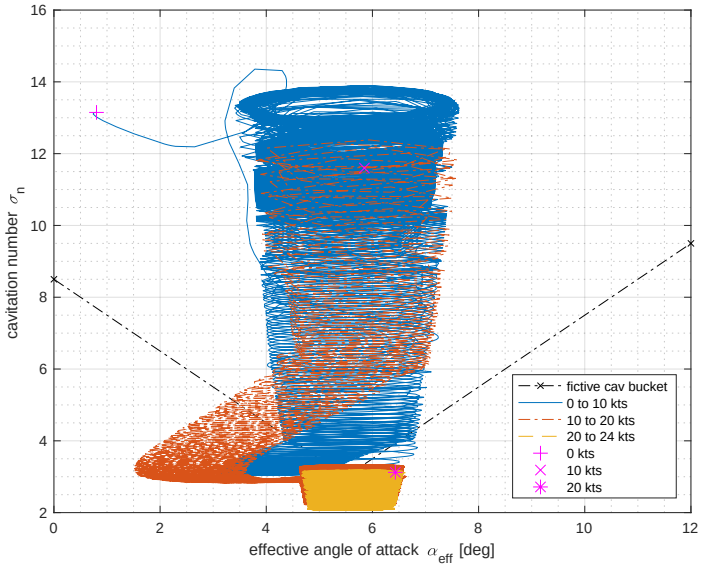

Figure 5.28: Intermediate sprints (IS) from 0 to 10, 10 to 20 and 20 to 24 kts in cavitation plot for mechanical adaptive pitch control (APC) strategy in design conditions.

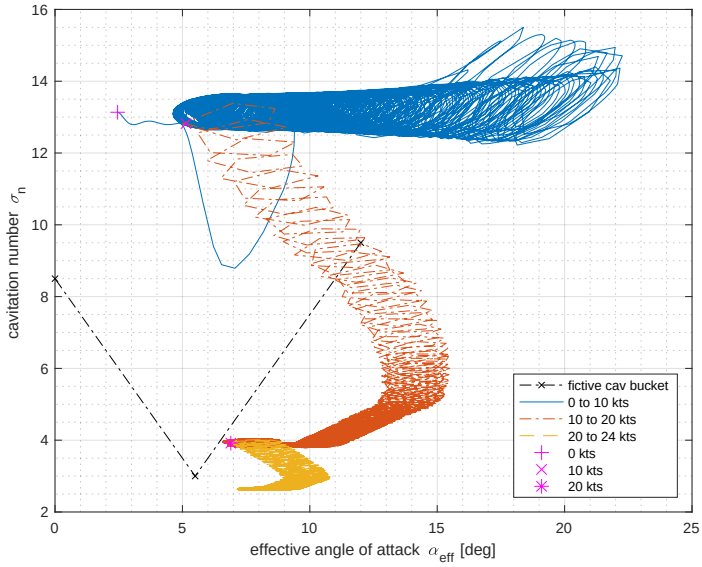

Figure 5.29: Intermediate sprints (IS) from 0 to 10, 10 to 20 and 20 to 24 kts in cavitation plot for parallel electric speed control (PESC) strategy in design conditions.

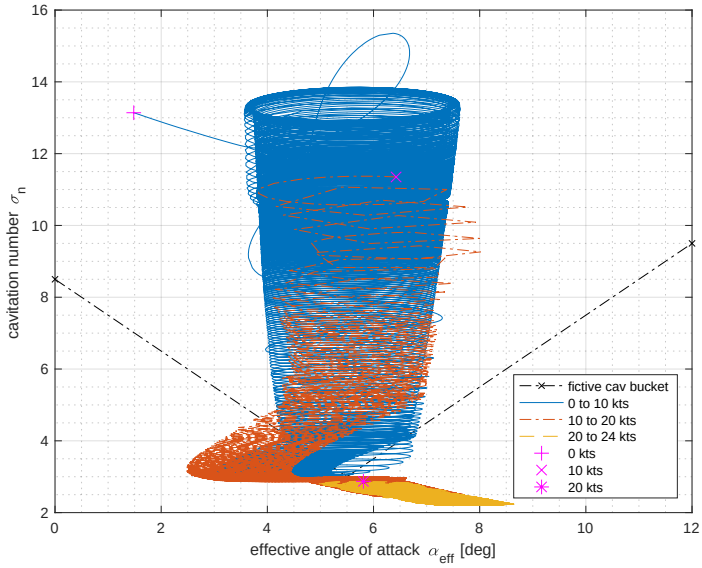

Figure 5.30: Intermediate sprints (IS) from 0 to 10, 10 to 20 and 20 to 24 kts in cavitation plot for parallel adaptive speed control (PAPC) strategy in design conditions.

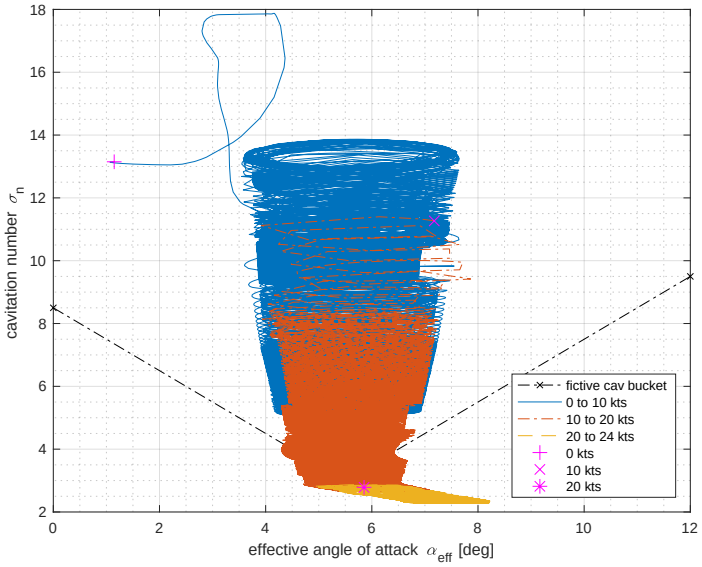

Figure 5.31: Intermediate sprints (IS) from 0 to 10, 10 to 20 and 20 to 24 kts in cavitation plot for slow parallel adaptive speed control (slow PAPC) strategy in design conditions.

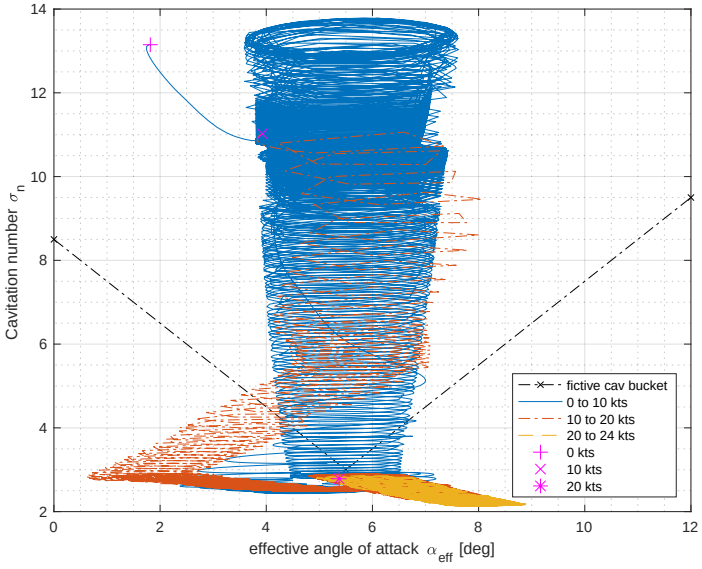

Figure 5.32: Intermediate sprints (IS) from 0 to 10, 10 to 20 and 20 to 24 kts in cavitation plot for fast parallel adaptive speed control (slow PAPC) strategy in design conditions.

form 10 to 20 kts and the slam start acceleration from 0 to 24 kts. In the operating envelope, Figure 5.21, during the intermediate sprint from 10 to 20 kts and the slam start acceleration from 0 to 24 kts, the engine operates very close to the operating envelope limits. In stationary conditions the air excess ratio λ can be as low as 1.4 according to the static operation map in Figure 5.9. Moreover, during acceleration, the turbocharger lag further deteriorates the air excess ratio. These low values of air exces ratio would lead to excessive smoke and particulate matter (PM) emissions (Nielsen *et al.* 2017a,b, 2018) and engine thermal loading. Therefore, a pitch reduction strategy or more conservative combinator settings, such as used in the baseline control strategy in Chapter 3 and 4, are required to improve the air excess ratio during acceleration, which would lead to even slower acceleration times. This control strategy does, however, provide a baseline strategy that is representative for the maximum feasible acceleration for a conventional control strategy with combinator curve control.

ADAPTIVE PITCH CONTROL

The adaptive pitch control (APC) strategy shows consistently fast acceleration during intermediate sprints from 0 to 10 kts and from 10 to 20 kts, in Table 5.8, and as concluded in Chapter 3. The slam start acceleration and the intermediate sprint to top speed, however, are just as slow as the MSC strategy, as APC can not benefit from the over-speed it uses during intermediate sprints at lower ship and engine speed. However, the air excess ratio λ is consistently maintained at a value of 1.45 or higher and the temperature only slightly exceeds the limit of 1340 K, with 50 K.

PARALLEL ELECTRIC SPEED CONTROL

While the parallel electric speed control (PESC) strategy accelerates significantly faster than the baseline MSC control strategy, it suffers from a seriously low air excess ratio due to the very limited engine envelope of this engine with conventional turbocharging, as shown in Table 5.8. This low air excess ratio would lead to excessive smoke production, PM emissions and thermal overloading. This seems to be in disagreement with the results in Geertsma *et al.* (2017d), which concluded that PESC provides fast acceleration, but the engine in the case study of Geertsma *et al.* (2017d) utilised Sequential Turbocharging (STC) with a significantly wider operating envelop and higher air excess ratio λ. The engine operating envelop in Figure 5.23 shows that during the intermediate sprint from 10 to 20 kts, the engine with conventional turbocharging operates very close to the temporary operating limit, near the operating point at which the air excess ratio during static conditions is at its lowest static value of 1.4, as shown in Figure 5.9. During the slam start acceleration, the engine benefits form a fast increase of engine speed due to the fast increasing electric drive torque, but the engine load runs into its limit when the pitch achieves its maximum value, even though the increase rate of pitch was reduced to postpone the engine hitting its limits. Thus, for optimum acceleration with an engine with a small operating envelope, pitch needs to be adopted during the acceleration manoeuvre, either with a pitch reduction strategy as discussed in Section 3.3 or with adaptive pitch control (APC) described in Section 4.2.

PARALLEL ADAPTIVE PITCH CONTROL

With PAPC the acceleration time for both the slam start manoeuvre and the intermediate sprints is more than halved compared to the baseline mechanical speed control strategy, as shown in Table 5.8. Moreover, the acceleration time for the slam start manoeuvre is similar to the acceleration time with gas turbine propulsion as reported in Geertsma *et al.* (2017d). Interestingly, according to Table 5.8, the lowest air excess ratio is achieved during the intermediate sprints, due to the engine speed increase and running near the theoretical propeller curve, as shown in Figure 5.24. Similar to APC, the air excess ratio λ is consistently maintained at a value of 1.45 or higher and the temperature only slightly exceeds the limit of 1340 K, with 50 K. With fast PAPC acceleration time can be further improved by approximately 20% at the cost of an increase in exhaust valve temperature T_{ev} and a higher rate of change of temperature dT/dt, as shown in Table 5.8. During intermediate sprints the exhaust valve temperature is 110K higher than the limit established from the maximum static temperature and during the slam start 20K, although the exhaust valve temperature could be limited by a charge pressure map as proposed in Section 4.3.3. However, during a slam start acceleration with PAPC the minimum air excess ratio is 1.6 due to the supporting torque from the electric drive, and the maximum exhaust valve temperature is 50 K below the maximum static temperature. Therefore, an air excess ratio of 1.6 would not deteriorate the acceleration times for the slam start manoeuvre and the engine is not pushed to its thermal overloading limits during a slam start acceleration. However, the cavitation plot in Figure 5.30 shows that during intermediate sprints the angle of attack is reduced due to the air excess ratio limitation, thus exceeding the cavitation bucket limitations. During operations, in which preventing cavitation is more important than fast acceleration, we propose slow adaptive pitch control, by reducing the maximum increase rate of fuel injection by a factor 3, as shown in Table 5.7. With these settings, slow PAPC maintains centred around its optimum angle off attack also during acceleration, further reducing the risk on cavitation, while taking up to two times the time to accelerate, which in most cases is still faster than the baseline MSC strategy. In conclusion, PAPC achieves superior acceleration performance without thermally overloding the engine and achieving near optimal fuel consumption, while slow PAPC can achieve operation within the cavitation bucket up to 18 to 20 kts, thus minimising the risk on cavitation.

For engines with a wide operating envelope, for example due to sequential turbocharging as proposed in Geertsma *et al.* (2017d), the torque control setpoint for PAPC can enable using the electric drive to provide power take-off. In the case study frigate presented in Geertsma *et al.* (2017d), which is the same case study as used in this Chapter, with a sequentially turbocharged version of the same diesel engine, this leads to a reduction in fuel consumption of 7% at a transit speed of 18 kts, and a reduction in generator running hours as the power supplied by the electric drive can supply all auxiliary and mission system loads. Therefore, an engine with a wide operating envelope, for example due to sequential turbocharging, can enable a further fuel consumption and emission reduction of 7% and a significant reduction in running hours.

5.7. CONCLUSIONS AND RECOMMENDATIONS

In this chapter, we have proposed the *parallel adaptive pitch control* (PAPC) strategy, which is based on the adaptive pitch control strategy proposed in Chapter 4 and uses the electric drive to improve acceleration performance and top speed, in particular at higher ship speeds. We have used the dynamic simulation models, benchmark manoeuvres and Measures of Performance proposed in Chapter 3 to answer Research Question 6 by comparing the performance of the proposed PAPC strategy with baseline mechanical speed control (MSC), without the pitch reduction strategy discussed in Section 3.3, parallel electric speed control (PESC) proposed in Geertsma *et al.* (2017d) and adaptive pitch control (APC) proposed in Chapter 4. The simulation experiment results demonstrate the following with regard to using the power split between the propulsion diesel engine and electric drive:

- PAPC achieves fast slam start and intermediate acceleration, twice as fast as the baseline MSC for the case study frigate, while better limiting engine thermal loading and thus causing less smoke and particulate matter (PM) emissions. The acceleration time for the slam start manoeuvre is similar to the acceleration time with gas turbine propulsion as reported in Geertsma *et al.* (2017d).
- PAPC improves intermediate acceleration from 20 to 24 kts and slam start acceleration compared to APC, again reducing acceleration time by a factor 2 or more. The speed of acceleration is a trade off with engine thermal loading, quantified by maximum exhaust valve temperature and rate of change of exhaust valve temperature.
- During situations with high manoeuvrability requirements, such as emergency situations, fast PAPC can actually reduce acceleration time by a further 20 % at the cost of a higher exhaust valve temperatures T_{ev}, rate of change of exhaust valve temperature dT_{ev}/dt and air excess ratio λ, which would lead to higher smoke and PM emissions.
- PAPC can achieve operation around the optimum angle of attack up to 18 to 20 kts ship speed. However, to prevent reduction of angle of attack during acceleration, for optimum cavitation behaviour the speed of acceleration should be reduced by a factor 2, still as fast as the baseline MSC control strategy.
- PAPC in combination with an engine with a wide operating envelope, for example due to sequential turbocharging, can enable a further fuel consumption and emission reduction of 7% and a significant reduction in running hours by switching of all diesel generators.

In summary, PAPC enables to select the optimum trade-off between cavitation risk, engine thermal loading and speed of acceleration by varying the fuel increase rate limitation R_X, while achieving the best possible fuel consumption above 15 kts. Below 15 kts fuel consumption can be reduced by running on the electric drive fed from the diesel generators, thus allowing maintaining maximum pitch and thus running at shaft speeds, below minimum main diesel engine speed.

6

ENERGY MANAGEMENT FOR HYBRID POWER GENERATION

Rinze GEERTSMA and Miltiadis KALIKATZARAKIS

Hybrid technology in marine vehicles can significantly reduce fuel consumption and local CO_2 emissions. It has been applied successfully to several ship-types, mostly with conventional, rule-based, strategies. To further improve performance, intelligent control strategies are necessary. This chapter, inspired by automotive research in energy management strategies, applies the Equivalent Consumption Minimisation Strategy (ECMS) to a ship powered by a hybrid propulsion plant with hybrid power supply that can be recharged with renewable shore power, thus partly answering Research Question 7: 'What control strategy can be used for the power split between various power sources in hybrid power supply to provide the best possible performance against an adaptive trade-off between the various conflicting MOEs?' This hybrid ship configuration has the additional challenge to determine the optimal power-split between three or more different power sources, in real-time, and to optimally deplete the batteries over the mission profile. To this end, a Mixed-Integer Non-Linear optimisation Problem is formulated and solved by combining Branch & Bound and Convex optimisation. Dynamic Programming (DP) is used to benchmark the real-time strategies, which are also compared to the current rule-based (RB) controller.

This chapter is organised as follows: Section 6.2 describes the system and case study tug, and Section 6.3 discusses the ECMS and causal control strategies, their control objectives and solution. The results of the comparison between the existing rule-based controller, the ECMS strategies and the causal controller are presented in Section 6.4. Finally, Section 6.5 summarises the conclusions of this chapter.

Parts of this chapter have been published in Control Engineering Practice **76** (2018), Kalikatzarakis *et al.* (2018). The research in this chapter has mainly been carried out by ir. Miltiadis Kalikatzarakis during his MSc. research under supervision of ir. R. D. Geertsma, CEng.

6.1. INTRODUCTION

THE shipping sector is responsible for 90% of global freight transportation, which has been increasing by 2.3% *annually* since 2000 (Shaheen *et al.* 2007; Stopford, 2008), and therefroe needs to drastically reduce its fossil fuel use. While stationary power consumers can progressively switch to renewable energy sources such as wind energy (Kumar *et al.* 2016), tidal energy and solar energy (Jamel *et al.* 2013), mobile power consumers often cannot be connected to the electric grid for renewable energy. Moreover, renewable fuels and fuel cells are not available for maritime application in the short term (Taljegard *et al.* 2014; van Biert *et al.* 2016). Therefore, the transportation field has to reside to stored energy for its renewable power supply, recharging the energy storage when connected to the main grid. However, only ship types that can connect to the grid regularly, such as ferries, can rely purely on energy storage. Other ship types can use energy storage to reduce fuel consumption, recharging the energy storage with renewable energy from the grid when moored alongside.

Hybrid propulsion and power supply architectures are capable of reducing fuel consumption and emissions by 10% to 35% according to the review in Chapter 2. However, advanced control strategies are required to regulate power production of all energy sources onboard in order to achieve these savings (Geertsma *et al.* 2017a; Grimmelius *et al.* 2011; Herdzik, 2013; Scibberas *et al.* 2015; Shiraishi *et al.* 2013; Vu *et al.* 2015, 2014; Yuan *et al.* 2016; Zhan *et al.* 2015) and Energy Management strategies are required to make optimum use of batteries over time and thus reduce fuel consumption and emissions (Sciarretta *et al.* 2004; Vu *et al.* 2015, 2014).

6.1.1. LITERATURE REVIEW

Hybrid power supply has recently become a realistic option for many maritime applications due to the development of power dense lithium-ion battery technologies, developed for the automotive industry. As argued in Capasso *et al.* (2014), lithium-ion batteries provide power and energy dense energy storage with good life cycle performance and have thus enabled electrical, hybrid and plug-in hybrid vehicles in the automotive market. Particularly, lithium-ion polymer batteries and lithium iron phosphate batteries provide high capacity at high discharge currents. Capasso *et al.* (2014) report experimental analysis that demonstrates the excellent performance of lithium iron phosphate batteries during high discharge current, and excellent charging efficiency of lithium-ion polymer batteries. These characteristics of lithium iron phosphate batteries and their thermal stability and relative safety have led to their application in towing vessels (Breijs *et al.* 2016; Drijver, 2013; Koperen, 2009; Volker, 2013), yachts (Bosich *et al.* 2013; Dedes *et al.* 2012; Grimmelius *et al.* 2011), ferries (Ovrum *et al.* 2015; Veneri *et al.* 2012; Zahedi *et al.* 2014), research (Capasso *et al.* 2016), naval (Doerry *et al.* 1996; Whitelegg *et al.* 2015), and offshore vessels (Zahedi *et al.* 2013), and tugs (de Groote *et al.* 2014), the case study for this chapter.

Advanced control in land-based hybrid electric vehicles has been a field of extensive research for almost twenty years (Ambuhl *et al.* 2010; Baumann *et al.* 1998; Chasse *et al.* 2011; Dib *et al.* 2014; Formentin *et al.* 2016; Guzzella *et al.* 2007; Johannesson *et al.* 2015; Kermani *et al.* 2012; Koot *et al.* 2005; Nuesch *et al.* 2014; Paganelli *et al.* 2000;

Salman *et al.* 2000; Sciarretta *et al.* 2004). For the automotive field, comparative studies have demonstrated that an optimal control-based approach can outperform rule-based approaches (Sciarretta *et al.* 2014). In particular, Sciarretta *et al.* (2014) demonstrate that various implementations of the Equivalent Consumption Minimisation Strategy (ECMS) can approximate the fuel economy of causual controllers, with low computational burden and limited calibration of control parameters. While initial research in this field focussed on charge sustaining strategies, the rise of Plug-in Hybrid Electric Vehicles (PHEV) has stimulated research into charge depleting ECMS strategies. The aim of such a charge depleting ECMS is to generate an optimal discharge trajectory for the battery (Guardiola *et al.* 2014). Ideally, progressive battery discharge, *blended-mode*, will be the output of the EMS, as the repetitive sequence of electrical charge depleting operation followed by charge sustaining operation is known to be far from optimal from a fuel economy standpoint (Guardiola *et al.* 2014; Sciarretta *et al.* 2014).

Energy management strategies, such as ECMS, can also reduce fuel consumption and emissions on ships with electric propulsion and hybrid power supply (Breijs *et al.* 2016; Haseltalab *et al.* 2016; Vu *et al.* 2015; Yuan *et al.* 2016) and ships with hybrid propulsion and hybrid power supply (Grimmelius *et al.* 2011). First, Vu *et al.* (2015) concludes that an ECMS strategy with a novel operating load estimation scheme on an electric tug with diesel electric propulsion and hybrid power supply can save up to 9% fuel, compared to the rule-based controller described in (Sciberras *et al.* 2012). However, the robustness of the estimation scheme against varying operating profiles is not investigated. Similarly, Yuan *et al.* (2016) report 17% savings for a similar tug with ECMS without knowledge or prediction of the future, compared to a charge-sustaining rule-based strategy. They both recognise that fuel economy is mainly attributed to the charge-depleting nature of ECMS rather than to its ability to identify more efficient operating modes for the propulsion plant. Haseltalab *et al.* (2016) demonstrate how multi-level Model Predictive Control can handle environmental disturbances and ship model uncertainties with a case study offshore vessel with electric propulsion and hybrid power supply. A comparative analysis with a conventional control solution is not documented. Breijs *et al.* (2016) establish the optimum power split for the hybrid power supply of a ferry with electric propulsion with a combination of a rule-based strategy for discrete decisions and ECMS. They report an additional 11% fuel consumption reduction due to their ECMS framework during actual sea trials. Finally, Grimmelius *et al.* (2011) demonstrate the feasibility of ECMS for hybrid propulsion with a simulation study, however they only utilise energy storage for electric power supply, use an inaccurate linear problem formulation, and lack a comparative analysis with a conventional control strategy. None of the studies discussed above compares the results with a causal, optimum, controller that has full knowledge of the operating profile, for example using dynamic programming, or addresses the robustness of its solution to a change in the operating profile.

6.1.2. AIM AND CONTRIBUTION

In this chapter, we investigate how much fuel consumption and local CO_2 emission reduction can be achieved by applying ECMS to a hybrid propulsion plant with hybrid power supply with and without future operating load estimation, and determine the ro-

Figure 6.1: Damen Azimuth Stern Drive 2810 Hybrid Tugboat, case study in this chapter.

bustness of the ECMS performance against varying operating profiles compared to the global optimum solution with a priori knowledge and determined with DP. We use a case study towing vessel with hybrid propulsion plant and hybrid power supply, as shown in Figure 6.2.

The novelty of this chapter is threefold. First, we validate the hybrid propulsion with hybrid power supply system model introduced in Chapter 3 with measurements and manufacturer data of te case study tug, in addition to the propulsion model validation covered in Chapter 3. Second, a novel approach is proposed for the on-line solution of the charge depleting ECMS control problem with discrete variables for the various engines and operating modes, by splitting the problem formulation in convex sub-problems, and combining branch and bound with convex optimisation. This approach is applied to an ECMS approach without and with operator load estimation. Third, the optimality and robustness of the two proposed strategies are compared with a rule-based strategy as applied on the tug in Figure 6.2 and the global optimum from Dynamic Programming (DP), assuming apriori knowledge on the operating profile.

6.2. SYSTEM DESCRIPTION & MODELLING

IN this chapter, we consider hybrid propulsion with hybrid power supply for ships. The propulsion system of the case study tug, shown in Figure 6.1, consists of two thrusters with fixed pitch propellers, two high-speed 4-stroke diesel engines with a combined power of 3680 kW (4935 hp) at 1600 rpm, two induction machines of 230 kW each and two lithium iron magnesium phosphate battery packs of 120 kWh each, as shown in Figure 6.2 and described in de Groote *et al.* (2014). The main engines can propel the vessel up to 13 knots, with a maximum bollard pull of 60 tons.

The model of the hybrid propulsion and power generation plant and its control is illustrated in Figure 6.4 and uses the modular, hierarchical and causal modelling approach, as discussed in (Colonna *et al.* 2007). While this dynamic approach is not required for accurate fuel consumption estimation, it allows to investigate other measures of performance such as engine thermal loading, manoeuvrability and cavitation noise as discussed in Chapter 3, (Geertsma *et al.* 2017c,d). In this chapter, we therefore use the

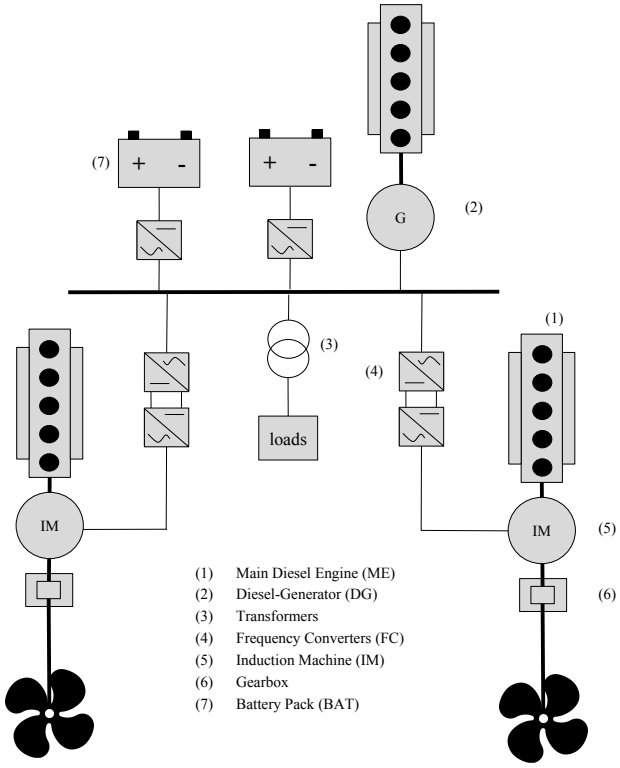

Figure 6.2: Hybrid propulsion with hybrid power supply, case study in this chapter.

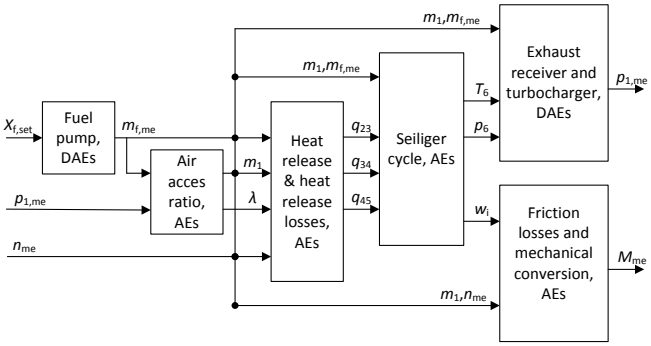

Figure 6.3: Schematic presentation of the diesel engine model and the interaction between its subsystems, consisting of Algebraic Equations (AE) or Differential and Algebraic Equations (DAE).

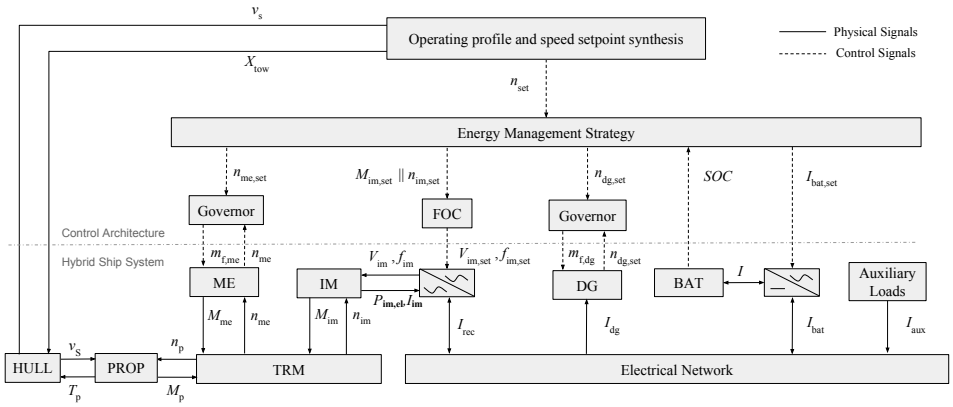

Figure 6.4: Schematic presentation & causality graph of the simulation model (propulsion and control system) showing coupling between models.

dynamic simulation model as the benchmark system agains which we establish the fuel economy performance of the various considered Energy Management strategies. The models of the mechanical propulsion plant, consisting of the main diesel engine (ME), governor (GOV), transmission (TRM), and propeller (PROP), are based on the validated Mean Value First Principle models of Chapter 3 (Geertsma *et al.* 2017c). The improvements in the diesel engine model as reflected in (3.17) and (3.57) are included in this model.

The operating profile of a tug is determined by the vessel speed v_s and the towing force, X_{tow}. The operating profile synthesis determines the speed setpoint for the model with a PI control loop. The energy management strategy proposed in Section 6.3 of this chapter subsequently determines the following control setpoints: speed setting of the main engines (MEs) $n_{me,set}$, speed or torque setting of the Induction Machines (IMs) $n_{im,set}$ or $M_{im,set}$ and current setting of the Battery (BAT) $i_{bat,set}$.

6.2.1. MODEL SUMMARY

In summary, the hybrid ship system model consists of 5 sub-models with a system of Differential and Algebraic Equations (DAEs) and 2 sub-models consisting of Algebraic Equations (AE) with the relations shown in Figure 6.4. The diesel engine model, a system of DAEs, consists of the state variables fuel injection per cylinder per cycle m_f, charge pressure p_1 and exhaust receiver pressure p_d. The induction machine and frequency converter model is a system of DAEs with 6 state variables for the direct and quadrature flux linkages of the stator, the rotor and the mutual flux Ψ_{qs}, Ψ_{ds}, Ψ_{qr}, Ψ_{dr}, Ψ_{md} and Ψ_{mq}, and the DAEs of the battery model consist of state variables terminal voltage u_t and battery state of charge S_{OC}. The gearbox and shaft-line model contains DAEs with state variable propeller speed n_p and the hull is a system of DAEs with state variable ship speed v_s. The diesel generator model consist of a system of DAEs with state variable diesel generator speed n_{dg}. Finally, the propeller model consist of a system of AE's.

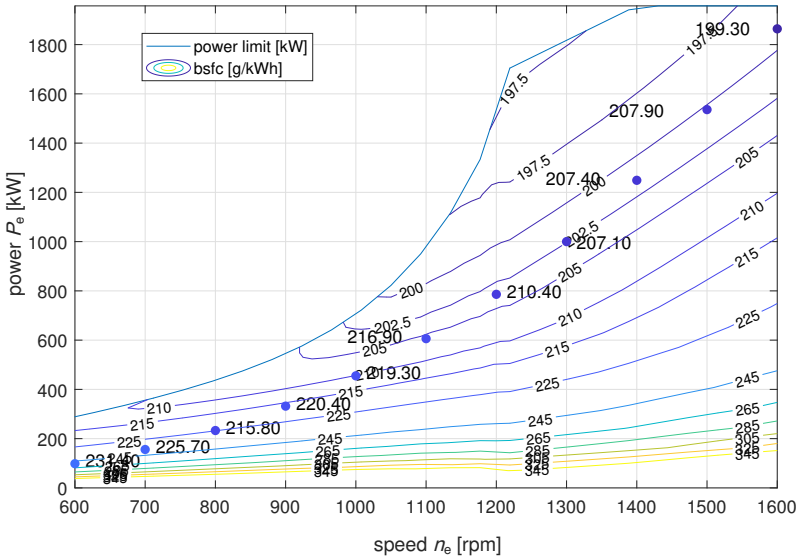

Figure 6.5: Fuel consumption map.

The primary control strategies of the propulsion plant are included in the model as the ECMS strategies investigated in this work are aimed at the secondary energy management, as indicated in Figure 6.4. The primary control strategy consist of speed control for the main diesel engine and diesel generator set controlling the control variable fuel injection setpoint $m_{\text{f,me,set}}$ for the main diesel engine and the variable fuel injection for the diesel generator $m_{\text{f,dg,set}}$, based on engine speed feedback. The primary control strategy of the IM consists of Field Oriented Control, controlling the control variables voltage and frequency V_{fc} and f_{fc} for the frequency converter, based on induction machine speed and current feedback. The resulting current subsequently has a mathematical relationship with the generator and battery current.

6.2.2. MODEL CALIBRATION AND VALIDATION

DIESEL ENGINE AND GOVERNOR

The parameters used in the diesel engine model have been obtained from three different sources. Most of the parameters are available from the manufacturer, and several have been estimated based on FAT data and diesel engine or general physics theory (Stapersma, 2010a,b,c). The comparison between actual measurements and the estimated fuel consumption, shown in Figure 6.5 and 6.6 demonstrates that the accuracy of the model is within +/- 5% down to a load of 5%. Further accuracy improvements could be made by including the effects of variable injection timing.

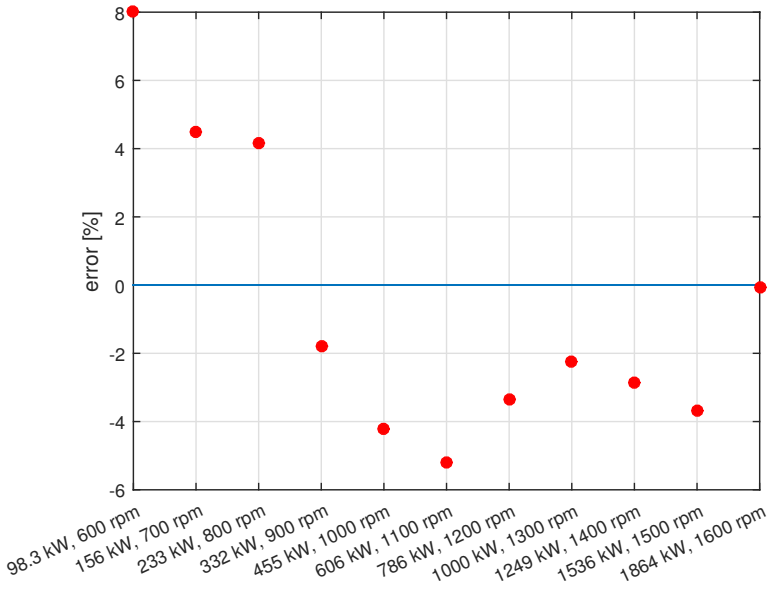

Figure 6.6: Fuel consumption relative errors.

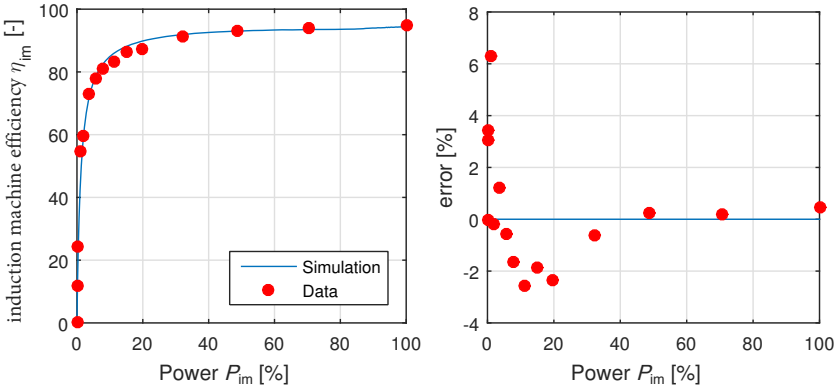

Figure 6.7: Combined efficiency of induction machine & frequency converter, and relative errors.

INDUCTION MACHINE AND FREQUENCY CONVERTER

The necessary parameters for the induction machines and frequency converters were estimated based on supplier data: part-load efficiency, no-load and locked-rotor test results. Figure 6.7 illustrates the combined efficiency of the induction machine and frequency converter, which is within +/- 3% of supplier data down to 3% load.

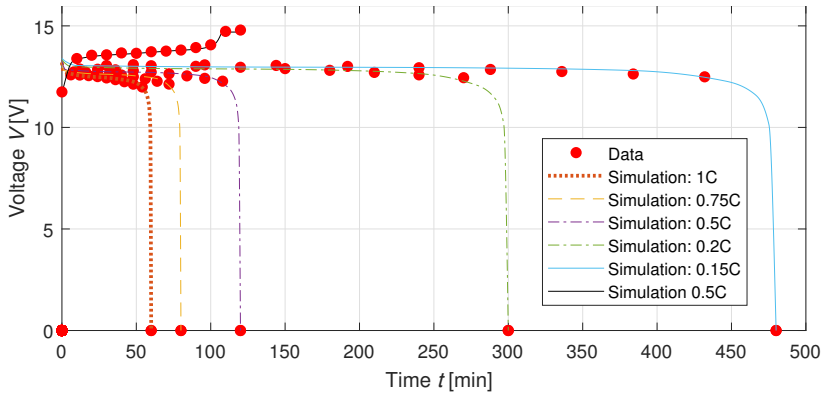

Figure 6.8: Battery model: simulation results and supplier data.

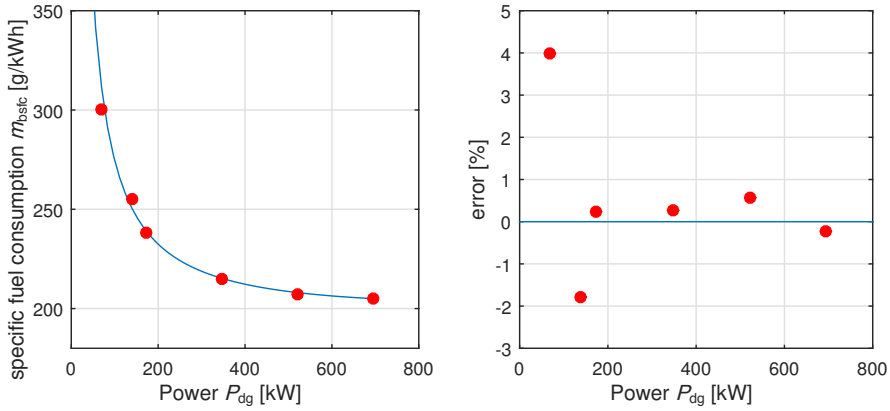

Figure 6.9: Simulated diesel generator fuel consumption and manufacturer's data.

BATTERY

We derived the battery values for $\vec{\mathbf{v}} = (v_1, ..., v_6) \in \mathbb{R}^6$ and $\mathbf{A} = (\alpha_{i,j}) \in \mathbb{R}^{3x2}, \mathbf{B} = (\beta_{i,j}) \in \mathbb{R}^{2x2}$ from a least-squares errors minimisation problem using typical supplier data of charge / discharge characteristics at different C-rates. A comparison between simulation results and the supplier data is shown in Figure 6.8.

DIESEL-GENERATOR SET

The model parameters for the diesel generator were estimated using supplier's data. Figures 6.9 and 6.10 give a comparison between estimated and actual values. In terms of fuel consumption the error has a maximum of 4% at 10% load, whereas the error of the efficiency of the synchronous generator is lower than 0.8% throughout, and almost negligent for a power factor of 0.8.

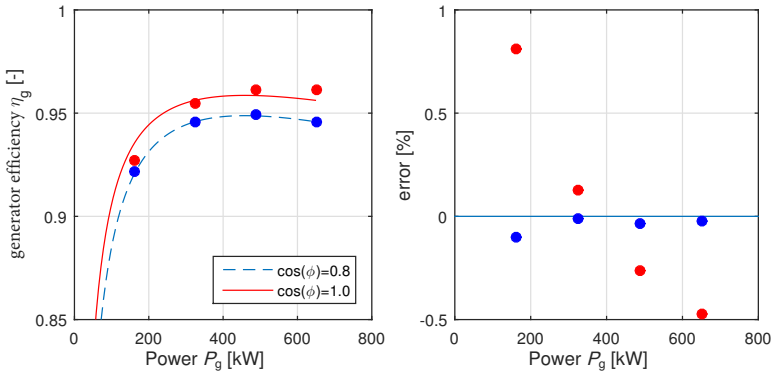

Figure 6.10: Synchronous generator efficiency and manufacturer's data.

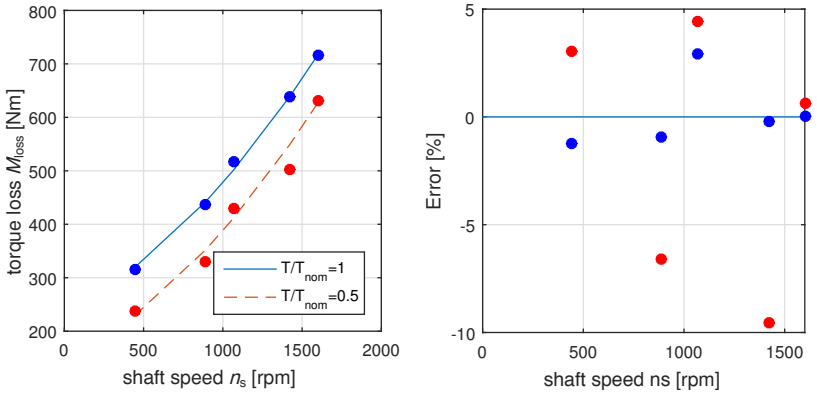

Figure 6.11: Simulated and actual torque losses of the gearbox.

PROPELLER

The model uses the results of the propeller open water tests for the Wageningen K_a5-75 propeller series with nozzle 19A (Kuiper, 1992), which is a well accepted method to model propeller thrust and torque within the assumptions of a homogeneous advance speed, perpendicular flow into the propeller and quasi static performance. Validation of the behaviour of the propeller model in the ship as a whole is covered in Chapter 3 (Geertsma *et al.* 2017c).

GEARBOX AND SHAFTLINE

The model parameters for the gearbox and shaft-line are estimated using on-board measurements. The differences can be seen in Figures 6.11, with a maximum error of 10%.

6.3. ENERGY MANAGEMENT STRATEGIES

THE Energy Management Strategies proposed in this chapter determine the load split between the main engines (MEs) and the induction machines (IMs) for hybrid propulsion and between the diesel generator (DG) and battery packs (BAT) for hybrid power generation. The speed setpoints for propulsion are determined by the speed setpoint from the operator for the MEs $n_{\text{me,set}}$, when running, and for the IMs $n_{\text{im,set}}$, when the MEs are of. The power split between the MEs and IMs, when both are running in parallel, is established with the torque setpoint for the IMs $M_{\text{im,set}}$. The speed setpoint for the DG, when running, and the BAT when the DG is off, is fixed with the 60Hz electrical network frequency, at 30 Hz, due to the 2 pole pairs P_{pp} of the synchronous generator. The power split between the DG and BAT, when both are operating in parallel, is established with the current setpoint for the frequency converter of the BAT $i_{\text{bat,set}}$. Therefore, the Energy Management Strategies have to determine the torque setting of the Induction Machines $M_{\text{im,set}}$, the current setting of the Battery $i_{\text{bat,set}}$ and the binary settings for switching the MEs, IMs, DG and BAT on or off $(b_{\text{dg}}, b_{\text{im}}, b_{\text{me}}) \in \mathbb{Z}_2$, as illustrated in Figure 6.4. The aim of the strategies is to minimise fuel consumption over the operating profile between two consecutive recharging opportunities, using real-time optimisation.

ECMS was initially introduced by Paganelli *et al.* (2000) and is based on the notion that battery can be seen as an auxiliary, reversible fuel tank. Therefore, by assigning a cost to electrical energy, it can be associated with a certain quantity of fuel. This cost is known as equivalence factor or co-state $s(t)$. It is the key control parameter of ECMS, and largely dictates its performance. The equivalence factor represents the chain of efficiencies through which fuel is transformed into electrical power and vice versa. As such, it changes for each operating condition of the power-train. In the original formulation of ECMS, the equivalence factor is a set of constants which can be interpreted as the average overall efficiency of the electric path for each operating mode (charge or discharge) for a given mission (Guzzella *et al.* 2007; Jager *et al.* 2013; Onori *et al.* 2016; Sciarretta *et al.* 2004, 2007). Since the entire mission is usually not known at the outset, any uncertainties about future operating conditions are transferred to uncertainty about the optimal value of the equivalence factor. State-to-costate feedback is applied in most studies, most commonly in the form of a PI- controller (Ambuhl *et al.* 2009, 2007; Chasse *et al.* 2009; Kessels *et al.* 2008). However, more advanced feedback laws have also been reported for land-based vehicles, which update the equivalence factor's values based on estimations about future operating conditions or driving pattern recognition (Musardo *et al.* 2005; Serrao *et al.* 2013; Sivertsson *et al.* 2015). Multiple co-states have also been reported, to include engine and catalyst temperatures in the control objective (Maamria *et al.* 2017).

In this work, two different approaches are investigated: The simplest scenario of an ECMS with constant equivalence factor, which has been discussed in Delprat *et al.* (2002), Guzzella *et al.* (2009), and Sciarretta *et al.* (2007) and applied in Won *et al.* (2005) with a unity value, and a more sophisticated approach of an adaptive equivalence factor based on operator load estimation, as discussed in Vu *et al.* (2015, 2014). The schematic representation of the adaptive strategy is illustrated in Figure 6.12. It consists of an optimiser that minimises the control objective subject to the applicable constraints, and a 'predictor' to estimate the equivalence factor according to Vu *et al.* (2015, 2014). The

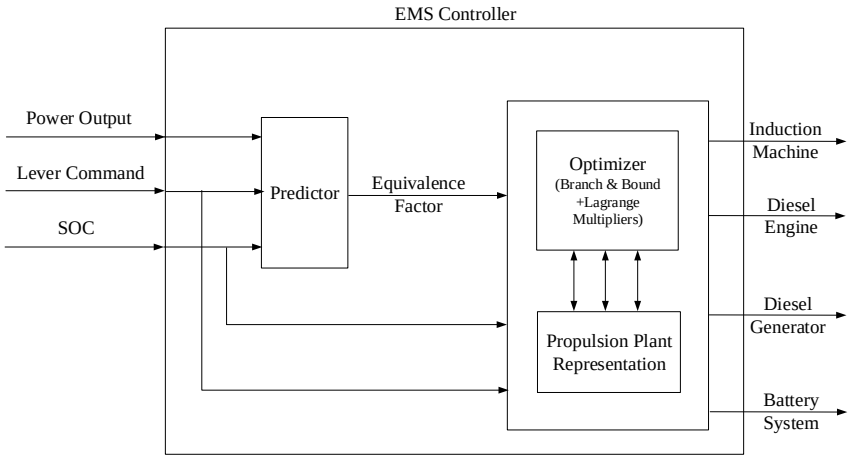

Figure 6.12: Schematic overview of the EMS controller.

constant equivalence factor approach is represented by the optimiser only, which has a fixed equivalence factor as its input.

In order to evaluate the performance of the proposed ECMS, we use the dynamic simulation model in Section 6.2 to compare ECMS against the performance of a rule-based controller and against the global optimum, established with Dynamic Programming (DP), assuming apriori knowledge of the operating profile. The rule based controller is described in Section 6.3.6 and the DP algorithm in Section 6.3.7.

6.3.1. MODEL REDUCTION

Ideally, the dynamic model presented in Section 6.2 would be used in the proposed strategies, however, real-time decisions would not be feasible due to its complexity and large number of state variables. Furthermore, quasi-static models suffice to a large extent for fuel economy estimation, as dynamic transient behaviour hardly influences total fuel consumption over an entire operating profile (Guzzella *et al.* 2007; Sciarretta *et al.* 2014; Serrao *et al.* 2007). For this reason, energy efficiency of each component will be estimated using efficiency maps, which are highly accurate for fuel consumption estimation, similar to the approach in many automotive ECMS (Sciarretta *et al.* 2014). These efficiency maps have subsequently been approximated by uni- and bivariate second-degree polynomials, due to their fine balance between accuracy and simplicity. Moreover, the convex character of these polynomials allows computationally fast online optimisation. The accuracy of this approach is discussed at the end of the section.

MAIN ENGINE

The fuel consumption map of the main engines can be approximated with a quadratic relationship with respect to power output P^*_{me} in W, and engine rotational speed n^*_{me}, as proposed in Shi *et al.* (2010), as follows:

$$\dot{m}^*_{\mathrm{f,me}}(t) = \begin{cases} \alpha_0 + \alpha_1 n^*_{\mathrm{me}}(t) + \alpha_2 P^*_{\mathrm{me}}(t) + \alpha_3 n^{*2}_{\mathrm{me}}(t) + \\ +\alpha_4 P^{*2}_{\mathrm{me}}(t) + \alpha_5 n^*_{\mathrm{me}}(t) P^*_{\mathrm{me}}(t), \;\; 0 < P^*_{\mathrm{me}} \leq 1 \\ 0, \;\; P^*_{\mathrm{me}} = 0, \end{cases} \tag{6.1}$$

with $\alpha_i \in (0,1),\ i = 1,...,5$ fitted parameters. The accuracy of this approach is illustrated in Figure 6.14.

INDUCTION MACHINE & FREQUENCY CONVERTER

The combined power losses are estimated based on torque output M^*_{im} in Nm, and shaft rotational speed n^*_{im}. Due to asymmetries in the efficiency between motoring and generating conditions, two different sets of coefficients are necessary, as follows:

$$P^*_{\mathrm{im+fc,loss}}(t) = \begin{cases} \epsilon_{\mathrm{i}1} n^*_{\mathrm{im}}(t) + \epsilon_{\mathrm{i}2} M^*_{\mathrm{im}}(t) + \epsilon_{\mathrm{i}3} n^{*2}_{\mathrm{im}}(t) + \\ +\epsilon_{\mathrm{i}4} M^{*2}_{\mathrm{im}}(t) + \epsilon_{\mathrm{i}5} n^*_{\mathrm{im}}(t), \\ M^*_{\mathrm{im}}(t), \;\; 0 < M^*_{\mathrm{im}} \leq 1 \\ 0, \;\; M^*_{\mathrm{im}} = 0 \end{cases} \tag{6.2}$$

$$P_{\mathrm{fc}}(t) = P_{\mathrm{im}}(t) + P_{\mathrm{im+fc,loss}}(t) \tag{6.3}$$

with $\epsilon_{ij} \in (0,1),\ i = 1,2,\ j = 0,....,5$ fitted parameters. The accuracy of this approach is illustrated in Figure 6.14.

DIESEL - GENERATOR

Fuel consumption of the diesel driving the generator represents a quadratic relationship with respect to rotational speed and power output. Because the diesel generator (DG) operates at constant speed, a one-dimensional polynomial can be used to approximate fuel consumption of the DG, as follows:

$$\dot{m}^*_{\mathrm{f,dg}}(t) = \begin{cases} \beta_0 + \beta_1 P^*_{\mathrm{dg}}(t) + \beta_2 P^{*2}_{\mathrm{dg}}(t), \;\; 0 < P^*_{\mathrm{dg}} \leq 1 \\ 0, \;\; P^*_{\mathrm{dg}} = 0, \end{cases} \tag{6.4}$$

with $\beta_i \in (0,1),\ i = 0,1,2$ fitted parameters. The accuracy of this approach is illustrated in Figure 6.14.

BATTERY

The Ragone efficiency is needed for the objective function (Sciarretta *et al.* 2007), and SOC and terminal voltage for the constraints. The open cell voltage is given by equation (3.94), and the efficiency depends on power output, as follows:

$$\eta_{\mathrm{bat}}(t) = \delta_0 + \delta_1 P_{\mathrm{bat}}(t) + \delta_2 P^2_{\mathrm{bat}}(t), \tag{6.5}$$

with $\delta_i,\ i = 0,1,2$ fitted parameters. In order to estimate state of charge and bounded battery power, the equivalent circuit of Figure 6.13 is used. When a current flows in the circuit, the following relations hold:

$$\left.\begin{aligned} i_{\mathrm{bat}}(t) &= \frac{P_{\mathrm{bat}}(t)}{u_{\mathrm{t}}(t)} \\ u_{\mathrm{oc}}(S_{\mathrm{OC}}(t)) - r\, i_{\mathrm{bat}}(t) &= u_{\mathrm{t}}(t) \end{aligned}\right\} \Rightarrow$$

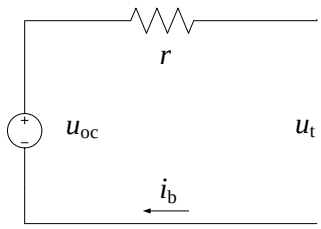

Figure 6.13: Battery equivalent circuit representation in the controller.

$$u_t^2(t) - u_{oc}(S_{OC}(t))\, u_t(t) + P_{bat}(t)\, r_{ec} = 0. \tag{6.6}$$

Solving equation (6.6) for power yields:

$$P_{bat}(t) = \frac{-u_t^2(t) + u_t(t)\, u_{oc}(S_{OC}(t))}{r_{ec}}. \tag{6.7}$$

Now, upper and lower limits for battery power can be determined:

$$P_{bat,max}(t) = \frac{u_{oc}(S_{OC}(t))\, u_{t,min} - u_{t,min}^2}{r_{ec}} \tag{6.8}$$

$$P_{bat,min}(t) = -\frac{u_{t,max}^2 - u_{oc}(S_{OC}(t))\, u_{t,max}}{r_{ec}}, \tag{6.9}$$

where $u_{t,min}$ and $u_{t,max}$ are the manufacturer's terminal voltage limits.

While the Energy Management Strategies (EMS) use state of charge S_{oc} as an exogenous input, the EMS strategy needs to ensure that the the SOC limitations are not violated while establishing the next iteration of settings. Therefore, the state of charge after one iteration is established with the more simple first order equivalent circuit (EC) model, illustrated in Figure 6.13, as opposed to the second order EC model in the dynamic model. This simple EC model is sufficiently accurate for this purpose as it only influences state of charge S_{oc} over one iteration of the Energy Management Strategy as opposed to the accumulative drift for the dynamic model. Therefore, within the Energy Management Strategies, state of charge S_{oc} is estimated as follows (Koot *et al.* 2005):

$$\begin{aligned} S_{OC}(t) &= \frac{Q_{bat}(t)}{Q_{bat,nom}} = \frac{Q_{bat}(t_0) - \sum_{t=0}^{t} \left(\frac{P_{bat}(t)}{u_{oc}(S_{OC}(t))} \Delta t \right)}{Q_{bat,nom}} \\ &= S_{OC}(t - \Delta t) - \frac{P_{bat}(t)\, \Delta t}{u_{oc}(S_{OC}(t))\, Q_{bat,nom}}. \end{aligned} \tag{6.10}$$

Finally, for the battery's rectifier, a constant efficiency η_{rec} is assumed, equal to 97.5%.

Figure 6.14 illustrates the accuracy of the relations used, relative to the benchmark simulation model, which is used to evaluate performance against. The induction machine reduced model, in the top-right graph, is within +/- 1% accurate in its normal

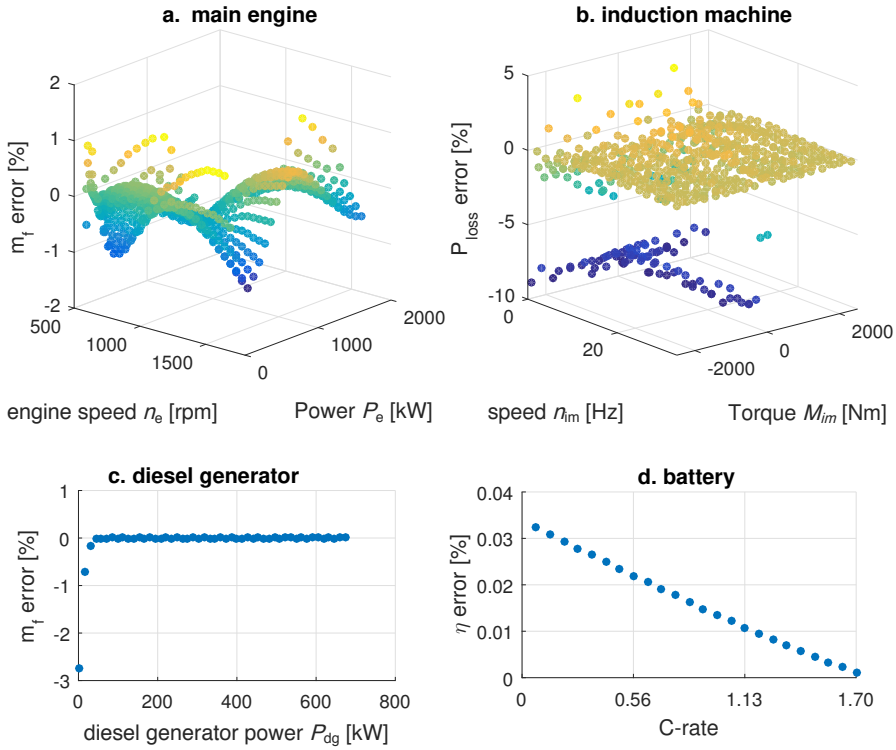

Figure 6.14: Fitting errors of Equations (6.1), (6.2), (6.4), (6.5).

operating region. While the model is not very accurate around the zero torque and zero speed region, this does not pose a problem for the optimisation process as the IM is indeed inefficient around these regions, and the EMS should avoid operating it. By over-estimating the losses around these regions, we actually bias the controller to avoid these regions altogether. For all other components, main engines, diesel generator and battery packs, the accuracy of the model is within 1% and therefore sufficiently accurate to be used for the ECMS approach.

6.3.2. OPTIMISATION PROBLEM FORMULATION

The control objective of ECMS is to establish the control variables BAT current i_{bat} when the DG is running, and IM torque M_{im} when the MEs are running, in order to minimise the instantaneous equivalent fuel consumption of the vessel $\dot{m}_{\text{f,eqv}}$, subject to propeller speed n_{p}, power demand for propulsion, P_{pd}, demanded auxiliary power P_{aux}, BAT state of charge S_{oc}, and three binary variables $(b_{\text{dg}}, b_{\text{im}}, b_{\text{me}}) \in \mathbb{Z}_2$ for the ON/OFF state of each component. BAT current i_{bat} and IM torque M_{im} are established from the ECMS control variables BAT power P_{bat} and IM power P_{im}, as follows:

$$i_{\text{bat}}(t) = \frac{P_{\text{bat}}}{\sqrt{3}u_{\text{line}}(t)\cos(f_p)} \tag{6.11}$$

$$M_{\text{im}}(t) = \frac{P_{\text{im}}(t)}{2\pi i_{\text{gb}} n_{\text{p}}(t)}. \tag{6.12}$$

While propulsion power demand P_{pd} and shaft speed are a result of the model dynamics against the specified shaft speed setting n_{set}, towing force X_{tow}, resistance curve $R(v_{\text{s}})$ and auxiliary load P_{aux} in the benchmark dynamic model, the reduced order model requires exogenous inputs propeller speed n_{p}, power demand for propulsion, P_{pd}, demanded auxiliary power P_{aux} and BAT state of charge S_{oc}. Propulsion power demand subsequently dictates ME power P_{me} when the IMs and MEs are running in parallel, or IM power P_{im} when the MEs are off, through the following equality:

$$P_{\text{me}}(t) = P_{\text{pd}}(t) - P_{\text{im}}(t). \tag{6.13}$$

Similarly, auxiliary power P_{aux} dictates DG power P_{dg} when the DG and battery packs are operating in parallel, or battery power P_{bat} when the DG is off, with the following equality:

$$P_{\text{dg}}(t) = P_{\text{aux}}(t) + 2\left(P_{\text{im}}(t) + b_{\text{im}}(t)P_{\text{im+fc,loss}}(t)\right) - P_{\text{bat}}(t). \tag{6.14}$$

6

The equivalent fuel consumption aims to reduce the global optimisation problem of minimising fuel consumption over the operating profile to an instantaneous optimisation of equivalent fuel consumption. To achieve this a cost is assigned to the use of the battery in discharge mode, equivalent to the expected amount of fuel consumption required to recharge the battery and a negative cost is assigned to charging the battery, equivalent to the expect amount of fuel to be saved when the battery is used to provide power (Paganelli *et al.* 2002). When the strategy aims to discharge to battery to its minimum SOC, this can be achieved by reducing the cost assigned to the use of the battery. Therefore, the equivalent fuel consumption is the sum of MEs and DG fuel consumption $\dot{m}_{\text{f,me}}$, $\dot{m}_{\text{f,dg}}$, and the artificial fuel consumption of the battery packs $\dot{m}_{\text{f,bat}}$, and can be defined as follows:

$$\dot{m}_{\text{f,eqv}}(t) = \sum_i \dot{m}_{\text{f,me}_i}(t) + \dot{m}_{\text{f,dg}} + \dot{m}_{\text{f,bat}}(t). \tag{6.15}$$

The artificial fuel consumption of the battery packs is proportional to the equivalence factor s, which differs whether the battery packs are being charged or discharged. In the original formulation of ECMS (Paganelli *et al.* 2000), the equivalence factor is a vector of values, one for charge and one for discharge $s(t) = [s_{\text{chg}}(t), s_{\text{dis}}(t)]$, as follows:

$$\begin{aligned} s_{\text{dis}} &= s(t)\eta_{\text{bat}}(P_{\text{bat}}(t)) \\ s_{\text{chg}} &= \frac{s(t)}{\eta_{\text{bat}}(t)} = s(t)\eta_{\text{bat}}^{-1}(P_{\text{bat}}(t)). \end{aligned} \tag{6.16}$$

However, since the original ECMS formulation, Kirk, (2012) showed that there is no need for multiple factors, since the efficiencies along the electrical path, apart from the battery packs, can be implicitly taken into account using one parameter, as follows:

$$\dot{m}_{\mathrm{f,bat}}(t) = c_{\mathrm{sfo,eqv}}(t) P_{\mathrm{bat}}(t) = \\ = \frac{\mathrm{s}(t)}{\eta_{\mathrm{bat}}(P_{\mathrm{bat}}(t))^{sgn(P_{\mathrm{bat}}(t))}} \frac{P_{\mathrm{bat}}(t)}{Q_{\mathrm{lhv}}}. \tag{6.17}$$

Utilising the model reduction defined in (6.1), (6.2), (6.4), (6.5) and (6.13) and (6.14), the equivalent fuel consumption of (6.15) can be summarised as a function of the five control variables $u_{\mathrm{c}} \triangleq [P_{\mathrm{bat}}, P_{\mathrm{im}}, b_{\mathrm{dg}}, b_{\mathrm{im}}, b_{\mathrm{me}}]$ and exogenous inputs $w_{\mathrm{e}} \triangleq [n_{\mathrm{p}}, P_{\mathrm{pd}}, P_{\mathrm{aux}}, S_{\mathrm{oc}}]$, as follows:

$$\begin{aligned} \dot{m}_{\mathrm{f,eqv}}(t) = {} & 2 b_{\mathrm{me}}(t) m_{\mathrm{f,me}}(n_{\mathrm{p}}(t), P_{\mathrm{pd}}(t), P_{\mathrm{im}}(t)) \\ & + b_{\mathrm{dg}}(t) m_{\mathrm{f,dg}}(P_{\mathrm{aux}}(t), P_{\mathrm{im}}(t), b_{\mathrm{im}}(t), n_{\mathrm{p}}(t)) \\ & + \frac{\mathrm{s}(t)}{\eta_{\mathrm{bat}}(P_{\mathrm{bat}}(t)) P_{\mathrm{bat}}(t)^{sgn(P_{\mathrm{bat}}(t))}} \frac{P_{\mathrm{bat}}(t)}{Q_{\mathrm{lhv}}}, \end{aligned} \tag{6.18}$$

where $s(t)$ is constant for ECMS and is established with the adaptive regime described in Section 6.3.5 for AECMS. The resulting optimisation problem definition is:

$$u_{\mathrm{c}}^{0}(t) = \arg\min_{u_{\mathrm{c}}} \dot{m}_{\mathrm{f,eqv}}(u_{\mathrm{c}}, w_{\mathrm{e}}(t), s(t)). \tag{6.19}$$

The inequality constraints of the optimisation problem include: the predefined SOC limitations to preserve battery lifetime using (6.10), as follows:

$$S_{OC_{min}} \leq S_{OC}(t) \leq S_{OC_{max}} \Rightarrow \\ S_{OC_{min}} \leq S_{OC}(t - \Delta t) - \frac{P_{\mathrm{bat}}(t)\, \Delta t}{u_{\mathrm{oc}}(S_{OC}(t)) Q_{\mathrm{bat,nom}}} \leq S_{OC_{max}}; \tag{6.20}$$

the operating envelope of the MEs from (6.13), as follows:

$$0 \leq P_{\mathrm{p,dem}}(t) - b_{\mathrm{im}}(t) P_{\mathrm{im}}(t) \leq P_{\mathrm{e,max}}(n_{\mathrm{e}}(t)) b_{\mathrm{e}}(t); \tag{6.21}$$

the operating envelope of the DG from (6.14), as follows:

$$0 \leq P_{\mathrm{aux}}(t) + 2 b_{\mathrm{im}}(t) \left(P_{\mathrm{im}}(t) + P_{\mathrm{im+fc,loss}}(t) \right) - P_{\mathrm{bat}}(t) + \\ \leq P_{\mathrm{gen,nom}} b_{\mathrm{dg}}(t); \tag{6.22}$$

power limitations of the BAT from (6.8) and (6.9), as follows:

$$-\frac{u_{\mathrm{t,max}}^2 - u_{\mathrm{oc}}(S_{OC}(t)) u_{\mathrm{t,max}}}{r} \leq \frac{P_{\mathrm{bat}}(t)}{\eta_{\mathrm{rec}}^{sgn(P_{\mathrm{bat}}(t))}} \leq \\ \leq \frac{u_{\mathrm{oc}}(S_{OC}(t)) u_{\mathrm{t,min}} - u_{\mathrm{t,min}}^2}{r}; \tag{6.23}$$

the operating envelope of the induction machines, as follows:

$$b_{im}(t) P_{\mathrm{im,min}} \leq P_{im}(t) \leq P_{\mathrm{im,max}} b_{im}(t); \tag{6.24}$$

and, finally, one extra constraint to force the energy management strategy to operate on the main engines when the vessel is towing:

$$b_{\mathrm{me}}(t) = \begin{cases} 1, \text{if } X_{\mathrm{tow}}(t) > 0 \\ 0, \text{if } X_{\mathrm{tow}}(t) = 0. \end{cases} \tag{6.25}$$

6.3.3. SOLUTION METHOD

The resulting optimisation problem can be classified as mixed integer non-linear program. Mixed integer non-linear programs are NP-Hard, so their solution time increases exponentially with the number of dimensions of the problem (Hillier, 2012). In Vu *et al.* (2014), heuristic search methods (genetic algorithms) are used to solve the optimisation problem. However, heuristic methods usually produce near-optimum solutions, whereas deterministic methods guarantee optimality of the solution (Hillier, 2012). Key factors in solving MINLPs fast enough are (1) the number of integer variables and (2) whether the problem has any special characteristics that can be exploited. In this case, three discrete variables exist, therefore a Branch & Bound method is applicable: It will generate only an $2^3 = 8$ node binary search tree, the sub-problems of which are *convex*, as Appendix A shows. Combining Branch & Bound with the method of Lagrange Multipliers to solve the arising convex sub-problems will result in limited computational time and guaranteed optimality of the solution for the defined problem formulation.

6.3.4. CONSTANT EQUIVALENCE FACTOR

In the first energy management strategy, in this work referred to as ECMS, a constant equivalence factor value has been adopted. The idea of a constant equivalence factor has been discussed in several studies in the past (Delprat *et al.* 2002; Guzzella *et al.* 2009; Sciarretta *et al.* 2007), mostly considering how close the resulting solution is to the global optimum. A constant equivalence factor only provides a solution close to the global optimum, when the battery usage is limited to a relatively narrow SOC range, as voltage and resistance do not vary much (Kim *et al.* 2011). In **??** we investigate the effect of battery's SOC, power input and output to the variation of the equivalence factor. Based on that analysis we have concluded that a constant equivalence factor provides a solution near the global optimum, regardless of the state of the battery packs.

Considering the battery as an auxiliary fuel tank, the value of the equivalence factor is chosen to reflect the nominal fuel consumption of the main engines, corrected for the nominal efficiency of the components between the battery packs and the shaft:

$$s = c_{\text{sfo,e}}\, \eta_{\text{rec}}\, \eta_{\text{im+fc}}\, Q_{\text{lhv}} = 2.165. \tag{6.26}$$

The key concept is that the use of the batteries will prevent low engine loading. Dedes *et al.* (2012) and Yuan *et al.* (2016) indicate that, when the load demand falls within the inefficient, low-loading region of the engine, its specific fuel consumption will be higher than the battery pack's. As a consequence, the controller will opt to either (1) switch off all of the engines and operate on the battery packs, or (2) increase engine loading to a more efficient operating point, using the excess power to recharge. The ECMS will chose between these options based on the value of the equivalence factor s, relative to the fuel consumption in the operating point with the increased engine loading, and is limited by the battery power and state of charge constraints. If the low loading operating point would be maintained for a long period in time, this could lead to a start-stop strategy, but this does not occur in the typical operating profile as demonstrated in Section 6.4 and Figure 6.20.

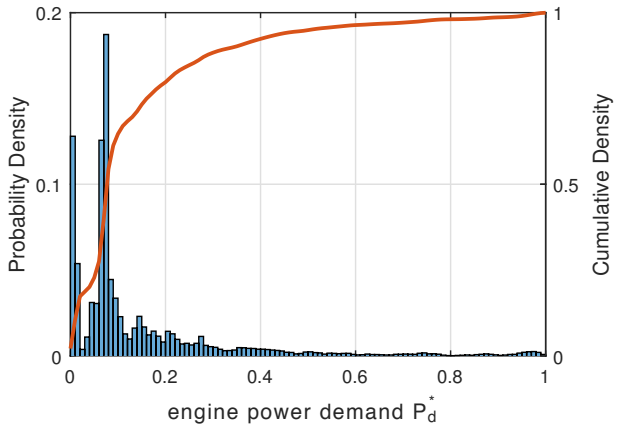

Figure 6.15: Measured power demand distribution of tugboats operating in the port of Rotterdam.

6.3.5. ADAPTATION BASED ON OPERATING LOAD ESTIMATION

In the second strategy, the equivalence factor is estimated on the basis of historical data: using tugboat measurements of operations in the port of Rotterdam, the probability distribution of normalised propulsion power demand $P^*_{\text{p,dem}}$ was compiled, shown in Figure 6.15, and combined with the propulsive load prediction scheme of Vu *et al.* (2015, 2014). This prediction scheme estimates upcoming load changes based on a stochastic approach over a future prediction horizon of 10 minutes, and is referred to as A-ECMS. The equivalence factor value is set equal to the inverse chain efficiency of the electrical path (battery - rectifier - frequency converter - induction motor) based on the predicted load:

$$s(t) = \prod_{i=1}^{4} \frac{1}{\eta_i \left(1 - \widehat{P}^*_{\text{p,dem}}(t)\right)}. \tag{6.27}$$

Furthermore, a penalty function has been used to guarantee that the SOC does not exceed the admissible limits, $S_{OC_{min}} \leq S_{OC}(t) \leq S_{OC_{max}}$, as follows:

$$\mu = \begin{cases} 1 - \left(\dfrac{S_{OC_a} - S_{OC}(t)}{\sigma}\right)^a & \text{for } S_{OC}(t) \leq S_{OC_a} \\ 1 & \text{for } S_{OC_a} \leq S_{OC}(t) \leq S_{OC_b} \\ 1 - \left(\dfrac{S_{OC}(t) - S_{OC_b}}{\sigma}\right)^a & \text{for } S_{OC}(t) \geq S_{OC_b}, \end{cases} \tag{6.28}$$

with:

$$\sigma = \frac{S_{OC_{max}} - S_{OC_{min}}}{2}$$

$$S_{OC_{min}} \leq S_{OC_a} \leq S_{OC_b} \leq S_{OC_{max}}.$$

Its effect can be seen in Figure 6.16, penalising for the SOC being close to the lower or upper bound $S_{OC_{min}}, S_{OC_{max}}$.

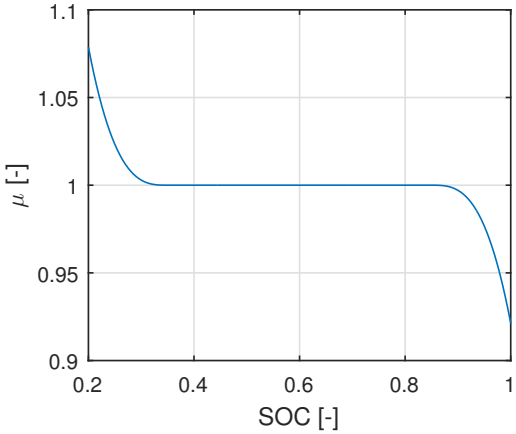

Figure 6.16: Effect of multiplicative penalty function $\mu(S_{OC})$ of (6.27).

6.3.6. RULE-BASED CONTROL

The rule-based controller in this chapter is used to compare the performance of the Energy Management Strategies with a commercially available rule-based controller, that has been applied to the actual case study tug. This controller switches between three operating modes for propulsion, as described in de Groote *et al.* (2014): standby, free sailing and towing mode. These three mode are defined, as follows:

- In standby mode, when the speed setting of the propulsion plant n_{set} ranges from 0 to 8.33 Hz, or 0 rpm to 500 rpm, the main engines (MEs) and diesel generator (DG) are switched of and the ship is propelled with the induction machines (IMs). Power to the IMs is provided by the battery packs (BAT) until they reach their minimum state of charge (SOC) S_{oc}, at 20% SOC. Then the DG is started and will provide electrical power to the IMs and charge the BAT at its maximum rate within the constraints of maximum DG power.
- In free sailing mode, when the speed setting of the propulsion plant n_{set} is higher than 8.33 Hz, or 500 rpm, either the DG or the MEs provides auxiliary and propulsion power. In the speed setting n_{set} range from 8.33 to 15 Hz, or 500 to 900 rpm, the MEs are switched off and the IMs provide propulsion power. The DG is switched on and provides electrical power for propulsion, auxiliaries and battery charging. The battery packs are charged at its maximum rate within the constraints of maximum DG power. In the speed setting n_{set} range from 15 Hz to 30 Hz, or 900 to 1800 rpm, the MEs provides power for propulsion and the IMs. Moreover, the IMs, driven by the MEs, operate as generator and provide electrical power to the auxiliary load and charge the BAT at its maximum rate within the constraints of maximum IMs power.
- In towing mode, the MEs are switched on regardless of the speed setting, in order to ensure full bollard bull is directly available without notice. The MEs provide power for propulsion and the IMs. Moreover, the IMs, driven by the MEs, operate

as generator, provide electrical power to the auxiliary load and charge the BAT at its maximum rate within the constraints of maximum IMs power.

6.3.7. GLOBAL OPTIMUM FOR KNOWN OPERATING PROFILE

The ECMS and A-ECMS are causal sub-optimal control strategies as they have very limited information on future operating conditions. Thus, their decision quality is limited. The entire mission is usually unknown from the outset, therefore adaptive controllers have to rely on estimations of future operating conditions. Because the operating profiles assessed in this chapter are known, the causal controllers can be compared with a non-causal optimal controller that has been determined using Dynamic Programming (DP). The generic DP MATLAB function of Elbert *et al.* (2013) and Sundstrom *et al.* (2010, 2009) has been used to provide the global optimum solution.

6.4. CONTROLLER EVALUATION

6.4.1. SIMULATION EXPERIMENTS

WITH the simulation models described in Section 6.2, we have analysed the fuel consumption for the case study tug with hybrid propulsion. The MATLAB Simulink R2014b software has been used on a PC with Intel Core i7 processor and 16GB memory to simulate the hybrid propulsion plant. To objectively assess the performance and robustness of the proposed suboptimal control system, we have compiled 6 variations of a real operating profile shown in Figure 6.17. Profile 1 is the standard profile, and is based on measurements of tugboats operating in the port of Rotterdam. Profiles 2 and 3 are two and three times the duration of the standard profile. Profile 4 represents a 'lighter' loading variation, in which vessel speed and bollard pull have been reduced in half, and profile 5 represents a shorter mission, of roughly half the duration of the standard profile. Finally, Profile 6 represents an extremely busy profile, consisting of tow jobs with heavy loads, and Profile 7 is an idle profile, in which the vessel is mostly free-sailing at low speeds. The difference between the first five 'original' missions (Profiles 1-5), the busy profile (Profile 6) and idle profile (Profile 7) are shown in Figure 6.18. The total time spent in stand-by, free-sailing and assisting modes is visualised.

6.4.2. RESULTS

Table 6.1 lists the fuel consumption m_f savings compared to rule-based (RB) controller in %, state of charge at the end of each mission $S_{OC,f}$ and average vessel efficiency η_{vessel} from the simulation experiments and mission profiles described in Section 6.4.1. These results confirm that DP yields the lowest fuel consumption for all operating profiles, with an average reduction of 8.6% compared to the currently used rule-based controller, which aims to maintain battery charge. The resulting savings are attributed to better utilisation of the battery packs, reflected by a lower SOC at the end of the mission shown in Figure 6.20, rather than the increased efficiency of the propulsion plant. In fact, the global optimum, established with DP, only marginally beats the rule-based controller's decisions in terms of plant efficiency and only for the longer operating profiles. Therefore, if a charge-sustaining solution was desired, the current rule-based controller provides near optimum solutions. This has been verified by imposing the constraint

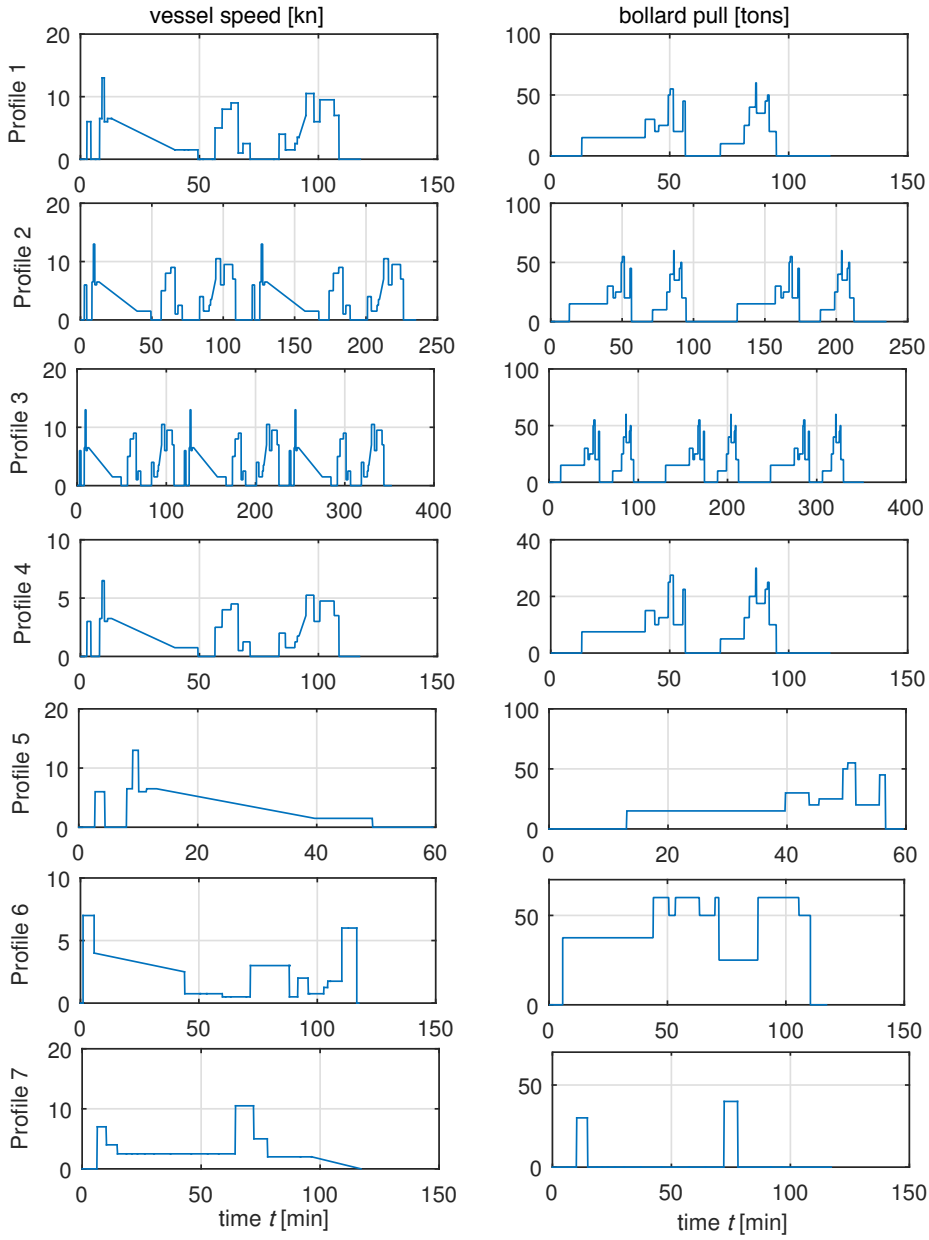

Figure 6.17: Simulated operating profiles.

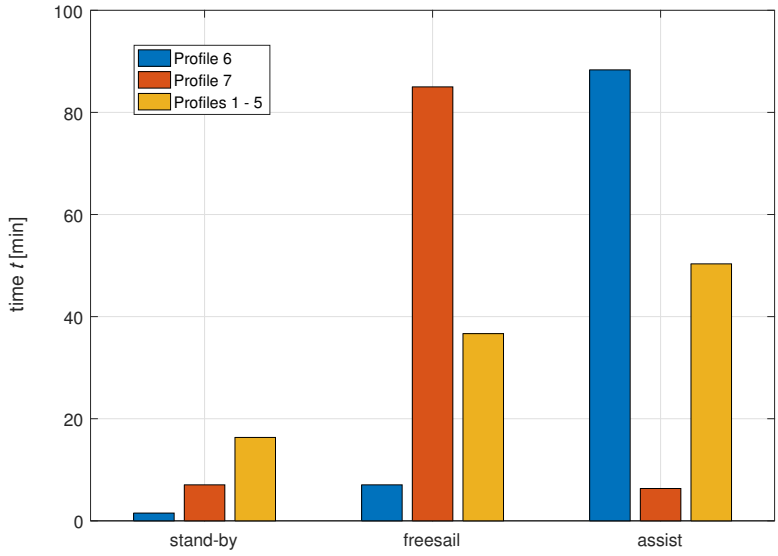

Figure 6.18: standard, idle and busy operating profiles - operating mode distribution.

$S_{OC_{f,DP}} = S_{OC_{f,RB}}$ to the causal controller and the results in Table 6.2, which demonstrate the rule-based controller achieves a solution within approximately 1% of the global optimum.

The cumulative saving of the ECMS strategy over all operating profiles is 3.7%, which is 2.1% less than the global optimum. For typical operating profiles, the saving of ECMS is 5% to 10%, but these savings are not robust for long or heavily loaded operating profiles. The AECMS strategy performs slightly better over the cumulative operating profiles at 4% savings, but ECMS performs better over the typical profile, while AECMS performs typically better at low loads, for example profile 4 and 7. Furthermore, the difference between the two strategies does not appear consistent and significant, therefore the adaptive algorithm does not perform consistently better. This is most probably caused by the short time window that the adaptive algorithm looks ahead and the uncertainty of the power demand distribution.

The state of charge and equivalence factor trajectories shown in Figure 6.20, demonstrate that the equivalence factor should mostly be increased or decreased when the mission length is increased or decreased. Future work should therefore focus on developing an algorithm that adapts equivalence factor based on the state of charge and remaining mission time or uses a predictive approach with a time window similar to mission length. The maximum additional fuel saving that can be achieved with such approaches is approximately 2%.

While the fuel savings that can be achieved with Energy Management Strategies are significant, the differences between the rule-based controller, both ECMS strategies and the global optimum are significantly smaller than in the study investigating the impact of

Table 6.1: Results from simulation experiments with rule-based (RB) control, Equivalent Consumption Minimisation Strategy (ECMS), adaptive ECMS (A-ECMS) and causal control with dynamic programming (DP) for operating profiles defined in Section 6.4.1

	EMS	Fuel		$S_{OC,f}$	η_{vessel}
		m_f [kg]	Savings [%] RB	[%]	[%]
Profile 1	DP	336.1	7.79	20	35.5
	RB	364.5	-	94	36.0
	ECMS	340.1	6.62	31	35.3
	A-ECMS	343.2	5.71	36	35.8
Profile 2	DP	846.8	3.49	20	36.6
	RB	876.9	-	94	36.1
	ECMS	869.6	0.83	33	36.0
	A-ECMS	857.9	2.27	27	36.0
Profile 3	DP	1104.3	2.62	20	36.4
	RB	1134.1	-	94	36.2
	ECMS	1118.6	1.36	35	36.1
	A-ECMS	1122.8	0.99	30	36.0
Profile 4	DP	259.6	10.5	27	35.6
	RB	290.0	-	100	35.1
	ECMS	270.1	6.89	20	34.9
	A-ECMS	264.3	8.96	20	35.0
Profile 5	DP	161.8	17.35	25	35.4
	RB	195.9	-	100	35.8
	ECMS	174.6	10.85	66	35.2
	A-ECMS	177.6	9.32	61	35.1
Profile 6	DP	1039.4	3.51	20	38.9
	RB	1077.3	-	95	38.6
	ECMS	1047.1	2.77	37	38.7
	A-ECMS	1046.3	2.81	33	38.5
Profile 7	DP	224.6	16.07	20	34.8
	RB	267.6	-	99	34.2
	ECMS	239.2	10.51	20	34.3
	A-ECMS	234.8	12.27	20	34.6

ECMS: Constant equivalence factor.

A-ECMS: Adaptive equivalence factor.

Table 6.2: Results from simulation experiments with rule-based (RB) control and causal control with dynamic programming (DP) when charge sustainment is imposed, for operating profiles defined in Section 6.4.1

	EMS	m_f [kg]	m_f [%]	η_{vessel} [%]	$S_{\text{OC,f}}$ [%]
Profile 1	DP	361.3		36.2	94
	RB	364.5	101.1	36.0	
Profile 2	DP	872.1		36.3	94
	RB	876.9	100.6	36.1	
Profile 3	DP	1130.0		36.1	94
	RB	1134.1	100.4	36.3	
Profile 4	DP	288.2		35.3	100
	RB	290.0	100.6	35.0	
Profile 5	DP	193.2		36.1	100
	RB	195.9	101.4	35.9	
Profile 6	DP	1065.4		38.8	95
	RB	1077.3	101.1	38.6	
Profile 7	DP	264.6		34.7	99
	RB	267.6	101.2	34.2	

various Energy Management Strategies for the plug-in hybrid vehicle benchmark studied in Sciarretta *et al.* (2014). For various operating profiles the difference between various rule-based and ECMS strategies in that study is reported to be 25% to 40%. Analysing the results of these studies, we attribute the smaller difference between various Energy Management Strategies for the tug to three main causes:

- The degree of freedom in control for the operating point of the main engines and the diesel generator is smaller for the tug case, because the energy management strategy cannot influence engine speed, while the planetary gearbox of the plug-in hybrid vehicle allows variable operating speed of the engine (Sciarretta *et al.* 2014). Main engine speed is fixed, because the relationship between engine speed and torque is fixed by the fixed pitch propeller characteristics in combination with the ships resistance curve. A controllable pitch propeller could enable variable engine speed. Diesel generator speed is fixed at constant frequency, because diesel generator speed dictates electrical network frequency. Diesel generator speed could be made variable, if a DC power distribution system was applied as proposed in Zahedi *et al.* (2014), who reported fuel savings of up to 15% with a DC power supply with energy storage, of which 7% was attributed to the use of energy storage with the energy management algorithm proposed in Zahedi *et al.* (2014), for a case study Off-shore Support Vessel (OSV). Future studies could therefore investigate the impact of controllable pitch propellers and DC power supply on Energy Management Strategies, although DC stability would have to to be addressed (Flower

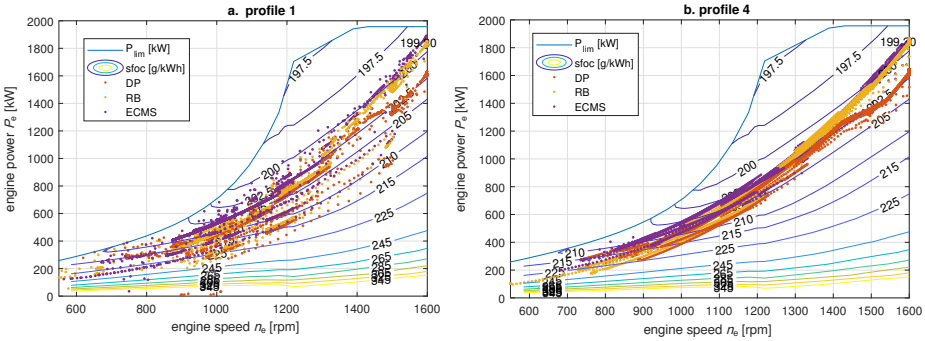

Figure 6.19: Operating points of the main engines in the operating envelope for causal global optimum control (DP), rule-based control (RBC) and ECMS during operating profiles 1 and 4.

et al. 2014; Haseltalab *et al.* 2017b; Herrera *et al.* 2017; Simmonds, 2014; Zahedi *et al.* 2013).

The operating points of the main engine during profile 1 and 4, shown in Figure 6.19, clearly demonstrate that all operating points of the main engine are close to the quadratic propeller curve discussed in Chapter 2, (Geertsma *et al.* 2017a). Causal global optimum control operates the engine at lower power, in order to reach minimum state of charge at the end of the operating profile, as shown in Figure 6.20, while the rule-based and ECMS strategies operate the engine at higher power, but do not achieve minimum state of charge. The global optimum strategy actually accepts the penalty of operating the main engines at a less efficient operating point, in the region where the gradient of fuel consumption as a function of torque is minimal, in order to ensure all stored battery energy is used. Moreover, global optimum control does not load the engine at its maximum load, suggesting an engine with reduced rating could be used, further reducing fuel consumption, as the smaller engine would be running at a higher relative load and thus lower fuel consumption. At maximum bollard pull, the induction machines would then run at full power in parallel with the main engines.

- In a significant part of the operating profile, during towing, the main engines are switched on, to ensure full bollard pull is directly available, without first having to start the main engines. In order to investigate the influence of this constraint, we have run the optimisation algorithms without the constraint to run the main engines during towing. The results in Table 6.3 demonstrate 2% to 3% additional fuel savings could be achieved if the main engines were not forced on during towing operations. While these savings are significant, they would require a proven reliable and very fast starting system for the main engines, that is equally reliable and safe as running with main engines on during towing continuously.
- A significant amount of fuel savings in plug-in hybrid vehicles is achieved by storing energy regenerated during braking in city traffic or downhill driving. The operating profile of ships does not feature a significant amount of braking or any alti-

tude fluctuation, although crane ships and ships with heave compensation can restore energy during crane or heave compensation operations, and these ship types could definitely benefit more from hybrid power supply as discussed in Chapter 2 (Geertsma *et al.* 2017a; Ovrum *et al.* 2015).

For the current equivalence factor, the battery packs appear to be well sized for 2 hour missions. Proportionally larger sized batteries would lead to a close to optimum performance of ECMS for longer operating profiles with the typical loading profile. Therefore, the proposed ECMS with the proposed propulsion architecture and battery pack size is likely to achieve close to optimum fuel savings for tugs that operate 2 hour missions mostly and can be recharged. ECMS without equivalence factor tuning does not appear to be robust against changes in operating profile length or loading, as the fuel savings for the alternative operating profiles are further away from the global optimum. Nevertheless, both ECMS and AECMS perform better than the current rule-based controller for all operating profiles investigated. Moreover, from this analysis we can conclude that optimum sizing of the battery packs should be established with an integrated co-design approach including the energy management strategy as proposed in Hofman *et al.* (2017), Murgovski *et al.* (2012), Silvas *et al.* (2017), and Xu *et al.* (2015).

The performance of the ECMS and AECMS strategies compared to the global optimum solution can be analysed with the state of charge and equivalence factor trajectories, as shown in Figure 6.20 and 6.21. These figures compare the state of charge and equivalence factor values of the causal controllers, to the optimal state of charge and equivalence factor, derived using the DP solution. The adaptive equivalence factor for typical operating Profile 1 is constantly higher than the optimal, penalising the use of the batteries. On the other hand, better results are achieved with the constant equivalence factor for typical operating Profile 1 due to its closer resemblance to the optimum one. When the equivalence factor of the DP solution varies more, due to long operating profiles or heavy loading, in most cases the AECMS follows the equivalence factor of the global optimum more closely. Finally, an estimation of an average, near - optimal equivalence factor, can be found by plotting used battery energy $E_B = Q_B \times (S_{OC,0} - S_{OC,f})$ as a function of achieved fuel savings, visualised in Figure 6.22. In fact, the derivative of this approximately linear pattern equals 178 g/kWh, corresponding to an equivalence factor value of 2.15, 0.7% lower than our initial estimate.

Figure 6.20 also demonstrates the rule-based controller only uses the battery packs occasionally. Moreover, without recharging, the battery packs would not reach its minimum state of charge for any of the investigated operating profiles. Therefore, a quick-win can be achieved by modifying the rule-based controller to not recharge the battery packs, or to only recharge the battery packs, when its SOC reaches a certain value and the main engines are running at high efficiency. Future research could investigate the impact of this modification of the rule-based controller with the methodology proposed in this work.

6.5. CONCLUSIONS

IN this chapter, we have investigated energy management in order to determine the optimum power split between the main diesel engine, diesel generators and battery

Table 6.3: Results from simulation experiments with rule-based (RB) control with towing mode, Equivalent Consumption Minimisation Strategy (ECMS) without towing constraint, and causal control with dynamic programming (DP) with and without towing constraint (wTC and woTC) for operating profiles defined in Section 6.4.1

	EMS	Fuel		$S_{OC,f}$	η_{vessel}
		m_f [kg]	Savings [%] RB	[%]	[%]
Profile 1	DP wTC	336.1	7.79	20	35.5
	RB	364.5	-	94	36.0
	ECMS	332.9	8.67	34	35.4
	DP woTC	328.1	9.98	20	35.6
Profile 2	DP	846.8	3.49	20	36.6
	RB	876.9	-	94	36.1
	ECMS	855.2	2.47	31	36.2
	DP woTC	832.8	5.25	20	36.7
Profile 3	DP	1104.3	2.62	20	36.4
	RB	1134.1	-	94	36.2
	ECMS	1107.8	2.32	34	36.2
	DP woTC	1092.3	3.68	20	36.6
Profile 4	DP	259.6	10.5	27	35.6
	RB	290.0	-	100	35.1
	ECMS	262.9	9.34	20	35.1
	DP woTC	251.6	13.24	23	35.7
Profile 5	DP	161.8	17.35	25	35.4
	RB	195.9	-	100	35.8
	ECMS	171.0	12.71	64	35.2
	DP woTC	157.8	19.45	22	35.4
Profile 6	DP	1039.4	3.51	20	38.9
	RB	1077.3	-	95	38.6
	ECMS	1043.5	3.13	36	38.7
	DP woTC	1035.4	3.89	20	38.9
Profile 7	DP	224.6	16.07	20	34.8
	RB	267.6	-	99	34.2
	ECMS	232.0	13.30	20	34.3
	DP woTC	216.6	18.85	20	34.8

ECMS: Constant equivalence factor.

A-ECMS: Adaptive equivalence factor.

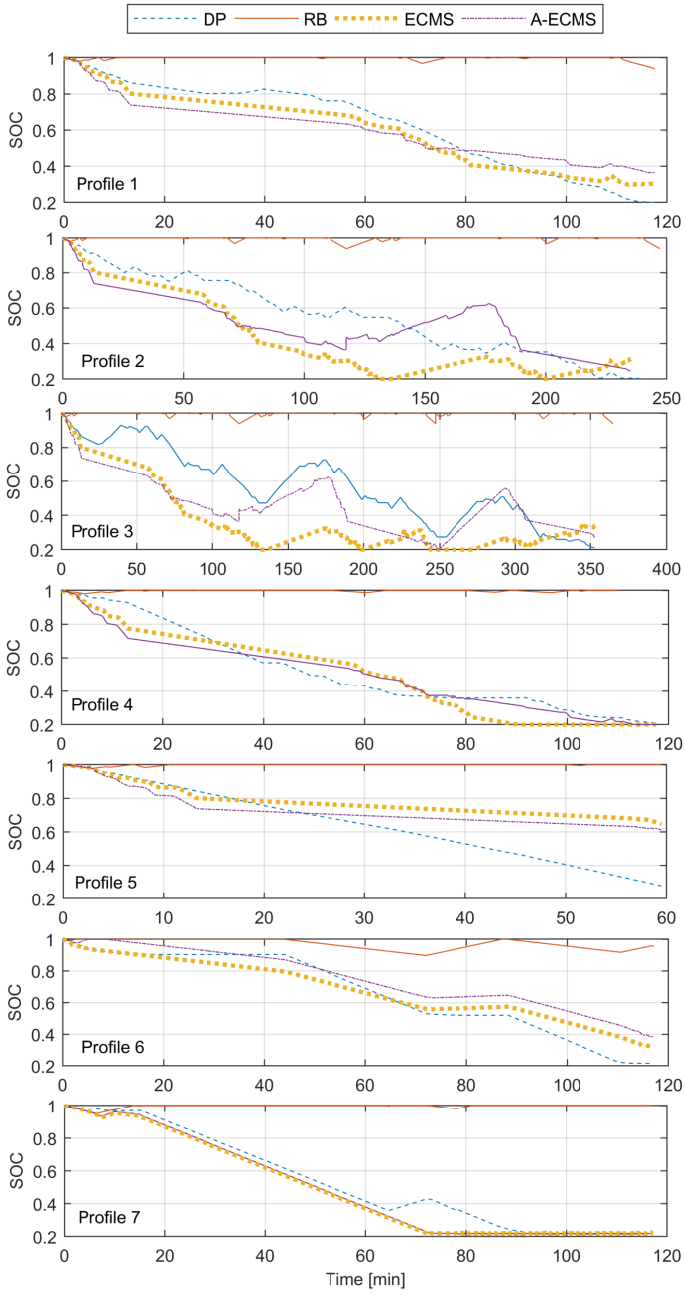

Figure 6.20: State of Charge (SOC) trajectories for all operating profiles.

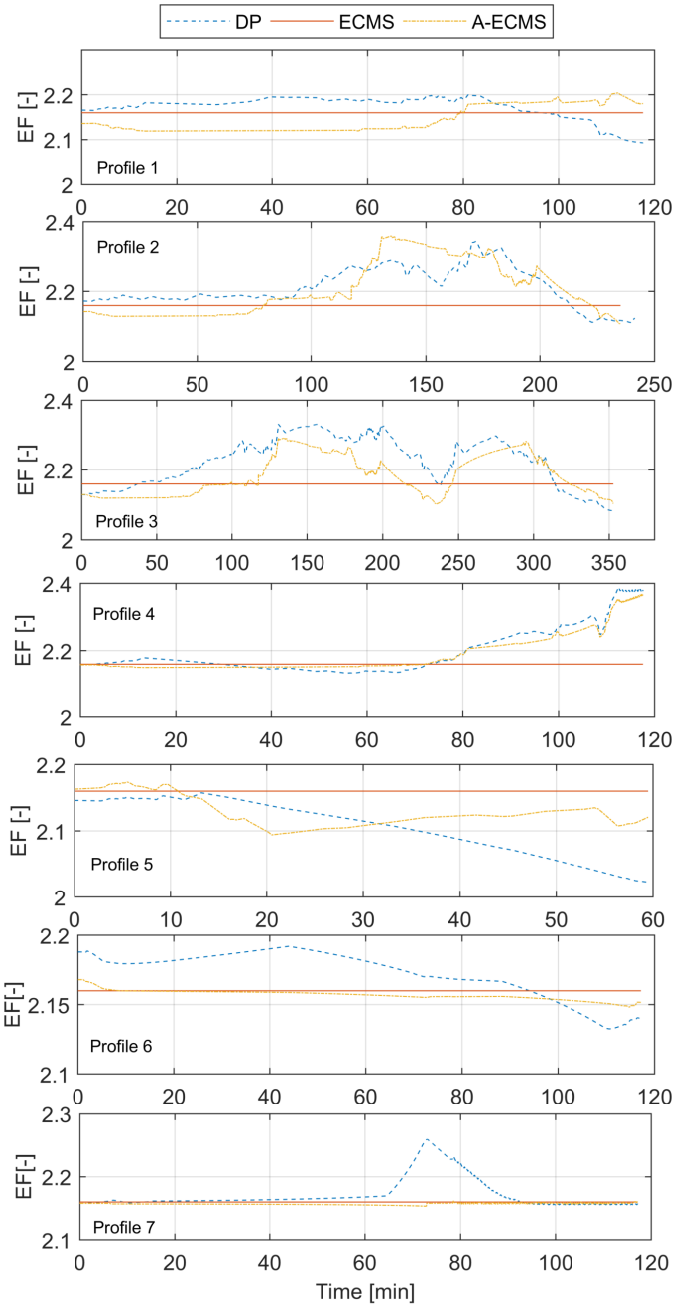

Figure 6.21: Equivalence Factor trajectories for all operating profiles.

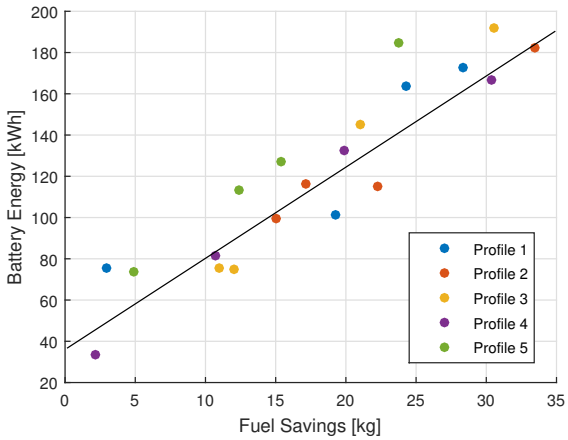

Figure 6.22: Battery energy as a function of achieved fuel savings.

packs of a ship with hybrid propulsion and hybrid power supply in order to minimise fuel consumption and CO_2 emissions and answer Research Question 7. We have applied two ECMS-based controllers to a tugboat and compared its fuel consumption with a rule-base controlled hybrid propulsion and power generation plant. The simulation experiments demonstrated that ECMS can contribute significantly to cleaner shipping, particularly if the batteries are recharged from the shore grid in between missions. Simulation results demonstrate that fuel savings and associated CO_2 emission reductions of 5% to 10% can be achieved with the proposed methods for a typical operating profile, within 1-2% of the global optimum solution. While the near optimum performance of ECMS is not robust against changes in operating profile length or heavy loading, ECMS does perform better than a charge sustaining rule-based controller and the charge sustaining global optimum for all operating profiles investigated. Furthermore, by testing the robustness of the strategies against contrasting profiles we demonstrated that, although better fuel economy than charge sustaining rule-based control is achieved in any case, the strategy can be improved by either including adaption of the equivalence factor based on remaining mission time or using a predictive approach with a prediction horizon as long as the time between recharging opportunities.

7

CONCLUSIONS AND RECOMMENDATIONS

In this PhD thesis, we have investigated how hybrid propulsion and power supply architectures and its advanced control strategies can reduce fuel consumption, CO_2, NO_x and PM emissions and underwater noise, improve acceleration performance, and limit engine loading to reduce maintenance, in order to answer the following problem statement: 'How can advanced control strategies for hybrid propulsion and power generation architectures autonomously achieve the best multi-objective trade-off for diverse ship operations?'

In this chapter, we will answer the research questions derived from this problem statement in Chapter 1, using three case studies: a patrol vessel with mechanical propulsion with CPP, a frigate with hybrid propulsion and a tug with hybrid propulsion and hybrid power supply. Then, we will propose the concept and design structure for autonomous control that can adapt the control system performance to changing ship functions and discuss the relation of the proposed adaptive layered control structure to the proposed control strategies: adaptive pitch control, parallel control for hybrid propulsion and energy management for hybrid power supply. Subsequently, we will address related future work to further develop and implement these control strategies and the adaptive layered control structure. This chapter is organised as follows: First, Sections 7.1 and 7.2 will discuss the candidate architectures and control strategies that were established in Chapter 2. Then, Sections 7.3 and 7.4 will discuss how the performance of these candidate architectures and control strategies can be quantified. Subsequently, the conclusions of the simulation studies will be discussed for adaptive pitch control, for propulsion with a controllable pitch propeller, in Section 7.5, for parallel adaptive pitch control, for hybrid propulsion, in Section 7.6, and for equivalent consumption minimisation strategies, for hybrid power supply, in Section 7.7, before discussing the concept and design structure for autonomous control that can adapt to changing ship functions, using these control strategies, in Section 7.8. Finally, we will propose future work to further develop and implement these strategies in Section 7.9, and provide a closing summary in Section 7.10.

7.1. CANDIDATE ARCHITECTURES

CHAPTER 2 has reviewed current and future power and propulsion system architectures and their associated control strategies for smart ships. The variety and complexity of these architectures poses an increasing amount of design choices to the ship and control system designer. In order to determine the optimal architecture, knowing the operational profile and the ship functions to be performed is essential. From the operating profile and ship functions, the candidate architectures for the ship can be established, based on the benefits and challenges for the various propulsion and power supply architectures in Table 2.1 and their application trends reported in Table 2.2, thus answering Research Question 1:

> *Which candidate propulsion and power generation architectures are suitable for which ship type and which combination of ship functions?*

Based on the review in Chapter 2 and its results in Table 2.1 and 2.2, we can derive the following general conclusions in answer to Research Question 1.

- Electrical propulsion is economically efficient and operationally effective when the mission and hotel loads are of a similar magnitude as the propulsion loads, for example in cruise ships, capital naval ships, and in offshore vessels that require the majority of its propulsive power for the dynamic positioning function. Then, the diesel generators can be switched on and off as required and alternately support all ship functions. However, if the propulsion load is significantly greater than the electrical mission and hotel loads together, then the conversion losses in the electrical propulsion drive increase fuel consumption and emissions while the electrical equipment drives up volume and weight;
- Hybrid propulsion is economically beneficial if the ship sails below 40% of its top speed a significant amount of time. This is applicable to ships that often perform the functions low speed sailing, patrolling or loitering, such as tugs, warships and patrol vessels and ships that often perform dynamic positioning such as offshore vessels and drilling and crane vessels. Hybrid propulsion, particularly in combination with hybrid power supply, can potentially also support ships sailing at constant speed in heavy weather conditions, as the direct drive main engine can then deliver constant torque while torque fluctuations are handled by the electric drive;
- Hybrid power supply is beneficial when the total electrical load has a great spread over time and can improve availability and reduce noise. The electrical load typically has a great spread over time for ships with functions that require large fluctuating loads, such as dredgers during dredging, heavy crane vessels during hoisting and lowering of loads and drilling vessels during drilling. The availability increase is of particular interest for ships that require high levels of dynamic positioning in order to safely perform functions such as loading and off-loading, performing maintenance on windturbines and drilling. The potential low noise operation on the electrical drive is required for ship functions such as underwater warfare patrol for naval vessels and operations in a noise restricted natural environment;

- Finally, DC power systems potentially bring down conversion losses and can run the generator at variable speed, reducing fuel consumption and associated emissions with up to 20%, for ships with electrical and hybrid propulsion, in particular when most electrical loads require variable speed drives for their functions. The increasingly electrically powered mission loads of naval vessels, for example rail guns and directed energy weapons, can also be more efficiently and effectively supported by DC power systems as they require pulsed loads, that can deteriorate both voltage and frequency stability of AC systems.

7.2. CANDIDATE CONTROL STRATEGIES

ONE of the most important aspects that determine whether the full potential of the selected architecture can be achieved in practice is the control strategy. As such, many intelligent control strategies have been investigated and applied in other applications such as the automotive industry and land based micro-grids. However, advanced control strategies have only most recently been investigated and applied in maritime applications, and only reductions in fuel consumption and emissions, of 15% to 35%, have been quantified for some cases, which is partly achieved by recharging batteries from the grid. Improvements in other criteria, such as propulsion availability, radiated noise and maintenance cost are crucial for effective hybrid power and propulsion systems as well. From the review of control strategies reported in literature, as presented in Table 2.3, Research Question 2 can be answered:

> *What candidate control strategies can be identified to improve on the MOEs fuel consumption, emissions, radiated noise, propulsion availability, manoeuvrability and maintainability due to engine mechanical and thermal loading?*

The review has identified three promising control strategies that utilise the degrees of freedom provided by the controllable pitch propeller (CPP), by the power split between the main engine and electric drive for hybrid propulsion, and by the power split between the diesel generator and the energy storage in hybrid power supply:

- Adaptive pitch control (APC) for diesel mechanical and hybrid propulsion with controllable pitch propellers, which combines the angle of attack approach for propeller pitch control (Vrijdag *et al.* 2010) with slow integrating speed control for diesel engine fuel injection, to achieve the identified advantages of torque control and to answer Research Question 5;
- Parallel adaptive pitch control (PAPC) for hybrid propulsion with CPP that uses a combination of slow integrating speed control for the main engines and torque control for the electric drive, both for electric motor assist and power take-off, to answer Research Question 6; and
- A novel approach for the on-line solution of the charge depleting Equivalent Consumption Minimisation Strategy ECMS control problem for hybrid propulsion with hybrid power generation that can also be used to generate the torque setpoint for the PAPC strategy proposed in Chapter 5 and to answer Research Question 7.

7.3. DYNAMIC SIMULATION MODEL

AFTER having established candidate architectures and control strategies for a particular ship type and its function based on the literature review in Chapter 2 or a quantitive mathematical model (Georgescu *et al.* 2018, 2017), thus answering Research Questions 1 and 2, a method is required to objectively and quickly quantify and assess the effectiveness of the system architecture and control strategy for diesel mechanical and hybrid propulsion systems and answer Research Question 3 and 4. While some of the MOEs listed in Section 1.1, such as manoeuvrability, radiated noise and thermal loading, depend on the dynamic behaviour of the various subsystems and their interaction, dynamic simulation models are required to answer Research Question 3:

> *What simulation model can be used to quantify MOEs fuel consumption, emissions, radiated noise, propulsion availability, manoeuvrability and maintainability due to engine mechanical and thermal loading?*

Chapter 3 has proposed a new diesel propulsion system model that can be parameterised with available manufacturer data. This model is based on a previous Mean Value First Principle (MVFP) model and has been improved to reflect modern turbocharger and Miller-timing behaviour based on advanced diesel engine theory. Subsequently, we have validated the MVFP diesel engine model with measurements in factory conditions and in operational conditions at sea with a case study naval vessel. The predictions of the diesel engine model were within 5% of most measurement values. Although exhaust gas temperatures were only predicted within 10% of the measurements, the engine thermal loading can be accurately quantified with the air excess ratio.

The baseline control strategy for mechanical propulsion with fixed combinator curves, acceleration limitations and pitch reduction strategy has been described. We have shown that this strategy can prevent engine overloading effectively while achieving conservative manoeuvrability, acceleration and cavitation behaviour. Quantitative validation has demonstrated that the propulsion system model credibly predicts propulsion system behaviour within 5% accuracy. Moreover, the wave model behaviour in Sea State 6 has been verified with the propulsion system model with modified parameters that reflect a frigate. The results of this model were found to match measurements on a frigate in Sea State 6. Moreover, we have proposed models for the induction machine and frequency converter for hybrid propulsion and simple models for the diesel generator, battery and auxiliary loads for hybrid power supply. Thus, we have proposed a simulation model for mechanical and hybrid propulsion and hybrid power generation, that can be used to to quantify MOEs fuel consumption, emissions, radiated noise, propulsion availability, manoeuvrability and maintainability due to engine mechanical and thermal loading, in answer to Research Question 3.

7.4. MEASURES OF PERFORMANCE

THE simulation models proposed in Chapter 3 can then be used to quantify performance. To this end, benchmark manoeuvres and associated measures of performance (MOPs) are required to quantify the performance of the propulsion plant on the following measures of effectiveness (MOEs): fuel consumption, rate of acceleration, engine thermal loading and propeller cavitation, to answer Research Question 4:

What benchmark manoeuvres and Measures of Performance (MOP) can quantify the MOEs listed above?

For this purpose, Chapter 3 has first proposed the following benchmark manoeuvres:

- Sail at constant speed in trial, design and off-design conditions;
- Accelerate from 0 kts to maximum speed with the slam start manoeuvre: increasing the lever setpoint to maximum virtual shaft speed at once (Altosole *et al.* 2012b).
- Accelerate in steps, for example from 0 to 5, 5 to 10 and 10 to 15 kts, in design conditions, referred to as intermediate sprints. The intermediate sprint manoeuvres are performed by increasing the virtual shaft speed from the setting corresponding to the initial ship speed to the setting corresponding to the final ship speed.

Subsequently, we have proposed the following MOPs, obtained from these benchmark manoeuvres:

- Fuel consumption per mile for trial, design and off-design conditions, presented as a function of ship speed during sailing at constant speed, as previously proposed in Klein Woud *et al.* 2012, Ch. 12, pp. 482-483;
- Acceleration time for intermediate sprints, for example from 0 to 5, 5 to 10 and 10 to 15 kts, and for slam start acceleration, for example from 0 to 15 kts, in design conditions;
- Average air excess ratio at constant speed for trial, design and off-design conditions, presented as a function of ship speed. This performance criterion serves as an indicator for engine thermal loading during constant speed sailing due to the average temperature;
- Minimum air excess ratio during intermediate sprints, for example from 0 to 5, 5 to 10 and 10 to 15 kts, and for slam start acceleration, for example from 0 to 15 kts, in design conditions. This performance criterion serves as an indicator for engine thermal loading due to acceleration manoeuvres;
- Air excess ratio fluctuation at constant speed for design and off-design conditions, presented as a function of ship speed. This performance criterion serves as an indicator for thermal stresses in the engine caused by waves due to temperature fluctuation;
- Cavitation plot of acceleration manoeuvres during intermediate sprints, for example from 5 to 10 and 10 to 15 kts, in design conditions.

These MOPs and the propulsion system model have been used to evaluate the performance of two operating modes of the conventional control strategy. Analysing these two control modes previously either required days of sea trials, or weeks of analysing various simulation time traces. Alternatively, the proposed MOPs can be determined within an hour of simulation time. Depending on the particular control strategy and operating conditions, fuel savings up to 30%, thermal loading reduction of 90 K and reductions of 50% in acceleration time can be achieved for the case study Patrol Vessel.

7.5. CONTROLLABLE PITCH PROPELLER

CHAPTER 4 has proposed the *adaptive pitch control* (APC) strategy for diesel mechanical or hybrid propulsion with controllable pitch propellers. This control strategy uses the degree of freedom in control provided by the controllable pitch propeller (CPP) to answer Research Question 5:

> *What control strategy can be used for controllable pitch propellers to provide the best possible performance against an adaptive trade-off between the various conflicting MOEs listed in Section 1.2?*

The APC strategy aims to maintain the required effective angle of attack α_{eff} by controlling propeller pitch P_{pd} and aims to provide the required engine speed with slow integrating speed control by controlling fuel pump injection X. The simulation models and Measures of Performance proposed in Chapter 3 were used to demonstrate the following:

- Adaptive pitch control (APC) robustly follows the requested virtual shaft speed, as the adaptive pitch setpoint is compensated by a speed setpoint correction;
- APC operates the propeller around its effective angle of attack. With current slow hydraulic pitch actuation systems the response is too slow to attenuate the wake flow disturbance due to waves, in particular due to the counter balance valve. However, the average angle of attack during manoeuvring remains close to the desired value;
- APC reduces fuel consumption and has the potential to reduce NO_x emissions, as the angle of attack setpoint can be used to run the engine at a predetermined operating curve, in this case the theoretical propeller curve. The operating curve can be selected based on the trade-off between the static CO_2 and NO_x emission maps. Moreover, particulate matter (PM) emissions can be reduced due to the smooth torque trajectory due to slow integrating speed control, although the reduction has not yet been quantified;
- APC maintains the air excess ratio λ at its required minimum value, thus limiting engine thermal loading. Varying the minimum air excess ratio depending on the ship function allows engine thermal loading to be adapted to the ships function. While the air excess ratio in dynamic conditions is not an exact indicator for engine thermal loading, alternatively an approach on charge pressure maps could be used;
- APC reduces acceleration time particularly during intermediates sprints, due to its consistent acceleration behaviour; and
- APC robustly prevents engine over- and under-speed.
- For the case study patrol vessel, the adaptive pitch control strategy reduces fuel consumption by 5% to 15% compared to the baseline transit mode in the ship speed range from 6 to 15 kts, and reduces acceleration time from 0 to 15 kts with the slam start procedure by 32% compared to the baseline manoeuvre mode and by 84% for an intermediate acceleration from 10 to 15 kts, without thermally overloading the engine.

In summary, APC enables to select the optimum trade-off between cavitation risk, engine thermal loading and speed of acceleration by varying the fuel increase rate limitation R_X and the minimum air excess ratio λ_{min}, while achieving the best possible fuel consumption.

7.6. HYBRID PROPULSION

In Chapter 5 we have proposed the *parallel adaptive pitch control* (PAPC) strategy, which is based on the adaptive pitch control strategy proposed in Chapter 4 and uses the electric drive to improve acceleration performance, in particular at higher ship speeds, and top speed for ships with hybrid propulsion. We have used the dynamic simulation models, benchmark manoeuvres and Measures of Performance proposed in Chapter 3 to compare the performance of the proposed PAPC strategy with baseline mechanical speed control (MSC) without the pitch reduction strategy discussed in Section 3.3, parallel electric speed control (PESC) as proposed in Geertsma *et al.* (2017d) and adaptive pitch control (APC) as proposed in Chapter 4, in order to answer Research Question 6:

> *What control strategy can be used for the power split between the propulsion engine and electric drive in hybrid propulsion to provide the best possible performance against an adaptive trade-off between the various conflicting MOEs?*

The simulation experiment results demonstrate the following with regard to using the power split between the propulsion diesel engine and electric drive:

- PAPC achieves fast slam start and intermediate acceleration, twice as fast as the baseline MSC for the case study frigate, while better limiting engine thermal loading and thus causing less smoke and particulate matter (PM) emissions.
- PAPC improves intermediate acceleration from 20 to 24 kts and slam start acceleration compared to APC, again reducing acceleration time by a factor 2 or more. The speed of acceleration is a trade-off with engine thermal loading, quantified by maximum exhaust valve temperature and rate of change of exhaust valve temperature.
- During situations with high manoeuvrability requirements, such as emergency situations, fast PAPC can actually reduce acceleration time by a further 20% at the cost of a higher exhaust valve temperatures T_{ev}, rate of change of exhaust valve temperature dT_{ev}/dt and air excess ratio λ, which would lead to higher smoke and PM emissions.
- PAPC can achieve operation around the optimum angle of attack up to 18 to 20 kts ship speed. However, to prevent reduction of angle of attack during acceleration, for optimum cavitation behaviour the speed of acceleration should be reduced by a factor 2, still as fast as the baseline MSC control strategy.
- PAPC in combination with an engine with a wide operating envelope, for example due to sequential turbocharging, can enable a further fuel consumption and emission reduction of 7% and a significant reduction in running hours, at a transit speed of 18 kts for the case study frigate with sequentially turbocharged diesel engines (Geertsma *et al.* 2017d).

In summary, PAPC enables to select the optimum trade-off between cavitation risk, engine thermal loading and speed of acceleration by varying the fuel increase rate limitation R_X and the minimum air excess ratio λ_{min}, while achieving the best possible fuel consumption above 15 kts, similar to APC, but PAPC reduces acceleration time of intermediate sprints at high speed and the slam start acceleration by 50%. Below 15 kts, fuel consumption can be reduced by running on the electric drive in speed control fed from the diesel generators, thus allowing maintaining maximum pitch and thus running at shaft speeds below minimum main diesel engine speed.

7.7. HYBRID POWER SUPPLY

In Chapter 6, we have investigated how much fuel consumption and local CO_2 emission reduction can be achieved by applying the *Equivalent Consumption Minimisation Strategy* (ECMS) to a hybrid propulsion plant with hybrid power supply with and without future operating load estimation, and determined the robustness of the ECMS performance against varying operating profiles compared to the global optimum solution with a priori knowledge and determined with DP, for a case study towing vessel with hybrid propulsion plant and hybrid power supply, to partly answer Research Question 7:

> *What control strategy can be used for the power split between various power sources in hybrid power supply to provide the best possible performance against an adaptive trade-off between the various conflicting MOEs?*

The simulation experiments have demonstrated the following:

- ECMS can contribute significantly to cleaner shipping, particularly if the batteries are recharged from the shore grid in between missions. Simulation results demonstrate that fuel savings and associated CO_2 emission reductions of 5% to 10% can be achieved with the proposed methods for a typical operating profile, within 1-2% of the global optimum solution;
- For the charge sustaining case, the baseline rule-based controller performed close to the global optimum with charge sustaining constraint, as established with dynamic programming (DP). The operating points of the main engines, in Figure 6.19, demonstrate that the limited engine operating envelope allows very limited degree of freedom in controlling the operating point of the main engine. These results seem to suggest that the problem of choosing the optimum operating point becomes one-dimensional: the energy management strategy only has to decide which prime mover delivers the power and not at which speed it is running. A simple rule based controller can be easily derived to determine the power at which the energy management strategy needs to switch to another power source;
- ECMS achieved near optimum performance for the design operating profile, but was not robust against changes in operating profile length or heavy loading, because the battery was either not completely discharged, for example due to a short operating profile, or was already discharged completely before the end of the operating profile, for example for a long operating profile. The performance can then be improved by either reducing or increasing the equivalence factor s. However,

ECMS does perform better than a charge sustaining rule-based controller and the charge sustaining global optimum for all operating profiles investigated;

- By testing the robustness of the strategies against contrasting profiles we demonstrated that, although better fuel economy than charge sustaining rule-based control is achieved in any case, the strategy can be improved by either including adaption of the equivalence factor based on remaining mission time or using a predictive approach with a prediction horizon as long as the time between recharging opportunities.

In summary, the simulation results of a case study tugboat with validated models show that, with unknown load demand, 6% additional fuel savings can be achieved with ECMS, while the simple ECMS with a constant equivalence factor s is not robust against changes in the operating profile.

7.8. AUTONOMOUS ADAPTATION TO SHIP FUNCTIONS

THE simulation study in Chapter 5, has demonstrated how the *parallel adaptive pitch control strategy* (PAPC) enables to select the optimum trade-off between cavitation risk, engine thermal loading and speed of acceleration by varying the fuel increase rate limitation R_X and the minimum air excess ratio λ_{min}, while achieving the best possible fuel consumption above 15 kts for a ship with hybrid propulsion and CPP. Moreover, the simulation study in Chapter 6 has demonstrated how the proposed *Equivalent Consumption Minimisation Strategy* (ECMS) for hybrid propulsion and power supply can utilise battery charge to reduce fuel consumption and CO_2 emissions. In this section, we discuss how these three novel control strategies can be combined in the layered control structure proposed in 2.9.4 for the mechanical and electrical system integration, based on the approach proposed for electrical system integration for microgrids in Guerrero *et al.* (2011) and discussed in Section 2.5.3. This section will propose the concept and design structure for autonomous control that can adapt the control system performance to changing ship functions and discusses the relation of the proposed autonomous control structure to the proposed control strategies: adaptive pitch control, parallel control for hybrid propulsion and energy management for hybrid power supply, in order to answer Research Question 8:

> *How can the performance trade-off between the various MOEs be autonomously adapted for changing ship functions?*

Figure 7.1 provides a schematic representation of the proposed adaptive layered control strategy for a ship with hybrid propulsion with CPP and hybrid power supply, for example the case study frigate with additional batteries or the case study tug with CPP. The proposed control strategy consists of 3 layers:

- The primary control layer consists of the low level *PID* feedback control strategies for the main diesel engine, the controllable pitch propeller (CPP), the induction machine drive, the diesel generator and the batteries. The main diesel engine is controlled with gain scheduled speed control, with fast *PI* speed control when the engine is running at its minimum engine speed n_e, and slow integrating speed

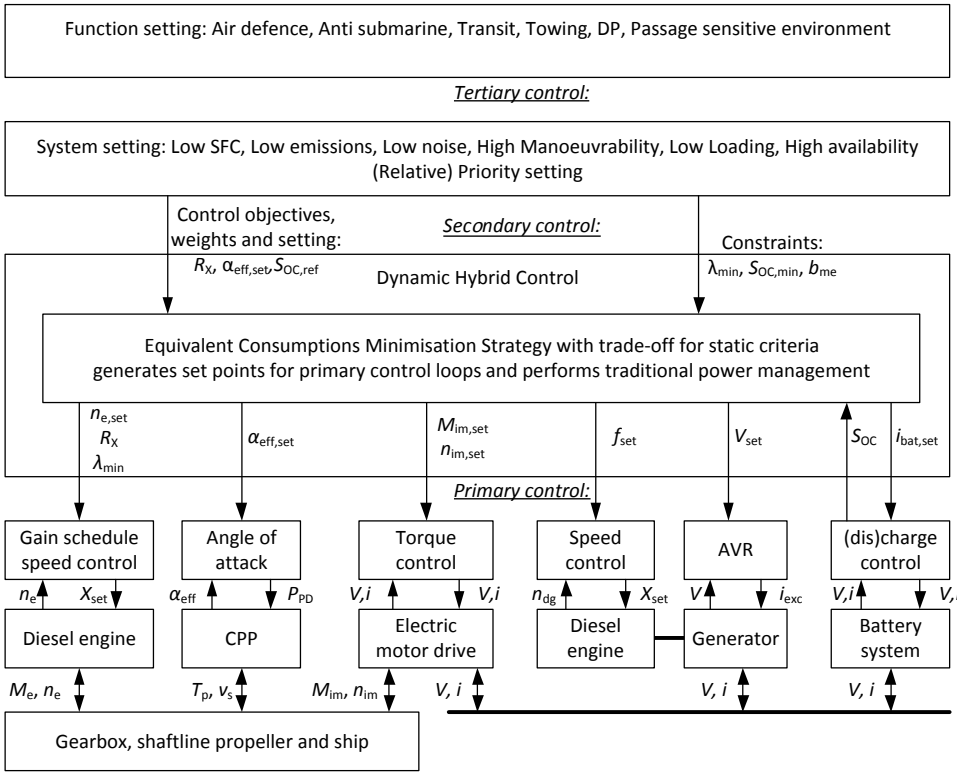

Legend:

α_{eff}	effective angle of attack	M_e	engine torque	S_{OC}	state of charge
λ_{min}	minimum air excess ratio	M_{im}	induction machine torque	$S_{OC,min}$	minimum state of charge
b_{me}	main engine on or off	n_{dg}	diesel generator speed	$S_{OC,ref}$	reference state of charge
f	Frequency	n_e	engine speed	T_p	propeller thrust
i	current	n_{im}	induction machine speed	V	voltage
i_{bat}	battery current	P_{pd}	propeller pitch ratio	v_s	ship speed
i_{exc}	excitation current	R_X	fuel increase rate limit	X_{set}	setpoint

Figure 7.1: Schematic presentation of proposed adaptive layered control strategy.

control above minimum speed as proposed in Chapter 4 and 5, with limitations for the fuel increase rate R_X and minimum air excess ratio λ_{min}. The CPP is controlled with *PI* control to maintain the desired effective angle of attack α_{eff}. The induction machine and its frequency converter are controlled with *PI* torque control when the main engine is running, and and additonal *PI* speed control loop when the induction machine is solely driving the shaft, in both cases using direct field oriented control, although any other modern machine drive control technique could also be used. The diesel generator is controlled with PI speed control to maintain the electrical network frequency and perform load sharing between multiple generators and with an Automatic Voltage Regulator (AVR) to maintain the electrical network voltage, although electrical system dynamics and generator engine

dynamics have not been addressed in this dissertation. Finally, the battery uses current control, while, again, the electrical system dynamics are not considered. In summary, all primary control strategies use existing *PI* control and receive their setpoints and, in some cases, limitations from the secondary control layer, therefore existing primary control equipment can be used.

- The secondary control layer provides the setpoints for the primary control layer and uses the Equivalent Consumption Minimisation Strategy (ECMS) proposed in Chapter 6. While the ECMS in Chapter 6 just considered fuel consumption and CO_2 emissions, future algorithms can also consist of an objective function that also considers NO_x emissions, engine running hours, engine loading and battery lifetime. Such a multi-objective optimisation would then utilise weight factors between the various objectives, which could depend on system settings. This control layer could be implemented on a programmable logic controller (PLC) as an extension of existing power management control and could also include traditional power management functions, such as the automatic starting and stopping of generators, voltage and frequency control and system protection as discussed in Section 2.3.3.

- The tertiary control layer provides the adaptivity to changing system settings and their priorities. While the details of this layer have not been worked out in this dissertation, this layer ensures for example that when low noise has a high priority that the effective angle of attack α_{eff} is maintained at its optimum value and the fuel increase rate limitation is maintained at its lowest value $R_{\text{X,cav}}$, while for high manoeuvrability the fuel increase rate limitation is allowed at its higher value $R_{\text{X,therm}}$ and the minimum air excess ratio λ_{min} might be relaxed to a lower value, in particular if low loading has a low priority. Similarly, the weights for the multi-objective ECMS could be changed depending on the system settings. In summary, the tertiary control setting translates system settings into control objectives, control objective weights, controller settings and constraints, which can be implemented in the integrated platform management system (IPMS) layer of the control system (Skowronek *et al.* 2016).

- Finally, the functional layer needs to translate the ships function into system setting and priorities, in order to prevent an operator is required to select the system settings, and to support more autonomous operation. This functional layer is envisioned to be part of the common services layer in the GAUDI architecture as proposed in Skowronek *et al.* (2016).

7.9. RECOMMENDATIONS FOR FUTURE WORK

7.9.1. CONTROLLABLE PITCH PROPELLER

CHAPTER 4 has demonstrated and discussed how *adaptive pitch control* (APC) can be used to contribute to the urgently required reduction of environmental impact while also improving acceleration performance and reducing engine thermal loading. In order to implement this strategy on future ships we propose the following future work:

- Experiments on engine testbeds should establish how much NO_x, smoke and particulate matter (PM) emissions can be reduced with this strategy, as an initial analysis in this chapter suggests the proposed approach can be used to address the quasi-static trade-off between fuel consumption and NO_x emissions based on static maps, and the smooth torque trajectory due to slow integrating speed control is expected to have a positive impact on smoke and PM emissions. Only very complex models in combination with experiments can accurately predict NO_x, smoke and PM emissions, due to the local effects in the combustion process. Therefore, we propose to derive static NO_x maps by running the considered engine across its operating enveloppe on a test bed, as opposed to only running the engine on the propeller curve or generator speed as dictated by classification societies and we propose to investigate the relationship between the air excess ratio λ and smoke and PM emissions by applying load steps, representative for the acceleration manoeuvres proposed in this dissertation, for example using the proposed propulsion system simulation model to generate the load for the load bank;

- In order to limit engine thermal loading more accurately based an a charge pressure based map approach, the exact relation between charge pressure and engine thermal loading, indicated by exhaust valve and exhaust receiver temperatures should be established with simulation studies verified by experiments, to improve the fuel injection limitation that prevents engine thermal overloading. Thus, the particular influence of cooling by the scavenge flow can be taken into account;

- The simulation studies in this dissertation assumed the actual angle of attack α_{eff} is available for the APC control strategy. While the experimental study in Vrijdag *et al.* (2010) demonstrated how the angle of attack can be established by measuring thrust and shaft speed and using the open water diagram of the propeller, the accuracy of the proposed approach needs to be established. Moreover, the simulation studies in this dissertation confirmed that the current pitch actuation is too slow to actually follow wake speed fluctuations due to waves as previously concluded in Vrijdag *et al.* (2010). Therefore, we propose to either consider developing faster pitch actuation in order to strive for pitch actuation that is fast enough to compensate wake speed fluctuation, while performing experimental studies to confirm continuous actuation does not cause increased wear on the propeller pitch actuation as concluded in Godjevac, (2009) and Godjevac *et al.* (2009), or to investigate the possibility of estimating the undisturbed wake flow, for example using extended Kalman filtering (EKF) techniques.

- APC compensates the pitch reduction during acceleration with an increase in engine speed, in order to maintain the virtual shaft speed n_{virt}. This interaction between the pitch setpoint and the engine speed setpoint, through the physical mechanism of the effective angle of attack α_{eff} can lead to an overshoot in the virtual shaft speed and thus ship speed during accelerations, as illustrated in Figure 4.5 and Figure 4.6. During the investigation of the sensitivity of the simulation results to various parameters, we found that the magnitude of the overshoot and the possibility of limiting this overshoot through controller settings very strongly depends on the value of the Vrijdag coefficient c_1 that is used to calibrate the effective

angle of attack with the cavitation bucket. We propose to perform a stability analysis to investigate the limitations that this mechanism causes for the application and parametrisation of APC, using the linear analysis proposed in Stapersma *et al.* (2017) and Vrijdag *et al.* (2017).

7.9.2. HYBRID PROPULSION

Chapter 5 has demonstrated how PAPC uses the combination of APC and parallel torque control of the electric drive to reduce acceleration time and engine thermal loading for hybrid propulsion with CPP. The reduction in acceleration time and engine thermal loading and the reduction of cavitation risk with the PAPC strategy strongly depends on the use of the controllable pitch propeller (CPP). As such, hybrid propulsion with a fixed pitch propeller (FPP) would not be able to achieve similar performance across all MOPs, as it lacks the degree of freedom in control to change engine speed for a given engine load. For ships with FPP, therefore, the only degree of freedom in control to improve acceleration performance is to use the electric drive torque to reduce engine load or increase engine speed during acceleration. This could be achieved with an additional torque provided by the electric drive, proportional to the error between the requested and actual virtual shaft speed. Alternatively, Model Predictive Control could be used to establish a torque setpoint trajectory for the electric drive using a cost function that weighs the cost of electric drive torque against the cost of the virtual shaft speed error, while constraining the increase rate and maximum torque of the electric drive. The propulsion system model could be based on the linearised propulsion system model proposed in Stapersma *et al.* (2017) and Vrijdag *et al.* (2017), updating the model parameters every time step, using measurements. The study should include an analysis wether this would lead to a robust control strategy, also under uncertainties due to weather conditions and measurement inaccuracies with an FPP and whether such an MPC strategy could also provide a slight improvement for the PAPC strategy with a CPP.

7.9.3. HYBRID POWER SUPPLY

Chapter 6 has demonstrated and discussed how energy management strategies can be used to reduce fuel consumption and CO_2 emissions for ships with hybrid propulsion and hybrid power supply with a fixed pitch propeller (FPP) and an engine with a limited operating envelope. Future work should focus on extending the energy management strategies to further cases, such as ships with controllable pitch propellers (CPP) and engines with wide operating envelopes, and on addressing the trade-off with other MOEs, such as manoeuvrability, radiated noise and thermal loading, as follows:

- The robustness analysis showed that the proposed energy management strategy can be improved by either including adaption of the equivalence factor based on remaining mission time or using a predictive approach with a prediction horizon as long as the time between recharging opportunities. Future work should focus on developing an algorithm that adapts the equivalence factor based on the SOC and remaining mission time or uses a predictive approach with a time window similar to mission length.

- The results in Chapter 6 suggest that for an engine with a small operating envelope and for a propulsion plant with a fixed pitch propeller, energy management has limited freedom of control to reduce fuel consumption and emissions. Future work should establish whether an engine with a wider operating envelope, for example due to sequential turbocharging as discussed in Geertsma *et al.* (2017d) provides additional benefits for energy management strategies.

- An energy management strategy for hybrid propulsion with a controllable pitch propeller (CPP) can also use propeller pitch P_{pd} or effective angle of attack α_{eff} as an additional degree of freedom in control. Future work should establish what reductions in fuel consumption and CO_2 emissions can be achieved with an energy management strategy that also uses CPP and how this energy management strategy, possibly in combination with the lower level strategies proposed in Chapter 4 and Chapter 5, can achieve an adaptive trade-off between MOEs fuel consumption, emissions, manoeuvrability, radiated noise and thermal loading. The dynamic simulation models proposed in Chapter 3 can then be used to also analyse dynamic performance and determine whether engine thermal loading can be reduced and acceleration times improved with hybrid propulsion and power generation.

- Energy management strategies are particularly focussed on minimising fuel consumption and CO_2 emissions. However, the approach is equally applicable to minimise any other MOP that can be described in a convex function of variables engine speed and power. For example, required maintenance for diesel engine or lifetime of batteries could be included in the instantaneous optimisation algorithm, either for a simple maintenance model based on running hours or a complex maintenance model that depends on engine speed and load. Future work should therefore be focussed on developing engine maintenance and battery lifetime models that can be included in the static instantaneous optimisation algorithms of ECMS. The dynamic performance in Measures of Performance that cannot be captured in quasi static maps, such as acceleration time and engine thermal loading, can then be achieved with primary control strategies such as adaptive pitch control (APC) and parallel adaptive pitch control (PAPC).

- The controller design should be included in optimisation studies of the hybrid propulsion and power generation plant, in order to determine to optimal sizing for the main engines, induction machines, diesel generators and batteries.

The case studies in this PhD thesis only used diesel engines for combustion power supply and batteries for energy storage. However, the proposed modelling approach can also be used to establish the dynamic performance of gas or dual fuel engines or gas turbines for combustion power supply, ultra capacitors or flywheels for stored power supply and could even include electrochemical power supplies, once dynamic fuel cell models have been developed and validated. The dynamic models of gas engines and fuel cells currently under development in the TU Delft GasDrive project could therefore be used for future multi-objective trade-off studies on hybrid power supply.

7.9.4. ELECTRICAL SYSTEM DYNAMICS

In this PhD thesis, electrical system dynamics were not considered, because the main focus was on quantifying MOEs related to the propulsion system and its diesel engines. Therefore, electrical system modelling was reduced to quasi static fuel consumption and efficiency maps. When electrical system dynamics need to be considered, for example to establish characteristics such as voltage and frequency stability or thermal loading of the diesel generators, dynamic simulation models should be developed. We propose the following dynamic models to be developed to model AC electrical system dynamics:

- The engine dynamics could be established with the diesel engine model proposed in Chapter 3, as this model in combination with a *PI* controller accurately represents engine dynamics and thus can be used to establish engine mechanical and thermal loading, electrical frequency and active power dynamics, for example for load sharing;
- The voltage dynamics could be established with a state space model of the typical synchronous generator in the dq-reference frame, similar to the induction machine model. This model could be used to establish the voltage stability of the system and to determine how energy storage can be used to improve voltage and frequency stability and to provide continuity of power supply during failure of a diesel generator.

The case studies in this PhD thesis only considered AC electrical systems. DC electrical systems allow to run the diesel engine at variable speed, potentially leading to a reduction in fuel consumption, emissions, noise and engine mechanical and thermal loading and should therefore be considered for future power supply systems. The dynamic models of DC electrical system components, currently under development in the TU Delft ShipDrive project could be used to perform similar studies that include DC electrical system dynamics (Haseltalab *et al.* 2017b, 2016).

7.9.5. LAYERED CONTROL STRATEGY

Section 7.9.3 has proposed to include alternative objectives in ECMS and to combine the ECMS with PAPC to enable an adaptive trade-off between MOEs fuel consumption, CO_2, NO_x, smoke and PM emissions, manoeuvrability, radiated noise, propulsion availability and maintainability due to engine mechanical and thermal loading. Future work should be focussed on the further validation and development of the proposed adaptive layered control strategy, as follows:

- A simulation study for a case study frigate can be used to establish the feasibility of combining the PAPC strategy with ECMS for a frigate with hybrid propulsion and hybrid power supply. While energy management in charge sustaining conditions for the case study tug hardly reduced fuel consumption, energy management might provide fuel savings for a ship with hybrid propulsion and power generation with CPP, due to the extra degree of freedom in control provided by propeller pitch and by an engine with a large operating envelope, for example due to sequential turbocharging;

- Various scenarios of operation should be established for ships with multiple functions and the optimum system setting should be established for each of these functions. Measurements from existing ships could be used to define typical operating scenarios, such as the operating profile of the case study tug in Section 6.4.1. In a similar approach, integrated platform management system (IPMS) loggings of frigates and patrol vessels could be used to define typical operating scenarios for frigates and patrol vessels. The simulation models proposed in Chapter 3 can then be used to compare system performance in these operating scenarios for various controller settings;
- The optimal relationships between control objectives, weights, setting and constraints and system settings could be established from the simulation studies discussed above and the tertiary control layer should be developed. Subsequently, the relationship between system settings and ship function should be established. Finally, the defined operating scenarios should be simulated while only providing the ship function as an input to the control strategy, thus validating the proposed approach.

After validating the proposed approach with the future work proposed above, the functional design for the hybrid propulsion and power supply could be included in the various design stages for future ships and further increase in technology readiness level could be achieved by hardware-in-the-loop studies to test the control strategies on real hardware and by validation studies on experimental facilities.

7.10. CLOSING SUMMARY

IN short, this thesis has first proposed a methodology to quantify performance improvements in fuel consumption, emissions, radiated noise, propulsion availability, manoeuvrability and maintainability due to applying hybrid propulsion and power generation architectures with autonomous control strategies for adaptive ships, and, second, proposed three novel control strategies that use the degrees of freedom in control from the controllable pitch propeller with *adaptive pitch control* (APC), the power split between the main engine and electric drive in hybrid propulsion with *parallel adaptive pitch control* (PAPC) and the power split between all power sources in hybrid power generation with the *equivalent consumption minimisation strategy* (ECMS), and, finally, proposed a layered control strategy that can autonomously adapt to various ship functions using APC and PAPC in its primary control layer and ECMS in its secondary control layer. The simulation studies have demonstrated that:

- for the case study patrol vessels, APC can reduce fuel consumption by 5% to 15% compared to the baseline transit mode in the ship speed range from 6 to 15 kts, and can reduce acceleration time from 0 to 15 kts with the slam start procedure by 32% compared to the baseline manoeuvre mode and by 84% for an intermediate acceleration from 10 to 15 kts, without thermally overloading the engine.
- for the case study frigate, PAPC can achieve twice as fast acceleration as the baseline mechanical speed control (MSC), while better limiting engine thermal loading and thus causing less smoke and particulate matter (PM) emissions, can achieve

the best possible fuel consumption in any condition at transit speeds above 15 kts and enable a further fuel consumption and emission reduction of 7% and significant reduction in diesel generator running hours, in combination with an engine with a wide operating envelope, and finally, can reduce the risk of cavitation by running the propeller within the cavitation bucket up to 18 kts, while accelerating as fast as baseline MSC.

- for the case study tug, ECMS can achieve fuel savings and associated CO_2 emission reductions of 5% to 10% for a typical operating profile, within 1-2% of the global optimum solution.

The proposed control strategies can all be combined in the adaptive layered control strategy proposed in Figure 7.1 for a ship with hybrid propulsion and hybrid power supply. This layered control strategy can adapt to changing ship functions autonomously if the proposed functional control layer is developed during the detailed design of a ship in order to link ship functions to system settings. The proposed hybrid propulsion and power generation architectures and associated control strategies can therefore contribute significantly to the urgently required reduction of the impact of shipping on the environment, while more autonomously achieving its increasingly diverse missions at sea with better manoeuvrability, higher availability and reduced maintenance. This will enable future shipping to achieve sustainable worldwide transport and to harvest more urgently required renewable energy from sources abundantly available in the worlds oceans.

ACKNOWLEDGEMENTS

THE research in this dissertation is part of the research programme 'ShipDrive: A Novel Methodology for Integrated Modelling, Control, and Optimisation of Hybrid Ship Sys- tems' with project number 13276, which is partly financed by the Netherlands Organisation for Scientific Research (NWO), domain Applied and Engineering Sciences (TTW) and by the Royal Netherlands Navy.

Figure 2.9, ©IFAC 2001, was reproduced from van Spronsen *et al.* 2001 with permission. Shipdrive partners Royal Netherlands Navy, IMTECH Marine and Damen Shipyards supplied Figure 1.1, 2.18 and 2.21. Special thanks goes to Youri Linden for preparing Figure 2.3.

The Royal Netherlands Navy supplied Figure 3.21. Figure 3.7, ©IFAC 2001, was reproduced from van Spronsen *et al.* 2001 with permission. Special thanks goes to Maarten de Boer and Ilham Hardy of Shipdrive Partner Damen Schelde Naval Shipbuilding for preparing and providing the validation data in FAT and SAT measurements in Chapter 3 and to dr. Arthur Vrijdag and prof. Douwe Stapersma for reviewing the manuscript of Geertsma *et al.* (2017c) and providing advice to improve the scientific quality and readability of that article, which forms the basis of Chapter 3.

Special thanks goes to dr. Arthur Vrijdag for providing advice to improve the scientific quality and readability of Geertsma *et al.* (2018), which forms the basis of Chapter 4.

Damen Shipyards supplied Figure 6.1. Special thanks goes to Damen Shipyards group for supplying all relevant information about the hybrid tug, along with their data logs regarding usual operating conditions in the port of Rotterdam, onboard measurements used for calibration of the gearbox model, sea trial data to calibrate the resistance curve and the commercially operated rule-based controller which have contributed to Kalikatzarakis *et al.* (2018), which forms the basis for Chapter 6.

A

CONVEXITY OF THE OPTIMISATION PROBLEM

A.1. INTRODUCTION

In Chapter 6 we aim to solve the mixed-integer non-linear Equivalent Consumption Minimisation Strategy (ECMS) problem for a ship with hybrid propulsion and power generation. The solution method proposed in Chapter 6 requires convex functions for the sub-models in the Branches of the complete problem formulation. Below, we give a mathematical proof that the continuous relaxation of the ECMS optimisation problem is convex and we discuss the assumption of a constant equivalence factor. This appendix is organised as follows: First, we introduce the definitions and theorems for the convexity proof in Section A.2. Then Section A.3 demonstrates that we can split the problem into three subproblems and proving convexity for each subproblem suffices to prove convexity of the combined problem. Then, we prove convexity for the three subproblems in Section A.4, A.5 and A.6. Finally, we discuss the impact of assuming a constant equivalence factor in Section A.7.

A.2. DEFINITIONS & THEOREMS

Below we have listed the necessary definitions and theorems for our proof:

Definition 1 (Convexity) *A function f is convex if dom f is a convex set and if for all $x,y \in$ dom f, and θ with $0 \leq \theta \leq 1$ we have:*

$$f\left(\theta x + (1-\theta)\, y\right) \leq \theta f(x) + (1-\theta)\, f(y).$$

Definition 2 (Positive semi-definite matrix) *A symmetric $n \times n$ real matrix M is said to be positive semi-definite if the scalar $z^T M z$ is non-negative for every non-zero column vector z of n real values.*

Parts of this chapter have been published in Control Engineering Practice **76** (2018) Kalikatzarakis *et al.* (2018).

A

Theorem 1 (First-order conditions) *Supposing f is differentiable (i.e., its gradient ∇f exists at each point in dom f, which is open). Then f is convex if and only if dom f is convex and:*

$$f(y) \geq f(x) + \nabla f(x)^{\intercal}(y - x).$$

for all $x, y \in \text{dom } f$.

Theorem 2 (Second-order conditions) *Supposing f is twice differentiable, that is, its Hessian or second derivative $\nabla^2 f$ exists at each point in dom f. Then f is convex if and only if dom f is convex and its Hessian is positive semidefinite.*

Theorem 3 (Convexity preservation: Weighted sums) *If $f_1, f_2, \ldots f_n$ are convex functions and $w_1, w_2, \ldots w_n \geq 0$, then the weighted sum:*

$$f = w_1 f_1 + \ldots + w_n f_n$$

is convex.

Theorem 4 (Convexity preservation: Composition) *Given the functions g in dom g and h in dom h, function f, defined by:*

$$f(x) = (h \circ g)(x) \text{ with } dom f = \{x \in dom\ g \mid g(x) \in dom\ h\},$$

is convex when one of the following statements is valid:

- *h is convex, $\tilde{h}$ is non-decreasing, and g is convex.*
- *h is convex, $\tilde{h}$ is non-increasing, and g is concave.*

where $\tilde{h}$ denotes the extended-value extension of function h, which assigns the value $+\infty$ $(-\infty)$ to points not in dom h for h convex (concave).

A.3. CONVEXITY OF THE PROBLEM

To assist readability, we use different notation to address each function and the decision variables, according to Table A.1. We will consider only the most general case for which all the components are operating. However, it will become evident that convexity holds for any combination of operating components.

The control objective can be written as follows:

$$f(x, y) = 2f_1(x) + f_2(x, y) + f_3(y),$$

according to the definitions in Table A.1.

According to Theorem 3, we need to show that each of $f_i,\ i = 1, 2, 3$ are convex. One complication is that Theorem 3 refers to functions defined on the same domain, which is not the case for f_1 and f_3. However, Theorem 3 applies in this case as well. If $f(x)|x \in \mathbb{F}$ and $g(y)|y \in \mathbb{G}$ are convex $h(x, y) = f(x) + g(y)$ is also convex in the domain $\{x \in \mathbb{F}|y \in \mathbb{G}\}$ by definition:

Let $z_1 = (x_1, y_1)$ and $z_2 = (x_2, y_2)$, then:

Table A.1: Notation used in this section.

Reference	New symbol
M_{im}	x
P_{bat}	y
$\dot{m}_{\text{f,eqv}}(M_{\text{im}})$	$f(x)$
$\dot{m}_{\text{f,e}}(M_{\text{im}})$	$f_1(x)$
$\dot{m}_{\text{f,dg}}(M_{\text{im}}, P_{\text{bat}})$	$f_2(x,y)$
$\dot{m}_{bat}(P_{\text{bat}})$	$f_3(y)$
$P_{\text{im,loss}}(M_{\text{im}})$	$q(x)$

$$
\begin{aligned}
h(\theta z_1 + (1-\theta) z_2) = h\left(\theta x_1 + (1-\theta) x_2, \theta y_1 + (1-\theta) y_2\right) = \\
= f(\theta x_1 + (1-\theta) x_2) + g\left(\theta y_1 + (1-\theta) y_2\right) \leq \\
\theta f(x_1) + (1-\theta) f(x_2) + \theta g(y_1) + (1-\theta) g(y_2) = \\
= \theta h(z_1) + (1-\theta) z_2
\end{aligned}
$$

A.4. MAIN DIESEL ENGINE FUEL CONSUMPTION

Function $f_1(x)$ can be written as a scalar composition of two functions, g and h, and convexity can be proven using Theorem 4. $g(x)$ refers to the normalised main engine power output as a function of induction machine torque output, and $h(g(x))$ indicates main engine's fuel consumption, as a function of power output and shaft speed (see equation (6.1):

$$
\begin{aligned}
f_1(x) &= (h \circ g)(x), \\
&\quad \text{with } dom f_1 = \{x \in dom\ g \mid g(x) \in dom\ h\} \\
h(z) &= c_0 + c_1 z + c_2 z^2, z \in (0, +\infty) \\
&\quad \text{where:} \quad c_0 = \dot{m}_{\text{f,nom}} b_{\text{e}} \left(a_0 + a_1 n^*_{sh}\right) \\
&\qquad\qquad\ \ c_1 = \dot{m}_{\text{f,nom}} b_{\text{e}} \left(a_2 + a_5 n^*_{sh}\right) \\
&\qquad\qquad\ \ c_2 = \dot{m}_{\text{f,nom}} b_{\text{e}} a_4 \\
g(x) &= c_3 - c_4 x, \ x \in [M_{\text{IM,min}}, M_{\text{IM,max}}] \\
&\quad \text{where:} \quad c_3 = P_{\text{p,dem}} \\
&\qquad\qquad\ \ c_4 = 2\pi n_{\text{sh}},
\end{aligned}
$$

and where $z = P_{\text{e}}$ is only meaningful when $z \in [0,1]$ i.e within the operating envelope of the engine. However, fuel consumption (function h) values are also defined outside this domain, which helps prove its convexity. The following applies:

- g is linear, therefore both convex and concave; and
- h is continuous and twice differentiable, with a positive second derivative $\frac{d^2h}{dz^2} = c_2 = a_4 \dot{m}_{\text{f,nom}}$. As such, it is convex and non-decreasing in $\mathbb{R}_{++}$.

Since g is both convex and concave, and h is convex and non-decreasing, f_1 is convex.

A

A.5. DIESEL - GENERATOR FUEL CONSUMPTION

Following the same procedure, $f_2(x)$ is written as $(h \circ g)(x,y)$. Here $g(x,y)$ refers to the normalised diesel generator's power output, being a function of the induction machine torque and battery power. $h(g(x,y))$ refers to fuel consumption as a function of power output from equation (6.4). Therefore:

$$
\begin{aligned}
f_2(x) &= (h \circ g)(x,y), \\
&\quad \text{with } dom f_2 = \{(x,y) \in dom\ g \mid g(x,y) \in dom\ h\} \\
h(z) &= b_{\text{dg}}\left(a_0 + a_1 z + a_2 z^2\right), z \in (0,1] \\
&\quad \text{where: } a_i > 0,\ i = 0,1,2 \text{ are given by equation (6.4)} \\
g(x,y) &= c_0 x + c_1 q(x) - y + c_2, \\
&\quad x \in [M_{\text{im,min}}, M_{\text{im,max}}], y \in [P_{\text{bat,min}}, P_{\text{bat,max}}] \\
&\quad \text{where:} \quad c_0 = b_{\text{im}} 4\pi n_{\text{sh}}, c_1 = 2b_{\text{im}}, c_2 = P_h b_{\text{im}} \\
&\qquad\qquad q(x) = c_{00} + c_{01} x + c_{02} x^2 \\
&\quad \text{with:} \quad \frac{c_{00}}{P_{\text{im,loss nom}}} = \left(a_{i1} n_{\text{sh}}^* + a_{i3} n_{\text{sh}}^{*2}\right) \\
&\qquad\qquad c_{01} = \frac{P_{\text{im,loss nom}}}{M_{\text{im,nom}}}\left(a_{i2} + a_{i5} n_{\text{sh}}^*\right) \\
&\qquad\qquad c_{02} = P_{\text{im,loss nom}} \frac{a_{i4}}{M_{\text{im,nom}}^2} \\
&\qquad\qquad a_{ij},\ i = 1,2\ \&\ j = 1,2,3,4,5.
\end{aligned}
$$

We can show that h is convex and non-decreasing in a similar way. Only proof that $g(x,y)$ is convex is needed and will be presented: g is twice differentiable for $\forall x,y \in \{\text{dom } g | x \neq 0\}$. For $x = 0$, the following applies:

$$
\begin{aligned}
\lim_{x \to 0^-}\left(g(x,y)\right) &= c_1 c_{00} + c_2 - y \\
\lim_{x \to 0^+}\left(g(x,y)\right) &= c_1 c_{00} + c_2 - y
\end{aligned}
$$

Since $c_{00} = f(a_{i1}, a_{i3})$ is the same both for motoring and generating conditions, then:

$$
\lim_{x \to 0^-}\left(g(x,y)\right) = \lim_{x \to 0^+}\left(g(x,y)\right)\ \forall y \in \text{dom } g.
$$

Furthermore:

$$
\begin{aligned}
\lim_{\epsilon \to 0}\left(\frac{g(0+\epsilon,y) - g(0,y)}{\epsilon}\right) &= c_0 + c_{01} \\
\lim_{x \to 0^-}\left(\frac{\partial g(x,y)}{\partial x}\right) = \lim_{x \to 0^+}\left(\frac{\partial g(x,y)}{\partial x}\right) &= c_0 + c_1 c_{01} \\
\lim_{\epsilon \to 0}\left(\frac{\frac{\partial g(0+\epsilon,y)}{\partial x} - \frac{\partial g(0,y)}{\partial x}}{\epsilon}\right) &= 2c_{02}.
\end{aligned}
$$

Since $c_{02} = f(a_{i4})$ changes value around $x = 0$, the first derivative of g is not differentiable. Therefore, we will use Theorem 1.

Let $z_1 = (x_1, y_1)$ and $z_2 = (x_2, y_2)$, then:

$$\left.\begin{array}{c} g(z_2) \geq g(z_1) + \nabla^{\mathsf{T}} g(z_1)(z_2 - z_1) \\ \\ \nabla g(z) = \begin{bmatrix} \dfrac{\partial g(z)}{\partial x} \\ \\ \dfrac{\partial g(z)}{\partial y} \end{bmatrix} = \begin{bmatrix} c_0 + c_1\,(c_{01} + 2x c_{02}) \\ -1 \end{bmatrix} \end{array}\right\} \Rightarrow$$

$$\begin{gathered} c_0 x_2 + c_1 q(x_2) - y_2 + c_2 \geq c_0 x_1 + c_1 q(x_1) - y_1 + c_2 + \\ + (c_0 + c_1\,(c_{01} + 2x_1 c_{02}))\,(x_2 - x_1) - (y_2 - y_1) \Rightarrow \\ \Rightarrow c_1 c_{02}\,(x_1 - x_2)^2 \geq 0, \end{gathered}$$

which is true for $\forall x_1, x_2 \in \text{dom}\ g$, considering:

- $c_1 = 2 > 0$; and
- $c_{02} = f(a_{i4}) > 0$ for both motoring and generating conditions, since $a_{i4} > 0,\ i = 1, 2$.

As such, g is convex, and since h is both convex and non-decreasing, f_2 is convex.

A.6. BATTERY EQUIVALENT FUEL CONSUMPTION

f_3 is a function of y of the following form:

$$f_3(y) = c_1 \frac{y}{\left(c_{00} + c_{01}|y| + c_{02}|y|^2\right)^{\text{sgn}(y)}},\ y \in [P_{\text{bat,min}}, P_{\text{bat,max}}]$$

where:
$$c_1 = \eta_{\text{rec}} \frac{s}{Q_{\text{lhv}}}$$
$$c_{00} = a_0$$
$$c_{01} = \frac{a_1}{n_s n_p}$$
$$c_{02} = \frac{a_2}{(n_s n_p)^2}$$
with $a_i,\ i = 0, 1, 2$.

f_3 is differentiable for $\forall y \in \{\text{dom}\ f_3 \mid y \neq 0\}$. For $y = 0$, the following apply:

$$\lim_{y \to 0^-} (f_3(y)) = \lim_{y \to 0^+} (f_3(y)) = 0$$
$$\lim_{\epsilon \to 0^+} \left(\frac{f_3(0+\epsilon) - f_3(0)}{\epsilon} \right) = \frac{c_1}{c_{00}}$$
$$\lim_{\epsilon \to 0^-} \left(\frac{f_3(0+\epsilon) - f_3(0)}{\epsilon} \right) = c_1 c_{00}.$$

Since $c_{00} = a_0 = 1$, then:

$$\lim_{\epsilon \to 0^+} \left(\frac{f_3(0+\epsilon) - f_3(0)}{\epsilon} \right) = \lim_{\epsilon \to 0^-} \left(\frac{f_3(0+\epsilon) - f_3(0)}{\epsilon} \right) = c_1.$$

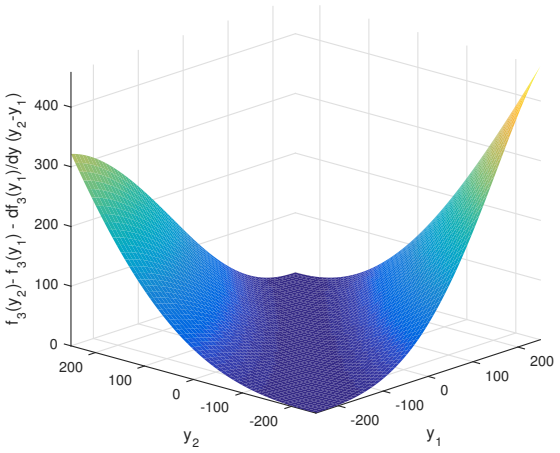

Figure A.1: Left hand-side of equation (A.1).

Therefore, f_3 is differentiable for $\forall\, y \in \text{dom}\, f_3$, with:

$$\frac{\partial f_3}{\partial y} = \frac{1}{\left(c_{00} + c_{01}|y| + c_{02}|y|^2\right)^{\text{sgn}(y)}} - \\ - y\left(\text{sgn}(y)\frac{c_{01}\text{sgn}(y) + 2c_{02}|y|\text{sgn}(y)}{\left(c_{00} + c_{01}|y| + c_{02}|y|^2\right)^{\text{sgn}(y)+1}}\right).$$

Convexity can be proven using Theorem 1:

$$f_3(y_2) \geq f_3(y_1) + \frac{\partial f_3}{\partial y}(y_1)(y_2 - y_1) \Rightarrow \\ \Rightarrow f_3(y_2) - f_3(y_1) - \frac{\partial f_3}{\partial y}(y_1)(y_2 - y_1) \geq 0. \tag{A.1}$$

Due to the complexity of the functions involved, the inequality was not solved analytically. Plotting the left-hand side over the whole range of (y_1, y_2), shown in Figure A.1, it can be seen that the inequality holds for $\forall\, y \in \text{dom}\, f_3$. Since all f_1, f_2, f_3 are convex, $f(x, y)$, being $\dot{m}_{\text{f,eqv}}$, is convex as well.

The power to the main diesel engine is a linear function of the power of the induction machine, therefore it is both convex and concave. The same applies to the constraint for the state of charge of the battery, which is a linear function of the battery power. Therefore, all the constraints of the problem, along with the objective function are convex.

A.7. CONSTANT EQUIVALENCE FACTOR s

In the following, we will explain why a constant equivalence factor can be considered for this optimal control problem using Pontryagin's Minimum Prinicple (PMP). PMP redefines the problem in terms of necessary local conditions, expressed by a set of first-order differential equations and an instantaneous minimisation (Kirk, 2012; Zak, 2003).

The *Hamilton-Jacobi-Bellman* (HJB) equation, indicates that searching for the optimal control input can be done by minimising the Hamiltonian:

$$u^*(t) = \underset{u(t)\in\mathscr{U}}{\operatorname{argmin}}\, H(t, x(t), u(t), r(t)), \tag{A.2}$$

where U is the set of admissible control values. From the Hamiltonian we can derive derive necessary, *but not sufficient*, conditions for optimality on u and s, as PMP shows:

$$\dot{x}^*(t) = \left.\frac{\partial H}{\partial s}\right|_{u^*(t)} = f\left(t, x^*(t), u^*(t)\right) \tag{A.3}$$

$$\begin{aligned}\dot{s}^*(t) = &-\left.\frac{\partial H}{\partial x}\right|_{u^*(t)} = -\frac{\partial L}{\partial x}\left(u^*(t), t\right) - \\ &- s^*(t)\frac{\partial f}{\partial x}\left(x^*(t), u^*(t), t\right)\end{aligned} \tag{A.4}$$

$$\begin{aligned}&H\left(t, u^*(t), x^*(t), s^*(t)\right) \le H\left(t, u(t), x^*(t), s^*(t)\right), \\ &\forall u(t) \in U(t),\ \forall t \in \left[t_0, t_f\right]\end{aligned} \tag{A.5}$$

$$x(t_0) = x_0,\ x(t_f) = x_{\text{final}}, \tag{A.6}$$

where L is the instantaneous cost, $x = S_{OC}$ is the state variable, and f represents the right hand side of the system dynamic equation. Considering the simple battery model, which consists of one constant resistor, the state of charge variation is:

$$\begin{aligned}\dot{x}^*(t) = \frac{\partial S^*_{OC}}{\partial t} &= -\frac{1}{\eta_{\text{bat}}^{sgn(i_{\text{bat}}(t))}}\frac{i_{\text{bat}}(t)}{Q_{\text{bat,nom}}} = \\ &= -\frac{1}{Q_{\text{bat,nom}}\eta_{\text{bat}}^{sgn(P^*_{\text{bat}}(t))}} \times \\ &\times\left(\frac{u_{\text{oc}}(x)}{2R} - \sqrt{\left(\frac{u_{\text{oc}}(x)}{2r}\right)^2 - \frac{P^*_{\text{bat}}(t)}{n_{\text{s}}n_{\text{p}}r}}\right),\end{aligned} \tag{A.7}$$

where the open cell voltage u_{oc} and battery efficiency are given by equations (3.94) - (6.5), respectively. Therefore:

$$\frac{\partial \dot{x}^*(t)}{dx} = \frac{\partial f}{\partial x}\left(x^*(t), u^*(t), t\right) = -\frac{1}{Q_{\text{bat,nom}}\eta_{\text{bat}}^{sgn(P^*_{\text{bat}}(t))}}$$

$$\frac{\partial}{\partial x}\left(\frac{u_{\text{oc}}(x(t))}{2r} - \sqrt{\left(\frac{u_{\text{oc}}(x(t))}{2r}\right)^2 - \frac{P^*_{\text{bat}}(t)}{n_{\text{s}}n_{\text{p}}r}}\right) =$$

$$= \frac{4\left(n_{\text{s}}n_{\text{p}}\right)^{\sigma_2}P^*_{\text{bat}}(t)}{Q_{\text{bat,nom}}} \times$$

$$\frac{\left(\frac{\nu_4}{2} + x^*(t)\nu_5 + \frac{\sigma_3}{2} + (\nu_4 + 2x^*(t)\nu_5 + \sigma_3\sigma_1)\frac{\sigma_5}{2\sigma_4} + \frac{\sigma_1}{2}\right)}{\left(a_0 n_{\text{s}}^2 n_{\text{p}}^2 + a_1 n_{\text{s}}n_{\text{p}}P^*_{\text{bat}}(t) + a_2 P^{*2}_{\text{bat}}(t)\right)^{sgn(P^*_{\text{bat}}(t))}}$$

A

$$\frac{1}{\left(v_3 + x^*(t)\,v_4 + \sigma_6 + x^*(t)^2\,v_5 + x^*(t)^3\,v_6 + \sigma_4\right)^2}, \tag{A.8}$$

where:

$$\begin{aligned}
\sigma_1 &= v_1 v_2 e^{v_2 x} \\
\sigma_2 &= 2sgn(P_B^*(t)) - 1 \\
\sigma_3 &= 3x^2 v_6 \\
\sigma_4 &= \sqrt{\sigma_5^2 - \frac{4RP_B^*(t)}{n_s n_p}} \\
\sigma_5 &= v_3 + x v_4 + \sigma_6 + x^2 v_5 + x^3 v_6 \\
\sigma_6 &= v_1 e^{v_2 x}
\end{aligned}$$

Using equation (A.4), we derive:

$$\dot{s}^*(t) = -\left.\frac{\partial H}{\partial x}\right|_{u^*(t)} = -\cancelto{0}{\frac{\partial L}{\partial x}} - s^*(t)\frac{\partial f}{\partial x} \Rightarrow \frac{\dot{s}^*(t)}{s^*(t)} = -\frac{\partial f}{\partial x} \tag{A.9}$$

The right hand side of equation (A.9), is given by equation (A.8), and is plotted in Figure A.2. As can be seen, its variation is relatively small compared to the absolute value of the equivalence factor (the value corresponding to the nominal sfc of the main engines is 2.36). To this end, we can safely assume that:

$$\frac{\dot{s}^*(t)}{s^*(t)} = -\frac{\partial f}{\partial x} \approx 0 \Rightarrow s^*(t) = \text{const} \tag{A.10}$$

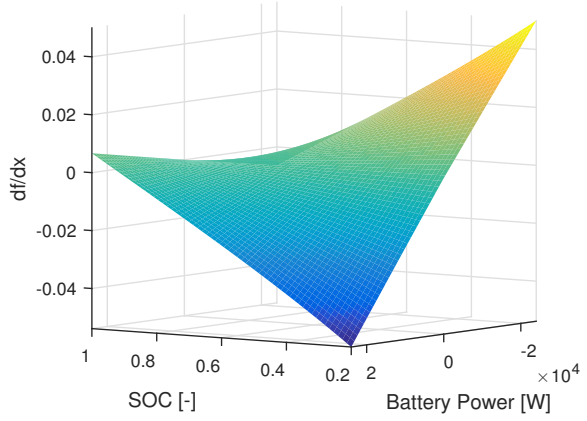

Figure A.2: Right hand-side of equation (A.9).

REFERENCES

Altosole, M., G. Benvenuto, M. Figari, and U. Campora (2009). "Real-time simulation of a COGAG naval ship propulsion system". In: *Proceedings of the Institution of Mechanical Engineers Part M: Journal of Engineering for the Maritime Environment*. Vol. 223:1, pp. 47–61.

Altosole, M., M. Figari, M. Martelli, and G. Orru (2012a). "Propulsion Control Optimisation for Emergency Manoeuvres of Naval Vessels". In: *Proceedings of the 11th International Naval Engineering Conference*.

Altosole, M., M. Marteli, and S. Vignolo (2012b). "A Mathematical Model of the Propeller Pitch Change Mechanism for the Marine Propulsion Control Design". In: *Proceedings of the 14th Congress of the International Maritime Association of the Mediteranean*. Vol. 2. Genova, Italy, pp. 649–656.

Altosole, M. and M. Martelli (2017). "Propulsion Control Strategies for Ship Emergency Manoeuvres". In: *Ocean Engineering*. Vol. 137, pp. 99–109.

Ambuhl, D. and L. Guzzella (2009). "Predictive reference signal generator for hybrid electric vehicles". In: *IEEE transactions on vehicular technology*. Vol. 58(9), pp. 4730–4740.

Ambuhl, D., A. Sciarretta, C. Onder, L. Guzzella, S. Sterzing, K. Mann, D. Kraft, and M. Kusell (2007). "A causal operation strategy for hybrid electric vehicles based on optimal control theory". In: *Proceedings of the 4th Symposium in Hybrid Vehicles and Energy Management*. Braunschweig, Germany, pp. 318–331.

Ambuhl, D., O. Sundstrom, A. Sciarretta, and L. Guzzella (2010). "Explicit optimal control policy and its practical application for hybrid electric powertrains". In: *Control Engineering Practice*. Vol. 18(12), pp. 1429–1439.

Amgai, R. and S. Abdelwahed (2014). "Power Management of Shipboard Power Systems Using Interaction Balance Principle". In: *Proceedings of the North American Power Symposium*. Pullman, Washington, USA, pp. 1–6.

Amini, H. and S. Steen (2012). "Theoretical and experimental investigation of propeller shaft loads in transient conditions". In: *International Shipbuilding Progress*. Vol. 59, pp. 55–82.

Asad, U. and M. Zheng (2014). "Exhaust Gas Reciculation for advanced diesel combustion cycles". In: *Applied Energy*. Vol. 123, pp. 242–252.

Astrom, K. J. and T. Hagglund (2001). "The future of PID control". In: *Control Engineering Practice*. Vol. 9(11), pp. 1163–1175.

Bakkeheim, J., T. A. Johansen, O. N. Smogelli, and A. J. Sorensen (2008). "Lyapunov-based integrator resetting with application to marine thruster control". In: *IEEE transactions on Control Systems Technology*. Vol. 16(5), pp. 908–917.

Baldi, F., H. Johnson, C. Gabrielii, and K. Andersson (2014). "Energy analysis of ship energy systems - the case of a chemical tanker". In: *International Journal of Thermodynamics*. Vol. 18(2), pp. 82–93.

Baldi, F., G. Theotokatos, and K. Andersson (2015). “Development of a Combined Mean Value-Zero Dimensional Model and Application for a Large Marine Four-Stroke Diesel Engine Simulation”. In: *Applied Energy*. Vol. 154, pp. 402–415.

Barcellos, R. (2013). “The hybrid propulsion system as an alternative for offshore vessels servicing and supporting remote oil field operations”. In: *Proceedings of the Annual Offshore Technology Conference*. Vol. 3. Houston, Texas, USA, pp. 1622–1631.

Barsingerhorn, J. S., J. S. Limburg, E. C. de Man, and V. A. Wieleman (2015). “Turbodrive”. BSc Thesis. The Netherlands: Faculty Mechanical, Maritime and Materials Engineering, Delft University of Technology.

Baumann, B., G. Rizzoni, and G. Washington (1998). “Intelligent control of hybrid vehicles using neural networks and fuzzy logic”. In: *SAE Technical Papers*.

Benvenuto, G. and U. Campora (2002). “Dynamic simulation of a high-performance sequentially turbocharged marine diesel engine”. In: *International Journal of Engine Research*. Vol. 3(3), pp. 115–125.

Benvenuto, G., U. Campora, and A. Trucco (2014). “Comparison of ship planting layouts for power and propulsion systems with energy recovery”. In: *Journal of Marine Engineering and Technology*. Vol. 13(3), pp. 3–15.

Betz, A. and G. Woschni (1986). “Energy Conversion Rate and Rate of Heat Release of Turbocharged Diesel Engines under Transient Conditions”. In: *MTZ Motortechnische Zeitschrift*. Vol. 47(7-8), pp. 263–267.

Blanke, M. and P. B. Nielsen (1990). “The marine engine governor”. In: *Proceedings of the 2nd Maritime Communications and Control Conference*, pp. 11–19.

Blanke, M., L. Pivano, and T. A. Johansen (2007). “An efficiency optimizing propeller speed control for ships in moderate seas - model experiments and simulation”. In: *IFAC Proceedings Volumes*. Vol. 7(1), pp. 329–336.

Blaschke, F. (1974). “New Method of Regulation for Rotating Field Machines”. In: *Siemens Forsch Entwicklungsbericht, Research Development Report*. Vol. 3(5), pp. 327–332.

Boonen, H.J. (2016). “Development of a hybrid propulsion simulation model”. In: *Proceedings of the 13th International Naval Engineering Conference*. Britsol, UK.

Bosich, D. and G. Sulligoi (2013). “Voltage Control on a Refitted Luxury Yacht Using Hybrid Electric Propulsion and LVDC Distribution”. In: *Proceedings of the 8th International Conference Ecological Vehicles and Renewable Energies*. Monte Carlo, Monaco, pp. 1–6.

Breijs, A. and E. El Amam (2016). “Energy Management - adapt your engine to every mission”. In: *Proceedings of the 13th International Naval Engineering Conference*. Bristol, UK, pp. 1–8.

Brynolf, S., F. Baldi, and H. Johnson (2016). “Shipping and the Environment”. In: Springer, Berlin, Heidelberg. Chap. Energy Efficiency and Fuel Changes to Reduce Environmental Impacts, pp. 295–339.

Burmeister, H.-C., W. Bruhn, O. J. Rodseth, and T. Porathe (2014). “Autonomous Unmanned Merchant Vessel and its Contribution towards the e-Navigation Implementation: the MUNIN Perspective”. In: *International Journal of e-Navigation and Maritime Economy*. Vol. 1, pp. 1–13.

Butcher, M., R. Maltby, and P. S. Parvin (2009). "Compact DC Power and Propulsion Systems - The Definitive Solution?" In: *Proceedings of the 3rd Engine As A Weapon Symposium*. Portsmouth, UK.

Caledonian Maritime Assets Limited (2015). "Hybrid Ferries Project".

Campora, U. and M. Figari (2003). "Numerical simulation of ship propulsion transients and full-scale validation". In: *Proceedings of the Institution of Mechanical Engineers, Part M: Journal of Engineering for the Maritime Environment*. Vol. 217:1, pp. 41–52.

Capasso, C. and O. Veneri (2014). "Experimental analysis on the performance of lithium based batteires for road full electrc and hybrid vehicles". In: *Applied Energy*. Vol. 136, pp. 921–930.

Capasso, C., O. Veneri, E. Notti, A. Sala, M. Figari, and M. Martelli (2016). "Preliminary design of the hybrid propulsion architecture for the research vessel G. Dalaporta". In: *Proceedings of the ESARS-ITEC 2016 Conference*. Toulouse, France.

Carlton, J. S. (2012). "Marine Propulsion and Propellers". In: 3rd. London, UK: Butterworth Heinemann.

Castles, G. and A. Bendre (2009). "Economic Benefits of Hybrid Drive Propulsion for Naval Ships". In: *Proceedings of the IEEE Electric Ship Technologies Symposium*. Baltimore, Maryland, USA, pp. 515–520.

Chasse, A., P. Pognant-Gros, and A. Sciarretta (2009). "Online implementation of an optimal supervisory control for a parallel hybrid powertrain". In: *SAE International Journal of Engines*. Vol. 2(1), pp. 1630–1638.

Chasse, A. and A. Sciarretta (2011). "Supervisory control of hybrid powertrains: An experimental benchmark of offline optimization and online energy management". In: *Control Engineering Practice*. Vol. 19(11), pp. 1253–1265.

Chen, L., T. L. Yip, and J. Mou (2017). "Provision of Emission Control Area and the impact on shipping route choice and ship emissions". In: *Transportation Research Part D: Transportation and the Environment*. Vol. in press.

Chen, S. and P. Flynn (1965). "Development of a Single Cylinder Compression Ignition Research Engine". In: *SAE Technical Paper of Combined Powerplant and Transportation Meeting*. Cleveland, Ohio, USA.

Cignitti, S., J. G. Andreasen, F. Haglind, J. M. Woodley, and J. Abildskov (2017). "Integrated working fluid-thermodynamic cycle design of organic Rankine cycle power sytem for waste heat recovery". In: *Applied Energy*. Vol. 203, pp. 442–453.

Colonna, P. and H. van Putten (2007). "Dynamic Modelling of Steam Power Cycles. Part I - Modelling Paradigm and Validation". In: *Applied Thermal Engineering*. Vol. 27(2), pp. 467–480.

Concli, F. and C. Gorla (2016). "Numerical Modelling of the Power Losses in Geared Transmissions: Windage, Churning and Cavitation Simluations with a New Integrated Approach that Drastically Reduces the Computational Effort". In: *Tribology International*. Vol. 103, pp. 58–68.

Coraddu, A., G. Dubbioso, S. Mauro, and M. Viviani (2013). "Analysis of twin screw ships asympetric propeller behaviour by means of free running model tests". In: *Ocean Engineering*. Vol. 68, pp. 47–64.

Coraddu, A., S. Gaggero, D. Villa, and M. Figari (2011). "A new approach in engine-propeller matching". In: *Proceedings of the 14th International Congress of the International Maritime Association of the Mediterranean, IMAM 2011*. Vol. 2, pp. 631–637.

Curley, R. (2012). "The Complete History of Ships and Boats". In: New York, New York, USA: Britannica Educational Publishing.

Danan, F. G. A., A. V. Weston, and B. N. J. Longepépé (2005). "The Electric Ship Technology Demonstrator Or How Two MoDs Are Derisking The All Electric Warship Concept". In: *Proceedings of the IMarEST All Electric Ship Conference 2005*. Versailes, France, pp. 109–125.

Dang, J., H. J. J. van den Boom, and J. Th. Ligtelijn (2013). "The Wageningen C- and D-Series Propellers". In: *Proceedings of the 12th FAST Conference*. Amsterdam, the Netherlands.

Dang, J., J. Brouwer, R. Bosman, and C. Pouw (2012). "Quasi-Steady Two-Quadrant Open Water Tests for the Wageningen Propeller C- and D-series". In: *Proceedings of the 29th Symposium on Naval Hydrodynamics*. Gothenburg, Sweden.

de Boer, M. J. and I. Hardy (2011). *Final dynamic simulations PS*. Tech. rep. E40800 / E1200.58. Damen Schelde Naval Shipbuilding.

de Groote, D. and R. van Koperen (2014). "Fuel Economy: hybrid solutions and beyond". In: *Proceedings International Tug Salvage & OSV Convention*. Hamburg, Germany, pp. 1–10.

De La Fuente, S. S. and A. R. Greig (2015). "Making shipping greener: comparative study between organic fluids and water for Rankine cycle waste heat recovery". In: *Journal of Marine Engineering and Technology*. Vol. 14:2, pp. 70–84.

Dedes, E. K., D. A. Hudson, and S. R. Turnock (2012). "Assessing the potential of hybrid energy technology to reduce exhaust emissions from global shipping". In: *Energy Policy*. Vol. 40, pp. 204–218.

Deleroi, K. H. E. (1995). "Simulation Study of Acceleration and Crash Stop Manoeuvres for Ship Machinery Systems." MSc Thesis. the Netherlands: Faculty Mechanical, Maritime and Materials Engineering, Delft University of Technology.

Delprat, S., T. M. Guerra, and J. Rimaux (2002). "Control strategies for hybrid vehicles: optimal control". In: *Proceedings of the 56th IEEE Vehicular Technology Conference*. Vol. 3, pp. 1681–1685.

Dib, W., A. Chasse, P. Moulin, A. Sciarretta, and G. Corde (2014). "Optimal energy management for an electric vehicle in eco-driving applications". In: *Control Engineering Practice*. Vol. 29, pp. 299–307.

Ding, Y. (2011). "Characterising Combustion in Diesel Engines". PhD thesis. The Netherlands: Faculty Mechanical, Maritime and Materials Engineering, Delft University of Technology.

Ding, Y., D. Stapersma, and H. T. Grimmelius (2012). "Using parametrized finite combustion stage models to characterize combustion in diesel engines". In: *Energy & Fuels*. Vol. 26, pp. 7099–7106.

Dixon, S. L. (1998). *Fluid mechanics and thermodynamics of thermomachinery*. 4th. Butterworth Heinemann.

Doerry, N., H. Robey, J. Amy, and C. Petry (1996). "Powering the Future with the Integrated Power System". In: *Naval Engineers Journal*, pp. 267–282.

Drijver, J. (2013). “Evaluation of Transmission Losses, Heat Flows and Temperatures of Propulsion Drive Lines”. MSc Thesis. The Netherlands: Faculty Mechanical, Maritime and Materials Engineering, Delft University of Technology.

Du, X. and W. Chen (2002). “Efficient Uncertainty Analysis Methods for Multidisciplinary Robust Design”. In: *AIAA journal*. Vol. 40(3), pp. 545–552.

Elbert, P., S. Ebbesen, and L. Guzzella (2013). “Implementation of Dynamic Programming for n- Dimensional Optimal Control Problems With Final State Constraints”. In: *IEEE Transactions on Control Systems Technology*. Vol. 21(3), pp. 924–931.

Emadi, A., K. Rajashekara, S. S. Williamson, and S. M. Lukic (2005). “Topological overview of hybrid electric and fuel cell vehicular power system architectures and configurations.” In: *IEEE Transactions on Vehicuar Technokogy*. Vol. 54(3), pp. 763–770.

Erdinc, O., B. Vural, and M. Uzunoglu (2009). “A dynamic lithium-ion battery model considering the effects of temperature and capacity fading”. In: *Proceedings of the International Conference on Clean Electric Power*, pp. 383–386.

Faber, E. (1993). “Some Thoughts in Diesel Marine Engineering”. In: *SNAME Transactions*. Vol. 101, pp. 537–582.

Figari, M. and C. Guedes Soares (2009). “Fuel consumption and exhaust emissions reduction by dynamic propeller pitch control”. In: *2nd International Conference on Marine Structures-Analysis and Design of Marine Structures*, pp. 543–550.

Flower, J. and C. Hodge (2014). “Stability and transient-behavioural assessment of power-electronics based dc-distribution systems. Part 4: Simple compensation to improve system performance”. In: *Journal of Marine Engineering and Technology*. Vol. 13(2), pp. 3–11.

Formentin, S., J. Guanetti, and S. M. Savaresi (2016). “Least costly energy management for series hybrid electric vehicles”. In: *Control Engineering Practice*. Vol. 48, pp. 37–51.

Gaggero, S., G. Tani, M. Viviani, and F. Conti (2014). “A Study on the Numerical Prediction of Propellers Cavitating Tip Vortex”. In: *Ocean Engineering*. Vol. 92, pp. 137–161.

Gao, L., S. Liu, and R. A. Dougal (2002). “Dynamic lithium-ion battery model for system simulation”. In: *IEEE transactions on components and packaging technologies*. Vol. 25(3), pp. 495–505.

Gawn, R. W. L. (1952). “Effect of Pitch and Blade Width on Propeller Performance”. In: *Transactions RINA*, pp. 157–193.

Geertsma, R. D. and N. A. Badon Ghijben (2014). “Experiences on Implementation of Electronic Incident Boards in the Royal Netherlands Navy”. In: *Proceedings of the 12th International Naval Engineering Conference*. Amsterdam, the Netherlands.

Geertsma, R. D., R. R. Negenborn, K. Visser, and J. J. Hopman (2016). “Torque Control for Diesel Mechanical and Hybrid Propulsion for Naval Vessels”. In: *Proceedings of the 13th International Naval Engineering Conference*. Bristol, UK, pp. 476–492.

— (2017a). “Design and Control of Hybrid Power and Propulsion Systems for Smart Ships: a Review of Developments”. In: *Applied Energy*. Vol. 194, pp. 30–54.

— (2017b). “Parallel Control for Hybrid Propulsion of Multifunction Ships”. In: *IFAC Proceedings Volumes*. Vol. 50(1), pp. 2296–2303.

Geertsma, R. D., R. R. Negenborn, K. Visser, and J. J. Hopman (2017c). "Pitch control for ships with mechanical and hybrid propulsion: Modelling, validation and performance quantification". In: *Applied Energy*. Vol. 206, pp. 1609–1631.

Geertsma, R. D., K. Visser, and R. R. Negenborn (2018). "Adaptive pitch control for ship with diesel mechanical and hybrid propulsion". In: *Applied Energy*. Vol. 228, pp. 2490–2509.

Geertsma, R. D., J. Vollbrandt, R. R. Negenborn, K. Visser, and J. J. Hopman (2017d). "A quantitative comparison of hybrid diesel-electric and gas-turbine-electric propulsion for future frigates". In: *Proceedings of the 2017 IEEE Electric Ship Technologies Symposium*, pp. 451–458.

Geertsma, R. D., A. V. Weston, J. Devlin, and W. Wright (2009). "Power System Survivability - How Can We Deliver?" In: *Proceedings of the Engine As A Weapon III conference*. Portsmouth, UK.

Gemmell, G., B. McIntyre, and M. Reilly (2014). "Is IFEP a Realistic Future Propulsion System for Flexible Frigates and Destroyers?" In: *Proceedings of the 12th International Naval Engineering Conference*. Amsterdam, the Netherlands, pp. 688–700.

Georgescu, I., R. D. Geertsma, A. Hasseltalab, K. Visser, R. R. Negenborn, M. Godjevac, and J. J. Hopman (2015). "ShipDrive: Novel design and control strategies for complex maritime smart ship system integration". In: *SWZ Maritime*.

Georgescu, I., M. Godjevac, and K. Visser (2018). "Efficiency constraints of energy storage for on-board power systems". In: *Ocean Engineering*. Vol. 162, pp. 239–247.

Georgescu, I., M. Godjevac, K. Visser, and J. J. Hopman (2017). "Early Eficiency Estimation of Hybrid and Electric Propulsion Systems on Board Ships". In: *Proceedings of the IEEE VPPC conference*.

Georgescu, I., Stapersma, and B. Mestemaker (2016). "Dynamic Behaviour of Gas and Dual-Fuel Engines: Using Models and Simulations to Aid System Integration". In: *Proceedings of the 28th CIMAC World Congress*. 126. Helsinki, Finland, pp. 1–13.

Gerritsma, J. (1989). "Bewegingen en sturen 1 - Golven". In: MT513, report 473-K. Faculty Mechanical, Maritime and Materials Engineering, Delft University of Technology.

Gerritsma, J. and W. Beukelman (1972). "Analysis of the Resistance Increase in Waves of a Fast Cargo Ship". In: *International Shipbuilding Progress*. Vol. 19(217), pp. 285–293.

Ghojel, J. I. (2010). "Review of the development and applications of the Wiebe functions: a tribute to the contribution of Ivan Wiebe to engine research". In: *International Journal of Engine Research*. Vol. 11, pp. 297–312.

Godjevac, M. (2009). "Wear and Friction in a Controllable Pitch Propeller". PhD thesis. Faculty Mechanical, Maritime and Materials Engineering, Delft University of Technology.

Godjevac, M., T. van Beek, H. T. Grimmelius, T. Tinga, and D. Stapersma (2009). "Prediction of Fretting Motion in a Controllable Pitch Propeller during Service". In: *Proceedings IMechE Part M: Journal of Engineering for the Maritime Environment*. Vol. 223(4), pp. 541–560.

Godjevac, M., J. Drijver, L. de Vries, and D. Stapersma (2016). "Evaluation of Losses in Maritime Gearboxes". In: *Proceedings IMechE, part M: Journal of Engineering for the Maritime Environment*. Vol. 230(4), pp. 623–638.

Grimmelius, H. T., J. C. Bakker, and A. F. Wesselink (2006). "The use of non linear models in the analysis of CPP actuator behaviour". In: *Marine Engineering Systems*. IMarEST. London, UK, pp. 240–254.

Grimmelius, H. T., E. Mesbahi, P. J. M. Schulten, and D. Stapersma (2007). "The Use of Diesel Engine Simulation Models in Ship Propulsion Plant Design and Operation". In: *Proceedings of the 25th CIMAC World Congress*. Vienna, Austria.

Grimmelius, H. T. and D. Stapersma (2000). "Control Optimisation and Load Prediction for Marine Diesel Engines using a Mean Value First Principle Model". In: *Proceedings of the MS&TES Conference*. Newcastle-upon-Tyne, UK, pp. 212–219.

— (2001). "The Impact of Propulsion Plant Control on Diesel Engine Thermal Loading". In: *Proceedings of the 22nd CIMAC World Congress*. Hamburg, Germany.

Grimmelius, H. T., P. de Vos, M. Krijgsman, and E. van Deursen (2011). "Control of Hybrid Ship Drive Systems". In: *Proceedings of the 10th Conference on Computer and its Applications in the Maritime Industry*. Hamburg, Germany, pp. 1–14.

Grune, L. and J. Pannek, eds. (2011). *Nonlinear Model Predictive Control, Theroy and Algorithms*. Communications and Control Engineering. Springer.

Guan, C., G. Theotokatos, P. Zhou, and H. Chen (2014). "Computational Investigation of Large Containership Propulsion Engine Operation at Slow Steaming Conditions". In: *Applied Energy*. Vol. 130, pp. 370–383.

Guardiola, C., B. Pla, S. Onori, and G. Rizzoni (2014). "Insight into the HEV/PHEV optimal control solution based on a new tuning method". In: *Control Engineering Practice*. Vol. 29, pp. 247–256.

Guerrero, J. M., J. Vasquez, J. Matas, L. G. de Vicuna, and M. Castilla (2011). "Hierarchical Control of Droop-Controlled AC and DC Microgrids - A General Approach Towards Standardization". In: *IEEE Transactions on Industrial Electronics*. Vol. 58(1), pp. 158–172.

Guillemette, J. R. and P. Bussières (1997). "Proposed Optimal Controller for the Canadian Patrol Frigate Diesel Propulsion System". In: *Proceedings of the 11th Ship Control Systems Symposium*. Southampton, UK, pp. 507–530.

Guzzella, L. and C. Onder (2009). *Introduction to modeling and control of internal combustion engine systems*. Berlin, Germany: Springer.

Guzzella, L. and A. Sciarretta (2007). *Vehicle propulsion systems*. Vol. 1. Berlin, Germany: Springer.

Han, H., X. Hou, J. Yang and. J. Wu, M. Su, and J. M. Guerrero (2016). "Review of Power Sharing Control Strategies for Islanding Operation of AC microgrids". In: *IEEE Transactions on Smart Grid*. Vol. 7(1), pp. 200–215.

Haseltalab, A. and R. R. Negenborn (2017a). "Adaptive control for a class of partially unknown non-affine systems: applied to autonomous surface vessels". In: *IFAC Proceedings Volumes*. Vol. 50-1, pp. 4252–4257.

— (2017b). "Predictive On-Board Power Management for All-Electric Ships with DC Distribution Architecture". In: *Proceedings of the Oceans Conference*. Aberdeen UK.

Haseltalab, A., R. R. Negenborn, and G. Lodewijks (2016). "Multi-Level Predicitive Control for Energy Management of Hybrid Ship in the Presence of Uncertainty and Environmental Disturbances". In: *IFAC Proceedings Volumes*. Vol. 49(3), pp. 90–95.

Hasse, K. (1969). “About the dynamics of adjustable-speed drives with converter-fed squireel cage induction motors (in German)”. PhD. Disseration. Darmstadt Tehcnishce Hochschule.

Hebner, R. E., F. M. Uriarte, A. Kwasinski, A. L. Gattozzi, H. B. Estes, A. Anwar, P. Cairoli, R. A. Dougal, X. Feng, H.- M. Chou, L. J. Thomas, M. Pipattanasomporn, S. Rahman, F. Katiraei, M. Steurer, M. O. Faruque, M. A. Rios, G. A. Ramos, M. J. Mousavi, and T. J. McCoy (2016). “Technical Cross-Fertilization between Terrestrial Microgrids and Ship Power Systems”. In: *Journal of Modern Power Systems and Clean Energy*. Vol. 4(2), pp. 161–179.

Hendricks, E. (1997). “Engine Modelling for Control Applications: A Critical Survey”. In: *Meccanica*. Vol. 32, pp. 387–396.

Herdzik, J. (2013). “Problems of propulsion systems and main engines choice for offshore support vessels”. In: *Zeszyty Naukowe/Akademia Morska w Szczecinie*.

Herrera, L., W. Zhang, and J. Wang (2017). “Stability analysis and controller design of DC microgrids with constant power loads”. In: *IEEE Transactions on Smart Grid*. Vol. 8(2).

Heywood, J. B. *et al.* (1988). *Internal combustion engine fundamentals*. Vol. 930. New York, New York, USA: McGraw-Hill.

Hillier, F. S. (2012). *Introduction to operations research*. New York, New York, USA: McGraw-Hill Education.

Hodge, C. G. and D. J. Mattick (1996). “The Electric Warship”. In: *IMarE Transactions*. Vol. 108(2), pp. 109–125.

— (1997). “The Electric Warship II”. In: *IMarE Transactions*. Vol. 109(2), pp. 127–137.

— (1998). “The Electric Warship III”. In: *IMarE Transactions*. Vol. 110(2), pp. 119–134.

— (1999). “The Electric Warship IV”. In: *IMarE Transactions*. Vol. 111(1), pp. 25–39.

— (2000). “The Electric Warship V”. In: *IMarE Transactions*. Vol. 112(1), pp. 27–37.

— (2001). “The Electric Warship VI”. In: *IMarE Transactions*. Vol. 113(2), pp. 49–58.

— (2008). “The Electric Warship Then, Now and Later”. In: *Proceedings of the 9th International Naval Engineering Conference*. Hamburg, Germany, pp. 556–565.

Hofman, T. and N. H. J. Janssen (2017). “Integrated design optimization of the transmission system and vehicle control for electric vehicles”. In: *IFAC Proceedings Volumes*. Vol. 50(1), pp. 10072–10077.

Holtrop, J. (1984). “A statistical re-analysis of resistance and propulsion data”. In: *International Shipbuilding Progress*. Vol. 28(363), pp. 272–276.

Hu, X., S. Li, and H. Peng (2012). “A comparative study of equivalent circuit mdoels for Li-ion batteries”. In: *Journal of Power Sources*. Vol. 198, pp. 359–367.

IMO MEPC 72 (2018). *Initial Strategy on greenhouse gas emissions from ship*. Tech. rep. April: International Maritime Organisation (IMO).

Jager, B. D., T. V. Keulen, and J. T. B. A. Kessels (2013). *Optimal control of hybrid vehicles*. Springer.

Jamel, M. S., A. A. Rahman, and A. H. Shamsuddin (2013). “Advances in the integration of solar thermal energy with conventional and non-conventional power plants”. In: *Renewable and Sustainable Energy Reviews*. Vol. 20(C), pp. 71–81.

Jauch, C., S. Tamilarasan, K. Bovee, L. Guvenc, and G. Rizzoni (2016). “Design and verification of driveability improving control for the EcoCAR2 Hybrid Electric Vehicle”. In: *Proceedings of the 2016 American Control Conference*. Boston, MA, USA.

— (2018). “Modeling for drivability and drivability improving control of HEV”. In: *Control Engineering Practice*. Vol. 70, pp. 50–62.

Jensen, J. P., A. F. Kristensen, S. C. Sorenson, N. Houbak, and E. Hendricks (1991). “Mean Value Modelling of a Small Turbocharged Diesel Engine”. In: *SAE Technical Papers*.

Johannesson, L., N. Murgovski, E. Jonasson, J. Hellgren, and B. Egardt (2015). “Predictive energy management of hybrid long-haul trucks”. In: *Control Engineering Practice*. Vol. 41, pp. 83–97.

Kalikatzarakis, M. (2017). “Energy Management for Hybrid Tugs”. MSc thesis. Faculty Mechanical, Maritime and Materials Engineering, Delft University of Technology.

Kalikatzarakis, M., R. D. Geertsma, E.-J. Boonen, K. Visser, and R. R. Negenborn (2018). “Ship energy management for hybrid propulsion and power supply with shore charging”. In: *Control Engineering Practice*. Vol. 76, pp. 133–154.

Karim, N., R. Lisner, H. Kazemi, and F. Annaz (2002). “Rule-based Power Management for the All-Electric Ship”. In: *Proceedings of the Australian University Power Engineering Conference*. Melbourne, Australia.

Kermani, S., S. Delprat, T.-M. Guerra, R. Trigui, and B. Jeanneret (2012). “Predictive energy management for hybrid vehicle”. In: *Control Engineering Practice*. Vol. 20(4), pp. 408–420.

Kessels, J. T. B. A., M. W. T. Koot, and P. P. J. van den Bosch (2008). “Online energy management for hybrid electric vehicles”. In: *IEEE Transactions on vehicular technology*. 3428-3440, 57(6).

Kim, N., S. Cha, and H. Peng (2011). “Optimal Control of Hybrid Electric Vehicles Based on Pontryagin’s Minimum Principle”. In: *IEEE Transactions on Control Systems Technology*. Vol. 19(5), pp. 1279–1287.

Kirk, D. (2012). *Optimal control theory: an introduction*. New York, USA: Prentice Hall.

Klein Woud, H. and D. Stapersma (2012). “Design of Propulsion and Electric Power Generation Systems”. In: London, UK: IMarEST.

Ko, J., D. Jin, W. Jang, C.-L. Myung, S. Kwon, and S. Park (2017). “Comparitive investigation of NOx emission characteristics from a Euro 6-compliant diesel passenger car over the NEDC and WLTC at various ambient temperatures”. In: *Applied Energy*. Vol. 187, pp. 652–662.

Koot, M. W. T., J. T. B. A. Kessels, B. de Jager, W. Heemels, W. van den Bosch, and M. Steinbuch (2005). “Energy Management Strategies for Vehicular Electric Power Systems”. In: *IEEE Transactions on Vehicle Technology*. Vol. 54(3), pp. 1504–1509.

Koperen, R. M. van (2009). “Conceptual design of an Environmentally Friendly Harbour Tug”. MSc thesis. The Netherlands: Faculty Mechanical, Maritime and Materials Engineering, Delft University of Technology.

Kouroutzis, S. and K. Visser (2016). “The Dynamic Behavior of Diesel Engines on Ships in Adverse Conditions”. In: *Maritime Technology and Engineering III: 3rd International Conference on Maritime Technology and Engineering (MARTECH 2016)*. Lisbon, Portugal.

Kretschmann, L., H. Burmeister, and C. Jahn (2017). “Analyzing the economic benefit of unmanned autonomous ships: An exploratory cost-comparison between an autonomous and a conventional bulk carrier”. In: *Research in Transportation Business and Management*. Vol. 25, pp. 76–86.

Kuiper, G. (1992). *The Wageningen Propeller Series*. publication 92-001. MARIN.

Kumar, Y., J. Ringenberg, S. S. Depuru, V. K. Devabhanktuni, J. W. Lee, E. Nikolaidis, B. Andersen, and A. Afjeh (2016). "Wind energy: Trends and enabling technologies". In: *Renewable and Sustainable Energy Reviews*. Vol. 53(C), pp. 209–224.

Kyrtatos, N. P. and I. Koumbarelis (1994). "Performance Prediction of Next Generation Slow Speed Diesel Engines during Ship Manoeuvres". In: *Transactions IMarE*. Vol. 106(1), pp. 1–26.

Lan, H., S. Wen, Ying-Yi Hong, D. C. Yu, and L. Zhang (2015). "Optimal sizing of hybrid PV/diesel/battery in ship power system". In: *Applied Energy*. Vol. 158, pp. 26–34.

Lashway, C. R., A. T. Elsayed, and O. A. Mohammed (2016). "Hybrid energy storage management in ship power systems with multiple pulsed loads". In: *Electric Power Systems Research*. Vol. 141, pp. 50–62.

Leites, K., A. Bauschulte, M. Dragon, S. Krummrich, and P. Nehter (2012). "Schibz - Design of different diesel based fuel cell systems for seagoing vessels and their evaluation". In: *ECS Transactions*. Vol. 42(1), pp. 49–58.

Li, S., R. R. Negenborn, and G. Lodewijks (2017a). "Closed-loop coordination of inland vessels operations in large seaports using hybrid logic-based benders decomposition". In: *Transportation Research Part E: Logistics and Transportation Review*. Vol. 97, pp. 1–21.

— (2017b). "Planning inland vessel operations in large seaports using a two-phase approach". In: *Computers & Industrial Engineering*. Vol. 106, pp. 41–57.

Linden, Y. (2017). "NOx-emission prediciton in a diesel engine using a two zone in-cylinder simulation model". MSc Thesis. The Netherlands: Faculty Mechanical, Maritime and Materials Engineering, Delft University of Technology.

Liu, C., R. R. Negenborn, X. Chu, and H. Zheng (2017a). "Predictive path following based on adaptive line-of-sight for underactuated autonomous surface vessels". In: *Journal of Marine Science and Technology*. Vol. in press.

Liu, C., R. R. Negenborn, H. Zheng, and X. Chu (2017b). "A state-compensation extended state observer for model predictive control". In: *European Journal of Control*. Vol. 36, pp. 1–9.

Loon, P. T. van and P. van Zon (2016). "From operational profile to hybrid propulsion". In: *Proceedings of the 24th international HISWA symposium on yacht design and yacht construction*. Amsterdam, The Netherlands, pp. 1–13.

Loyd, C., R. Simpson, and G. Reid (2003). "The Type 45 Destroyer – Powering to Success". In: *Proceedings of the IMarEST All Electric Ship Conference 2003*. London, UK, pp. 198–207.

Maamria, D., A. Sciarretta, F. Chaplais, and N. Petit (2017). "Online Energy Management System (EMS) Including Engine and Catalysts Temperatures for a parallel HEV". In: *IFAC Proceedings Volumes*. Vol. 50(1), pp. 8913–8920.

Mahon, L. L. J. (1992). "Diesel Generator Handbook". In: 1st. Oxford, GB: Butterworth-Heinemann. Chap. Parallel Operation of Generating Sets.

MAN Diesel SE (2008a). *Operating and Maintenance Manual for Marine Plants Diesel Engine 28/33D*. Technical Report. Augsburg, Germany: MAN Diesel SE.

— (2008b). *Project Guide for Marine Plants Diesel Engine 28/33D Prelim*. Tech. rep. Augsburg, Germany: MAN Diesel SE.

Martelli, M. (2014). “Marine Propulsion Simulation”. In: Warsaw / Berlin: De Gruyter Open Ltd.

Martelli, M. and M. Figari (2017). “Real-time model-based design for CODLAG propulsion control strategies”. In: *Ocean Engineering*. Vol. 14, pp. 265–276.

Martelli, M., M. Figari, M. Altosole, and S. Vignolo (2014a). “Controllable pitch propeller actuating mechanism, modelling and simulation”. In: *Proceedings IMechE, Part M: Journal of Engineering for the Maritime Environment*. Vol. 228(1), pp. 29–43.

Martelli, M., M. Viviani, M. Altosole, M. Figari, and S. Vignolo (2014b). “Numerical modelling of propulsion, control and ship motions in 6 degrees of freedom”. In: *Proc IMechE, Part M: Journal of Eng. for the Maritime Environment* 228.4, pp. 373–397.

Mattick, D. J., M. Benatmane, N. McVea, and R. Gerrard (2005). “The Electric Ship Technology Demonstrator: 12 Inches To The Foot”. In: *Proceedings of the IMarEST All Electric Ship Conference 2005*. Versailles, France.

McCoy, T. J. (2002). “Trends in ship electric propulsion”. In: *Proceedings of the IEEE Power Engineering Society Transmission and Distribution Conference*. Vol. 1, pp. 343–346.

MER (2008). “Offshore Propulsion: Powering the Offshore Industry”. In: *Marine Engineers Review*, pp. 18–22.

Mestemaker, B. T. W. and I. Georgescu (2014). *Diesel and Dual Fuel Engine Model*. unpublished rep. Kinderdijk, The Netherlands: MTI Holland BV.

Miedema, S. A. and Z. Lu (2002). “The Dynamic Behaviour of a Diesel Engine”. In: *Proceedings of the WEDA XXII Conference*. Denver, Colorado, USA.

Miller, R. H. (1947). “Supercharging and internal cooling for high ouput”. In: *ASME Transactions*. Vol. 69, pp. 453–7.

Millo, F., F. Mallamo, E. Pautasso, and G. Ganio Mego (2006). “The Potential of Electric Exhaust Gas Turbocharging for HD Diesel Engines”. In: *SAE Technical Papers*. Detroit, Michigan, USA.

Mizuno, N., Y. Miyazaki, and Y. Kudo (2010). “Marine engine control with multivariable adaptive extremum control scheme”. In: *IFAC Proceedings Volumes*, pp. 155–160.

Mondejar, Maria E., F. Ahlgren, M. Thern, and M. Genrup (2017). “Quasi-steady state simulation of an organic Rankine cycle for waste heat recovery in a passenger vessel”. In: *Applied Energy*. Vol. 185(2), pp. 1324–1335.

Moreno, V. M. and A. Pigazo (2007). “Future Trends in Electric Propulsion Systems for Commercial Vessels”. In: *Journal of Maritime Research*. Vol. IV(2), pp. 81–100.

Murgovski, N., L. Johannesson, J. Sjoberg, and B. Egardt (2012). “Component sizing of a plug-in hybrid electric powertrain via convex optimization”. In: *Mechatronics*. Vol. 22, pp. 106–120.

Musardo, C., G. Rizzoni, Y. Guezennec, and B. Staccia (2005). “A-ECMS: An Adaptive Algorithm for Hybrid Electric Vehicle Energy Mangement”. In: *European Journal of Control*. Vol. 11, pp. 509–524.

Naval Sea Systems Command (NSSC) (2007). *Next Generation Integrated Power System Technology Development Roadmap*. report ADA519753.

Negenborn, R., Z. Lukszo, and H. Hellendoorn, eds. (2010). *Intelligent Infrastructures*. Vol. 42. Intelligent Systems, Control and Automation: Science and Engineering. Springer.

Nielsen, K. V., M. Blanke, and L. Eriksson (2017a). “Control-Oriented Model of Molar Scavenge Oxygen Fraction for Exhaust Recirculation in Large Diesel Engines”. In:

Transactions ASME, Journal of Dynamic Systems, Measurement and Control. Vol. 139, pp. 0210071–9.

Nielsen, K. V., M. Blanke, L. Eriksson, and M. Vejlgaard-Laursen (2017b). "Adaptive feedforward control of exhaust gas recirculation in large diesel engines". In: *Control Engineering Practice*. Vol. 65, pp. 26–35.

— (2018). "Marine diesel engine control to meet emission requirements and maintain maneuverability". In: *Control Engineering Practice*. Vol. 76, pp. 12–21.

Nuesch, T., M. Wang, P. Isenegger, C. H. Onder, R. Steiner, P. Macri-Lassus, and L. Guzzella (2014). "Optimal energy management for a diesel hybrid electric vehicle considering transient PM and quasi-static NOx emissions". In: *Control Engineering Practice*. Vol. 29, pp. 266–276.

Olivares, D. E., A. Mehrizi-Sani, A. H. Etemadi, C. A. Canizares, R. Iravani, M. Kazerani, A. H. Hajimiragha, O. Gomis-Bellmunt, M. Saeedifard, R. Palma-Behnke an G. A. Jimenez-Estevez, and N. D. Hatziargyriou (2014). "Trends in Microgrid Control". In: *IEEE Transactions on Smart Grid*. Vol. 5(4), pp. 1905–1919.

Ong, C.-M. (1998). "Dynamic Simulation of Electric Machinery". In: Upper Saddle River, NJ, USA: Prentice Hall PTR. Chap. 6, pp. 167–258.

Onori, S., L. Serrao, and G. Rizzoni (2016). *Hybrid Electric Vehicles: Energy Management Strategies*. Berlin, Germany: Springer.

O'Rourke, R. (2009). "Navy DDG-1000 and DDG-51 Destroyer Programs: Background, Oversight Issues, and Option for Congress". In: *Congressional Research Service, report ADA 500951*.

Öster, H. (2010). "Low Loss Concept Offers Improved Performance at Lower Cost". In: *Twentyfour7, Wärtsilä Stakeholder Magazine*. 3, pp. 45–47.

Ovrum, E. and T. F. Bergh (2015). "Modelling Lithium-Ion Battery Hybrid Ship Crane Operation". In: *Applied Energy*. Vol. 152, pp. 162–172.

Paganelli, G., S. Delprat, T. M. Guerra, J. Rimaux, and J. J. Santin (2002). "Equivalent Consumption Minimization Strategy For Parallel Hybrid Powertrains". In: *Proceedings of the 55th IEEE Vehicular Technology Conference*, pp. 2076–2081.

Paganelli, G., T. M. Guerra, S. Delprat, J. J. Santin, M. Delhom, and E. Combes (2000). "Simulation and assessment of power control strategies for a parallel hybrid car". In: *Proceedings IMechE Part D: Journal of Automobile Engineering*. Vol. 214(7), pp. 705–717.

Pang, K. M., N. Karvounis, J. H. Walther, and J. Schramm (2016). "Numerical Investigation of soot formation and oxidation processes under large two-stroke marine diesel engine-like conditions using integrated CFD-chemical kinetics". In: *Applied Energy*. Vol. 169, pp. 874–887.

Papalambrou, G., S. Samokhin, S. Topaloglou, N. Planakis, and K. Zenger (2017). "Model Predictive Control for Hybrid Diesel-Electric Marine Propulsion". In: *IFAC Proceedings Volumes*. Vol. 50-1, pp. 11064–11069.

Park, H., J. Sung, S. Pekarek, P. Stone, D. Opila, R. Meyer, I. Kolmanovsky, and R. DeCarlo (2015). "Real-Time Model Predictive Control for Shipboard Power Management Using the IPA-SQP Approach". In: *IEEE transactions on Control Systems Technology*. Vol. 23(6), pp. 2129–2143.

Parker, M. N., R. D. Geertsma, C. G. Hodge, A. Macalindin, and O. J. Simmonds (2009). "The impact of Future Combat System Loads on Power System Design". In: *Proceedings of the Engine As A Weapon III conference*. Portsmouth, UK.

Pasini, G., G. Lutzemberger, S. Frigo, S. Marelli, M. Ceraolo, R. Gentili, and M. Capobianco (2016). "Evaluation of an Electric Turbo Compound System for SI engines: A numerical Approach". In: *Applied Energy*. Vol. 162, pp. 527–540.

Patel, M. R. (2012). *Shipboard propulsion, power electronics, and ocean energy*. CRC Press.

Perera, L. P. and C. Guedes Soares (2017). "Weather routing and safe ship handling in the future of shipping". In: *Ocean Engineering*. Vol. 130, pp. 684–695.

Psoma, A. and G. Sattler (2002). "Fuel cell systems for submarines: from the first idea to serial production". In: *Journal of Power Sources*. Vol. 106, pp. 381–383.

Rampen, P. and A. Breijs (2014). "Energy Management System Optimising Trial Results". unpublished report.

Raptosasios, S., N. F. Sakellaridis, R. G. Papagiannakis, and D. T. Hountalas (2015). "Application of a multi-zone combustion model to investigate the NOx reduction potential of two-stroke marine diesel engines using EGR". In: *Applied Energy*. Vol. 157, pp. 814–823.

Ren, Y., L. Li, J. Brindley, and L. Jiang (2016). "Nonlinear PI control for variable pitch wind turbine". In: *Control Engineering Practice*. Vol. 50, pp. 84–94.

Roedler, G. J. and C. Jones (2005). *Technical Measurement, a coll. project of PSM, INCOSE and Industry*. Technical Report INCOSE-TP-2003-020-01 v1.0. INCOSE.

Roskilly, A. P., P. C. Taylor, and J. Yan (2015). "Energy storage systems for a low carbon future - in need of an integrated approach". In: *Applied Energy*. Vol. 137, pp. 463–466.

Rubis, C. J. and T. R. Harper (1986). "Governing Ship Propulsion Gas Turbine Engines". In: *SNAME Transactions*. Vol. 94, pp. 283–308.

Salman, M., N. J. Schouten, and N. A. Kheir (2000). "Control strategies for parallel hybrid vehicles". In: *Proceedings of the IEEE American Control Conference*. Vol. 1(6), pp. 524–528.

Sapra, H., M. Godjevac, K. Visser, D. Stapersma, and C. Dijkstra (2017). "Experimental and simulation-based investigations of marine diesel engine performance against static back-pressure". In: *Applied Energy*. Vol. 204, pp. 78–92.

Sattler, G. (2000). "Fuel cells going on-board". In: *Journal of Power Sources*. Vol. 86, pp. 61–67.

Scappin, F., S. H. Stefansson, F. Haglind, A. Andreasen, and U. Larsen (2012). "Validation of a Zero-Dimensional Model for Predicition of NOx and Engine Performance for Electronically Controlled Marine Two-Stroke Diesel Engines". In: *Applied Thermal Engineering*. Vol. 37, pp. 344–252.

Schlesinger, S., R. E. Crosbie, R. E. Gagne, G. S. Innis, C. S. Lalwani, J. Loch, R. J. Sylvester, R. D. Wright, N. Kheir, and D. Bartos (1979). "Terminology for model credibility". In: *Simulation*, pp. 103–104.

Schulten, P. J. M. (2005). "The Interaction between Diesel Engines, Ship and Propellers during Manoeuvring". PhD thesis. Faculty Mechanical, Maritime and Materials Engineering, Delft University of Technology.

Schulten, P. J. M., R. D. Geertsma, and K. Visser (2017). "Energy As A Weapon, part 2". In: *Proceedings of the Engine As A Weapon VII conference*. Bristol, UK.

Schulten, P. J. M. and D. Stapersma (2003). "Mean Value Modelling of the gas exchange of a 4-stroke diesel engine for use in powertrain applications". In: *SAE Technical Papers*.

— (2007). "A study of the validity of a complex simulation model". In: *Journal of Marine Engineering and Technology*. Vol. 10.

Sciarretta, A., M. Back, and L. Guzzella (2004). "Optimal control of parallel hybrid electric vehicles". In: *IEEE Transactions on control systems technology*. Vol. 12(3), pp. 352–363.

Sciarretta, A. and L. Guzzella (2007). "Control of hybrid electric vehicles". In: *IEEE Control systems*. Vol. 27(2), pp. 60–70.

Sciarretta, A., L. Serrao, P. C. Dewangan, P. Tona, E. N. D. Bergshoeff, C. Bordons, L. Charmpa, P. Elbert, L. Eriksson, T. Hofman, *et al.* (2014). "A control benchmark on the energy management of a plug-in hybrid electric vehicle". In: *Control Engineering Practice*. Vol. 29, pp. 287–298.

Scibberas, E. A., B. Zahawi, D. J. Atkinson, and A. Juando (2015). "Electric auxiliary propulsion for improved fuel efficiency and reduced emissions". In: *Proceedings IMechE Part M: Journal of Engineering for the Maritime Environment*. Vol. 229(1), pp. 36–44.

Sciberras, E. A. and R. A. Norman (2012). "Multi-Objective Design of a Hybrid Propulsion System for Marine Vessels". In: *IET Electrical Systems in Transportation*. Vol. 2(3), pp. 148–157.

Sears, L. C., R. D. Gerrard, B. G. Salter, and C. New (2010). "Integrating the Power and Propulsion System for the Queen Elizabeth Class Aircraft Carriers". In: *Proceedings of the 10th International Naval Engineering Conference*. Portsmouth, UK, pp. 432–440.

Seenumani, G., J. Sun, and H. Peng (2012). "Real-time Power Management of Integrated Power Systems in All Electric Ship Leveraging Multi Time Scale Property". In: *IEEE transactions on Control Systems Technology*. Vol. 20(1), pp. 232–240.

Serrao, L., C. J. Hubert, and G. Rizzoni (2007). "Dynamic modeling of heavy-duty hybrid electric vehicles". In: *Proceedings of the ASME International Engineering congress and Expo*. Vol. 16, pp. 121–128.

Serrao, L., A. Sciarretta, O. Grondin, A. Chasse, Y. Creff, D. Di Domenico, P. Pognant-Gros, C. Querel, and L. Thibault (2013). "Open issues in supervisory control of hybrid electric vehicles: A unified approach using optimal control methods". In: *Oil and Gas Science and Technology*. Vol. 68(1), pp. 23–33.

Shaheen, S. A. and T. E. Lipman (2007). "Reducing greenhouse emissions and fuel consumption: Sustainable approaches for surface transportation". In: *IATSS Research*. Vol. 31(1), pp. 6–20.

Shi, W. (2013). "Dynamics of energy system behaviour and emissions of trailing suction hopper dredgers". PhD thesis. The Netherlands: Faculty Mechanical, Maritime and Materials Engineering, Delft University of Technology.

Shi, W., H. T. Grimmelius, and D. Stapersma (2010). "Analysis of Ship Propulsion System Behaviour and the Impact on Fuel Consumption". In: *International Shipbuilding Progress*. Vol. 57, pp. 35–64.

Shi, W., X. Xie, C.-C. Chu, and R. Gadh (2015). "Distributed Optimal Energy Management in Microgrids". In: *IEEE Transactions on Smart Grid*. Vol. 6(3), pp. 1137–1146.

Shiraishi, K., S. Minami, K. Kobayashi, and M. Kodera (2013). "Development of A Hybrid Tugboat Propulsion System". In: *MTZ industrial*. Vol. 3(2), pp. 36–43.

Shu, G., Y. Liang, H. Wei, J. Zhao, and l. Liu (2013). “A review of waste heat recovery on two-stroke IC engine aboard ships”. In: *Renewable and Sustainable Energy Reviews*. Vol. 19, pp. 385–401.

Silvas, E., T. Hofman, N. Murgovski, L. F. P. Etman, and M. Steinbuch (2017). “Review of Optimization Strategies for System-Level Design in Hybrid Electric Vehicles”. In: *IEEE Transactions on Vehicuar Technokogy*. Vol. 66(1), pp. 57–70.

Silvas, E., T. Hofman, A. Serebrenik, and M. Steinbuch (2015). “Functional and Cost-based Automatic Generator for Hybrid Vehicles Topologies”. In: *IEEE/ASME Transactions on Mechatronics*. Vol. 20, pp. 1561–1572.

Simmonds, O. J. (2014). “DC: Is it the Alternative Choice for Naval Power Distribution?” In: *Journal of Marine Engineering and Technology*. Vol. 13:3, pp. 37–43.

Singh, A., B. Grant, R. DeFour, C. Sharma, and S. Bahadoorsingh (2016). “A review of Induction Motor Fault Modelling”. In: *Electric Power Systems Research*. Vol. 133, pp. 191–197.

Sivertsson, M. and L. Eriksson (2015). “Design and evaluation of energy management using map-based ECMS for the PHEV benchmark”. In: *Oil and Gas Science and Technology*. Vol. 70(1), pp. 195–211.

Skaar, I., K. Angeltveit, and M. Urheim (2012). “Wärtsilä LLC Helps Achieve Highest Possible ERN Number”. In: *Wärtsilä Technical Journal*. 1, pp. 40–46.

Skowronek, J., M. Ditzel, J. C. Scheurs, L. Franke, and P. Rozendaal (2016). “GAUDI: innovative architecture for integrated maritime mission systems in support of advanced optimised manning concepts”. In: *Proceedings of the 13th International Naval Engineering Conference*. Bristol, UK.

Smogeli, O. N., A. J. Sorensen, and K. J. Minsaas (2008). “The concept of anti-spin thruster control”. In: *Control Engineering Practice*. Vol. 16, pp. 465–481.

Sorensen, A. J. (2005). “Structural issues in the design and operation of marine control systems”. In: *Annual reviews in control*. Vol. 29, pp. 125–149.

Sorensen, A. J. and O. N. Smogeli (2009). “Torque and power control of electrically driven marine propellers”. In: *Control Engineering Practice*. Vol. 17, pp. 1053–1064.

Stapersma, D. (1994). “The importance of (e)mission profile for naval ships”. In: *Proceedings of the 7th International Naval Engineering Conference*. Plymouth, UK, pp. 83–100.

— (2005). “Matching Propulsion Engine with Propulsor”. In: *Journal of Marine Engineering and Technology*. Vol. 4(2), pp. 25–32.

— (2010a). *Diesel Engines - A Fundamental Approach to Performance Analysis, Turbocharging, Combustion, Emissions and Heat Transfer*. 8th print. Vol. 1: Performance Analysis. NLDA.

— (2010b). *Diesel Engines - A Fundamental Approach to Performance Analysis, Turbocharging, Combustion, Emissions and Heat Transfer*. 8th print. Vol. 2: Turbocharging. NLDA.

— (2010c). *Diesel Engines - A Fundamental Approach to Performance Analysis, Turbocharging, Combustion, Emissions and Heat Transfer*. Vol. 3: Combustion. NLDA.

— (2010d). *Diesel Engines - A Fundamental Approach to Performance Analysis, Turbocharging, Combustion, Emissions and Heat Transfer*. 6th print. Vol. 4: Emissions and heat transfer. NLDA.

Stapersma, D., P. J. M. Schulten, and H. T. Grimmelius (2004). "A Fresh View on Propulsion Control". In: *Proceedings of the 7th International Naval Engineering Conference*. Amsterdam, The Netherlands, pp. 221–240.

Stapersma, D. and A. Vrijdag (2017). "Linearisation of a ship propulsion system model". In: *Ocean Engineering*. Vol. 142, pp. 441–457.

Stapersma, D., A. Vrijdag, and H. T. Grimmelius (2009). "A Fresh View on Propulsion Control II". In: *Proceedings of the 14th International Ship Control Systems Symposium*. Ottawa, Canada.

Stefanopoulou, A. and R. Smith (2000). "Maneuverability and smoke emission constraints in marine diesel propulsion". In: *Control Engineering Practice*. Vol. 8, pp. 1023–1031.

Stopford, M. (2008). *Maritime Economics*. 3rd. London, UK: Routledge.

Sudhoff, S. D., K. A. Corzine, S. F. Glover, H. J. Hegner, and H. N. Robey (1998). "DC Link Stabilized Field Oriented Control of Electric Propulsion Systems". In: *IEEE Transactions on Energy Conversion*. Vol. 13(1), pp. 27–33.

Sudhoff, S. D., S. D. Pekarek, R. R. Swanson, V. S. Duppalli, D. C. Horvath, A. E. Kasha, R. Lin, B. D. Marquet, P. R. O'Regan, H. Suryanarayana, and Y. Yan (2015). "A Reduced Scale Naval DC Microgrid to Support Electric Ship Research and Development". In: *Proceedings of the 6th IEEE Electric Ship Technologies Symposium*, pp. 464–471.

Sui, C., E. Song, D. Stapersma, and Y. Ding (2017). "Mena value modelling of diesel engine combustion based on parameterized finite stage cylinder process". In: *Ocean Engineering*. Vol. 136, pp. 218–232.

Sulligoi, G., S. Castellan, M. Aizza, D. Bosisch, L. Piva, and G. Lipardi (2012). "Active Front-End for Shaft Power Generation and Voltage Control in FREMM Frigates Integrated Power System: Modelling and Validation". In: *Proceedings of the 21st SPEEDAM Conference*. Sorrento, Italy, pp. 452–457.

Sulligoi, G., A. Vicenzutti, V. Arcidiacono, and Y. Khersonsky (2016). "Voltage stability in large marine-integrated electrical and electronic power systems". In: *IEEE transactions on industry applications*. Vol. 52(4), pp. 3584–3594.

Sundstrom, O., D. Ambuhl, and L. Guzzella (2010). "On implementation of dynamic programming for optimal control problems with final state constraints". In: *Oil and Gas Science and Technology*. Vol. 65(1), pp. 91–102.

Sundstrom, O. and L. Guzzella (2009). "A generic dynamic programming Matlab function". In: *Proceedings of the 18th IEEE International Conference on Control Applications*. Saint Petersburg, Russia, pp. 1625–1630.

Taljegard, M., S. Brynolf, M. Grahn, K. Andersson, and H. Johnson (2014). "Cost-effective choices of marine fuels in a carbon-constrained world: results from a global energy model". In: *Environmental Science and Technology*. Vol. 48, pp. 12986–12993.

Taskar, B., K. K. Yum, S. Steen, and E. Pedersen (2016). "The effect of waves on engine-propeller dybamics and propulsion performance of ships". In: *Ocean Engineering*. Vol. 122, pp. 262–277.

Taylor, D. W. (1933). *The Speed and Power of Ships: a Manual of Marine Propulsion*. Washington D.C., USA: Press of Ransdell, Inc.

Terwisga, T. van, E. vn Wijngaarden, J. Bosschers, and G. Kuiper (2007). "Achievements and Challenges in Cavitation Research on Ship Propellers". In: *International Shipbuilding Progress*. Vol. 54. IOS Press, pp. 165–187.

Theotokatos, G. and V. Tzelepis (2015). “A Computational Study on the Performamnce and Emission Parameters Mapping of a Ship Propulsion System”. In: *Proceedings IMechE Part M: Journal of Engineering for the Maritime Environment*. Vol. 229(1), pp. 58–76.

Tian, Y., B. Xia, M. Wang, W. Sun, and Z. Xu (2014). “Comparison study on two model-based adaptive algorithms for SOC estimation of lithium-ion batteries in electric vehicles”. In: *Energies*. Vol. 7(12), pp. 8446–8464.

Topaloglou, S., G. Paplambrou, and N. Kyrtatos (2016). “Energy management controller design for hybrid ship propulsion during transient operation”. In: *Proceedings of the 28th CIMAC*. 50. Helsinki, Finland, pp. 1–9.

Trzynadlowski, A. M. (2001). “Control of Induction Motors”. In: San Diego, California, USA: Academic Press.

UN (2017). *The emissions gap report 2017*. Tech. rep. United Nations Environment Programme.

Unamuno, E. and J. A. Barrena (2015). “Hybrid AC/DC microgrids - part II: Review and Classification of control strategies”. In: *Renewable and Sustainable Energy Reviews*. Vol. 52, pp. 1123–1134.

van Biert, L., M. Godjevac, K. Visser, and P. V. Aravind (2016). “A review of fuel cell systems for maritime applications”. In: *Journal of Power Sources*. Vol. 327, pp. 345–364.

van Spronsen, P. J. and R. Toussain (2001). “An Optimal Control Approach to Preventing Marine Diesel Engine Overloading aboard *Karel Doorman* Class Frigates”. In: *IFAC Proceedings Volumes*. Vol. 34(7), pp. 23–30.

van Straaten, O. F. A. and M. J. de Boer (2012). “Optimum propulsion engine configuration from fuel economic point of view”. In: *Proceedings of the 11th International Naval Engineering Conference*. Edinburgh, UK.

Vanderpump, D., M. Benatmane, and P. T. Murray (2002). “The Type 45 Destroyer Power and Propulsion System”. In: *Proceedings of the 6th International Naval Engineering Conference*. Glasgow, UK, pp. 61–74.

Veneri, O, F Migliardini, C Capasso, and P Corbo (2012). “Overview of electric propulsion and generation architectures for naval applications”. In: *Conference proceedings ESARS-ITEC 2012*.

Vettor, R. and C. Guedes Soares (2016). “Development of a ship weather routing system”. In: *Ocean Engineering*. Vol. 123, p. 1014.

Vie, R. (1998). “Commercial Experience with Electric Propulsion on Passenger Cruise Vessels”. In: *Proceedings of the IMarE All Electric Ship Conference*. London, UK, pp. 1–9.

Visser, K., R. D. Geertsma, A. Hasseltalab, and R. R. Negenborn (2017). “Marine Engineering at the Heart of the Autonmous Vessel”. In: *SWZ Maritime*, pp. 18–22.

Volker, T. (2013). “Hybrid Propulsion Concepts on Ships”. In: *Zeszyty Naukowe Akademii Morskiej w Gdyni*. Vol. 79, pp. 66–76.

Vrijdag, A. (2009). “Control of Propeller Cavitation in Operational Conditions”. PhD thesis. The Netherlands: Faculty Mechanical, Maritime and Materials Engineering, TU Delft.

— (2014). “Estimation of Uncertainty in Ship Performance Predictions”. In: *Journal of Marine Engineering and Technology*. Vol. 13(3), pp. 45–55.

Vrijdag, A., P. J. M. Schulten, D. Stapersma, and T. van Terwisga (2007). "Efficient Uncertainty Analysis of a Complex Multidisciplinary Simulation Model". In: *Journal of Marine Engineering and Technology*. Vol. 10.

Vrijdag, A. and D. Stapersma (2017). "Extension and application of a linearised ship propulsion system model". In: *Ocean Engineering*. Vol. 143, pp. 50–65.

Vrijdag, A., D. Stapersma, and T. van Terwisga (2008). "Trade-offs in Ship Propulsion Control: Engine Overloading and Cavitation Inception in Operational Conditions". In: *Proceedings of the 9th International Naval Engineering Conference*. Hamburg, Germany, pp. 82–93.

— (2009). "Systematic modelling, verification, calibration and validation of a ship propulsion simulation model". In: *Proceedings IMarEST Part A: Journal of Marine Engineering and Technology*. Vol. 8(15), pp. 3–20.

— (2010). "Control of Propeller Cavitation in Operational Conditions". In: *Journal of Marine Engineering and Technology*. Vol. 16, pp. 15–26.

Vu, T. L., A. A. Ayu, J. S. Dhupia, and A. K. Adnanes (2015). "Power Management for Electric Tugboats Through Operating Load Estimation". In: *IEEE transactions on Control Systems Technology*. Vol. 23(6), pp. 2375–2382.

Vu, T. L., J. S. Dhupia, A. A. Ayu, L. Kennedy, and A. K. Adnanes (2014). "Optimal power management for electric tugboats with unknown load demand". In: *Proceeding of the IEEE American Control Conference*. Oregon, USA, pp. 1578–1583.

Waag, W., C. Fleischer, and D. U. Sauer (2014). "Critical review of the methods for monitoring of lithium-ion batteries in electric and hybrid vehicles". In: *Journal of Power Sources*. Vol. 258, pp. 321–339.

Waard, D. S. de (2015). "Parameterization of ship propulsion drives and their fuel efficiency under different operatiobal modes and configurations". In: *Proceedings of the Engine As A Weapon VI conference*. Bath, UK, pp. 44–57.

Wang, Y., L. Lin, S. Zeng, J. Huang, A. P. Roskilly, Y. He, X. Huang, and S. Li (2008). "Application of the Miller cycle to reduce NOx emissions from Petrol Engines". In: *Applied Energy*. Vol. 85, pp. 463–474.

Wesselink, A. F., D. Stapersma, and D. van den Bosch (2006). "Non-linear aspects of propeller pitch control". In: *Proceedings of the 8th International Naval Engineering Conference*. London, UK.

Whitelegg, I., R. W. G. Bucknall, and B. T. Thorp (2015). "On electric warship power system performance when meeting the energy requirements of electromagnetic railguns". In: *Journal of Marine Engineering and Technology*. Vol. 14(2), pp. 85–102.

Wijsmuller, M. and T. Hasselaar (2007). "Optimisation of the Propulsion Arrangement in Emergency Towing Vessels". In: *Ship and Boat International*, pp. 34–37.

Wirasingha, S. G. and A. Emadi (2011). "Classification and Review of Control Strategies for Plug-In Hybrid Electric Vehicles". In: *IEEE Transactions on Vehicular Technology*. Vol. 60, pp. 111–120.

Won, J.-S., R. Langari, and M. Ehsani (2005). "An energy management and charge sustaining strategy for a parallel hybrid vehicle with CVT". In: *IEEE Transactions on Control Systems Technology*. Vol. 13(2). 313-320.

Wrobel, K., J. Montekwa, and P. Kujula (2017). "Towards the assessment of potential impact of unmanned vessels in maritime transportation safety". In: *Reliability Engineering and System Safety*. Vol. 165, pp. 155–169.

Xiros, N. (2002). "Robust Control of Diesel Ship Propulsion". In: London, UK: Springer-Verlag.

Xiros, N. I. (2014). "PID Marine Engine Speed Regulation under Full Load Conditions for sensitivity $H-\infty$ norm Specifications against Propeller Disturbance". In: *Journal of Marine Engineering and Technology*. Vol. 3(2), pp. 3–11.

Xu, L., C. D. Nueller, J. Li, M. Ouyang, and Z. Hu (2015). "Multi-objective component sizing based on optimal energy management strategy of fuel cell electric vehicles". In: *Applied Energy*. Vol. 157, pp. 664–674.

You, Y. (2018). "A study on the maneuverability of a twin-screw LNGC under machinery failure". In: *Ocean Engineering*. Vol. 155, pp. 324–350.

Yuan, L. C. W., T. Tjahjowidodo, G. S. G. Lee, R. Chan, and A. K. Adnanes (2016). "Equivalent Consumption Minimization Strategy for hybrid all-electric tugboats to optimize fuel savings". In: *Proceedings of the American Control Conference*, pp. 6803–6808.

Zaccone, R. and M. Figari (2017). "Energy efficient ship voyage planning by 3D dynamic programming". In: *Journal of Ocean Technology*. Vol. 12:4, pp. 49–71.

Zaccone, R., E. Ottaviani, M. Figari, and M. Altosole (2018). "Ship voyage optimization for safe and energy-efficient navigation: A dynamic programming approach". In: *Ocean Engineering*. Vol. 153, pp. 215–224.

Zadeh, M. K., B. Zahedi, M. Molinas, and L. E. Norum (2013). "Centralised Stabilizer for Marine DC Microgrid". In: *Proceedings of the 39th Annual Conference of the IEEE Industrial Electronics Society*. Vienna, Austria, pp. 3359–3363.

Zahedi, B. and L. E. Norum (2013). "Modelling and Simulation of All-Electric Ships with Low-Voltage DC Hybrid Power Systems". In: *IEEE Transactions on Power Electronics*. Vol. 28(10), pp. 4525–4537.

Zahedi, B., L. E. Norum, and K. B. Ludwigsen (2014). "Optimised Efficiency of All-Electric Ship by DC Hybrid Power Systems". In: *Journal of Power Sources*. Vol. 255, pp. 341–354.

Zak, S. H. (2003). *Systems and control*. New York, New York, USA: Oxford University Press.

Zeldovich, Y. B. (1946). "The Oxidation of Nitrogen in Combustion and Explosions". In: *Acta Physicochimica URSS*. Vol. 21(4), pp. 577–628.

Zhan, K., H. Gao ad H. Chen, and Z. Lin (2015). "Optimal retrofitting of a hybrid propulsion system using NSGA-II algorithm for trailing suction hopper dredger". In: *Proceedings of the IEEE Electric Ship Technologies Symposium*, pp. 201–206.

Zhang, Z., X. Huang, J. Jiang, and B. Wu (2010). "A Load-sharing Control Scheme for a Microgrid with a Fixed Frequency Inverter". In: *Electric Power Systems Research*. Vol. 80, pp. 311–317.

Zhao, F., W. Yang, W. W. Tan, W. Yu, J. Yang, and S. K. Chou (2016). "Power management of vessel propulsion system for thrust efficiency and emission mitigation". In: *Applied Energy*. Vol. 161, pp. 124–132.

Zheng, F., Y. Xing, J. Jiang, B. Sun, J. Kim, and M. Pecht (2016). "Influence of different open circuit voltage tests on state of charge online estimation for lithium-ion batteries". In: *Applied Energy*. Vol. 183, pp. 513–525.

Zheng, H., R. R. Negenborn, and G. Lodewijks (2017a). “Closed-loop scheduling of waterborne AGVs for energy-efficient Inter Terminal Transport”. In: *Transportation Research Part E: Logistics and Transportation Review*. Vol. 105, pp. 261–278.

— (2017b). “Fast ADMM for Distributed Model Predictive Control of Cooperative Waterborne AGVs”. In: *IEEE transactions on Control Systems Technology*. Vol. 25(4), pp. 1406–1413.

Ziegler, J. and N. Nichols (1942). “Optimum Settings for automatic controllers”. In: *Transactions ASME, Journal of Dynamic Systems, Measurement and Control*. Vol. 64, pp. 759–768.

Zinner, K. (1980). *Aufladung von Verbrennungsmotoren*. 2. Auflage. Berlin, Heidelberg, New York: Springer-Verlag.

NOMENCLATURE

Greek Symbols

α	crank angle [deg]
α_{eff}	effective angle of attack [deg]
α_{i}	shock free entry angle onto the leading edge of the propeller profile [deg]
α_{Z}	*Zinner* turbine area decrease factor
α_{wk}	angle of the vertical wave movement at the propeller centre [rad]
β	hydrodynamic pitch angle [rad]
χ	the ratio between the specific heats at constant pressure and air
δ_{f}	fuel addition factor
ΔT	time step over which the rate is limited
η	efficiency
η_{q}	heat release efficiency
η_{R}	relative rotative efficiency of the propeller
κ	specific heat ratio
λ	air excess ratio
λ_{CR}	length ratio of the crank rod to the crank shaft radius
ω_{b}	base frequency [rad/s]
ω_{e}	frequency of the rotating reference frame [rad/s]
ω_{i}	induction machine shaft speed [rad/s]
ω_{r}	electrical rotor speed [rad/s]
ω_{wv}	wave radial frequency in [rad/s]
π	pressure ratio of turbine or compressor
Ψ	flux linkage per second [V]
Ψ_{sc}	non-dimensional scavenge flow
ρ_{e}	angle of the rotating reference frame relative to the a phase of the stator [rad]
ρ_{sw}	density of seawater [kg/m^3]
σ_{f}	stoichiometric air to fuel ratio of the fuel
σ_{n}	cavitation number
$\tau_{\text{p,d}}$	time delay for filling the exhaust receiver [s]
τ_{p}	time constant representing pitch actuation delay [s]
τ_{X}	fuel injection time delay [s]
θ	pitch angle [rad]
θ_{red}	pitch angle reduction [rad]
θ_0	pitch at which zero thrust is achieved [deg]
ε	parasitic heat exchanger effectiveness

ε_c	geometric compression ratio
ζ	significant wave amplitude [m]

Roman Symbols

a, b, c	Seiliger parameters for isochoric, isobaric and isothermal combustion
A_{eff}	effective area of the turbine [m^2]
$a_{\text{gb}}, b_{\text{gb}}, c_{\text{gb}}$	gearbox loss function parameters
a_η, b_η, c_η	polynomial coefficients of the turbocharger
b_{dg}	binary setting for switching the diesel generator (DG) on or off
b_{im}	binary setting for switching the induction machine (IM) on or off
b_{me}	binary setting for switching the main engine (ME) on or off
c	capacitance [F]
c_1	Vrijdag coefficient to calibrate the effective angle of attack
c_{p}	specific heat at constant pressure [J/kgK]
$C_{\text{Q}}, C_{\text{T}}$	torque and thrust coefficient
c_{v}	specific heat at constant volume [J/kgK]
c_f	friction factor (fraction of nominal power)
c_{sfo}	specific fuel oil consumption [kg/kWh]
D	propeller diameter [m]
D_{B}	bore diameter [m]
D_{p}	propeller diameter [m]
D_{ref}	direct induction machine field control reference
f_{t}	thrust deduction factor
f_{w}	wake fraction
f_p	power factor
g	standard gravity [m/s^2]
h^{L}	lower heating value of fuel at ISO conditions [kJ/kg]
i	current [A]
i_{e}	number of cylinders of the engine
i_{gb}	gearbox reduction ratio
J	moment of inertia [kgm]
k_{e}	number of revolutions per cycle
K_{ID}	induction machine field reference reset rate
K_{IT}	induction machine torque reference reset rate
K_{I}	reset rate
K_{PD}	induction machine field reference gain
K_{PT}	induction machine torque reference gain
k_{p}	number of propellers
K_{Q}	propeller torque coefficient
k_{w}	wave number in [1/m]
L	length [m]
L_{set}	lever setpoint after rate limitation [%]
L_{u}	unlimited lever setpoint [%]

M	torque [kNm]
m	mass in cylinder [kg]
$\dot{m}_\mathrm{f}$	fuel consumption [kg/s]
m_bsfc	brake specific fuel consumption [kg/kWh]
m_f	fuel injected per cylinder per cycle [kg]
M_i	indicated torque [kNm]
$M_\mathrm{loss,grad}$	torque loss gradient
M_loss	torque loss [kNm]
M_l	gearbox torque loss [kNm]
$\dot{m}_\mathrm{t}$	total mass flow at nominal conditions [kg/s]
n	rotational speed [Hz]
n_bld	polytropic expansion coefficient of blowdown
n_exp	polytropic exponent for expansion
n_e	engine speed [Hz]
N_virt	virtual shaft speed [rpm]
n_virt	virtual shaft speed [Hz]
P	power [kW]
p	pressure [Pa]
p_∞	ambient water pressure at the center-line of the propeller [Pa]
p_max	maximum pressure during combustion in the Seiliger cycle [Pa]
$P_\mathrm{pd,0}$	pitch ratio at which zero thrust is achieved
P_pd	Propeller pitch to diameter ratio at 70% of the radius
P_pp	the number of pole pairs of an electric machine
p_v	vapour pressure of water at ambient temperature [Pa]
P_os	overspeed limitation gain
P_us	under-speed limitation gain
Q	heat [kJ]
q	specific heat release [kJ/kg]
Q_bat	battery capacity [Ah]
q_hl	specific heat loss [kJ/kg]
Q_lhv	lower heating value of fuel at ISO conditions [kJ/kg]
Q_p	open water propeller torque [kNm]
Q_ref	quadrature induction machine field control reference
R	gas constant [J/kgK]
R_a	gas constant of air [J/kgK]
R_CS	crank shaft radius [m]
r_c	effective compression ratio
r_eo	ratio of volume at Seiliger point 6 relative to 1
r_ht	heat transfer ratio between blowdown heating and scavenge cooling
$R_\mathrm{L+}, R_\mathrm{L-}$	maximum, minimum increase rate of the lever setpoint [1/s]
$R_\mathrm{P+}, R_\mathrm{P-}$	maximum, minimum pitch increase rate [1/s]
R_Pr	pitch reduction rate [1/s]

r_r	rotor resistance [Ω]
r_s	stator resistance [Ω]
$r_\mathrm{T,TC}$	driving temperature ratio of the turbocharger
R_v	ship resistance [kN]
$R_\mathrm{X,cav}$	fuel increase rate limitation to prevent cavitation [1/s]
$R_\mathrm{X,therm}$	fuel increase rate limitation to prevent thermal overloading [1/s]
s	equivalence factor or co-state
s_byp	bypass slip factor for flow around cylinder
s_sc	scavenge slip ratio without bypass air
s_sl	slip ratio of the scavenge process with bypass air
S_OC	state of charge
T	temperature [K]
t	time [s]
T_1	temperature at the start of compression [K]
T_bld	*Zinner* blowdown temperature [K]
T_ev	exhaust valve temperature [K]
T_p	thrust [N]
T_slip	temperature of the air slip during scavenging [K]
u	voltage [V]
u_c	control variables for the control problem
V	Cylinder volume [m^3]
V_1	cylinder volume at the start of compression [m^3]
v_a	advance speed of water into the propeller [m/s]
v_a	advance speed of water into the propeller [m/s]
v_h	hydrodynamic velocity [m/s]
v_s	ship speed [m/s]
v_w	wakefield disturbance due to waves [m/s]
w	specific work [kNm/kg]
w_e	exogenous inputs for the control problem
w_i	specific indicated work [kNm/kg]
X	fuel pump injection [%]
X_ct	portion of heat released at constant temperature
X_cv	portion of heat released at constant volume
x_c	compression stroke effectiveness factor
X_I	fuel injection setpoint from integrating speed control [%]
x_M	equivalent inductance [Ω]
x_m	mutual inductance [Ω]
X_PI	fuel injection setpoint from fast *PI* speed control [%]
x_r	rotor self-inductance [Ω]
x_s	stator self-inductance [Ω]
$X_{\mathrm{lim},\lambda}$	fuel injection limitation to limit air acces ratio λ [%]
z	water depth at propeller center [m]

Superscripts

*	normalised value, relative to nominal value
e	in the synchronously rotating reference frame

Subscripts

ic	slow integrating speed control
max	maximum
mins	minimum speed setpoint [rpm]
min	minimum
os	overspeed
set	setpoint
a	air
amb	ambient
aux	auxiliary electrical load demand
b	after the compressor, before the intercooler
bat	battery
BDC	when cylinder is at bottom dead centre
c	charge air after the intercooler
chg	charge
com	compressor
comb	combustion
CR	crank rod
d	exhaust receiver
dg	diesel generator
dis	discharge
dr	direct component of the rotor
ds	direct component of the stator
e	engine
EC	when the exhaust valve closes
el	electric
em	electromagnetic
EO	when the exhaust valve opens
eqv	equivalent
ew	entrained water
ex	turbine exit
FAT	FAT conditions
fc	frequency converter
g	exhaust gas
gb	gearbox
gen	synchronous generator
i	state in the Seiliger cycle according to Figure 3.6
IC	when inlet valve closes
id	assuming no heat loss

ij	from state i to state j in the Seiliger cycle
im	induction machine
inl	inlet duct
is	assuming isentropic conditions
lim	limitation
line	network line
loss	losses
m	mechanical
mar	margin
max	maximum value
md	direct component of mutual (flux linkage)
me	main diesel engine
min	minimum
mq	quadrature component of mutual (flux linkage)
nom	nominal value
oc	open cell
p	propeller
pd	demand for propulsion
qr	quadrature component of the rotor
qs	quadrature component of the stator
rec	rectifier
ref	reference
S	stroke
s	equilibrium
set	setpoint
sl	shaftline
t	terminal
TC	turbocharger
TDC	when cylinder is at top dead centre
tot	total
tur	turbine

CURRICULUM VITÆ

Rinze Dirk GEERTSMA

19-11-1975 Born in Kollum, the Netherlands.

EDUCATION

1988–1994 Grammar School
Stedelijk Gymnasium, Leeuwarden, the Netherlands

1994–1999 Officers Degree
Royal Netherlands Naval Academy, Den Helder, the Netherlands

1998–1999 Master of Science in Marine Engineering (electrical), with distinction
University College London, UK

2014–2018 Doctor of Philosophy in Marine Engineering
Delft University of Technology, the Netherlands
Thesis: Autonomous control for adaptive ships with hybrid propulsion and power generation
Promotors: Prof. dr. R. R. Negeborn and Prof. ir. J. J. Hopman
Supervisor: ir. K. Visser

AWARDS

1999 Ship Design Exercise award at University College London

1999 Best student award in Marine Engineering at University College London

PROFESSIONAL QUALIFICATION

2008 Chartered Engineer

PROFESSIONAL EXPERIENCE

Cdr (E) Rinze Geertsma, MSc, CEng, MIMarEST is an experienced naval engineering officer with a strong interest in applying revolutionary technology on current and future naval vessels to improve their performance, reduce their environmental footprint and increase their autonomy, while leaving key decisions to human operators and maintainers. He currently is senior officer energy and smart maintenance in the Life Cycle Modelling section of the Netherlands Defence Materiel Organisation with the Netherlands Ministry of Defence. This dissertation is the result of his PhD research at Delft University of Technology and Netherlands Defence Academy into adaptive control strategies for hybrid and autonomous ship systems from september 2014 to 2018.

Cdr (E) Rinze Geertsma has achieved a dozen publications in engineering conferences and has achieved four publications in high quality Q1 scientific journals. He is a chartered engineer, active member of the IMarEST, committee member of the IMarEST Benelux branch, chairmen of the international Ship Control System Symposium (iSCSS), associate editor of the Journal of Marine Engineering and Technology, member of the IMarEST publications Supervisory Board and highly engaged to improve and acknowledge professional development of engineers through KIVI and IMarEST.

Previously, he was responsible for the specification and design of automation systems for future and current ships in the Royal Netherlands Navy, introducing interactive electronic incident boards, developing advisory systems for unmanned machinery control rooms and integrating platform and combat systems information for improved command advice. He has extensive operational experience as Marine Engineering Officer of HNLMS de Ruyter and HNLMS Tromp and as Deputy Marine Engineering Officer of HNLMS van Speijk, going through the complete training cycle, including FOST, both as a DMEO and as an MEO, and successfully managing a technical team of over 50 engineers. Earlier experience includes research and development project management, system and project engineering and in service support.

LIST OF PUBLICATIONS

9. A. Coraddu, M. Kalikatzarakis, L. Oneto, G.-J. Meijn, M. Godjevac, **R. D. Geertsma**, *Ship diesel engine performance modelling with combined physical and machine learning approach*, Conference Proceedings of the 15th international Ship Control Systems Symposium (2018).

8. **R. D. Geertsma**, K. Visser, R. R. Negenborn, *Adaptive pitch control for ship with diesel mechanical and hybrid propulsion*, Applied Energy **228**, pp. 2490-2509 (2018).

7. M. Kalikatzarakis, **R. D. Geertsma**, E.-J. Boonen, K. Visser, R. R. Negenborn, *Ship energy management for hybrid propulsion and power supply with shore charging*, Control Engineering Practice **76**, pp. 133-154 (2018).

6. **R. D. Geertsma**, R. R. Negenborn, K. Visser, J. J. Hopman *Pitch control for ships with mechanical and hybrid propulsion: Modelling, validation and performance quantification*, Applied Energy **206**, pp. 1609-1631 (2017).

5. **R. D. Geertsma**, J. Vollbrandt, R. R. Negenborn, K. Visser, J. J. Hopman, *A quantitative comparison of hybrid diesel-electric and gas-turbine-electric propulsion for future frigates*, Proceedings of the 2017 IEEE Electric Ship Technologies Symposium pp. 451-458 (2017).

4. **R. D. Geertsma**, R. R. Negenborn, K. Visser, J. J. Hopman, *Parallel Control for Hybrid Propulsion of Multifunction Ships*, IFAC Proceedings Volumes **50(1)** pp. 2296-2303 (2017).

3. P. J. M. Schulten, **R. D. Geertsma**, K. Visser, *Energy As A Weapon, part 2*, Proceedings of the Engine As A Weapon VII conference (2017).

2. **R. D. Geertsma**, R. R. Negenborn, K. Visser, J. J. Hopman, *Design and Control of Hybrid Power and Propulsion Systems for Smart Ships: a Review of Developments*, Applied Energy **194**, pp. 30-54 (2016).

1. **R. D. Geertsma**, R. R. Negenborn, K. Visser, J. J. Hopman, *Torque Control for Diesel Mechanical and Hybrid Propulsion for Naval Vessels*, Proceedings of the 13th International Naval Engineering Conference (2016).